Determining the Mechanisms of Long-Term Pain in Childhood Cancer Survivorship

Tameille Valentine

A thesis submitted in partial fulfilment of the requirements of Nottingham Trent University for the degree of Doctor of Philosophy

April 2023

Publication and Abstracts

Publication

T. Valentine, L. Hardowar, J. Elphick-Ross, R. P. Hulse and M. Paul-Clark (2022). "The Role of Vascular-Immune Interactions in Modulating Chemotherapy Induced Neuropathic Pain." *Frontiers in Pharmacology*.

Abstracts

T. Valentine, A. Hargreaves, A. Coutts and R. P. Hulse. "Determining the Mechanisms of Long Term Pain in Childhood Cancer Survivorship". Oral presentation presented at The PGR STAR Conference; Nottingham, 8th and 9th June 2021 [Online].

T. Valentine, L. Hardowar, A. Hargreaves, A. Coutts and R. P. Hulse. "Determining the Mechanisms of Long Term Pain in Childhood Cancer Survivorship". Oral presentation presented at Physiology 2021; Online, 12th - 16th July 2021.

T. Valentine, L. Hardowar, A. Coutts and R. P. Hulse. "TOP2-Associated TrkA Activation, A Possible Mechanism of Long Term Pain in Childhood Cancer Survivorship". Oral presentation presented at Europhysiology 2022; Copenhagen, 16th - 18th September 2022.

Abstract

Chemotherapy-induced peripheral neuropathy (CIPN) commonly occurs following platinum-based chemotherapy (e.g. cisplatin). Neonatal exposure to cisplatin results in a delayed but lasting chronic pain, that persists into adulthood, decreasing quality of life. Presently, there are no preventative treatments and no condition-tailored analgesia so current analgesia that are being utilized are either ineffective or result in long-term adverse effects. Furthermore, it may negatively impact on chemotherapy treatment, preventing the administration of chemotherapy at the optimal effective doses and premature discontinuation of therapy. If we are able to understand the mechanisms involved, then we will be able to develop effective preventative and therapeutic strategies. Previous research has demonstrated the involvement of tropomyosin receptor kinase A (TrkA) modulation in causing aberrant nerve fibre growth and development of pain. This thesis investigated the effect of cisplatin treatment and the role of TrkA signalling using both in vitro and in vivo analysis. In vitro models were also explored to identify a modulator of TrkA function.

Firstly, both the in vitro and in vivo models were successfully developed. Isolated dorsal root ganglion (DRG) sensory neurons exposed to varying concentrations of cisplatin for 24 hours displayed a decrease in neurite outgrowth with increasing concentrations of cisplatin, demonstrating neurodegeneration. Similarly, following 24-hours cisplatin treatment, SH-SY5Y cells exhibited a decrease in cell viability with increasing concentrations of cisplatin. Using this cell line model, TrkA expression levels appeared to remain unchanged. However, there was a dose-dependent increase in TrkA phosphorylation following 24-hours cisplatin treatment. In vivo, cisplatin resulted in a persistent but delayed onset of chronic pain in the form of mechanical hypersensitivity, demonstrating peripheral sensory neuronal sensitization. Mechanical hypersensitivity was accompanied by aberrant nerve fibre growth. Administration of cisplatin along with the TrkA inhibitor GW441756, thereby blocking TrkA signalling, ameliorated cisplatin-induced mechanical hypersensitivity and prevented cisplatin-induced aberrant nerve fibre growth. Consequently, the next step was to identify a possible source of TrkA phosphorylation. Notably, cisplatin induced a DNA damage response, evidence by an upregulation in p53 as well as increased phosphorylation of p53 and histone H2A.X, key DNA damage markers.

Novel findings included upregulation of the DNA topoisomerase, TOP2, by cisplatin. Furthermore, in vitro inhibition of TOP2, using doxorubicin, suppressed both cisplatin-induced TrkA phosphorylation in SH-SY5Y cells and cisplatin-induced nociceptor activation in DRG sensory neurons. These results indicate that CIPN is TrkA dependent, which is regulated by TOP2, a modulator of TrkA phosphorylation and nociceptor sensitization. Hence a new analgesic target may have been found in TOP2.

Acknowledgements

Firstly, I would like to thank God for sending this opportunity my way and providing me with the self-motivation, ambition, discipline and persistence required to complete this project and write this thesis. Thanks to my Director of Studies, Dr Richard Hulse, for seeing my potential and accepting me onto this project. You have taught me so much over the years and have definitely shaped the researcher I am today. Thank you for being such a supportive, approachable, open-minded, patient and engaging supervisor. You always valued my research ideas, entrusted me to work independently in the laboratory and was always available when I needed assistance. I could not have asked for a better supervisor. Thanks to the rest of my supervisory team, Dr Amanda Coutts, Dr Alan Hargreaves and Dr Carl Nelson, for your guidance and support throughout my project. Additionally, thank you to David Boocock and Clare Coveney for your expertise and assistance with the omics work conducted in this thesis.

I am grateful to all my colleagues in the Interdisciplinary Science and Technology Centre (ISTeC) for providing a positive and enjoyable working environment. Thank you to Arnold Tan, Satinderdeep Kaur, Dr Alice Murphy and Dr Awais Younis for all your help within the laboratory. Thank you to Nikita Lad (my Western blotting mentor), Cristina Parenti and Merell Billacura for your support and friendship both in and out of the laboratory; you made those long and stressful days a bit more manageable. A particular thank you to Lydia Hardowar for welcoming me into the Hulse research group; your humour as well as being a fellow horror enthusiast definitely allowed me to de-stress and create some memorable moments over the years.

To the personal trainers at PureGym West Bridgford, thanks for helping me get through the writing of my thesis. Being stuck at home all day, it was refreshing to be greeted daily with your friendliness and enthusiasm. Your classes kept me energized and was always the highlight of my days. Lastly and certainly not least, I am indebted to my family; my twin sister, Tineille Valentine-Templeton, my mom, Marilyn Valentine and my aunt Roslyn Valentine. Thank you for always supporting me, believing in me and encouraging me to be the best version of myself possible. Even when times got difficult, you guys kept me motivated. This thesis is dedicated to you three as well as my nieces KaliRose and AylaRae, who always kept me smiling even in the most stressful of time.

Abbreviations

AP	Apurinic or Apyrimidinic
APE	AP endonuclease
APS	Ammonium persulphate
ASCO	American Society of Clinical Oncology
ATF-3	Activating transcription factor-3
ATM	Ataxia-telangiectasia mutated
ATP	Adenosine triphosphate
ATR	Ataxia-telangiectasia and RAD3-related
AUC	Area under the curve
BC	Boundary cap
BDNF	Brain-derived neurotrophic factor
BER	Base excision repair
BRCA2	Breast and ovarian cancer susceptibility protein 2
BSA	Bovine serum albumin
Ca^{2+}	Calcium ion
CC3	Cleaved caspase-3
CCI	Chronic constriction injury
CCSS	Childhood Cancer Survivor Study
CDH	Chronic daily headache
CGRP	Calcitonin gene-related product
CIPA	Congenital insensitivity to pain with anhidrosis
CIPN	Chemotherapy-induce peripheral neuropathy
CNS	Central nervous system
CO_2	Carbon dioxide
CPT	Current perception threshold
CREB	cAMP response element-binding protein
CRPS	Complex regional pain syndrome
CS	Cockayne syndrome
DDR	DNA damage response
DEG	Differentially expressed gene
DMEM	Dulbecco’s Modified Eagle Medium
DMSO	Dimethyl sulphoxide

DNA	Deoxyribonucleic acid
Dox	Doxorubicin hydrochloride
DRG	Dorsal root ganglion
dRP	Deoxyribose phosphate
DSB	Double-strand break
ECL	Enhanced chemiluminescence
EORTC	European Organisation for Research and Treatment of
FBS	Foetal bovine serum
FC	Fold change
FD	Familial dysautonomia
FDR	False discovery rate
FEN-1	Flap endonuclease-1
FMN	Facial motoneuron
GABA	γ-aminobutyric acid
GEO	Gene expression omnibus
GG-NER	Global genome nucleotide excision repair
GO	Gene Ontology
GPCR	G-protein-coupled receptor
HBSS	Hanks' Balanced Salt Solution
HR	Homologous recombination
HSV	Herpes simplex virus
i.p.	intraperitoneal
i.pl.	intraplantar
i.v.	intravenous
IASP	International Association for the Study of Pain
IB4	Isolectin B4
IENF	Intraepidermal nerve fibre
IL-	Interleukin-
KEGG	Kyoto Encyclopedia of Genes and Genomes
LPS	Lipopolysaccharide
MAPK	Mitogen-activated protein kinase
mDNA	mitochondrial deoxyribonucleic acid
Mg^{2+}	Magnesium ion
mRNA	messenger ribonucleic acid

Na^+	Sodium ion
NaCl	Sodium chloride
NCV	Nerve conduction velocity
NDS	Neuropathy disability score
NER	Nucleotide excision repair
NGF	Nerve growth factor
NGN	Neurogenin
NHEJ	Non-homologous end joining
NMDA	N-methyl-d-aspartate
NPC	No primary antibody control
NS	Nociceptive specific
NSS	Neuropathy symptom score
NT	Neurotrophin
OCT	Optimal cutting temperature
PACAP	Pituitary adenylate cyclase-activating polypeptide
PAG	Periaqueductal grey
PBS	Phosphate buffered saline
PCNA	Proliferating cell nuclear antigen
PFA	Paraformaldehyde
PGP9.5	Protein gene product 9.5
PI3K	Phosphatidylinositol 3-kinase
Pif-α	Pifithrin-α hydrobromide
PKC	Protein kinase C
PLC	Phospholipase C
PNS	Peripheral nervous system
PPI	Protein-protein interaction
QLQ	Quality of Life Questionnaire
QOL	Quality of Life
RFC	Replication factor C
RIPA	Radioimmunoprecipitation assay
R-ODS	Rasch-built Overall Disability Scale
ROS	Reactive oxygen species
RPA	Replication protein A
RUNX	Runt related transcription factor

RVM	Rostral ventromedial medulla
SAP	Sensory action potential
SCG	Superior cervical ganglion
SDS	Sodium dodecyl sulfate
SEM	Standard error of the mean
sICAM-1	Soluble intercellular adhesion molecule 1
SNI	Spared nerve injury
SP	Substance P
SSB	Single-strand break
ssDNA	Single-stranded DNA
TBS(-T)	Tris-buffered saline (-Tween 20)
TC-NER	Transcription coupled nucleotide excision repair
TEMED	Tetramethyl ethylenediamine
TFIIH	Transcription factor II human
TNF-α	Tumour necrosis factor α
TOP	DNA topoisomerase
Trk	Tropomyosin receptor kinase
TRP	Transient receptor potential
TRPA	Transient receptor potential Ankyrin
TRPC	Transient receptor potential Canonical
TRPM	Transient receptor potential Melastatin
TRPML	Transient receptor potential Mucolipin
TRPP	Transient receptor potential Polycystin
TRPV	Transient receptor potential Vanilloid
WDR	Wide dynamic range
XP	Xeroderma pigmentosum

Table of Contents

List of Figures

List of Tables

Chapter 1: General Introduction

1.1 Nociception and pain

Pain is an acute protective process, playing an essential role in the survival of an organism. It is defined by the International Association for the Study of Pain (IASP), as "an unpleasant sensory and emotional experience associated with the actual or potential tissue damage, or described in terms of such damage." Nociception is the neural process by which the body detects and responds to stimuli that are potentially tissue damaging and therefore perceived as painful. This neural process is dependent upon function of the somatosensory nervous system, which coordinates our perception of pain.

1.2 The somatosensory nervous system

The somatosensory nervous system contributes to the perception of pain and consists of two parts; the central nervous system (CNS) and the peripheral nervous system (PNS). The CNS is made up of the brain and spinal cord, which are involved with the processing of sensory information through modulation of neural signals via inhibitory and facilitatory processes. The spinal cord consists of a central core of grey matter surrounded by white matter (see Figure 1.1). The grey matter primarily contains neuronal cell bodies and is divided into dorsal horns and ventral horns. The white matter contains bundles of axons. Dorsal roots extend from the dorsal horns of the spinal cord to the dorsal root ganglion (DRG), a cluster of sensory neurons that project sensory nerve fibres to all parts of the body to form the PNS. The DRG is made up of a heterogeneous population of cells that includes supporting glia and blood vessels. Rodents typically have 30 or 31 pairs of DRGs; 8 pairs of cervical, 13 pairs of thoracic, 5 or 6 pairs of lumbar and 4 pairs of sacral DRGs [1]. Similarly, humans have 31 pairs of DRGs but slightly different numbers; 8 pairs of cervical, 12 pairs of thoracic, 5 pairs of lumbar, 5 pairs of sacral and 1 pair of 1 coccygeal DRGs [2]. Nociceptors, "pain-sensing" neurons, are one of the sensory neuronal subsets located in the DRG.

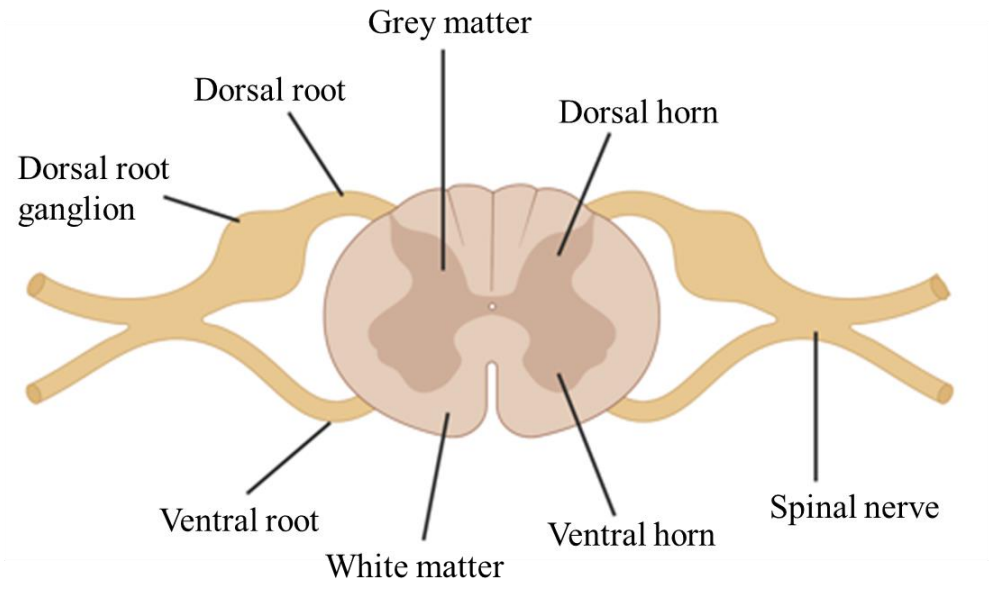

Figure 1.1 A cross-sectional view of the spinal cord. The grey matter primarily contains neuronal cell bodies and is divided into dorsal horns and ventral horns. The white matter contains bundles of axons. Dorsal roots extend from the dorsal horns and ventral roots extend from the ventral horns. They merge to form a spinal nerve. Along the dorsal root is a dorsal root ganglion (DRG), a cluster of sensory neurons that project sensory nerve fibres to all parts of the body to form the PNS. Created with Biorender.com

1.2.1 Nociceptors

Classification of peripheral sensory neurons (Aβ, Aδ and C fibres) are based largely on their diameter, myelination state and conduction velocity (which is affected by both fibre diameter and myelination state) [3]. The larger the fibre diameter and thicker the myelin sheath, the greater the conduction velocity. A-fibres have large diameters and are myelinated while C fibres have small diameters (0.2-1.5 µm) and are unmyelinated. A-fibres can further be subdivided into Aβ-fibres, which are larger (6-12 µm) and thickly myelinated, and Aδ-fibres, which are smaller (1-5 µm) and thinly myelinated [4, 5]. Hence the order of conduction velocity for these fibres from fastest to slowest is Aβ > Aδ > C [6]. Aβ-fibres act mainly as low-threshold mechanoreceptors, Aδ-fibres are both mechanoreceptors and nociceptors, and C-fibres account for the majority of nociceptors [7]. More than half of all somatosensory neurons are C-fibres [8] and they can be either peptidergic or non-peptidergic [9]. See Figure 1.2 for a summary.

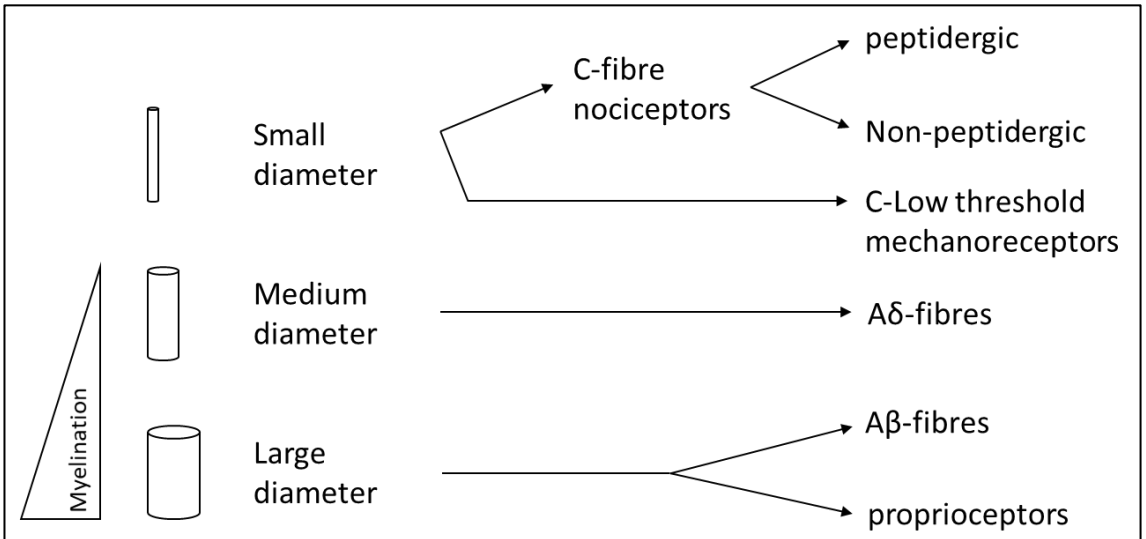

Figure 1.2 Classification of somatosensory neurons. Somatosensory neurons can be classed into three broad categories based on their diameter and myelination state. Large diameter Aβ-fibres are thickly myelinated, medium diameter Aδ-fibres are thinly myelinated and small diameter C-fibres are unmyelinated. Numerous subpopulations then exist. For example, C-fibres are mostly nociceptors, which can be peptidergic ($TrkA^+$ and release the neuropeptides CGRP and SP) or non-peptidergic ($TrkA^-$ and do not release CGRP or SP). Diagram adapted and modified from (15).

DRG sensory neurons are pseudo unipolar cells extending projection both to the CNS and also primary afferent sensory nerve fibres that possess specialized nerve endings to innervate varying tissues including the skin, joints and viscera. These specialized nerve endings contain specific channels and receptors, including voltage-gated sodium channels (Na_V), voltage-gated potassium channels (K_V), voltage-gated calcium channels (Ca_V) and transient receptor potential (TRP) channels, which are directly activated by different stimulus modalities (mechanical, thermal and chemical). Interaction with the extrinsic and intrinsic environment results in their activation, leading to membrane depolarization and transduction of an electrical signal (action potential). This action potential is conveyed and interpreted by the thalamus and cortex regions of the brain, allowing us to perceive sensation and pain. Peripheral sensory neurons have the capacity to detect innocuous stimulation (non-painful or not damaging to normal tissue such as touch, poke) as well as noxious stimuli (painful or damaging to normal tissue such as heat, cold, pinch). Nociceptors can also be classed dependent upon modality; mechanical (respond to intense pressure), thermal (respond

to extreme hot temperatures (> 45°C) or extreme cold temperatures (< 5°C)), mechano-thermal (respond to both mechanical and thermal stimuli), polymodal (respond to noxious mechanical, thermal and chemical stimuli) or silent (insensitive to mechanical and thermal stimuli) [3]. Silent nociceptors, however, are thought to become sensitive to mechanical and thermal stimulation once sensitized by inflammatory mediators such as cytokines, bradykinin, serotonin, histamine, prostaglandins and leukotrienes [10]. Based on electrophysiological studies, Aδ-fibres can further be subdivided into type I and type II Aδ-fibres. Type I Aδ-fibres, which are high-threshold mechanical nociceptors, respond to both mechanical and chemical stimuli and their heat activation temperature thresholds are quite high (> 50 °C). However, maintained heat stimulation results in decreased activation temperature thresholds and sensitization upon tissue injury. These fibres transmit pain signals in response to noxious mechanical stimuli. Type II Aδ-fibres have very high mechanical thresholds and lower heat activation temperature thresholds (~43 °C). These fibres transmit pain signals in response to noxious heat stimuli. C-fibres are typically polymodal, however some have been shown to fall in the other classes described above [10, 11].

The expression of numerous biochemical markers such as transient receptor potential (TRP) channels are also used to distinguish nociceptor subtypes at the molecular level as they are differentially expressed in somatosensory neurons. TRP channels are non-selective cation channels which, in mammals, can be classified into 6 subfamilies; TRPC (Canonical), TRPV (Vanilloid), TRPM (Melastatin), TRPP (Polycystin), TRPML (Mucolipin) and TRPA (Ankyrin) [12]. Primary afferent nociceptors have been shown to express TRPV1, TRPV2, TRPV3, TRPV4, TRPM8 and TRPA1; sensory transducers for thermal, chemical and mechanical stimuli [13]. All these TRP channels are thermos-sensitive with different activation temperature thresholds; TRPV1 is activated at temperatures ≥ 42 °C, TRPV2 at temperatures ≥ 52 °C, TRPV3 at temperatures ≥ 33 °C, TRPV4 at temperatures ~27-34 °C, TRPA1 at temperatures ≤ 17 °C and TRPM8 at temperatures ≤ 25 °C [3, 14]. Furthermore, these ion channels are activated by chemicals which can be found in natural products; capsaicin (chilli peppers), mustard oil and menthol (mint leaves) activate TRPV1, TRPA1 and TRPM8 respectively [13, 15]. TRPA1 is activated by garlic/onion [15].

TRPV1 is extensively explored as nociceptive DRG neurons are found to have high levels of TRPV1 [16]. During development, a wide range of DRG neurons transiently

express TRPV1. However, its expression gradually becomes restricted to the peptidergic subset of sensory neurons following downregulation in non-peptidergic neurons [17]. A subset of TRPV1-expressing nociceptive sensory neurons also express TRPA1 [15, 18]. TRPM8, on the other hand, is not co-expressed with TRPA1 and TRPV1 [18, 19].

As mentioned, DRG neurons are pseudo-unipolar in nature. They have a single axon which bifurcates, sending axonal projections to innervate both the spinal cord (central) and the target organ (peripheral). These primary afferent axons terminate in the dorsal horn of the spinal cord [20], which is divided into a series of parallel laminae (I-V) [21, 22]. Laminae I and II are located in the superficial dorsal horn while laminea III-V are located deeper. Laminae termination pattern varies for the different nociceptor subtypes [22, 23] (see Figure 1.3). Peptidergic C-fibres mainly terminate within lamina I and outer lamina II (II_o) whereas non-peptidergic C-fibres mainly terminate within inner lamina II (II_i). Aβ-fibres, which are large but low-threshold, terminate within laminae III-IV whereas Aδ-fibres, which are large but high-threshold, terminate

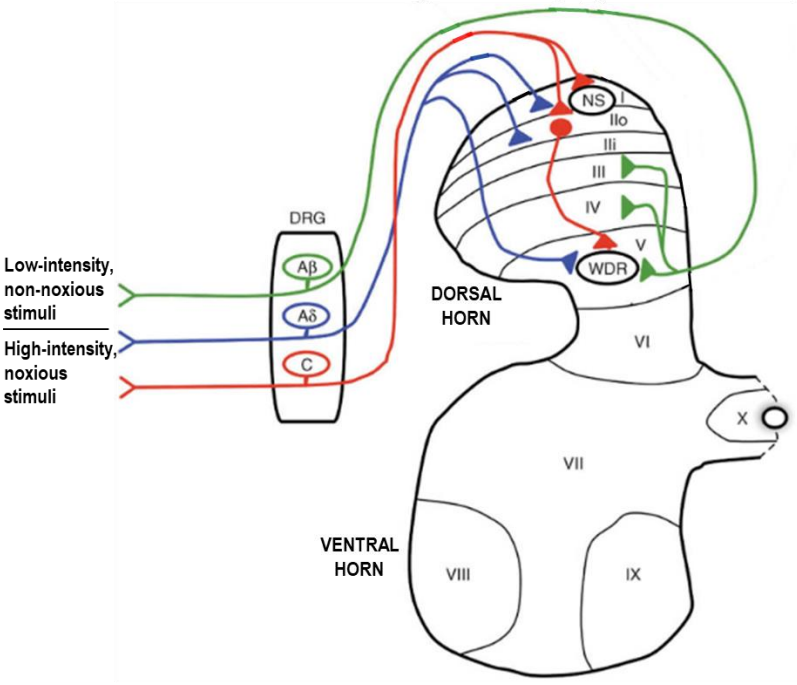

Figure 1.3 Connections between primary afferent fibres and the spinal cord. Primary afferent fibres (Aβ in green, Aδ in blue and C in red) terminate in the dorsal horn of the spinal cord, which is divided into a series of parallel laminae (I-V). Nociceptive specific (NS) cells are mainly located in the superficial dorsal horn (laminae I–II), whereas most wide dynamic ranges (WDRs) are found deeper (lamina V). Diagram adapted and modified from (22).

mainly within lamina I. Lamina V receives direct inputs from Aβ-fibres and Aδ-fibres and indirect input from C-fibres.

Nociceptors, also referred to as first-order sensory neurons, detect noxious stimuli from the periphery and transmit this sensory information to the dorsal horn in the form of an action potential. Excitatory neurotransmitters, primarily glutamate, are released from these first-order sensory neurons and activate second-order neurons. They transmit the noxious signal up the spinal cord and into the brain to the thalamus. Third-order neurons, which reside in the thalamus, then pass the signals to the relevant somatosensory cortex area of the brain where it is perceived as pain [9, 24]. This route of signal transmission is the ascending pathway (see Figure 1.4). A descending pathway forms a feedback loop which either facilitates or inhibits pain transmission via the release of excitatory (glutamate) or inhibitory (γ-aminobutyric acid (GABA) and/or glycine) neurotransmitters respectively [25].

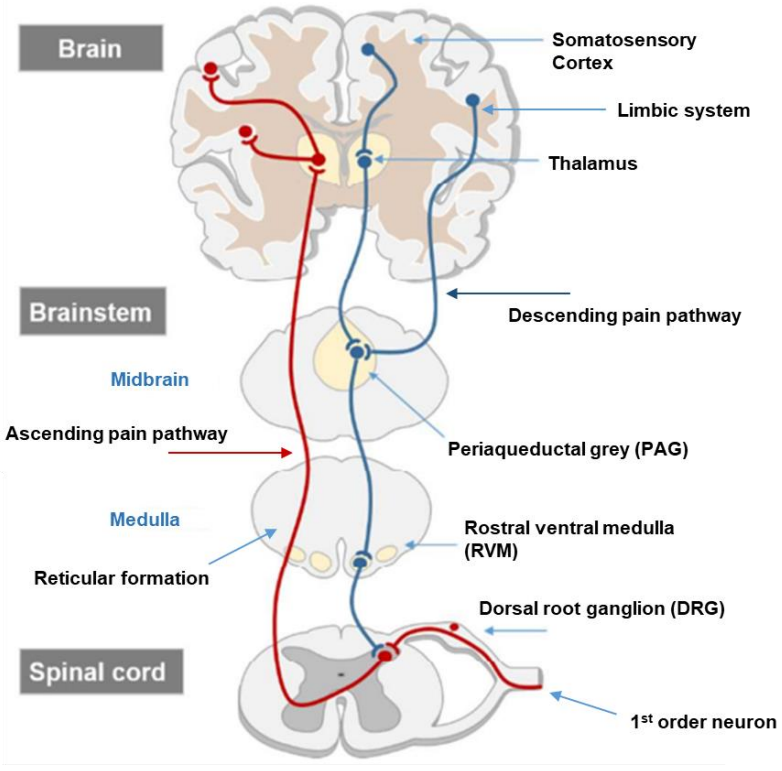

Figure 1.4 The nociceptive pathway. Signal transmissions are conducted via two routes, an ascending pathway (red) and a descending pathway (blue). The ascending pathway carries sensory information up the spinal cord to the brain where it is processed as pain. The descending pathway goes from the brain, down the spinal cord to the dorsal horn. This forms a feedback loop which either facilitates or inhibits pain transmission. Diagram adapted and modified from (25).

1.2.2 Nociceptor development

Nociceptors are primary somatosensory neurons that develop from neural crest stem cells that migrate out of the neural tube, producing cells of the DRG [26]. Using mice, it has been discovered that neurogenesis of sensory neurons occur in two successive waves; the first wave occurs between embryonic day (E) 9.5 and E11.5 and generates large-diameter tropomyosin receptor kinase (Trk) C^+ and $TrkB^+$ neurons and the second wave occurs between E10.5 and E13.5 and generates small-diameter $TrkA^+$ neurons [27, 28]. Neurotrophic factors act through these Trk receptors [29]. TrkA is primarily the receptor for nerve growth factor (NGF), TrkB for brain-derived neurotrophic factor (BDNF) and neurotrophin-4/5 (NT4/5), and TrkC for neurotrophin-3 (NT3). The first wave, driven by neurogenin2 (NGN2), produces mechanoreceptive and proprioceptive neuronal subtypes whereas the second wave, driven by neurogenin1 (NGN1), produces predominantly nociceptive neurons [27]. These two waves have also been identified in the development of chick DRG [30–32]. Although such tracing studies have not been performed in human DRGs, Blanchard et al., demonstrated similar roles of NGN1 and NGN2 in the subtyping of neurons [33]. Human embryonic and mouse fibroblasts were selectively reprogrammed into DRG sensory neurons following ectopic expression of NGN1 or NGN2 (co-expressed with the transcription factor Brn3A). These induced sensory neurons acquired key properties of the three sensory neuronal subtypes and exhibited selective expression of Trk receptors. A later study in mice [34] revealed a third wave which arises significantly later, after E11.5, and comes from the boundary cap (BC), a cellular structure located at the entry and exit points of peripheral nerve roots. These BC-derived cells migrate along the nerve roots and into the DRG, generating mainly small-diameter $TrkA^+$ nociceptive neurons, as well as satellite cells. Hence, DRGs can be described as the cell body of sensory neurons which are surrounded by a layer of satellite glial cells.[2].

DRG neurons are divided into distinct neuronal subpopulations based on their expression of the runt related transcription factors RUNX1 and RUNX3 [35]. RUNX3 expression has been shown to be confined to $TrkC^+$ proprioceptive DRG neurons but not $TrkB^+$ DRG neurons [35, 36]. On the other hand, RUNX1 expression is restricted to $TrkA^+$ nociceptors [35, 37]. Initially, all embryonic nociceptors express TrkA [38]. These nociceptive neurons express the neuropeptides calcitonin gene-related peptide

(CGRP) and substance P (SP) [39]. Postnatally, during the 3 weeks after birth in mice, TrkA expression is lost in approximately half of all nociceptors as there is a switch from expressing TrkA to expressing Ret [39, 40]. This gives rise to two subpopulations; $TrkA^+$ peptidergic neurons that express the neuropeptides CGRP and substance P, and $TrkA^-$ non-peptidergic neurons that bind to isolectin B4 (IB4). RUNX1 appears to play a role in this subdivision [35, 37]. Kramer et al. [35] demonstrated that subsequent to ectopic expression of RUNX1 in $TrkA^+$ DRG neurons, there was repressed expression of CGRP. Additionally, Chen et al. [37] revealed that persistent RUNX1 expression is responsible for transition from $TrkA^+$ to Ret^+ nociceptors as lumbar DRG from postnatal day (P) 60 $RUNX1^{-/-}$ mice displayed an increase in the percentage of $TrkA^+$ neurons and a decrease in the percentage of Ret^+ neurons compared to controls. RUNX1 appears to suppress TrkA expression and promote Ret expression. Hence, in $TrkA^+$ DRG neurons, maintained expression of RUNX1 drives a non-peptidergic phenotype ($TrkA^-$) whereas downregulation of RUNX1 expression drives a peptidergic phenotype ($TrkA^+$). Kramer et al. [35] also showed that in addition to not being expressed in $TrkB^+$ DRG neurons, RUNX3 is also not expressed in Ret^+ DRG neurons.

1.2.3 TrkA signalling pathway

TrkA, a transmembrane protein belonging to the Trk receptor family, is encoded by the *NTRK1* gene and located on chromosome 1q21-q22 [41]. Other members of the family include TrkB and TrkC which are encoded by the *NTRK2* and *NTRK3* genes respectively. TrkA consists of an extracellular domain, a transmembrane domain and a juxtamembrane intracellular region that contains the tyrosine kinase domain [42, 43]. The extracellular domain (ligand-binding domain) consists of a cysteine-rich cluster (Trk-d2 or C1), a leucine-rich domain (Trk-d1 or LRR1-3), another cysteine-rich cluster (Trk-d3 or C2) and two immunoglobulin-like domains (Trk-d4 and Trk-d5; also referred to as Ig1 and Ig2). Critical tyrosine residues are located within the tyrosine kinase domain; three within the activation loop (Y670, Y674 and Y675) and two on either side of the tyrosine kinase domain (Y490 and Y785). A structure of the TrkA receptor is illustrated in Figure 1.5. These five tyrosine residues have been identified as auto-phosphorylation sites [44–46]. Phosphorylation of Y490 is required for the binding of Shc and FRS-2 and for activation of the mitogen-activated protein

kinase (MAPK) and phosphatidylinositol 3-kinase (PI3K) signalling pathways. Phosphorylation of Y785 is required for the binding of phospholipase Cγ1 (PLCγ1), which activates protein kinase C (PKC) signalling and can also influence synaptic plasticity as it promotes Ca^{2+} mobilization. Phosphorylation of the other three tyrosine residues, Y670, Y674 and Y675, is associated with Trk activation and enhances kinase activity.

TrkA is regarded as the high affinity receptor for NGF [47–49]. NGF binds to the extracellular domain in the Trk-d5 (Ig2) domain of the Trk receptor [50]. The binding of NGF to TrkA results in its activation via homodimerization and subsequent auto-phosphorylation [47, 51]. The NGF-bound TrkA receptors are then internalized. The activation of TrkA triggers intracellular signalling and subsequent activation of multiple signalling pathways including PLCγ1-PKC, MAPK (also known as Ras-MEK-ERK) and PI3K-Akt, which have been shown to promote the growth, survival, differentiation and synaptic plasticity of neurons [52, 53]. The various signalling pathways are illustrated in Figure 1.6.

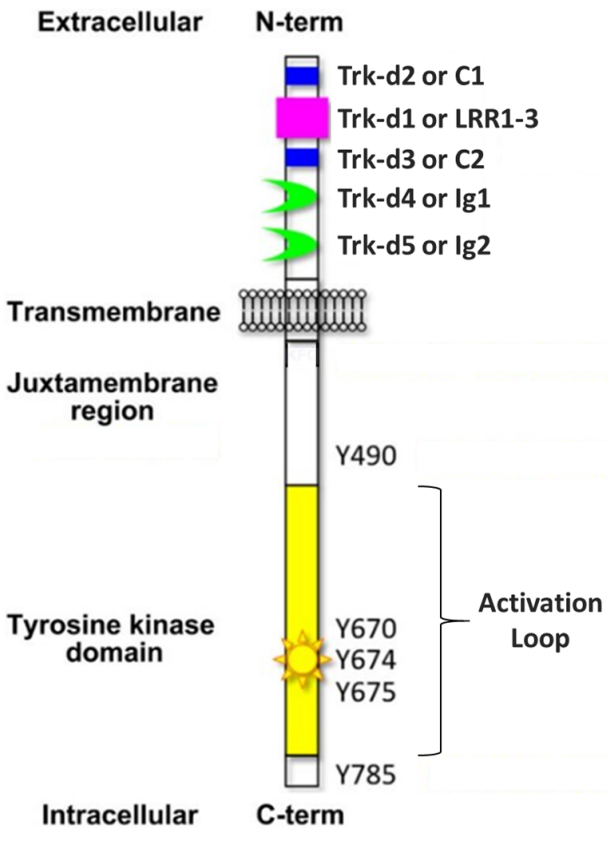

Figure 1.5 Diagram of the TrkA receptor. TrkA consists of an extracellular domain, a transmembrane domain and a juxtamembrane intracellular region which contains the tyrosine kinase domain. The extracellular domain (ligand-binding domain) consists of a cysteine-rich cluster (Trk-d2 or C1) followed by a leucine-rich domain (Trk-d1 or LRR1-3) then another cysteine-rich cluster (Trk-d3 or C2) and two immunoglobulin-like domains (Trk-d4 and Trk-d5; also referred to as Ig1 and Ig2). Critical tyrosine residues are located within the tyrosine kinase domain; three within the activation loop (Y670, Y674 and Y675) and two on either side of the tyrosine kinase domain (Y490 and Y785). These five tyrosine residues have been identified as auto-phosphorylation sites. Diagram adapted and modified from (43).

It has also been shown that TrkA can be activated in the absence of NGF, through the G-protein-coupled receptor (GPCR) ligands adenosine and pituitary adenylate cyclase-activating polypeptide (PACAP) [54–56]. Using PC12 cells, both ligands were capable of activating TrkA receptor in the absence of NGF, although this was prolonged compared to NGF activation. Similar to NGF activation, the use a TrkA inhibitor, K252a, inhibited this increased activation. Furthermore, both adenosine and PACAP induced activation of AKT (protein kinase B) and resulted in increased cell survival subsequent to the withdrawal of NGF. In addition, TrkA receptors can be auto-phosphorylated by endogenous protein kinases. This phosphorylated state can also be prolonged through either upregulation of theses kinases or downregulation of TrkA phosphatases.

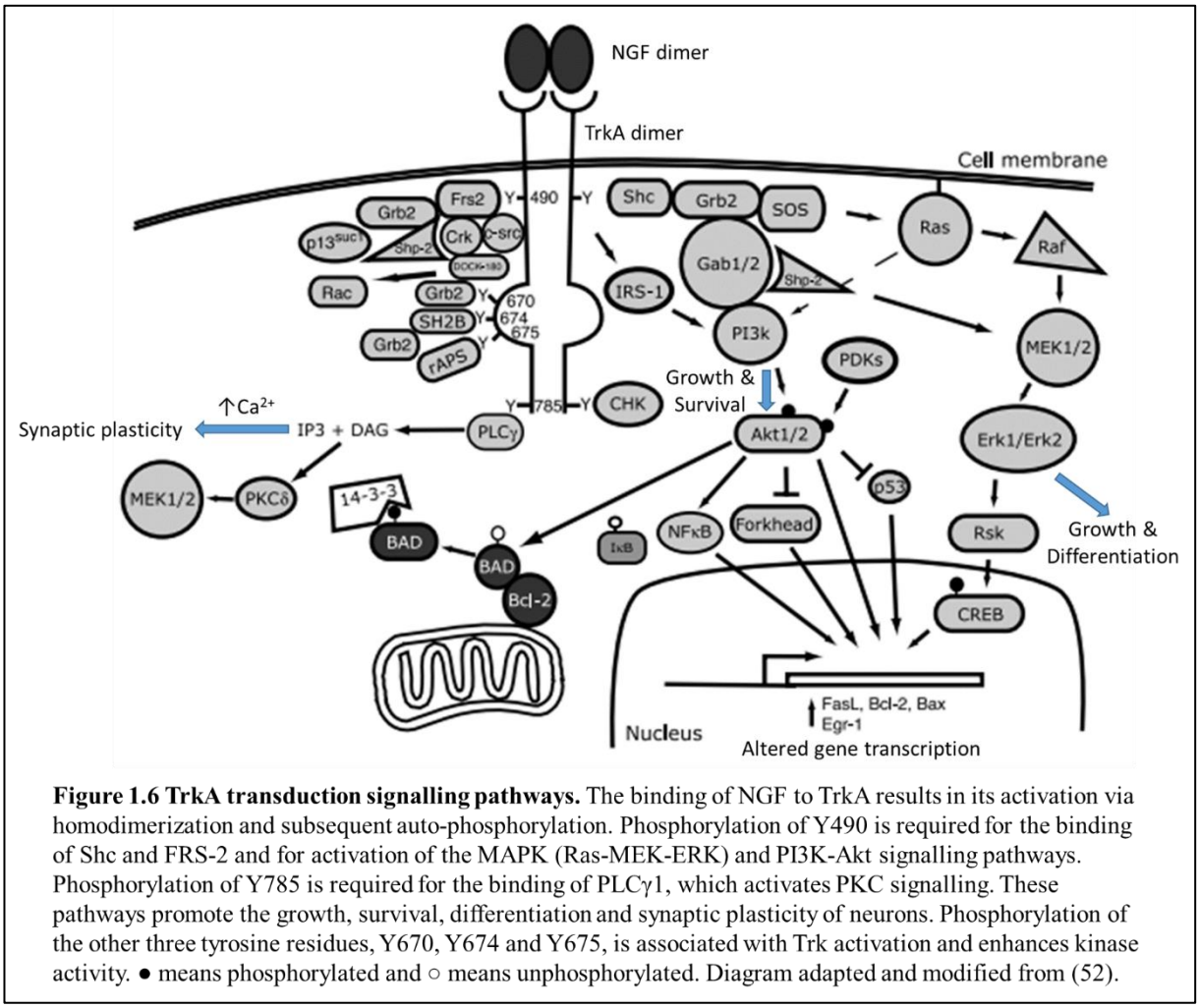

Figure 1.6 TrkA transduction signalling pathways. The binding of NGF to TrkA results in its activation via homodimerization and subsequent auto-phosphorylation. Phosphorylation of Y490 is required for the binding of Shc and FRS-2 and for activation of the MAPK (Ras-MEK-ERK) and PI3K-Akt signalling pathways. Phosphorylation of Y785 is required for the binding of PLCγ1, which activates PKC signalling. These pathways promote the growth, survival, differentiation and synaptic plasticity of neurons. Phosphorylation of the other three tyrosine residues, Y670, Y674 and Y675, is associated with Trk activation and enhances kinase activity. ● means phosphorylated and ○ means unphosphorylated. Diagram adapted and modified from (52).

Activation of TrkA signalling pathway has proven vital to the sensitization of nociceptors [57], growth of sensory neurons [58] and onset of pain and chronic pain states [59, 60]. It was discovered that unrelated patients suffering from congenital insensitivity to pain with anhidrosis (CIPA), which is characterized by the inability to respond to noxious stimuli (insensitivity to pain) [61], all possessed a mutation (deletion mutation, splice mutation, missense mutation) in the tyrosine kinase domain of the TrkA receptor [62]. Additionally, patients suffering from osteoarthritis, which is characterized by pain and stiffness in the joints [63], displayed increased levels of NGF and TrkA in their chondrocytes (specialized cells found in cartilage tissue) compared to those isolated from normal individuals [64]. Moreover, inhibiting TrkA reduced pain in various rat models of arthritis [60] and osteoarthritis [59].

1.3 Neuropathic pain and nociceptor sensitization

Neuropathic pain is pain that arises from a lesion or disease of the somatosensory nervous system. Disease of the somatosensory system such as diabetes, Parkinson's disease, Alzheimer's disease, multiple sclerosis, shingles, neuralgia and HIV infection or AIDS can all result in neuropathic pain. This type of pain is usually chronic as it tends to persist. In the UK, chronic pain affects almost 28 million adults [65]. Symptoms commonly described by patients include spontaneous pain, hyperalgesia, allodynia, dysesthesia (an unpleasant, abnormal sensation) and paresthesia (tingling or numbness). Spontaneous pain is pain that occurs without stimulation and takes the form of a shooting, burning or stabbing pain. Hyperalgesia describes an exaggerated pain response to a normal noxious stimulus whereas allodynia describes a pain response to an innocuous (non-noxious) stimulus [66]. This can be further defined as primary hyperalgesia, when increased perception of pain occurs at the site of injury or area exposed to the noxious stimulus, and secondary hyperalgesia, when increased perception of pain occurs in the surrounding uninjured area. In addition to pain, patients have also reported experiencing anxiety and depression, fatigue and sleep disturbances. Rodent models subjected to nerve injury have displayed behavioural hypersensitivity to both mechanical and thermal stimuli, evidenced by a decrease in their withdrawal threshold and withdrawal latency, respectively [67–72]. A graphical representation of the difference between hyperalgesia and allodynia can be seen in Figure 1.7.

These behavioural changes are a consequence of hypersensitivity in the sensory nervous system and is in part associated with peripheral nociceptor sensitization. Sensitization is the process whereby primary afferent nociceptors have a heightened response to stimulation depicted as a nociceptor having a reduced activation threshold and/or enhanced response to stimulation due to increased sensitivity. This heightened response can initiate at the peripheral and/or central level. Primary hyperalgesia is predominantly due to peripheral nociceptor sensitization [73] whereas secondary hyperalgesia is mediated by central nociceptor sensitization [73, 74].

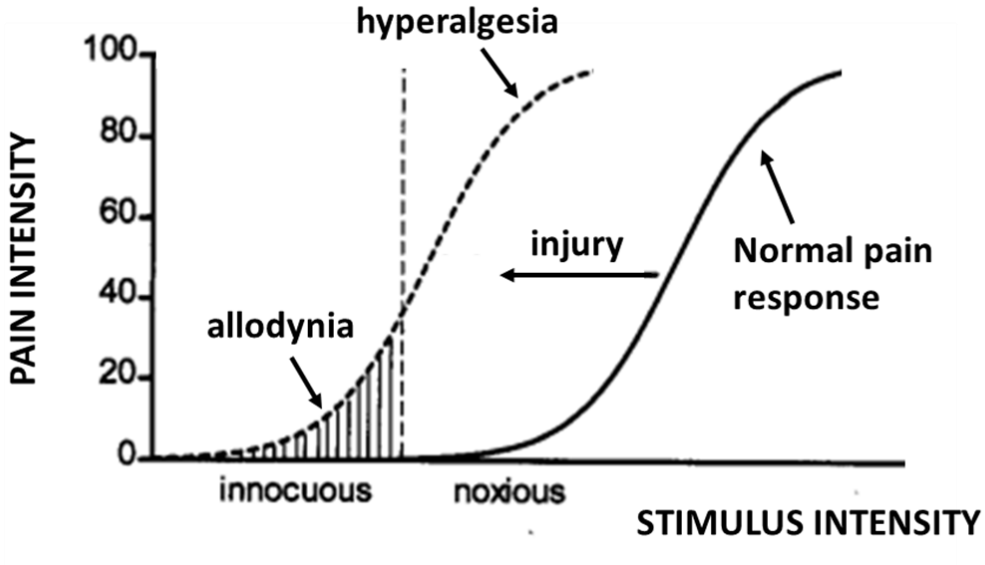

Figure 1.7 Difference between hyperalgesia and allodynia. A normal pain response is shown as a solid line. Following an injury, the individual experiences increased sensitivity to pain, shown as a dashed line. This can be described as an exaggerated pain response to a normal noxious stimulus (hyperalgesia) or a pain response to an innocuous (non-noxious) stimulus (allodynia). Diagram adapted and modified from (66).

Upon nerve damage, nociceptors become activated, releasing the primary neurotransmitter, glutamate as well as the neuropeptides CGRP and SP. Additionally, a nerve trauma, such as a nerve injury, induces local inflammation leading to the release of inflammatory mediators including bradykinin, adenosine triphosphate (ATP), serotonin, NGF and protons [7, 24, 75–77]. This results in an "inflammatory soup" consisting of a wide array of signalling molecules. These signalling molecules

bind to nociceptors, which express one or more cell-surface receptors (TRP channels, G protein-coupled receptors, tyrosine kinases) on the peripheral nociceptor terminal. In addition, this damage can increase in the concentration of protons (e.g. due to mitochondrial mishandling) which in turn increases the acidity of the environment and activates TRPV1, accounting for enhanced activation of this channel following nerve injury. Binding of these signalling molecules to the receptors on the peripheral nociceptor terminals influences ion channels in close proximity, increasing the influx of Ca^{2+} and depolarizing the membranes, which in turn induces activation of mitogen and protein kinases [78]. Subsequent phosphorylation of terminal receptors and channels, such as TRPV1, increases excitability of the nociceptors through reducing the threshold at which these ion channels open and/or prolonging opening times. As a result, this causes nociceptor sensitization and is referred to as peripheral sensitization. Sensitization of these primary afferent nociceptors increases the frequency at which action potentials are generated. This state of hyper-excitability results in a stronger synaptic input being received by the dorsal horn of spinal cord, thereby enhancing pain sensation. Activation of these kinases can also lead to activation of various signalling pathways to activate neuron function, for example TrkA receptor activation leading to nerve fibre growth (as discussed in section 1.2.3). Tissue damage also induces an inflammatory response, initiated by surrounding and infiltrating non-neural cells including macrophages, mast cells, neutrophils and endothelial cells [9]. These inflammatory cells release inflammatory mediators, such as tumour necrosis factor α (TNF-α), interleukin-1β (IL-1β) and IL-6, contributing to the "inflammatory soup" and providing an additional source for nociceptor activation and subsequent sensitization.

Similarly, this state of hyper-excitability can be established in the CNS. When it does, it enhances nociceptive processing, leading to central sensitization [79]. There is a decrease in the activation threshold for pain stimuli in central second-order neurons within the dorsal horn of the spinal cord, causing increased responsiveness to normal and/or subthreshold inputs from primary afferents [80]. A number of mechanisms can cause enhanced synaptic transfer in the CNS, leading to the development of central sensitization, including glutamate/N-methyl-d-aspartate (NMDA) receptor-mediated sensitization, disinhibition and microglial activation [9]. During normal nociceptive transmission, primary afferent neurons release neuropeptides (CGRP, SP) and the

neurotransmitter, glutamate, as a means of transmitting peripheral sensory information to the spinal cord and brain. Glutamate is a major excitatory neurotransmitter in the nervous system in vertebrates and is present in high concentrations in the DRG and spinal cord [81]. The glutamate receptor, (NMDA), is normally blocked by magnesium ions (Mg^{2+}) causing them to be silent [82]. Sustained release of glutamate and these neuropeptides is sufficient to depolarize the membrane, removing Mg^{2+} from the NMDA receptor pore and activating the receptor. The consequence of this is increased Ca^{2+} influx into the central neurons, enhanced synaptic activity and hyper-excitability, leading to pain hypersensitivity.

Disinhibition is a decreases in inhibitory transmission [83]. The inhibitory neurotransmitters, γ-aminobutyric acid (GABA) and/or glycine are continuously released by inhibitory interneurons, under normal conditions, decreasing the excitability of output neurons of lamina I and thus protecting against over-excitation of neural excitatory circuits [84]. Upon injury, these inhibitory mechanisms can be lost, enhancing depolarization and excitation of central neurons [83, 85]. Additionally, peripheral nerve injury triggers the release of ATP, which activates microglia via its $P2X_4$ receptor, causing the release of BDNF [86, 87]. BDNF has been shown to disrupt anion balance and promote hyper-excitability through its interaction with TrkB in lamina I neurons, leading to the development of central sensitization and behavioural hypersensitivity [86–89]. The cytokines and chemokines released by activated microglia can also modulate excitatory and inhibitory transmission across synapses, contributing to central sensitization [90].

In some instances, a phenomenon known as contralateral sensitization may occur whereby a unilateral lesion or injury results in a bilateral effect. For example, peripheral nerve injury in one limb can result in hypersensitivity in both the injured and uninjured limb. This has been observed in clinical patients suffering from unilateral osteoarthritis pain [91], unilateral postherpetic neuralgia [92] and complex regional pain syndrome (CRPS) [93] as well as in rodent models of monoarthritis [94, 95] and inflammation [96, 97].

1.3.1 Neonatal nerve injury versus adult nerve injury

It has been discovered that the age that peripheral nerve damage occurs impacts upon somatosensory processing and pain development [98, 99]. Animal studies have revealed that unlike adults, peripheral nerve damage early in life (neonates and infants) does not elicit neuropathic pain immediately, however, pain hypersensitivity emerges later in life [70, 100–102]. Spared nerve injury (SNI) in rat pups aged 3, 10 and 21 days did not exhibit mechanical allodynia at any time-point up to 28 days post-surgery [70, 102]. In contrast, SNI in adult rats aged, P33 and older, resulted in persistent mechanical hypersensitivity from 7 days post-surgery, with a decrease in withdrawal threshold compared to the controls. Similar observations were made following chronic constriction injury (CCI); surgery at P10 did not elicit a decrease in withdrawal threshold at any time-point up to 28 days post-surgery. However, CCI in adult rats resulted in persistent mechanical hypersensitivity from 7 days post-surgery, with a decrease in withdrawal threshold by at least 45 % compared to contralateral controls. In longer term studies [100, 101], SNI at P10, in both rats and mice, also did not cause mechanical hypersensitivity for the first 2-3 weeks post-surgery. However, at P31, 21 days post-surgery, significant mechanical hypersensitivity developed and persisted until the end of the study at P54 [100]. This delayed onset of mechanical hypersensitivity following nerve injury (SNI) at P10 was not only observed in rats but mice [101]. Both adult (P33) mice and rats displayed significant mechanical hypersensitivity at 4 days and 7 days post-surgery, respectively. However, SNI at P10 did not elicit mechanical hypersensitivity until P31 and P35 for mice and rats, respectively. In both studies, though, there was no impact on heat sensitivity. See Table 1.1 for a summary of these animal models.

Clinical experiences have also revealed that early-life injury has long-term consequences on somatosensory processing and pain perception [103, 104]. Flexor reflex threshold testing, which is used to measure sensation, was performed on premature infants following local tissue damage. There was a decrease in mean flexor reflex threshold to half of that of the contralateral side, indicative of hypersensitivity [103]. Similarly, repeated stimulation in infants aged 27.5-35 gestational weeks exhibited a significant decrease in mean withdrawal threshold compared to baseline [104]. It appears that early life experience of procedural pain alters sensory function

in neonates, such that later in life they present with hypersensitivity at the affected area but acute pain may also induce global hyposensitivity [99].

Table 1.1 Animal models demonstrating neonatal vs adult nerve injury

Species	Type of Injury	Age of Injury	Pain-like Behaviour	Reference
Sprague-Dawley rats	Spared nerve injury (SNI)	P3, P10 and P21	No mechanical allodynia at any time-point up to 28 days post-surgery	Howard et al. 2005 [70]
		P33	Persistent mechanical hypersensitivity from 7 days post-surgery	
		P60	Persistent mechanical hypersensitivity from 1 day post-surgery	
Sprague-Dawley rats	Chronic constriction injury (CCI)	P10	No mechanical hypersensitivity at any time-point up to 28 days post-surgery	
		Adult	Mechanical allodynia from 7 days post-surgery	
Sprague-Dawley rats	Spared nerve injury (SNI)	P3, P10 and P21	No mechanical hypersensitivity at 7 days post-surgery	Costigan et al., 2009 [102]
		P33 and Adult	Mechanical hypersensitivity at 7 days post-surgery	
Sprague-Dawley rats	Spared nerve injury (SNI)	P10	Persistent mechanical hypersensitivity from 3 weeks post-surgery	Vega-Avelaira et al., 2012 [100]
Sprague-Dawley rats	Spared nerve injury (SNI)	P10	Mechanical hypersensitivity from 4 weeks post-surgery	McKelvey et al., 2015 [101]
		P33	Persistent mechanical hypersensitivity from 1 week post-surgery	
CD1 mice	Spared nerve injury (SNI)	P10	Mechanical hypersensitivity onset at 3 weeks post-surgery	
		P33	Mechanical hypersensitivity from 4 days post-surgery	

Activation of inflammatory signalling pathways and neuroplasticity have both been attributed to the development of pain hypersensitivity. Numerous studies have shown that unlike adult nerve injury (SNI) which is accompanied by microglia activation 7 days post-surgery [100–102, 105, 106], subsequent to neonatal nerve injury, there is no or very low detection of activated microglia at 7 days post-surgery. However, two of those studies that investigated long-term effects of early nerve injury demonstrated

that the delayed onset of hypersensitivity experienced 21 days post-surgery was accompanied by increased microglia activation [100, 101]. IBA-1 was used as the microglia marker in all studies but one, which used CD68 [102]. Activated microglia release proinflammatory cytokines, which is believed to be responsible for this delayed onset of chronic pain in adulthood subsequent to infant nerve injury. Moss et al. [105] illustrated microglia activation and mechanical allodynia in P10 rats subsequent to intrathecal injection of lipopolysaccharide (LPS). In another comparison study between infant (P10) and adult (P33) rodents [101], infant rodents which experienced nerve injury displayed no behavioural pain hypersensitivity until P38 for rats and P31 for mice. On the other hand, rapid decrease in mechanical threshold was observed in adult rodents within seven days following nerve injury. A closer look at the inflammatory response illustrated an initial anti-inflammatory immune response in the dorsal horn following infant nerve injury, which switches to a proinflammatory response upon reaching adolescence. In contrast, nerve injury in adult rodents initiated a proinflammatory response. Furthermore, it was discovered that following early life nerve injury, neuropathic pain is not absent but only suppressed, as blocking anti-inflammatory activity in the dorsal horn of infant rats caused significant decrease in withdrawal threshold following nerve injury.

However, it does not appear that the absence of activated microglia is the issue but immaturity of immune response signalling following peripheral nerve injury as Moss et al. [105] revealed that intrathecal injection of cultured ATP-stimulated microglia did not result in tactile allodynia in P10 rats. However, injections performed at P16 and P21 caused allodynia, with injections at P21 producing a similar response to that seen in adults. Furthermore, a study performed by Hathway et al. [107] illustrated this difference in neural signalling. Brief stimulation of rat peripheral C-fibres at low frequency evoked long-lasting mechanical hypersensitivity and induced microglia activation in the dorsal horn of adult rats but failed to cause hypersensitivity and activate microglia in neonatal rats.

Another difference observed between neonatal and adult nerve injury is the trigger of collateral sprouting, whereby intact axons grow into denervated regions [108–112]. Neonatal nerve injury (from birth to P7) resulted in the sprouting of adjacent intact primary afferent terminals into the denervated regions within the dorsal horn, leading to abnormal distributions during development when compared to adults. It was shown

that sprouting involved both A-fibres and C-fibres [109, 110]. This declined progressively with the age that the nerve injury occurred [109, 113]. Animals wounded at P0 or P7 displayed prolonged sprouting, which lasted for several weeks after wound healing, as well as long-lasting hypersensitivity and reduced mechanical thresholds [109]. On the other hand, animals wounded at P14 and P21 displayed a weak sprouting response, similar to that observed in wounded adults. A study illustrated that peripheral injury in neonates resulted in much faster and more extensive neuron loss compared to older animals [114]. Studies have demonstrated that these new sprouted terminals innervate inappropriate central regions, forming new functional connections with neurons in the dorsal horn [108, 110–112], thereby possibly contributing to the persistent hypersensitivity observed in adults who have experienced neonatal nerve injury. Studies have revealed that subsequent to peripheral nerve injury, low-threshold non-nociceptive Aβ-fibres (which normally reside in laminae III-V) sprouted into laminae I and II, forming new connections with nociceptive neurons [115–117]. Such event modified sensory processing, leading to the development of pain from innocuous stimuli. However, it appears that only if the injury occurs within the first postnatal week that this central sprouting is observed [113].

Due to the plasticity of the immature nervous system during the neonatal period, nerve damage early in life can disrupt the normal development of nociceptive pathways, resulting in prolonged changes in structure and function, altering pain processing, which can last into adulthood [99, 118, 119]. These changes include central sensitization, neuroimmune priming and collateral sprouting, all of which can lead to enhanced sensitivity to pain.

1.4 Chemotherapy-induced peripheral neuropathy (CIPN)

It has been reported by the World Health Organization that trachea, bronchus and lung cancers are one of the top 10 leading causes of death worldwide in 2019, with the number of deaths rising from 1.2 million in 2000 to 1.8 million in 2019 [120]. According to Cancer Research UK, every year in the UK there are around 375,000 new cancer cases and more than 166,000 cancer deaths (2016-2018) [121]. Macmillan Cancer Support estimated that in 2020 there are 3 million people living with cancer in the UK and it is predicted that this number will rise to nearly 3.5 million by 2025, 4

million by 2030 and 5.3 million by 2040 [122]. Cancer survival is improving and has doubled in the last 40 years in the UK [121]. In the early 1970s the median survival time after a cancer diagnosis was one year, by 2007 it was six years [123] and by 2011 it was ten years [124]. This is because of the development of improved treatments and diagnostics. Current and new treatments include radiotherapy, surgical intervention, immunotherapy, cryotherapy and chemical intervention such as chemotherapy. Unfortunately, despite increasing life expectancy, patients suffer from increasingly apparent quality of life issues arising from the disease and/or treatment [125–128].

Chemotherapy is a form of chemical drug therapy used for the treatment of cancer. These drugs are cytotoxic to rapidly dividing cells. However, there is no distinction between cancer cells and healthy somatic cells. As a result, healthy cells in the body also become damaged during treatment. The main areas of the body that may be affected by chemotherapy include the bone marrow, hair follicles and the digestive system [129, 130]. The number of cells produced by the bone marrow can be reduced due to chemotherapy. These include white blood cells, red blood cells and platelets. A reduction in white blood cells results in neutropenia, making the individual more vulnerable to infections. Reduced number of red blood cells leads to anaemia and a reduction in the number of platelets causes increased bleeding and bruising. Additionally, individuals exhibit hair loss due to damaged hair follicles as well as nausea, vomiting, constipation, diarrhoea and appetite changes which arise from damage to the digestive system.

Chemotherapy drugs are also known to affect nerve fibres, damaging the peripheral nervous system (PNS) resulting in a condition referred to as chemotherapy-induced peripheral neuropathy (CIPN). Commonly used chemotherapeutic agents that give rise to CIPN include platinum based drug (cisplatin and oxaliplatin), taxanes (paclitaxel), proteasome inhibitors (Bortezomib) and vinca alkaloids (vincristine) [131–134]. The platinum based drugs have shown a high incidence of sensory neuropathy (70-100 %) [135–137], cisplatin being most neurotoxic compared to oxaliplatin and carboplatin [138–141]. Taxanes also have a high neuropathy incidence (11-87 %) [135]. Peripheral neuropathy can be classified into three categories; sensory, motor and autonomic. Sensory neuropathy refers to damage to the sensory nerves (e.g. touch, temperature and pain). Common symptoms of sensory neuropathy include numbness, tingling in the hands and feet and chronic pain [132, 142, 143].

Motor neuropathy occurs when the motor nerves, which are responsible for controlling the movement of all muscles under conscious control (e.g. walking, talking and grasping), are damaged. Motor effects such as muscle cramps and distal weakness have been experience following treatment with vincristine [132, 133, 143, 144], oxaliplatin [133, 145], and taxanes [132, 143, 146]. Autonomic neuropathy refers to damage to autonomic nerves, which are responsible for regulating functions of the body that people do not control consciously (e.g. breathing, heartbeat and bladder function). Autonomic neuropathy has been rarely observed amount most chemotherapy agents, mainly vincristine, which has been reported to result in constipation, orthostatic hypotension and urinary retention [131, 133, 147].

1.4.1 Aetiology and pathophysiology of CIPN

As mentioned above, a wide range of chemotherapy agents leads to the development of CIPN. However, the molecular targets and mechanisms of action vary between the different chemotherapy agents. One of the main cellular components that are affected by the platinum based drugs is the DRGs [148–151]. Cisplatin induces peripheral sensory neurotoxicity [138–141] by binding to the deoxyribonucleic acid (DNA) of DRGs and forming cisplatin-DNA adducts [143, 148, 152–155]. It has been shown that the formation of cisplatin-DNA cross-links structurally distorts the DNA [156] and unwinds it [157]. This in turn interferes with its normal functioning, including DNA replication and transcription, essential processes for neuronal survival and function, eventually resulting in neuronal apoptosis [134, 138, 158].

DRGs have increased susceptibility to cisplatin [136, 138, 159, 149, 160–164]. They are not protected by the blood-brain barrier because the vasculature within the DRGs are “leaky” due to the presence of an abundant fenestrated capillary network [165–167]. This increased permeability makes these tissues easily accessible to circulating compounds [148–151] and therefore allows pharmacological agents and drugs to accumulate in these tissues. Clinical studies [136, 161, 164] and preclinical rodent studies [159, 160, 163] have investigated tissue accumulation of the chemotherapeutic agent cisplatin, administered via intravenous, intracarotid or internal iliac artery injection for clinical patients or intraperitoneal injection for rodents. These studies highlight significant accumulation of cisplatin in DRGs and peripheral sensory nerves compared to other tissues following administration. Those same studies revealed that

tissues protected by the blood-brain-barrier, such as the brain and spinal cord, had the lowest accumulation of cisplatin. Therefore CIPN associated with cisplatin is characterized as a peripheral neuropathy that includes predominantly sensory neuropathy [131, 133, 148, 162, 168–170], as well as motor and autonomic neuropathies [133, 169, 171, 172].

It has also been suggested that other contributing factors of cisplatin-induced neurotoxicity include oxidative stress, mitochondrial dysfunction, changes in Ca^{2+} homeostasis and increased production of pro-inflammatory mediators [163, 173–175]. Cisplatin also binds to mitochondrial DNA (mDNA) in DRG neurons [150], forming cisplatin-mDNA adducts, impairing mitochondrial DNA replication and transcription and resulting in morphological changes in the mitochondria [150, 176] as well as alterations in protein synthesis and disruption of the electron transport chain [174, 177, 178]. Neuronal mitochondrial damage leads to cellular ATP depletion and increased production of reactive oxygen species (ROS), which in turn can cause oxidative DNA damage [150, 158, 179, 180]. All these events lead to mitochondrial membrane depolarization, increased intracellular Ca^{2+} levels and activation of apoptotic pathways [150, 176, 181, 182] alongside increased production of pro-inflammatory mediators [175], which further damages the mitochondria. In addition to peripheral neurotoxicity, cisplatin has also been reported to cause ototoxicity (hearing loss and tinnitus) and nephrotoxicity [183–185].

Unlike cisplatin, oxaliplatin induces two clinically distinct forms of peripheral neuropathy; acute and chronic [186]. Similar to cisplatin, the chronic oxaliplatin neuropathy results from morphologic and functional changes in the DRGs. On the other hand, acute neuropathy is induced by the chelating effect of the oxaliplatin metabolite, oxalate, on extracellular Ca^{2+}, which in turn increases Na^{+} conductance [187]. Oxalate also has a direct effect on voltage-gated Na^{+} channels, resulting in prolonged opening of the channels and increased axonal excitability [188, 189]. Both vincristine and paclitaxel target β-tubulin [134]. Vincristine inhibits microtubule formation, which in turn can lead to mitotic arrest and cell death [148, 190, 191]. In contrast, the mechanism behind paclitaxel-induced neuropathy involves microtubule stabilization; however, the resulting impact appears similar. Paclitaxel suppresses dynamic instability and depolymerisation of microtubules, preventing its disassembly and resulting in cell cycle arrest and ultimately apoptotic cell death [148, 192]. Both

vincristine and paclitaxel affect Ca^{2+} homeostasis [174, 193], through mitochondrial dysfunction, leading to abnormal neuronal excitability [142, 177, 194–196]. Additionally, vincristine and paclitaxel have shown to induce both oxidative stress and inflammation [180, 195, 197–200] as well as cause loss of intraepidermal nerve fibres, specifically Aδ and C fibres, leading to cold and heat allodynia [201]. Bortezomib, being a proteasome inhibitor, is believed to be associated with proteasome inhibition and microtubule stabilization, which in turn gives rise to tubulin dynamics alteration [202, 203]. It appears that Bortezomib interferes with microtubule and mitochondrial function, increasing microtubule polymerization and decreasing mitochondrial axonal transport and function in sensory neurons [204, 205]. Proteasome inhibition has shown to induce DNA damage and defective translation of messenger ribonucleic acids (mRNAs) in DRG neurons, important contributing factors to the sensory pathophysiology observed following Bortezomib treatment [206]. Furthermore, Bortezomib leads to an increase in reactive oxygen species in DRG neurons [180, 207, 208] as well as causes endoplasmic reticulum stress and eventually apoptosis [209]. Similar to other chemotherapeutic drugs, dysregulation of Ca^{2+} homeostasis [210] is also induced.

1.4.2 Clinical evaluation of CIPN

The evaluation of peripheral neuropathy involves performing a combination of differing measures. These include nerve conduction study of sensory and motor nerves (measures changes in conduction velocity), needle electromyography (measures electrical activity in response to a nerve's stimulation of the muscle) and current perception threshold (CPT) testing (selectively evaluates the larger myelinated Aβ fibres, the lightly myelinated Aδ fibres and the unmyelinated C fibres in sensory nerves through different frequencies of electrical stimulus), as well as deriving a neuropathy disability score (NDS) and a neuropathy symptom score (NSS) [211–214].

Patients suffering from CIPN tend to demonstrate a decrease in nerve conduction velocity due to nerve fibre degeneration, which can result in decreased length, decreased diameter and/or demyelination [215]. Needle electromyography is more commonly used to assess damage to the motor nerves, with measurements taken at rest and with contraction. The presence of abnormal activity, at rest, denotes active

denervation, and little or no response, when the muscle is contracted, is a possible indication of peripheral neuropathy [216]. Alternatively, CPT testing evaluates the function of sensory nerve fibres. The different sensory nerve fibres are stimulated at different frequencies; 2,000 Hz stimulates the larger myelinated Aβ fibres, 250 Hz stimulate the smaller lightly myelinated Aδ fibres, and 5 Hz stimulate the unmyelinated C fibres. A reduced CPT value is indicative of hypersensitivity whereas an elevated CPT value is indicative of hyposensitivity, signifying loss of nerve function [217]. In clinical patients, there appears to be a correlation between the changes in their CPT values and their degree of neurotoxicity [218]. NDS and NSS are utilized to assess neuropathy signs and symptoms, with a higher score signifying greater severity of neuropathy.

Furthermore, the functioning of autonomic nerves can be examined by performing autonomic function tests and the tilt-table test (measures and monitors heart rate and blood pressure under different conditions), urinalysis and bladder function tests and gastrointestinal tests [219, 220]. Clinical trials have used the European Organisation for Research and Treatment of Cancer Quality of Life Questionnaire for patients with chemotherapy-induced peripheral neuropathy (EORTC QLQ-CIPN20) to quantify symptoms and impairments of sensory, motor and autonomic neuropathy [221, 222] as well as the Rasch-built Overall Disability Scale for patients with chemotherapy-induced peripheral neuropathy (CIPN-R-ODS) to provide linear measurement of CIPN-related disability [223]. Findings have associated CIPN with a decrease in quality of life.

According to Seretny et al.[224], the incidence of CIPN was 68.1 % when measured within the first month following chemotherapy, 60.0 % after 3 months of chemotherapy and 30.0 % after 6 months or more. Chemotherapy-induced peripheral neuropathy is a dose-limiting effect [131, 143, 148], with symptoms typically developing within the first two months of treatment, progressing as chemotherapy continues and then alleviating once treatment is completed. However, cisplatin seems to be an exception. Vincristine-induced neuropathy is usually reversible when therapy is discontinued but it can occasionally be irreversible [225–228]. Symptoms of both bortezomib-induced neuropathy and taxane-induced neuropathy usually improve or resolve within months after treatment has ended [148, 225, 229]. With regards to paclitaxel peripheral neuropathy, it appears to persist longer in older patients and in

those who experience severe neuropathy [230]. In contrast, a "coasting" phenomenon is observed exclusively in platinum-based chemotherapy, particularly cisplatin, whereby neuropathic symptoms worsen for weeks or months following cessation of therapy [131, 143, 148]. Despite "coasting" being observed after oxaliplatin treatment, cumulative oxaliplatin-induced peripheral neuropathy has been reported to be partially reversible in approximately 80% of patients and completely resolved in approximately 40% within 6-8 months once treatment has ended [132]. The higher the dose of drug administered and the longer the duration of treatment, the greater the neurotoxicity. This has caused increasing clinical concerns regarding the reduction of treatment to a suboptimal level or even cessation of treatment [143, 231, 232].

1.4.3 CIPN in childhood cancer survivors

CIPN is a common side effect of cancer treatment in both adult [127, 233, 234] and paediatric [235–238] patients. However, symptoms experienced in paediatric patients persist into adulthood, with sensory and motor neuropathy, pain and functional impairments being observed in adults who survived children cancers [170, 237, 239, 240]. These individuals were compared with their siblings, who served as controls. Pain was reported by ~50 % of childhood cancer survivors [237, 240], which they attributed as an adverse side effect of their cancer treatment. Additionally, it was that the younger the age of exposure to chemotherapy, the greater the severity [237]. A diagnostic age of ≤3 years was associated with a higher risk of reporting pain conditions compared to a diagnostic age of 4-20 years.

Most instances of CIPN in survivors of childhood cancers have been associated with vincristine and the platinum-based agents as they are more routinely used in this population [241]. However, vincristine has shown to result in predominantly motor deficits in paediatric patients [242]. Furthermore, cisplatin-treated children have displayed more severe residual CIPN compared to children treated with vincristine [235].

1.4.4 Painkilling Treatment

Presently, there are no effective preventative strategies or treatment for CIPN [234, 236, 243, 244]. Several interventions have been trialled but have shown to have low

benefits (acetylcysteine, carbamazepine, glutamate/glutamine, retinoic acid, gabapentin and nortriptyline/amitriptyline) or no evidence of efficacy (acetyl-L-carnitine, nimodipine, lamotrigine) [233, 243, 245]. Additionally, some of these treatments were shown to cause adverse effects such as nausea, vomiting, fatigue, dizziness, drowsiness and somnolence [246]. Recently, the use of a range of interventions, both pharmacological and non-pharmacological, have been recommended against by the American Society of Clinical Oncology (ASCO) [234]. These include amitriptyline, L-carnosine, cannabinoids, glutathione, glutamate, calcium/magnesium infusion, vitamin E, vitamin B, carbamazepine, venlafaxine, gabapentin/pregabalin, oxcarbazepine, N-acetylcysteine, minocycline, metformin, recombinant human leukemia inhibitory factor, exercise therapy and acupuncture. The use of opioids has been shown to be effective in controlling neuropathic pain [247, 248], however, there appears to be a high prevalence of opioid addiction [249]. There is also concern behind co-administering gabapentin with opioids, as it is associated with increased risk of respiratory depression [250].

According to ACSO guidelines, only duloxetine currently has moderate recommendation for the treatment of CIPN [234]. Duloxetine is a serotonin and noradrenaline reuptake inhibitor and has shown to help neuropathic pain in established CIPN [245, 251–253]. A randomized, double-blinded, placebo-controlled, cross-over clinical trial of 231 patients with painful CIPN demonstrated the effectiveness of duloxetine for pain management in neuropathy [252]. There was a greater reduction in pain in patients who received duloxetine compared to those who received placebo, as well as a greater decrease in numbness and tingling. However, some associated side effects of duloxetine include headache, nausea, somnolence, anxiety and dry mouth [246] Although there is no recommendation for acupuncture by ASCO, a systematic review, consisting of 19 randomised controlled trials and involving 1174 people, illustrated that acupuncture not only significantly improved pain but also NCV [254]. Additionally, there is growing evidence for the positive effect of exercise on CIPN-induced symptoms [255–257]. In a randomized controlled trial, the impact of exercise on CIPN was investigated in metastasized colorectal cancer patients [257]. In the intervention group, individuals who participated in an eight-week supervised exercise program, neuropathic symptoms remained stable over time (from baseline to after the intervention period, as well as from baseline to a 4-weeks follow-up period). In

contrast, CIPN in the control group significantly worsened over time. Furthermore, the intervention group demonstrated significant improvement in strength and balance function, unlike the control group. Furthermore, the high concentration (8% w/w) capsaicin patch (179 mg) has been shown to be effective in providing pain relief in CIPN patients [258–261]. There was also evidence of sensory nerve fibre regeneration [259, 260], with 93 % nerve fibre recovery observed 24 weeks following exposure to the capsaicin patch [259]. Importantly, Bienfait et al. [261] demonstrated significantly better efficacy in patients who received repeated applications, particularly three or more, compared to patients who received fewer applications.

1.4.5 DNA damage response (DDR) and DNA repair pathways

The primary mechanism to detect and repair cisplatin-DNA adducts is the nucleotide excision repair (NER) pathway [152, 262–264], as it is associated with the removal of bulky lesions. Studies have revealed that the severity of CIPN depends on the efficiency of this DNA repair machinery to repair cisplatin-DNA adducts [152, 265]. Cisplatin not only binds to nuclear DNA, but also to mitochondrial DNA [150, 266, 267]. Unlike the nucleus, the NER DNA repair pathway is not present in the mitochondria [268, 269], accounting for mitochondrial dysfunction as a significant contributory factor in cisplatin neurotoxicity. An increase in the repair of cisplatin-DNA adducts has also been associated with cisplatin resistance [270, 271]. In addition to the NER pathway, it has been revealed that the base excision repair (BER) pathway is also involved in the response to cisplatin damage in DRGs [272], which is associated with the repair of base modifications and single-strand breaks (SSBs). Cisplatin results in an increase in the production of ROS, which also damages DNA by creating base modifications and SSBs [215,216]. Both NER and BER have been linked to p53 signalling pathway [275, 276]. Furthermore, studies have shown that p53 promoted DNA repair and protected against cisplatin-induced DNA damage and apoptosis [277–279], supporting the involvement of p53 in the modulation of various DNA damage response pathways [280]. Other repair pathways including homologous recombination (HR) and non-homologous end joining (NHEJ) have been demonstrated to be involved in the repair of cisplatin-induced DNA damage [281–283]. Both processes repair double-strand breaks (DSBs) [284] and cisplatin has been shown to produce DNA DSBs [285, 286].

In response to DNA damage and DNA replication stress, ataxia-telangiectasia mutated (ATM) and ataxia-telangiectasia and RAD3-related (ATR) are activated [287–289]. These protein kinases are key regulators of the DNA damage response (DDR), a complex signalling pathway which allows for the detection and repair of damaged DNA. When ATM and ATR are activated, DDR is initiated and results in the phosphorylation of a spectrum of substrates [288, 290, 291]. Two such substrates include p53 [292, 293] and histone H2A.X [294, 295], hence they are often utilized as markers of DNA damage.

In normal cells, the protein level of p53 is low, due to Mdm2; the major regulator of p53 which is responsible for its degradation [296, 297]. Following peripheral nerve injury, p53 protein levels have been demonstrated to increase [298, 299]. Phosphorylation of p53 inhibits the binding of Mdm2 and thereby results in its stabilization, by preventing its degradation [300]. In response to DSBs, H2A.X is phosphorylated at serine-139 to form γH2A.X, accounting for the increased expression levels of γH2A.X observed following DNA damage [294, 301–304]. γH2A.X then serves as a platform for the accumulation and retention of the numerous coordinators of DDR signalling [305–316].

The NER pathway, used for the detection and repair of bulky lesions, consists of two sub-pathways; global genome (GG-NER) and transcription coupled (TC-NER) [317, 318]. GG-NER recognizes and repairs lesions anywhere in the genome whereas TC-NER repairs lesions at actively transcribing genes. With exception to the mechanism by which DNA damage is initially recognized, these two sub-pathways are identical. In GG-NER, initial detection of DNA damage involves the xeroderma pigmentosum group C protein complex, XPC-RAD23B. On the other hand, stalling of the RNA polymerase II complex initiates TC-NER, which is then displaced by Cockayne syndrome (CS) proteins CSA and CSB. The subsequent steps are identical with the binding of XPA and the heterotrimeric replication protein A (RPA) to the damaged site and recruitment of the transcription factor II human (TFIIH) complex. Unwinding of the double helix on either side of the lesion is carried out by the helicases XPB and XPD, subunits of the TFIIH complex. The strand with the lesion is then cleaved at the 3' and 5' ends by the endonucleases XPG and XPF/ERCC1, respectively, removing the oligonucleotide containing the lesion. The detached oligonucleotide is ~30 nucleotides long. Using the intact strand as a template, the gap generated is filled by

DNA replication proteins including DNA polymerases δ ε, or κ and replication factor C (RFC), and sealed by a DNA ligase (ligase I or III).

The BER pathway, used for the detection and repair of base modifications and SSBs, is initiated by DNA glycosylases [319]. These highly specialized enzymes recognize and cleave the damaged DNA base, generating an apurinic or apyrimidinic (AP) site. An AP endonuclease (APE), APE-1, then cleaves the AP site, creating a 3' hydroxyl terminus and a 5' deoxyribose phosphate (dRP) terminus. DNA polymerase β fills the single nucleotide gap as well as removes the dRP residue via its phosphodiesterase activity. As a result, a 5' phosphate end is created, which is sealed by DNA ligase III. This is commonly referred to as short-patch repair. For the replacement of more than one base (~2-10 nucleotides), long-patch repair, proliferating cell nuclear antigen (PCNA), flap endonuclease-1 (FEN-1), DNA polymerase δ and DNA ligase I are involved [320]. PCNA serves as a sliding clamp and FEN-1 excises the dRP residue.

DSBs can be repaired by either HR or NHEJ [321]. HR requires a homologous DNA sequence, usually the sister chromatid, for DNA repair and is error-free. In contrast, NHEJ does not require a DNA template so it is faster, however, it is error-prone. HR commences with the binding of the MRN protein complex (MRE11-Rad50-Nbs1) to the damaged DNA. At the break, a process known as DNA end resection occurs, generating 3' single-stranded DNA (ssDNA) overhangs. The newly created ssDNA ends are coated by RPA, stabilizing the ends and protecting them from nucleases. This is called a ssDNA nuclofilament. Next, Rad51 is loaded onto the ssDNA with the help of the breast and ovarian cancer susceptibility protein 2 (BRCA2). Rad51 replaces the RPA, creating a nucleoprotein filament. Rad51 initiates the search for a homologous region on the sister chromatid to serve as a template and is crucial for strand invasion. Upon identification of a homologous region, the ssDNA end invades the homologous dsDNA, forming a D-loop. DNA polymerase then extends the 3' of the invading strand using the homologous region as a template and DNA ligase I seals the end. The newly repaired DNA strand is an exact replica of the original.

NHEJ is initiated by the binding of the Ku70/Ku80 heterodimeric protein to the DSB site. Next, DNA protein kinase catalytic subunits, DNA-PKcs, are recruited and attach to the Ku proteins. DNA-PKcs allow for the subsequent recruitment of Artemis, a nuclease, and the MRN protein complex. Artemis is then phosphorylated and the Artemis- DNA-PKcs complex, having nuclease activity, cleaves the ssDNA segment

from the dsDNA, creating 2 blunt ends. The ends are joined, resynthesis completed by DNA polymerases μ and λ, and then sealed by DNA ligase IV. In contrast to HR, the newly repaired DNA strand does not resemble the original DNA as nucleotides are lost via this process.

1.4.6 Preclinical models of CIPN

Rodent models are used to explore the underlying mechanisms attributed to CIPN. From this point onwards, CIPN would be used to signify cisplatin-induced peripheral neuropathy. Rodent models include models that mirror adult and childhood associated CIPN, with adult and neonatal rodents. These approaches consist of interventions that consider clinical scenarios [322, 323]. One major issue is the disparities which remain across the literature with differing dosing regimens presented [323]. CIPN is a dose-limiting side effect, which occurs in a dose-dependent and time-dependent manner [148, 324]. The severity of CIPN increases with higher cumulative doses and longer times of exposure to cisplatin [161, 224]. Dosing schedules utilized include either a single administration of the agent [325] or multiple doses per week, over a duration of one or several weeks [326–330]. This has resulted in cumulative doses of cisplatin ranging from (2-23 mg/kg).

In vitro models include both neuronal cell lines (SH-SY5Y, PC12, 50B11) as well as primary DRG sensory neurons that have been isolated from living tissue or organs. These cells are treated with varying concentrations of cisplatin for various time-points, usually 24 hours, and subsequently analyzed using an array of techniques, most commonly cell viability assays and immunofluorescence to assess the toxicity of cisplatin. This allows investigation of the effects of cisplatin on neuritogenesis and neuronal function mediated by an inflammatory response or changes in neuropeptide release. With regards to in vivo rodent models, dosing regimen involves either a single dose or multiple doses over a period of one week or several weeks of either intraplantar (i.pl.), intraperitoneal (i.p.) or intravenous tail vein (i.v.). This has led to a wide range of cumulative doses being utilized [323]. The rodents are then subjected to pain behaviour tests to assess mechanical and thermal hypersensitivity as well as electrophysiological test to assess changes in nerve conduction velocity (NCV) [331].

One of the hallmarks of CIPN is peripheral sensory neurodegeneration, which includes intraepidermal nerve fibre (IENF) degeneration [332–334]. In vitro, cisplatin treatment has exhibited a decrease in the number of neuronal cells demonstrating neuritogenesis and a dose-dependent decline in cell viability [335–339]. In vivo, cisplatin treatment has shown to result in a reduction in both PGP9.5+ve and CGRP+ve IENFs [333–335, 340, 341], indicative of sensory neurodegeneration. In addition, rodents exposed to cisplatin typically display increased sensitivity to mechanical stimuli [325, 326, 328–330, 333–335, 340, 342–344, 331, 345–349], either as mechanical allodynia or mechanical hyperalgesia. Rodents also display increased sensitivity to heat, thermal hyperalgesia [325, 328, 335, 340, 347]. However, there has been conflicting views as some studies have failed to demonstrate thermal hyperalgesia [326, 343, 346]. This discrepancy can possibly be accounted for by difference in the method of drug administration (intravenous vs intraperitoneal) or dosing regimens (resulting in a wide cumulative dose range) employed. Furthermore, electrophysiological testing has demonstrated that cisplatin treatment leads to reduction in both motor and sensory NCV [152, 341, 350], which was greater in sensory nerves.

Despite the lack of understanding about the impact of chemotherapeutics on nociception and development and childhood cancer survivorship, there are now preclinical models exploring this [340, 351, 352]. Early life exposure to chemotherapy resulted in a persistent but delayed onset of chronic pain in these rodent models. In the vincristine model [351], neonatal exposure to vincristine (P11) caused a delayed onset (P26) of mechanical hypersensitivity that persisted into adulthood (P54). On the other hand, neonatal exposure to cisplatin (P7) [340] caused a delayed onset (P22) of mechanical and thermal hypersensitivity, both of which also persisted into adulthood (P42). In the vincristine model, the development of pain was associated with a significant reduction in IENF density in the plantar skin (P33). In contrast, the cisplatin model illustrated alterations in IENF density from degeneration shortly post-treatment (P16), prior to the onset of pain, to aberrant nerve fibre growth subsequent to the onset of pain (P45). See Table 1.2 for a summary of preclinical models of CIPN involving early life exposure to chemotherapy. This increase in aberrant nerve fibre growth is thought to be TrkA modulated as it was accompanied by an increase in TrkA+ve sensory neurons. According to Fitzgerald [29], during development, there is

a switch in the TrkA signal transduction pathway from growth and survival to hyperalgesia, providing further support for the involvement of TrkA signalling in the onset of neuritogenesis and hypersensitivity observed following cisplatin treatment. We wish to now investigate the reason behind this persistent but delayed onset of chronic pain following early life exposure to platinum-based chemotherapeutic agents.

Table 1.2 Preclinical models of CIPN involving early life exposure to chemotherapy

Species	Chemotherapy Agent	Age of exposure and Regimen	Route	Cumulative Dose	Outcome	Reference
Wistar rats	Cisplatin	P7 1 mg/kg; 5 daily injections	i.p.	5 mg/kg	Persistent mechanical and thermal hypersensitivity from P22 until P42 Reduction in IENF density in the plantar skin from P16-P20 Increase in IENF density in the plantar skin at P45	Hathway et al. 2018 [344
Sprague –Dawley rats	Vincristine	P11 60 µg/kg; 5 injections on P11, 13, 17, 19 and 21	i.p.	300 µg/kg	Persistent mechanical hypersensitivity from P26 until P54 No thermal hypersensitivity Significant reduction in IENF density in the plantar skin at P33	Schappacher et al., 2017 [355]

1.5 Research hypothesis

In this thesis, it was hypothesized that early exposure to cisplatin results in DNA damage and modulation of TrkA receptors. Initially, there is a period of neurodegeneration, which triggers a DNA damage response. The TrkA receptors on nerve fibres becomes activated, leading to increased nerve growth and disruption to the normal development of nociceptive pathways. Subsequently, this results in peripheral sensory neuronal sensitization and the onset of chronic pain, which is experienced by adults following childhood chemotherapy.

1.6 Research objectives

1) Validate that cisplatin treatment results in DNA damage and activation of the TrkA receptor. (In vitro model)
2) Validate that cisplatin treatment induces nerve growth and peripheral sensory neuronal sensitization. (In vivo model)
3) Investigate TrkA signalling to determine its involvement in the development of increased sensitivity to pain following cisplatin treatment.
4) Identify a source of TrkA activation following cisplatin treatment.

Each results chapter has its own specific hypotheses and experimental aims.

Chapter 2: General Methodology

2.1 Animals

All experimental procedures involving animals were performed in accordance with the UK Home office animals (Scientific procedures) Act 1986, under the project licence (PPL) P39888F91, and reviewed by Nottingham Trent University Animal Welfare and Ethics Review Boards. All efforts were made to abide by the 3Rs principles of replacement, reduction and refinement. Where applicable, animal work was replaced, the number of animals utilized per experiment was reduced to a minimum and experiments were refined to minimize pain, suffering and distress of the animals.

All rodents used in this thesis were purchased from Charles River (Kent, UK). Male Wistars Han rats (~250g, 8 weeks) were used in the in vivo nerve growth factor (NGF) studies (n=54). Male and female neonatal Wistars Han rats (~30g) were used in the in vivo studies for the behavioural assessment of cisplatin-induced pain (male n=8, female n=10). Wistar rats were used because the previous cisplatin rodent model [340] was created using this breed. In addition, in house bred C57/BL6J pups (7-14 days) were used for in vitro DRG neuron cultures. These mice were more readily available as they were already being utilized in the laboratory for the collection of other tissues. All rodents were housed within the Bioscience Support Facility (BSF) at Nottingham Trent University, in triplicates, in Techniplast Sealsafe Plus cages. Each cage was equipped with corncob bedding and sizzle-nest (Datesand Ltd., Cheshire, UK). Environmental enrichment was provided in the form of wooden chew blocks and cardboard fun tunnels (Datesand Ltd., Cheshire, UK). All rodents were supplied with an irradiated Rodent 2018 Envigo Global Certified Diet (Envigo Laboratories U.K. Ltd., Oxon, UK) and autoclaved tap water *ad libitum*. Environmental conditions were all in accordance with the 'Code of Practice for the Housing and Care of Animals Used in Scientific Procedures' and consisted of targeted parameters for temperature (20-24 ℃) and humidity (45-65 %) and at least fifteen air changes per hour. At the BSF, all rodents received animal technician support care under 12:12 hour light dark cycles (light on 7am-7pm) and bedding materials were changed once per week.

2.2 Nociceptive behavioural testing

The mechanical withdrawal threshold was measured using von Frey monofilament hairs [353] and the thermal withdrawal latency was measured using the Hargreaves test [354]. These tests allowed for the assessment of mechanical and thermal hypersensitivity respectively. All behavioural tests were performed and recorded blinded i.e. information regarding treatment groups was unknown by the experimenter as references were only made using cage and animal numbers. Testing was performed in a quiet room with ambient lighting. The plantar surface on both the right and left hind paws were subjected to nociceptive testing. For each experiment, prior to any animals being dosed, two reciprocal baseline reading were required. The animals were monitored pre and post behavioural assessment to ensure their welfare.

2.2.1 Habituation

Prior to the start of any experiment, rats were acclimatized to the research unit and personal licence (PIL) holder, myself, by means of animal handling, for a period of 1 week. On the day of behavioural testing, rats were allowed 5 minutes of habituation, to acclimatize to the testing enclosure and become settled, before any tests were performed.

2.2.2 Assessment of mechanical withdrawal threshold

For the von Freys monofilament hairs test, rats were placed into clear Perspex enclosures (Bioseb, USA), which sat on mesh flooring to allow visualization and access to the plantar surface of the hind paws from beneath. Von Frey monofilament hairs (Bioseb, USA) of increasing forces were applied to the plantar surface, at right angle, until the hair bent. This meant that a constant force was exerted and allowed for differentiation from a prick. Withdrawal of the paw from the stimuli would indicate a positive response and be recorded as “X”. No response would indicate a negative response and be recorded as “I”. Testing was done in ascending order of force and each monofilament was applied a maximum of five times to each hind paw. The forces utilized depended on the response of the rats. It was ensured that both a 0 % withdrawal response (IIIII) and a 100 % withdrawal response (XXXXX) was obtained for each rat. The forces used ranged from 2-100 g. As a measure to avoid a

false positive reading, testing was only performed when the rat was alert but stationary. Three rats were tested simultaneously, allowing time for the paws to recover. GraphPad Prism v9.0 was then used to generate a force-response curve, by plotting the percentage withdrawal response (ranging from 0-100 %) against the force applied (ranging from 2-100 g). From the sigmoidal curves produced, the logEC50 value was calculated; this is the force that resulted in 50 % withdrawal from the stimuli. The logEC50 values were then plotted, as withdrawal threshold (g), against time, to display the change in withdrawal threshold over time.

2.2.3 Assessment of thermal withdrawal threshold

For the Hargreaves test, rats were placed into clear Perspex enclosures (Bioseb, USA), which sat on a transparent glass pane. A mobile infrared heat source was positioned under the glass pane, focused on the plantar surface of the hind paw, and a heat stimulus at constant intensity (60 units was used throughout this research) was applied. Once the heat source was switched on, it started a digital timer which automatically stopped when the paw was withdrawn, allowing the withdrawal latency to be recorded. Exposure to the heat source was limited to a maximum of 20 seconds to avoid any possible sensitization or tissue damage. Testing was performed three times on each hind paw. Similar to the von Freys monofilament hairs test, three rats were tested simultaneously, allowing a period of time between stimulations to prevent sensitization. Additionally, as a measure to avoid a false positive reading, testing was only done when the rat was alert but inactive. Using Excel, the three repeat readings per hind paw were averaged and the data for each treatment group merged. GraphPad Prism v9.0 was then used to plot withdrawal latency (s), against time, to display the change in withdrawal latency over time.

2.3 Rodent models

2.3.1 NGF-induced pain model

A rat model of NGF-induced sensory neuropathy was used to investigate the effect of NGF on pain behaviour and IENF nerve growth as well as determine whether inhibition of NGF/TrkA signalling, using a TrkA inhibitor (GW441756), could prevent or ameliorate those effects. Wistar Hans rats were randomly separated into 3

cohorts (control, NGF and NGF+TrkA inhibitor). Two different methods of drug administration were trialled (see Table 2.1 for experimental details). All drugs were delivered into the right hind paw, midsole, in a total volume of 20 µL. The left hind paw served as a control for each rat.

2.3.2 Cisplatin-induced pain model

A rat model of cisplatin-induced neuropathic pain [340] was used to investigate the effect of cisplatin on pain behaviour and nerve growth as well as determine whether inhibition of TrkA signalling, using a TrkA inhibitor (GW441756), could prevent or ameliorate those effects. Wistar Hans rats were randomly separated into 3 cohorts (control, cisplatin and cisplatin+TrkA inhibitor). Rats were then injected intraperitoneally (i.p.) with either phosphate buffered saline (PBS) for the vehicle control or cisplatin. At a later time-point, rats in the cisplatin+TrkA inhibitor group that were previously treated with cisplatin were i.p. injected with GW441756, a selective and potent TrkA inhibitor [355, 356] (see Table 2.1 for experimental details).

Table 2.1 Experimental details for the NGF-induced and cisplatin-induced pain models

	Experimental group	Drug delivery	Drug concentration	Animal number	Sex
NGF Experiment 1	Control	PBS (i.pl.)	0.01 M	6	males
	NGF	NGF (i.pl.) PBS (i.p.)	1 µM 0.01 M	6	males
	NGF+TrkA inhibitor	NGF (i.pl.) GW441756 (i.p.)	1 µM 2 mg/kg	6	males
NGF Experiment 2	Control	PBS (i.pl.)	0.01 M	6	males
	NGF	NGF (i.pl.)	1 µM	8	males
	NGF+TrkA inhibitor	A mixture of NGF + GW441756 (i.pl.)	1 µM 100 nM	8	males
Cisplatin Experiment	Control	PBS (i.p.)	0.01 M	6 6	males females
	Cisplatin	Cisplatin (i.p.)	0.1 mg/kg	6 8	males females
	Cisplatin+TrkA inhibitor	A mixture of Cisplatin + GW441756 (i.p.)	0.1 mg/kg 0.5 mg/kg	6 6	males females

2.3.3 Tissue harvesting and processing

Rats were terminally anaesthetised using sodium pentobarbital (i.p, 60mg/kg) and death confirmed by cervical dislocation. Plantar skin was extracted from both the right and left hind paws (World Precision Instruments USA). An appropriate sample was removed and any underlying muscle that was attached to the plantar skin was trimmed away. Once retrieved, each piece of tissue was cut vertically into two segments; half for protein analysis and half for immunofluorescence.

2.3.4 Tissue processing for protein analysis

Tissue for protein analysis was placed into a bijou and either stored on dry ice or placed into liquid nitrogen. When frozen, the tissues were transferred to a -80 ℃ freezer for storing until required.

2.3.5 Tissue processing for immunofluorescence

Tissue for immunohistochemistry was fixed by submerging in 4% paraformaldehyde (PFA) for 24 hours at 4 ℃. Following PFA submersion, tissues were cryoprotected in 30 % sucrose and stored at 4 ℃ overnight. Plantar skin tissues were then embedded in optimal cutting temperature (OCT) (VWR International, UK) and either stored at -80 ℃ or processed for cryosectioning. 20 µm thick sections of plantar skin were sectioned onto labelled SuperFrost Plus Microscope Slides (VWR International, UK) using Leica cryostat CM1860 UV (UK), which was set to -20 ℃. Three to four sections were mounted onto each slide. Slides were stored in slide boxes at -80 ℃ until required for immunohistochemistry staining.

2.4. Cell culture

2.4.1 SH-SY5Y cell culture

The human neuroblastoma cell line, SH-SY5Y, was obtained from Dr. Amanda Coutts (Nottingham Trent University, UK). Due to Covid-19, rodents were no longer easily accessible. To salvage the remaining time, our primary cell model was substituted with a cell-line model. We were given a frozen cryovial containing 1 ml of SH-SY5Y cell suspension in freezing medium: 90 % foetal bovine serum (FBS) and 10%

dimethyl sulphoxide (DMSO). Prior to collection, cell culture medium was prepared by supplementing Dulbecco's Modified Eagle Medium (DMEM) (Gibco, UK) with 10 % FBS and 1X penicillin/streptomycin. This was then filtered using a 0.2µm Minisart filter unit (Sartorius Stedim Biotech, UK) fixed onto a 50 ml luer syringe.

Frozen cryovials were thawed rapidly, by putting into a 37 ℃ water bath, transferred to 75 cm^2 cell culture flasks containing pre-heated cell culture medium and placed into an incubator at 37°C in a humidified environment containing 5% carbon dioxide (CO_2) and the cells allowed to grow. If not otherwise stated, all incubations were performed in this incubator at the stated settings. The following day, the medium was discarded and replaced with fresh cell culture medium to get rid of any residual DMSO. Cells were left to grow, in the incubator, in 75 cm^2 cell culture flasks until they reached 90-100 % confluency, at which point they were split and seeded onto cell culture plates or gelatin-coated 90 mm petri dishes for further experiments. The type of plate and number of cells seeded were based on the experiment to be performed. Cell culture medium was replaced every 2-3 days.

2.4.2 Cell maintenance

For cell maintenance and passaging, the cell culture medium was removed and the cells washed with 4 ml PBS. Next, 4 ml of 0.05% Trypsin (Sigma-Aldrich, UK) was added to the cell culture flask and the flask incubated for 2-3 minutes. This was done to enzymatically dissociate the cells. After incubating, the flask was removed from the incubator, gently tapped to assist with detachment of the cells and visualized using a brightfield light microscope to confirm that the cells were detached. Once confirmed, enzymatic dissociation was stopped by adding 8 ml of cell culture medium to the flask. The cell mixture was transferred to a 15 ml falcon tube and centrifuged at 1000 x g for 2 minutes. The supernatant was discarded and the pellet re-suspended in 12 ml cell culture medium. At this point, if more cells were required, 1 ml of cell suspension was transferred to a new 75 cm^2 flask containing 14 ml pre-heated cell culture medium.

For cell counting, 10 µl of cell suspension was pipetted under a sterilized 22 x 22 mm glass coverslip (VWR International, UK) into one of the chambers of a haemocytometer (Mill Science Neubauer) and the number of cells present in the four corner regions of the centre grid were manually counted using a light microscope

(Leica DM IL). The value obtained was averaged and multiplied by 10^4 to give the total number of cells/ml. The cell suspension was then thoroughly, but gently mixed and seeded at the required density onto gelatin-coated 90 mm petri dishes or cell culture plates containing fresh pre-heated culture medium. At the first splitting event, some cell suspension was left in the falcon for freezing. This was centrifuged at 1000 x g for 2 minutes, the supernatant discarded and the cell pellet re-suspended in 1 ml of freezing medium. This was then transferred to a cryovial and stored at - 80 ℃ overnight. The following day, the cryovial was moved to a liquid nitrogen tank.

2.4.3 Primary cell culture

2.4.3.1 Plate preparation

For immunofluorescence of DRG cell culture, coverslips were first sterilized by pre-soaking in 70 % ethanol for 10 minutes, washed with PBS and transferred to the wells of a transparent, flat bottom 24-well plate (Corning Costar, Fisher Scientific, UK). The plate was then pre-treated with 300 µl of poly-L-lysine (Sigma-Aldrich, UK, P4707) and incubated overnight at 37 ℃. The following day, the poly-L-lysine was removed, the wells washed with 300 µl sterile distilled water and allowed to air dry. The wells were then coated with 300 µl laminin (5 ug/ml prepared in PBS) (Sigma-Aldrich, UK, L2020) and incubated at 37 ℃ for a minimum of 2 hours. Prior to using, the laminin was removed and the wells allowed to air dry.

For calcium assay, a 96-well plate was pre-treated with 50 µl of poly-L-lysine and incubated overnight at 37 ℃. The following day, the poly-L-lysine was removed, the wells washed with 50 µl sterile distilled water and allowed to air dry. The wells were then coated with 50 µl laminin (1 ug/ml prepared in PBS) and incubated at 37 ℃ for a minimum of 2 hours. Prior to using, the laminin was removed and the wells allowed to air dry.

2.4.3.2 Dorsal Root Ganglia (DRG) isolation

C57/BL6J mice (P7-14 male and female), were decapitated via Schedule 1. Dissection tools were disinfected using 70 % IMS, prior to the start of dissecting and between mice. Once the mice were terminated, they were collected. A laminectomy was performed to retrieve the spinal column. The mouse was laid on its front, facing

downwards. The skin was separated from the dorsal muscle by inserting a scissors, from the neck, between the skin and dorsal muscle and opening it. The skin was then cut along the dorsal midline, from the neck down to the tail, revealing the muscular structure and connecting tissues surrounding the spinal column. An incision was made above the tail bone to separate the spinal column from the tail bone. The ribs on both sides were cut and connective tissue dissected away, allowing the spinal column to be removed. Once retrieved, the spinal column was placed in a bijou containing Hanks' Balanced Salt Solution (HBSS) (Gibco, UK) and stored on ice for further dissecting. The spinal column was then opened by cutting along both sides of vertebral bone from the cervical end straight down until the sacral region. The spinal cord was gently removed, revealing the DRGs and connecting nerves. As many DRGs as possible were collected and placed into a bijou containing cold DRG prepared medium: Ham's F12 medium (Gibco, UK) supplemented with 1X N2 supplement (Gibco, UK), 0.3 % bovine serum albumin (BSA) (Sigma-Aldrich, UK, A9576) and 1X penicillin/streptomycin (Gibco, UK). DRGs were then enzymatically dissociated by incubating in 0.125 % collagenase solution (Sigma-Aldrich, UK, C9407) at 37 ℃ for a maximum of 2 hours.

Following incubation, the cells were mechanically broken down by trituration to form a single cell suspension, and transferred to a falcon tube containing a 15 % BSA cushion (1 ml 30 % BSA solution and 1 ml cell culture medium). The cell suspension was then centrifuged at 1600 revolutions per minute (rpm) for 10 minutes at room temperature with no brake, using an Eppendorf Centrifuge 5702 (UK). The supernatant was discarded, along with the myelin interface and any debris, and the pellet re-suspended in DRG culture medium. The cell suspension was then distributed equally among the wells of a cell culture plate. Plates were kept in an incubator and the cells allowed to grow. DRG culture medium was replaced every 2-3 days.

2.4.3.3 Splenocyte isolation

C57/BL6J mice (P7-14), were decapitated via Schedule 1 procedure by a third party. Dissection tools were disinfected using 70 % IMS, prior to the start of dissecting and between mice. Once the mice were terminated, they were collected. The mouse was laid on its back, facing upwards. An incision into the skin was made using scissors. The skin was then pulled back, separating it from the underlying muscle and exposing

the peritoneal cavity. The spleen is located on the left side of the mouse so the mouse was laid on its right side. A small snip into the muscle wall on the left side was made and the spleen removed. Any connective tissue was trimmed off and the spleen was placed into a bijou containing cold washing medium: RPMI 1640 medium (Invitrogen, UK), penicillin-streptomycin (Sigma-Aldrich, UK) and foetal bovine serum (FBS) (Invitrogen, UK). The spleens were mechanically broken down into a single cell suspension and strained through a 40 µm cell strainer (Fisher Scientific, UK) into a falcon tube. Splenocyte culture medium: RPMI 1640 medium, penicillin-streptomycin, FBS, l-glutamine (Invitrogen, UK), sodium pyruvate solution (Sigma-Aldrich, UK) and monothioglycerol (Sigma-Aldrich, UK) was added to the falcon tube and the cell suspension centrifuged at 1500 rpm for 3 minutes at room temperature with no brake. The supernatant was discarded and the pellet re-suspended in red blood cell lysing buffer (Sigma-Aldrich, UK, R7757) for a maximum of 30 seconds. The cells were then washed twice by adding splenocyte culture medium, centrifuging at 1500 rpm for 3 minutes at room temperature with no brake and discarding the supernatant. After washing, the pellet was re-suspended in splenocyte culture medium and distributed equally among the wells of a 6-well plate. Plates were kept in an incubator and the cells allowed to grow. Splenocyte culture medium was replaced every 2-3 days.

2.4.4 Cell seeding for experimentation

Prior to cell splitting, the required number of petri dishes were coated with 5 ml of 0.15 % gelatin (Sigma-Aldrich, UK, G9391) and incubated for 30 minutes. The gelatin was then removed and the petri dishes allowed to air dry. For protein analysis, SH-SY5Y cells were seeded at ~$1x10^6$ cells per petri dish. Splenocytes were equally distributed among the wells of a 6-well plate. For cell viability assays, SH-SY5Y cells were seeded at ~$3x10^4$ cells per well of a 96-well plate. For calcium assays, DRGs were equally distributed among the wells of a 96-well plate. For immunofluorescence, DRGs were equally distributed among the wells of a coverslipped 24-well plate.

2.5 Immunofluorescence

2.5.1 Immunohistochemistry of DRG cell culture

All incubation steps at room temperature were performed on the bench top. DRG culture medium was removed and cells washed once with 300 µl of PBS for 5 minutes. The cells were then fixed to their coverslips by incubating in 300 µl of 4 % PFA for 15 minutes at room temperature. The PFA was removed and the cells washed again with 500 µl of PBS for 5 minutes. The cells were then permeabilized in 500 µl of permeabilizing solution (Table 2.2) for 5 minutes. Subsequently, non-specific binding sites were blocked by incubating in 300 µl of blocking solution (Table 2.2) for 1 hour at room temperature. After blocking, the cells were incubated in primary antibody (Table 2.3) overnight at 4 ℃. Primary antibodies were diluted in blocking solution. The following day, the primary antibody was removed, cells washed three times using 500 µl of PBS for 5 minutes each and incubated in secondary antibody (Table 2.3) for 2 hours at room temperature, protected from light. Secondary antibodies were diluted in permeabilizing solution. Cells were then washed three times using 500 µl of PBS for 5 minutes each. For the final wash, DAPI (Table 2.2) was added to the PBS in a 1:1000 dilution. The coverslips were then carefully removed from the wells and place cell-side down onto SuperFrost microscope slides upon a drop of Vectashield anti-fade mounting media (2BScientific, UK, H-1000-10). The coverslips were gently pressed against the microscope slides to release any air bubbles. 2-3 coverslips were added onto each slide. Slides were labelled and stored at 4 ℃ until they were ready to be imaged.

2.5.2 Immunohistochemistry of plantar skin

All incubation steps at room temperature were performed on the bench top. Tissue sections mounted on microscope slides were placed onto a humidified Simport stain tray system (Scientific Laboratory Supplies, UK, MIC4162), which contained water to provide a humidified environment. A no primary antibody control (NPC) was included as a negative control. An ImmunoPen (Millipore, UK) was used to draw a hydrophobic ring around the mounted tissue on each slide. Tissue sections were washed three times with PBS for 10 minutes each. Tissue sections were then permeabilized in permeabilising solution (Table 2.2) for 5 minutes. Subsequently, non-specific binding sites were blocked by incubating in blocking solution (Table 2.2)

for 1 hour at room temperature. After blocking, tissue sections were incubated in primary antibody (Table 2.3) for 72 hours at 4 ℃, except for the NPC which remained in blocking solution as primary antibodies were diluted in blocking solution. After the incubation period, the primary antibody (or blocking solution for the NPC) was removed, tissue sections washed three times with PBS for 10 minutes each and incubated in secondary antibody (Table 2.3) for 2 hours at room temperature, protected from light. Secondary antibodies were diluted in permeabilising solution. Tissue sections were then washed three times with PBS for 10 minutes each. For the final wash, DAPI was added to the PBS in a 1:1000 dilution. Slides were carefully dried, 1-2 drops of Vectashield anti-fade mounting media were added onto each slide and glass coverslips were delicately placed on top of the slides. The coverslips were gently pressed against the microscope slides to release any air bubbles. Slides were labelled and stored at 4 ℃ until they were ready to be imaged.

Table 2.2 List of reagents used for immunofluorescence

Solution	Composition	Supplier (Product Code)
0.01 M PBS (Phosphate buffered solution)	10 mM phosphate buffer, 2.7 mM potassium chloride, 137 mM sodium chloride, pH 7.4 at 25 ℃	Sigma-Aldrich, UK (P4417)
Permeabilising solution	0.2% Triton X-100 dissolved in 0.01M PBS	For Triton X-100 Sigma-Aldrich, UK (X100)
Blocking solution	5% BSA and 0.2% Triton X-100 dissolved in 0.01M PBS	For BSA Sigma-Aldrich, UK (A9418)
DAPI	20µg/mL DAPI dissolved in distilled water	For DAPI Sigma-Aldrich, UK (D9542)

2.6 Cell viability

Cells were seeded in a 96-well plate at a concentration of 3×10^4 cells per well, in 100 µl of culture medium. The following day, cells were treated as required, in a total

volume of 100 µl per well. Once treated, cells were incubated for 24 hours at 37°C and 5% CO_2. The following day, 10 µl of Cell Proliferation Reagent WST-1 (Roche Diagnostics, UK) was added to each well and cells were placed in an incubator for 4 hours at 37°C and 5% CO_2. After 4 hours, the plate was shaken on a shaker for 1 minute and the absorbance for each well measured using the Tecan plate reader Infinite 200Pro (Life sciences, UK). The measured absorbance directly correlates to the number of viable cells. The wavelength setting was selected as 440 nm. A row of wells containing only culture medium, 100 µl per well, was used as the blank control.

Table 2.3 List of primary and secondary antibodies used for immunofluorescence and Western blotting

	Target	Species	Dilution Factor	Supplier (Product Code)
Primary Antibodies	TrkA	Rabbit	1:250	Cell Signaling, UK (2505)
	Phospho TrkA (P-TrkA)	Rabbit	1:250	Cell Signaling, UK (9141)
	p53	Mouse	1:1000	Cell Signaling, UK (2524)
	Phospho p53 (P-p53)	Mouse	1:1000	Cell Signaling, UK (9286)
	Phospho Histone H2A.X (λH2A.X)	Rabbit	1:1000	Cell Signaling, UK (2577)
	ATF-3	Rabbit	1:1000	Santa Cruz Biotechnology, US
	TOP2A+TOP2B (Topoisomerase II α and β)	Rabbit	1:10,000	abcam, UK (ab109524)
	NGF	Goat	1:1000	Sigma-Aldrich, UK (N8773)
	β-actin (Housekeeping)	Mouse	1:1000	Cell Signaling, UK (8457)
	β-actin (Housekeeping)	Rabbit	1:1000	Abcam, UK
	β3-tubulin	Guinea pig	1:500	Synaptic Systems, Germany (302 304)
	Cleaved Caspase 3 (CC3)	Rabbit	1:400	Cell Signaling, UK (9661)
	Calcitonin Gene-Related Peptide (CGRP)	Rabbit	1:5000	Sigma-Aldrich, UK (C8198)
	Protein Gene Product 9.5 (PGP9.5)	Rabbit	1:100	Sigma-Aldrich, UK (AB1761)
	Anti-rabbit	Biotinylated	1:500	R&D systems, UK
Secondary Antibodies	Anti-rabbit	Goat	1:1000	Cell Signaling, UK (7074)
	Anti-mouse	Horse	1:1000	Cell Signaling, UK (7076)
	Anti-goat	Rabbit	1:1000	abcam, UK (ab6741)
	Anti-rabbit	Donkey	1:500	Invitrogen, US Alexa Fluor 555
	Anti-guinea pig	Goat	1:500	Invitrogen, US Alexa Fluor 488
	Anti-rabbit	Streptavidin	1:5000	Invitrogen, US (S32355) Alexa Fluor 555 conjugated

2.7 Protein expression analysis

2.7.1 Protein extraction

SH-SY5Y cells were lysed, on ice, using radioimmunoprecipitation assay (RIPA) lysing buffer (Sigma-Aldrich, UK, R0278). RIPA buffer was supplemented with a protease/phosphatase inhibitor cocktail (Cell Signaling Technology, UK, 5872S). Cell culture medium was removed from each petri dish and cells washed once with 5 ml of cold PBS for 5 minutes. The PBS was removed and the cells incubated in lysis buffer (Table 2.4) for 10 minutes at 4 ℃, swirling the plates occasionally. The cells were then rapidly scraped off the petri dishes using cell scrapers (Sigma-Aldrich, UK, CLS3010), transferred to cold 1.5 ml Eppendorf tubes and incubated for a further 30 minutes at 4 ℃. All samples were then centrifuged at 14,000 rpm for 15 minutes at 4 ℃. The protein lysate was transferred to new cold 1.5 ml Eppendorf tubes and either the total protein quantified immediately or stored at -80 ℃ for protein quantification.

Table 2.4 List of reagents used for protein expression analysis

Solution	Composition	Supplier (Product Code)
Lysis buffer	RIPA buffer protease/phosphatase inhibitor (100X)	Sigma-Aldrich, UK (R0278) Cell Signaling, UK (5872S)
Protein ladder	Precision Plus Protein Dual Xtra Standards (2–250 kD)	Bio-Rad, UK (1610377)
Running buffer	25 mM Tris base 192 mM Glycine 0.1 % SDS	Sigma-Aldrich, UK Fisher Scientific, UK (BP381) Fisher Scientific, UK (BP166)
Transfer buffer	25 mM Tris base 192 mM Glycine 20 % v/v Methanol	Sigma-Aldrich, UK Fisher Scientific, UK (BP381) Fisher Scientific, UK
Washing buffer (TBST)	20 mM Tris base 150 mM NaCl 0.1 % Tween-20	Sigma-Aldrich, UK Sigma-Aldrich, UK (S7653) Sigma-Aldrich, UK (P1379)
Blocking solution	20 mM Tris base 150 mM NaCl 0.1 % Tween-20 5 % BSA	Sigma-Aldrich, UK Sigma-Aldrich, UK (S7653) Sigma-Aldrich, UK (P1379) Fisher Scientific, UK (BP1600)
ECL mix (Clarity Western ECL Substrate)	Equal volumes of Peroxide Reagent and Luminol/Enhancer Reagent	Bio-Rad, UK (1705061)

2.7.2 Total protein quantification

Total protein quantification was performed using the Bradford protein assay. If samples were frozen, the were first thawed at 4 ℃. In new 0.5 ml Eppendorf tubes, each sample was appropriately diluted using distilled water. Protein standards (0, 0.05, 0.1, 0.2, 0.3, 0.4, 0.5 and 0.6 mg/ml) were prepared using BSA powder. 10 µl of each standard and sample was pipetted, in triplicate, into individual wells of a transparent, flat bottom 96-well plate. 200 µl of protein assay dye reagent concentrate (Bio-Rad, UK), diluted 1:5 in distilled water and filtered, was added to each well containing standard or sample. The plate was then incubated on a shaker (100 rpm) at room temperature for 8 mins before placing into the Tecan plate reader Infinite 200Pro. The wavelength was set at 595 nm and colorimetric analysis performed. Optical density measurements provided were exported to Microsoft Excel. A standard curve plot was generated and used to calculate the total protein concentration of the samples through interpolation. Once determined, the values were multiplied by the dilution factor to give the final concentration.

2.7.3 Western blotting

For each experiment, equal amounts of protein were utilized for each sample. The volume of cell protein lysate required were calculate before the start of each experiment. Cell protein lysate were mixed with 4x Laemmli buffer (Bio-Rad; UK), to which 10% 2-mercaptoethanol (Sigma-Aldrich, UK, M6250) was added prior to using. Samples were briefly vortexed, denatured on a heating block at 95 ℃ for 5 minutes and briefly centrifuged. The protein ladder (Table 2.4) and samples were loaded on manually prepared gels (see Table 2.5 for composition) and ran in running buffer (Table 2.4) at 90 V until sufficient separation was achieved, usually between 90-105 minutes. Proteins were then transferred from the gels onto methanol pre-soaked PVDF membranes (Sigma-Aldrich, UK) via wet transfer. This was ran in transfer buffer (Table 2.4) at 90 V for ~90 minutes, on ice. Following the transfer process, the membranes were soaked in Ponceau S solution (Sigma-Aldrich, UK, P7170) to confirm that protein transfer was successful. Upon confirmation, the membranes were washed using washing buffer (Table 2.4) until all the staining was removed and blocked by incubating in blocking solution (Table 2.4) for 1 hour at room temperature, on a rocker (75 rpm). The membranes were then incubated overnight in

primary antibody (Table 2.3) at 4 ℃, on a roller (30 rpm). Primary antibodies were diluted in blocking solution (Table 2.4).

The next day, the membranes were washed three times in washing buffer (Table 2.4) for 10 minutes each, shaking at 75 rpm. Following washing, the membranes were incubated in secondary antibody (Table 2.3) for 1 hour at room temperature, on a roller (30 rpm). Secondary antibodies were diluted in blocking solution (Table 2.4). The membranes were then washed three times in washing buffer (Table 2.4) for 10 minutes each, shaking at 75 rpm. During the final wash, the enhanced chemiluminescence (ECL) mix (Table 2.4) was prepared. The membranes were visualized using the gel documentation system and GeneSys software. Images were exported and saved for densitometry analysis. In some instances, once the membranes have been visualized, they were washed three times in washing buffer (Table 2.4) for 10 minutes each, shaking at 75 rpm, and re-probed with a housekeeping gene antibody (Table 2.3) as described above. This served as a loading control. Densitometry analysis was performed using the Fiji software (Image J2) version 2.15.0 (https://imagej.net/software/fiji/).

2.7.4 Mass spectrometry

Lysates prepared from SH-SY5Y cells (50 µg protein) were purified and digested (Trypsin) using Protifi S-Trap Micro Spin columns. See sections 2.7.1 and 2.7.2 for details on sample preparation. Digested peptides were re-suspended to a final concentration of 5% (v/v) acetonitrile in 0.1% (v/v) formic acid (Fluka Analytical, Buchs, Switzerland) for liquid chromatography separation using an Eksegent expert nano LC 452 upstream of a Sciex TripleTOF 6600 mass spectrometer. Samples (4 µl) were injected and separated on a YMC Triart-C18 pre-column (5 mm, 3 µm, 300 µm ID) at a flow rate of 10uL/min and 57 min gradient elution. Acquisitions were made both in data dependent (IDA) as well as independent (SWATH) manners. Raw data was searched against Swissprot export of the human proteome June 2021 using DIANN.

2.7.5 Proteome profiler array analysis

2 ml of Array Buffer 6 (Table 2.6) was pipetted into each well of the 4-well multi-dish containers provided. A membrane was then placed into each well, the dishes covered and the membranes incubated for 1 hour on a rocker. This served to block the membranes. During membrane blocking, samples were prepared by adding the required volume of each sample (maximum 1 ml) to 0.5 ml of Array Buffer 4 (Table 2.6), in separate tubes. The content of each tube was then adjusted to a final volume of 1.5 ml using Array Buffer 6 (Table 2.6). Following this, 15 µl of reconstituted detection antibody cocktail (Table 2.6) was added to each sample, the samples mixed well and incubated for 1 hour at room temperature. Once incubation was complete, Array Buffer 6 (Table 2.6) was removed from each well of the 4-well multi-dish containers, the prepared sample/antibody mixtures added onto the membranes and the dishes covered. These were then incubated overnight at 4 ℃, on a rocker.

The next day, the membranes were washed three times in 1X Wash Buffer (Table 2.6) for 10 minutes each, shaking at 64 rpm. Following washing, the membranes were incubated in Streptavidin-HRP (Table 2.6) for 30 minutes at room temperature, on a shaker. The membranes were then washed three times in 1X Wash Buffer (Table 2.6) for 10 minutes each, shaking at 64 rpm. Excess wash buffer was removed from each membrane before they were placed on the bottom sheet of the plastic sheet protector. Chemi Reagent Mix (Table 2.6) was prepared and 1 ml was pipetted onto each membrane. The membranes were then covered with the top sheet of plastic sheet protector, air bubbles removed and membranes incubated for 1 minute. Following incubation, the top plastic sheet protector was removed, excess Chemi Reagent Mix blotted off and the membranes covered with plastic wrap. The membranes were then visualized using the gel documentation system and GeneSys software. Images were exported and saved for densitometry analysis. Densitometry analysis was performed using the Fiji software (Image J2) version 2.15.0 (https://imagej.net/software/fiji/).

2.8 Calcium activity assay

TRPV1 activity in DRG cell cultures was measured using the Fluo-4 Direct calcium assay kit (Intvitrogen, US). Prior to the assay, cells were seeded to a minimum of 2000 cells/well in a flat-bottom 96 well plate. Cells were treated for 24 hours, in a total

volume of 100 µl. 2X Fluo-4 Direct calcium reagent loading solution was prepared by adding 10 ml of Fluo-4 Direct calcium assay buffer and 200 µl of 250 mM probenecid stock solution to one bottle of Fluo-4 Direct calcium reagent. Any remaining solution was stored at -20 ℃ for future use. From each well, 60 µl of

Table 2.5 Gel composition of prepared gels for Western blotting

Type of gel	Gel Composition	Supplier (Product Code)
Resolving gel (10 %)	30 % Bis-acrylamide	Sigma-Aldrich, UK (A3699)
	Resolving Buffer (1.5M Tris, 0.4 % SDS, pH 8.8)	National Diagnostics (NAT1268)
	10% Sodium Dodecyl Sulfate (SDS)	Fisher Scientific, UK (BP166)
	10% Ammonium persulphate (APS)	Thermo Scientific, UK (17874)
	Tetramethyl ethylenediamine (TEMED)	Sigma-Aldrich, UK (T9281)
	Distilled water	N/A
Stacking gel (4 %)	30 % Bis-acrylamide	Sigma-Aldrich, UK (A3699)
	Stacking Buffer (0.5M Tris, 0.4 % SDS, pH 6.8)	National Diagnostics (NAT1270)
	10% Sodium Dodecyl Sulfate (SDS)	Fisher Scientific, UK (BP166)
	10% Ammonium persulphate (APS)	Thermo Scientific, UK (17874)
	Tetramethyl ethylenediamine (TEMED)	Sigma-Aldrich, UK (T9281)
	Distilled water	N/A

medium was removed, leaving 40 µl. To each well, 2X Fluo-4 Direct calcium reagent loading solution was added and the plate incubated for 1 hour at 37 ℃, 5 % CO_2. During incubation, the agonist (capsaicin) was prepared at 5X concentration in a new flat-bottom 96 well plate. Following incubation, fluorescent readings before and after the addition of capsaicin were measured using the Tecan plate reader Infinite 200Pro, which was pre-heated to 37 ℃. Wavelength settings selected were 488 nm excitation

and 516 nm emission. Before the addition of capsaicin, baseline fluorescence readings were taken. 20 µl of capsaicin was then added to all treatment groups, down column 1, and fluorescence responses at 10 second intervals over a 300 second time period were immediately measured. Hence the baseline fluorescence reading would be at t=0 and the first reading following capsaicin stimulation would be at t=10. This process was repeated across the columns of the plate for 6-8 repeats. A multichannel pipette was used to ensure that all treatment groups were measured simultaneously. Precaution was taken not to disturb the cells or introduce air bubbles when adding capsaicin.

Table 2.6 List of reagents used for proteome profiler array analysis

Solution	Composition	Supplier (Product Code)
Array buffer 4	Buffered protein base with preservatives	R&D Systems, UK (895022)
Array buffer 6	Buffered protein base with preservatives	R&D Systems, UK (893573)
Wash buffer	25X concentrated solution of buffered surfactant with preservative. Diluted to 1X using distilled water	R&D Systems, UK (895003)
Detection antibody cocktail	Biotinylated antibody cocktail. Reconstituted with 100 µl distilled water	R&D Systems, UK (893560)
Streptavidin-HRP	Streptavidin conjugated to horseradish-peroxidase. Diluted in Array buffer 6	R&D Systems, UK (893019)
Chemi reagent mix	Equal volumes of Chemi Reagent 1 and Chemi Reagent 2	R&D Systems, UK (894287, 894288)

2.9 Statistical analysis

For cell viability assays, the average absorbance reading was calculated for each treatment group and that of the blank control was subtracted from all treatment groups to account for background absorbance. All average absorbance readings were then normalized to that of the vehicle control, as a percentage, and plotted using GraphPad Prism v9.0. Standard curve plots for total protein concentration were generated in Microsoft Excel by plotting absorbance against concentration (mg/ml) and drawing a

line of best fit. The protein concentration of each sample was determined by substituting its absorbance value into the equation of the line of best fit.

Images obtain from immunofluorescence, Western blotting and proteome profiler array experiments were analyzed using the Fiji software (Image J2) version 2.15.0 (https://imagej.net/software/fiji/) and the data exported to GraphPad Prism v9.0. For densitometry analysis of Western blots, a box was first drawn around each band. The software measures the density of the band and subtracts the local background, producing a peak. For each experimental run, the area under the peaks for each treatment group was calculated and expressed as a percentage of the total size of all the peaks in that run. These values were used as the band intensities. The band intensity of the target protein was divided by that of the loading control, β-actin, thereby normalizing protein expression levels. For phosphorylated proteins, this normalized expression level was then expressed relative to that of the total. For densitometry analysis of proteome profiler array spots, a box was first drawn around each pair of duplicate spot representing each cytokine. Similar to Western blotting analysis, the area under each peak generated was calculated and these values were used as the spot intensities. The intensities for each cytokine pair was averaged and average intensity of the negative control spot (PBS) was subtracted from that of all the other cytokine spots.

For the calcium assays, all fluorescence readings were exported into Microsoft Excel. The lowest fluorescence reading was selected as the background reading and subtracted from all other fluorescence readings. For each run, the time course fluorescence readings following the addition of capsaicin (t=10 until t=300) were divided by their own respective baseline fluorescence reading to give a fold change of capsaicin-induced calcium fluorescence intensity (F/F_0). Using GraphPad Prism v9.0, the mean fold change for each treatment group was plotted against time. The measure of TRPV1 activity was interpreted as the area under the curve (AUC) of this time course.

GraphPad Prism v9.0 was used for the plotting of graphs and statistical analyses. The error bars on graphs were presented as mean ± standard error of the mean (SEM). The n value represented the number of individual animals or individual cultures in a treatment group. Comparisons between groups were done using either a t-test (compares the means of two groups), a one-way ANOVA (compares multiple groups

with only one variable e.g. treatment) or a two-way ANOVA (compares multiple groups with only one variable e.g. treatment over time). For multiple comparisons, the Bonferroni method calculated adjusted p-values, which were used to determine statistical significance as follows: $p < 0.05$ (*), $p < 0.01$ (**), $p < 0.001$(***) and $p < 0.0001$(****).

For mass spectrometry, differentially expressed genes (DEGs) were selected using a fold change (FC) of 1 (i.e. $\log2FC \geq 0$) and an adjusted $P < 0.05$. A clustergram was generated in MATLAB.

Chapter 3: Characterization of the cisplatin model for cisplatin-induced peripheral neuropathy in childhood cancer survivors

3.1 Introduction

Cisplatin induces peripheral sensory neurotoxicity [138–141] by binding to the DNA of dorsal root ganglia sensory neurons (DRGs) and forming cisplatin-DNA adducts [143, 148, 152–155]. This in turn damages the DNA and eventually results in neuronal apoptosis [134, 138, 158]. DRGs and peripheral sensory nerves, which relay sensory neural messages from the periphery to the central nervous system, have increased susceptibility to cisplatin [136, 138, 159, 149, 160–164], allowing for its accumulation in these tissues [136, 159–161, 163, 164]. Therefore CIPN associated with cisplatin is characterized as a peripheral neuropathy that includes predominantly sensory neuropathy [131, 133, 148, 162, 168–170], as well as motor and autonomic neuropathies [133, 169, 171, 172]. CIPN is a common side effect of cancer treatment in both adult [127, 233, 234] and paediatric [235–238] patients. However, fewer studies have explored the underpinning mechanistic causation of paediatric CIPN.

3.1.1 Clinical aspects of CIPN

Common symptoms of sensory neuropathy include numbness, tingling in the hands and feet which progresses in a "glove and stocking" distribution to the wrists and ankles, and chronic pain [132, 137, 142, 143, 244, 357, 358]. A "coasting" phenomenon is observed exclusively in platinum-based chemotherapy, particularly cisplatin, whereby neuropathic symptoms worsen for weeks or months following cessation of therapy [131, 143, 148, 225, 244, 357]. In relation to paediatric patients, these individuals present symptoms that tend to persist into adulthood, with sensory and motor neuropathy, pain and functional impairments being observed in adults who survived children cancers [170, 235, 237, 239, 240]. These individuals were compared with their siblings, who served as controls. Childhood cancer survivors have shown to display symptoms of CIPN >7 years post treatment [359, 360]. A clinical follow-up study to evaluate the adverse late effects of early exposure to chemotherapy (median age at diagnosis 5 years) was conducted in adult survivors (median age 32 years) of childhood cancer (extracranial solid tumours), who were at least 10 years

post-diagnosis [170]. Sensory impairment was assessed using the sensory subscale of the Total Neuropathy Score and the prevalence of sensory impairment was evidenced by a score of ≥1. The study found that in the patients who were treated with cisplatin, 20 % of the survivors had sensory impairment a median of 25 years from diagnosis. Despite this known clinical phenomenon, little is known about how these cytotoxic agents impact the developing human and in particular the somatosensory nervous system.

As mentioned, chronic pain is a typical adverse effect of CIPN which develops as a consequence to peripheral sensory neuron damage [127, 169, 237, 242, 361–366]. Pain was reported by ~50 % of childhood cancer survivors [237, 240], which they attributed as an adverse side effect of their cancer treatment. Additionally, the younger the age of exposure to chemotherapy, the greater the severity [237]. A diagnostic age of ≤3 years was associated with a higher risk of reporting pain conditions compared to a diagnostic age of 4-20 years. This pain can presents as allodynia or hyperalgesia [246, 367]. Allodynia is pain due to a stimulus that does not normally provoke pain whereas hyperalgesia (sometimes referred to as hypersensitivity) is an increased sensitivity to a painful stimulus. Furthermore, following cisplatin treatment, patients have experienced nerve conduction velocity (NCV) changes [358, 368–371], exhibiting decreased sensory NCV and reduced sensory action potential (SAP) amplitude along the nerves. Axonal degeneration, evident by loss of nerve fibres alongside secondary damage to myelin sheath, have been demonstrated from nerve biopsies [136, 164, 371, 372], possibly accounting for these NCV alterations.

Childhood cancer survivors affected by CIPN also suffer from increasingly apparent quality of life (QOL) issues that present later in life [239, 360, 373, 374]. CIPN has been known to cause fatigue, cognitive and psychological impairment as well as negative social outcomes, which will impact upon education and work as these children develop. The prevalence of a chronic condition in childhood cancer survivors who were 5-14 years post diagnosis was 68 % [360]. This increased with increasing age to 77 % at 15-24 years post diagnosis, 85 % at 25-36 years post diagnosis and 88 % at 40-49 years post diagnosis, respectively. In addition, other symptoms which have been described include paresthesia, muscle cramps and distal weakness as well as constipation, orthostatic hypotension and urinary retention [131–133, 143]. However, no standardized measurement for the assessment of CIPN exists [375–377], resulting

in a variety of objective clinical-rated tools and subjective patient-reported outcome scales being utilized. Evaluation of these tools and scales have revealed a significant discrepancy between the clinician-based and patient-reported measures, with clinicians often underestimating the severity of the patient experience [377, 378]. Furthermore, there was low correlation among scales that currently used to measure CIPN as well as issues with validity, reliability, sensitivity and reproducibility [376, 377, 379]

3.1.2 Preclinical models of CIPN

Rodent models are used to explore the underlying mechanisms attributed to CIPN. These include models that mirror adult and childhood associated CIPN, with adult and neonatal rodents. These approaches consist of interventions that consider clinical scenarios [322, 323]. One major issue is the disparities which remain across the literature with differing dosing regimens presented [323]. CIPN is a dose-limiting side effect, which occurs in a dose-dependent and time-dependent manner [148, 324]. The severity of CIPN increases with higher cumulative doses and longer times of exposure to cisplatin [161, 224]. Dosing schedules utilized include either a single administration of the agent [325] or multiple doses per week, over a duration of one or several weeks [326–330]. This has resulted in cumulative doses of cisplatin ranging from (2-23 mg/kg).

One of the hallmarks of CIPN is peripheral sensory neurodegeneration, which includes intraepidermal nerve fibre (IENF) degeneration [332–334]. Cisplatin treatment, in both rodent models and cell lines, has shown to result in neurodegeneration [333, 334, 340, 335, 338, 380]. For one in vitro study [335], 50B11 cells (embryonic rat DRG neuronal cell line) treated with 2-10 µg/ml cisplatin exhibited decreased neurite growth, with a reduction in total growth per cell and a decrease in the percentage of cells demonstrating neuritogenesis. In another study using DRG explants from rats and different strains of mice [338], cisplatin treatment inhibited neurite outgrowth in a dose-dependent in all DRGs. A similar effect of reduced neurite length following cisplatin treatment was observed in both PC12 cells (rat pheochromocytoma cell line) and rat DRG neurons [380]. In rodent models that were administered cisplatin over a period of 3 weeks (cumulative dose ranging from 12-23 mg/kg) [333–335], plantar skin was collected and IENF examined. There was evidence to suggest a reduction in

PGP9.5+ve IENF in the cisplatin-treated cohort compared to the vehicle control. To explore nociceptors, researchers have studied the effect of cisplatin treatment on CGRP+ve IENFs [340, 341]. The data also suggested a reduction following cisplatin treatment.

In addition, rodents exposed to chemotherapeutic agents typically display increased sensitivity to mechanical stimuli following cisplatin treatment [325, 326, 328–330, 342–344, 331, 345–349], either as mechanical allodynia or mechanical hyperalgesia. The rodent models mentioned above [333–335, 340] were all subjected to pain behaviour tests prior to tissue removal. This involved the application of a pin-prick to the hind paw and measurement of withdrawal threshold. Cisplatin treatment resulted in either mechanical allodynia [333–335] or mechanical hyperalgesia [340], evident by a decrease in the withdrawal threshold of the rodents. Additionally, thermal hyperalgesia [335, 340], increased sensitivity to heat, is common and was observed in the cisplatin-treated groups compared to the controls. However, there has been conflicting views with regards to whether cisplatin results in thermal hyperalgesia [325, 328, 347] or not [326, 343, 346]. Comparing the experiments, different methods of drug administration (intravenous vs intraperitoneal) as well as dosing regimens (cumulative dose ranging from 2-23 mg/kg) were utilized. It is uncertain whether this contributed to the difference in results obtained, illustrating the importance of standardization when performing these assessments.

3.1.3 DNA damage

As mentioned above, the primary neural tissue affected by the platinum based chemotherapy agents is the DRG [148–151]. It has been shown that the formation of cisplatin-DNA cross-links structurally distorts the DNA [156] and unwinds it [157]. This in turn interferes with its normal functioning, including DNA replication and transcription, essential processes for neuronal survival and function. It has also been suggested that other contributing factors of cisplatin-induced neurotoxicity include oxidative stress, mitochondrial dysfunction and changes in Ca^{2+} homeostasis [163, 173, 174]. Cisplatin also binds to mitochondrial DNA (mDNA) in DRG neurons [150], forming cisplatin-mDNA adducts, impairing mitochondrial DNA replication and transcription and resulting in morphological changes in the mitochondria [150, 176] as well as alterations in protein synthesis and disruption of the electron transport

chain [174, 177, 178]. Neuronal mitochondrial damage leads to cellular adenosine triphosphate (ATP) depletion and increased production of reactive oxygen species (ROS), which in turn can cause oxidative DNA damage [150, 158, 179, 180]. All these events lead to mitochondrial membrane depolarization, increased intracellular Ca^{2+} levels and activation of apoptotic pathways [150, 176, 181, 182] alongside increased production of pro-inflammatory mediators [175].

Cisplatin treatment has been shown to cause an increase in the number of cleaved caspase-3 positive (CC3+ve) neurons, both in cisplatin-treated cells [335] as well as DRGs extracted from cisplatin-treated rodents [340]. However, despite this increased expression of CC3, a marker of apoptosis (programmed cell death), following cisplatin treatment, there was no effect on DRG cell populations [340]. In response to DNA damage and DNA replication stress, ataxia-telangiectasia mutated (ATM) and ataxia-telangiectasia and RAD3-related (ATR) are activated [287–289]. These protein kinases are key regulators of the DNA damage response (DDR), a complex signalling pathway which allows for the detection and repair of damaged DNA. When ATM and ATR are activated, this initiates the DDR and results in the phosphorylation of a spectrum of substrates [288, 290, 291]. Two of these substrates include p53 [292, 293] and histone H2A.X [294, 295], hence they are often utilized as markers of DNA damage.

In normal cells, the protein level of p53 is low, due to Mdm2; the major regulator of p53 which is responsible for its degradation [296, 297]. Following peripheral nerve injury, p53 protein levels have been demonstrated to increase [298, 299]. Phosphorylation of p53 inhibits the binding of Mdm2 and thereby results in its stabilization, by preventing its degradation [300]. In response to double-strand breaks (DSB), H2A.X is phosphorylated at serine-139 to form γH2A.X, accounting for the increased expression levels of γH2A.X observed following DNA damage [294, 301–304]. γH2A.X then serves as a platform for the accumulation and retention of the numerous coordinators of DDR signalling [305–316].

3.1.4 Hypothesis

Early life exposure to cisplatin induces DNA damage, leading to neurodegeneration of the peripheral sensory nerve fibres and subsequent disruption in the normal

development of nociceptive pathways. Approaching adulthood, chronic pain ensues in the form of pain hypersensitivity. This delayed onset of chronic pain is characteristic of the CIPN which develops in childhood cancer survivors following cisplatin treatment.

Specific Hypotheses

5) Cisplatin treatment is cytotoxic, resulting in sensory neuronal degeneration and cell death.
6) Damage to the peripheral sensory neurons following early life exposure to cisplatin causes a delayed onset of chronic pain, depicted by increased sensitivity to pain.
7) Cisplatin treatment induces a DNA damage response.

Experimental aims

1) To assess the cytotoxicity of cisplatin and determine an effective dosing concentration.
2) To develop an in vitro model of CIPN and utilize it to validate that cisplatin treatment results in neurodegenerative and induces a DNA damage response.
3) To develop an in vivo model of CIPN and utilize it to validate that early life exposure to cisplatin causes a delayed onset of chronic pain.

3.2 Method

3.2.1 Cisplatin induction and behavioural testing

Neonatal Wistar Hans rats (weaned at P21, see chapter 2 for animal details) were injected twice on non-consecutive days with cisplatin (0.1mg/kg, i.p., n=4) at Postnatal day (P) 14 and 16). An additional cohort of age-matched rats was injected with PBS (i.p., n=3) and were used as vehicle controls. Mechanical withdrawal thresholds (using von Frey monofilament hairs test) were measured as described in Section 2.2.2. Testing was performed pre-dosing to obtain a baseline value, 24 hours post-dosing and then twice a week for 3 weeks.

3.2.2 Immunocytochemistry of DRG culture

DRGs were extracted from neonatal (P7) C57/BL6J mice and cultured on coverslips in 24-well plates (see Sections 2.4.3.1 and 2.4.3.2 for full details). After 6 days, the cultures were treated with varying concentrations of cisplatin (0, 5, 10 and 20 µg/ml) for 24 hours. Immunofluorescence staining was then performed using primary antibodies targeted to Beta (β)3-tubulin and cleaved caspase-3 (CC3) and suitable secondary antibodies, Alexa Fluor 488 Goat anti-Guinea Pig and Alexa Fluor 555 Donkey anti-Rabbit, respectively (see Section 2.5.1 for immunofluorescence and antibody details). Cells were additionally incubated in a nuclear stain DAPI. DRG neurons were visualized using the EVOS M7000™ Imaging System microscope (ThermoFisher Scientific; USA) and images obtained were processed and analysed using the Fiji software (Image J2) version 2.15.0 (https://imagej.net/software/fiji/). Neurite length was measured using the Neurite Tracer plugin (https://imagej.net/plugins/snt/). Cells were selected at random and the free hand drawing tool was used to trace along the lengths of neurites (stained by β3-tubulin).

3.2.3 Cell viability

SH-SY5Y cells were cultured as described in Section 2.4.1 and treated the following day with varying concentrations of cisplatin (0, 0.1, 1, 2, 5 and 10 µg/ml) for 24 hours. A cell viability assay was performed using Cell Proliferation Reagent WST-1 (see Section 2.6 for full details).

3.2.4 Western blotting

Protein was extracted from SH-SY5Y cells treated with varying concentrations of cisplatin (0, 1, 2 and 5 μg/ml) and quantified using the Bradford assay (see Sections 2.7.1 and 2.7.2 for full details). Western blotting was performed for determining protein expression of p53, phospho-p53 (P-p53) and γH2A.X (see Section 2.7.3 for protocol and antibody details). The housekeeping protein, β-actin, was used as the loading control. For p53 and P-p53, 30 μg of protein was loaded into each well and for γH2A.X, 50 μg of protein was loaded into each well. The protein expression levels of all target proteins were normalized to that of β-actin. For P-p53, this normalized expression level was then expressed relative to that of total p53. All graphs were plotted using GraphPad Prism v9.0. A one-way ANOVA was performed for the analysis of p53 and P-p53 expression levels whereas a t-test was performed for the analysis of γH2A.X expression level.

3.2.5 Data analysis

For the behavioural test, withdrawal threshold (g) was plotted against time (Postnatal Day) using GraphPad Prism v9.0 and analysis performed using a two-way ANOVA, compared to the vehicle control.

For immunofluorescence of the DRG cell culture, the neurite lengths obtained for each cisplatin concentration were averaged and a graph plotted using GraphPad Prism v9.0. Analysis was performed using a one-way ANOVA, compared to the control (0 μg/ml). Prior to any measurements being done, the scale bar was calibrated to a known length. For immunohistochemistry of plantar tissue, IENF density was determined by counting the number of nerve fibres per 1000 μm, for a minimum of three randomly selected areas, for each treatment group. A branch-point was denoted by a "V" shape. The number of branch-points per 1000 μm was counted. For each result, a graph was plotted using GraphPad Prism v9.0. Analysis was performed using a one-way ANOVA, compared to the control.

For cell viability, a graph of Cell Viability (%) versus Cisplatin Concentration (μg/ml) was plotted using GraphPad Prism v9.0 and analysis performed using a one-way ANOVA, compared to the control (0 μg/ml).

For Western blotting, graphs of protein expression level versus cisplatin concentration (μg/ml) were plotted. GraphPad Prism v9.0 was used to plot all graphs. Analysis of p53 and P-p53 expression levels were performed using a one-way ANOVA, whereas a t-test was implemented for γH2A.X expression level; all comparisons were done to the control (0 μg/ml).

3.3 Results

3.3.1 Cisplatin results in increased mechanical sensitivity

There was a significant effect of treatment on the development of mechanical hypersensitivity [F (1,22) = 70.92, p < .0001]. As previously demonstrated [340], administration of cisplatin in neonatal rats resulted in a delayed onset of mechanical hypersensitivity, which was observed from P23 (**p<0.01) and continued until the end of the experiment at P38 (****p<0.0001) (Figure 3.1). The cisplatin-treated rats experienced a significant decrease in mechanical withdrawal threshold compared to the vehicle controls (P23 vehicle 31.667±5.667 g vs cisplatin 11.667±1.054 g **p<0.01; P25 vehicle 37.333±7.168 g vs cisplatin 12.333±0.919 g ****p<0.0001; P28 vehicle 31.667±5.667 g vs cisplatin 14.167±0.833g **p<0.01; P30 vehicle 37.333±7.168 g vs cisplatin 11.333±1.202 g ****p<0.0001; P35 vehicle 31.667±5.667 g vs cisplatin 10.167±1.046 g ***p<0.001; P38 vehicle 37.333±7.168 g vs cisplatin 11.667±1.054 g ****p<0.0001).

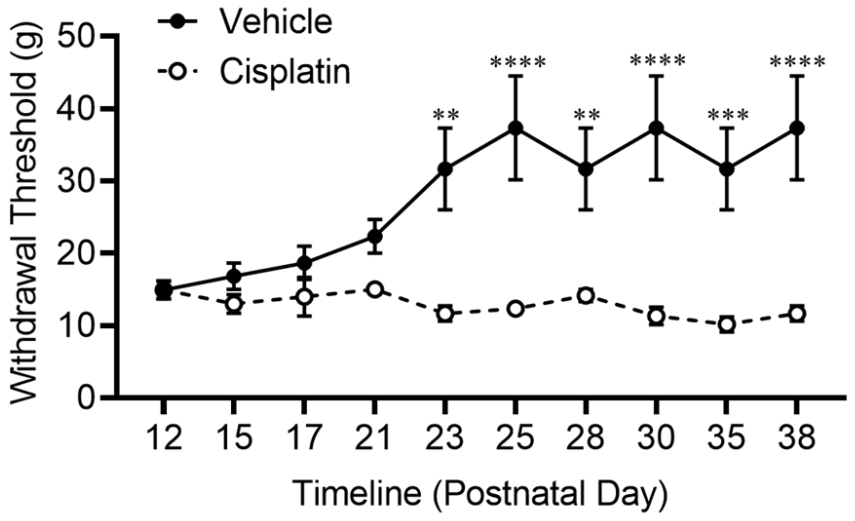

Figure 3.1 Cisplatin results in increased mechanical sensitivity. Neonatal Wistar rats (~30g) were intraperitoneal injected with cisplatin (0.1mg/kg) at Postnatal day (P) 14 and 16. Increased mechanical allodynia was observed from P23 until the end of experiment at P38. **p < 0.01, ***p < 0.001 and ****p < 0.0001, Two-way ANOVA compared to vehicle group; n = 3 for vehicle and n = 4 for cisplatin. Error bars are mean ± SEM.

3.3.2 Cisplatin causes sensory neuronal degeneration in vitro

Treatment also had significant effects on both neurite length [F (3,177) = 4.008, p < .01] and cell viability [F (5, 48) = 9.056, p < .0001]. DRG sensory neurons, which were isolated, cultured and treated for 24 hours with varying concentrations of cisplatin, showed a decrease in neurite outgrowth following cisplatin treatment when compared to the vehicle control (vehicle 135.97±12.827 g; 10 µg/ml cisplatin 99.582±8.841 g, *p<0.05; 20 µg/ml cisplatin 99.901±7.026 g, *p<0.05). (Figure 3.2A-E). There was no effect observed on average neurite length following treatment with 5 µg/ml of cisplatin (control 135.97±12.827 g vs. 5 µg/ml cisplatin 138.572±15.322 g). No CC3 staining was detected.

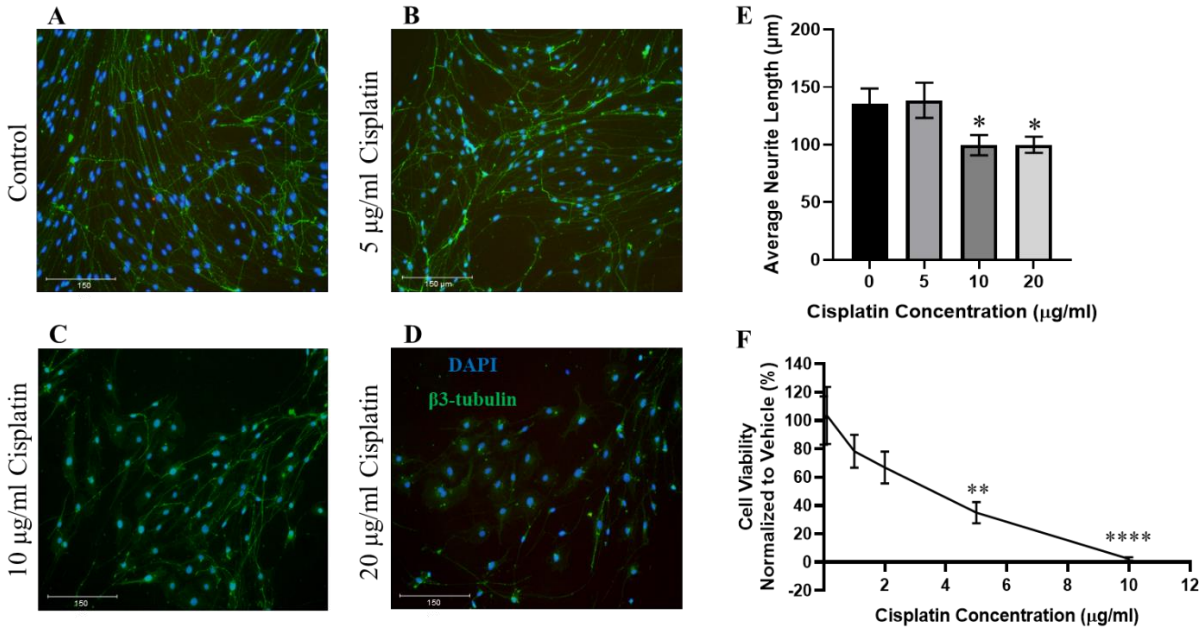

Figure 3.2 Cisplatin causes sensory neuronal degeneration. Dorsal root ganglia (DRGs) from neonatal mice (P7) were isolated, enzymatically dissociated, seeded and allowed to grow for 6 days. The cultures were then treated with varying concentrations of cisplatin (0, 5, 10 and 20 µg/ml) for 24 hours and immunocytochemistry performed using the neuronal-specific marker, β3-tubulin and apoptotic marker, cleaved caspase 3 (CC3). Representative images [A-D] and quantification of neurite length [E] showed that as cisplatin concentration increased, there was a decrease in neurite outgrowth. *p < 0.05, one-way ANOVA compared to control (0 µg/ml). Scale bar = 150 µm. Error bars are mean ± SEM. No CC3 staining was observed. SH-SY5Y cells, seeded at ~3 x 10^4 cells per well, were treated the following day with varying concentrations of cisplatin (0, 0.1, 1, 2, 5 and 10µg/ml) for 24 hours and a cell viability assay performed using Cell Proliferation Reagent WST-1 [F]. Similarly, there was a decrease in cell viability with increasing concentration of cisplatin. **p < 0.01 and ****p < 0.0001, one-way ANOVA compared to control (0 µg/ml); n = 3. Error bars are mean ± SEM.

The human neuroblastoma cell line, SH-SY5Y, exhibited a decline in cell viability following 24-hours treatment with increasing concentrations of cisplatin (Figure 3.2F). In a dose-dependent manner, cell viability was reduced following 24-hours treatment with 5 µg/ml cisplatin (34.956±7.57 % cell viability, **p<0.01) and 10 µg/ml cisplatin (2.395±1.212 % cell viability, ****p<0.0001).

3.3.3 Cisplatin induces the DNA damage response (DDR) in neurons

Cisplatin had significant effects on both p53 [F (3, 12) = 7.529, p < .01] and P-p53 [F (3, 12) = 3.412, p < .01] expression levels. 24-hours treatment with 5 µg/ml cisplatin induced DNA damage response in SH-SY5Y cells (Figure 3.3A-C). There was a dose-dependent increase in both p53 and P-p53 expression levels, with significant increase following treatment with 5 µg/ml cisplatin, when compared to the vehicle control (p53 = 361.312±121.7 **p<0.01; P-p53 = 263.956±140.181 **p<0.01). Additionally, 24-hours treatment with 5 µg/ml cisplatin led to a significant increase in γH2A.X expression level (271.276±224.795 ***p<0.001), compared to the vehicle control (Figure 3.3D).

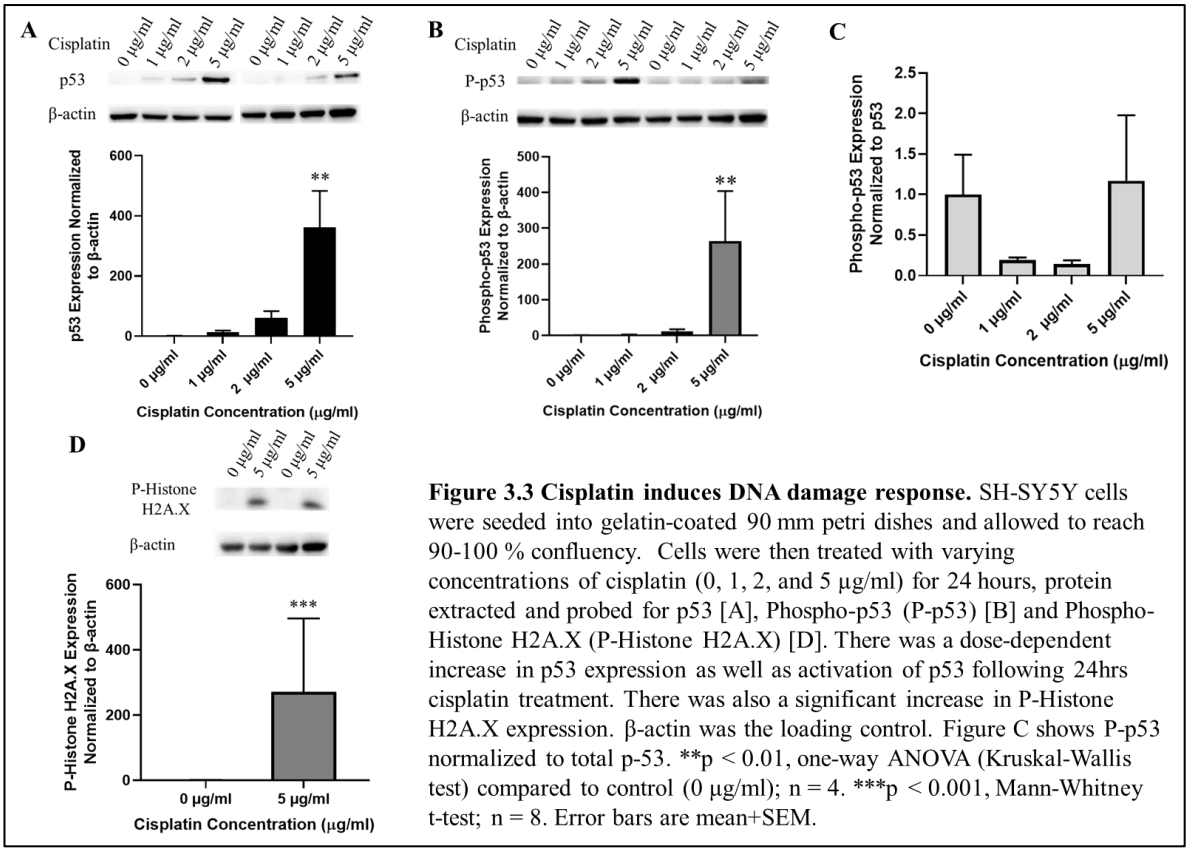

Figure 3.3 Cisplatin induces DNA damage response. SH-SY5Y cells were seeded into gelatin-coated 90 mm petri dishes and allowed to reach 90-100 % confluency. Cells were then treated with varying concentrations of cisplatin (0, 1, 2, and 5 µg/ml) for 24 hours, protein extracted and probed for p53 [A], Phospho-p53 (P-p53) [B] and Phospho-Histone H2A.X (P-Histone H2A.X) [D]. There was a dose-dependent increase in p53 expression as well as activation of p53 following 24hrs cisplatin treatment. There was also a significant increase in P-Histone H2A.X expression. β-actin was the loading control. Figure C shows P-p53 normalized to total p-53. **p < 0.01, one-way ANOVA (Kruskal-Wallis test) compared to control (0 µg/ml); n = 4. ***p < 0.001, Mann-Whitney t-test; n = 8. Error bars are mean+SEM.

3.4 Discussion

Early life treatment with cisplatin results in alterations in nociceptive behavioural withdrawal responses in rodents, comparative to those clinical signs described by adult survivors of childhood cancer. Neonatal exposure to cisplatin leads to a prominent remodelling of the peripheral sensory nervous system, depicted by alterations in sensory neuritogenesis and IENF innervation. This remodelling occurs in conjunction to a prominent cisplatin-induced DNA damage response, implicating this pathway in the development of cisplatin-induced sensory neuropathy.

3.4.1 Preclinical models of CIPN

As highlighted in the clinic, young patients are exposed to cytotoxic agents that include the outlined chemotherapeutic agents. Young individuals are growing at an enormous rate, which includes the developing sensory nervous system. Studies have shown that pain and nerve injury early in life, both in rodents and humans, causes long-term changes to a developing somatosensory and pain systems [29, 98, 99]. As a result, neuropathic pain is rarely observed in children before adolescence, however, neonatal injury tends to trigger neuropathic pain in adults [101, 381, 382], accounting for this delayed and long-lasting pain phenotype observed following early life exposure to chemotherapy. A correlation between the incidence of neuropathic pain and the age at which nerve damage occurred was also observed [382]. According to the Childhood Cancer Survivor Study (CCSS) [383], a large multi-institutional cohort study of 5-year survivors of childhood and adolescent cancer, the age of diagnosis which contained the highest number of participants was 1-3 years. In our rodent model, dosing commenced at P14, which is equivalent to a human age of 1 month - 2 years [384–386], making our model comparable for the evaluation of CIPN associated with early life exposure to chemotherapy. In our preclinical cisplatin model, we also demonstrated a persistent, but delayed onset of chronic pain following early life exposure to cisplatin, complementing these clinical studies as well as exhibiting the "coasting" phenomenon that has been reported to be observed exclusively in platinum-based chemotherapy [131, 143, 148, 225, 244, 357]. Research has also illustrated this coasting phenomenon in adult cancer patients whereby adult survivors of testicular cancer have experienced peripheral neuropathy which persisted longer than 10 years after cisplatin treatment [387, 388].

In our model, rodents exposed to cisplatin early in life developed mechanical hypersensitivity. This increased sensitivity to mechanical stimuli was evident by a decrease in withdrawal threshold when compared to the vehicle control. These findings coincide with that of numerous other researchers whose rodent models also demonstrated delayed onset of mechanical hypersensitivity subsequent to cisplatin treatment, despite differences in species of rodents (rats [329, 330, 343, 348, 349] versus mice [327, 331, 344, 346, 389]), age (neonatal [340] versus adult [325, 326, 328, 335]), method of dosing (intraperitoneal [326, 328, 331, 343, 344, 389] versus intravenous [325]) as well as dosing size and regimen (cumulative doses <5 mg/kg [325, 348] versus 5-15 mg/kg [327, 330, 335, 340, 346, 349] versus >15 mg/kg [328, 329, 331, 389]). In our rodent model, a small cumulative dose of 0.2 mg/kg, administered as two intraperitoneal injections of 0.1 mg/kg each, was sufficient to produce a similar effect as the larger doses reported. In a similar experiment performed using neonatal rats [340], whereby cisplatin was administered as five intraperitoneal injections of 1 mg/kg, given from P7, for five consecutive days (cumulative dose 5 mg/kg), the mechanical hypersensitivity which developed was delayed until P22. In our model, even though a lower dose of cisplatin was administered and dosing began at a later age (P14), mechanical hypersensitivity was also delayed until P23. Additionally, there was no difference in body weight between the control animals and the cisplatin-treated animals, meaning that our rodents did not lose weight following treatment. The cisplatin dose that was administered here (human equivalent dose 0.912 mg/m^2 [390]) is much lower than that which is typically given in a clinical setting (mean dose of 429.4 mg/m^2) [170], however, the welfare of the rodents has to be taken into consideration. Due to the difference in body size between rodents and humans, the dosing needs to be more appropriate for the rodents. When it comes to administering cytotoxic agents to animals, animal welfare requires monitoring through clinical signs including body weight. A loss in body weight greater than a certain criterion will require the experiment to be terminated and the animals killed [391]. Therefore, it is crucial to use the most appropriate drug regimen to induce the expected phenotypes whilst bearing in mind those welfare considerations. Here, we were able to develop a suitable CIPN model for childhood chemotherapy whereby sensory neuropathy was induced with the administration of a lower dose of cisplatin, thereby sustaining the welfare of the rodents utilized in this study. However, this has to be taken into account when it comes to translatability. The typical higher doses that are

administered in the clinic would be of greater toxicity and hence result in more severe symptoms.

In the clinic, cumulative doses of chemotherapy administered to children vary greatly between patients [170, 383]. As seen in a study performed by Ness et al. [170], cumulative doses ranged from 92.7-1045 mg/m^2 for cisplatin and from 1.5-95.9 mg/m^2 for vincristine. The CCSS study [383] showed the 10th percentile and 90th percentile cumulative doses of cisplatin to be 171.1 mg/m^2 and 848.1 mg/m^2 respectively. The cumulative dose depends on the dose and duration of drug administration, which in turn is influenced by the stage of cancer; the later the stage, the higher the dose and/or the longer the cycles of drug administration. In a study performed by Gregg et al. [161], a linear relationship between cumulative dose of cisplatin administered and tissue platinum levels was observed in neural tissue. Cisplatin neurotoxicity was also demonstrated to correlate with tissue platinum levels. Consequently, the higher the dose of cisplatin administered, the greater the neurotoxicity [392]. DRGs are the primary neural tissue affected by platinum based chemotherapy agents [148–151]. The higher the dose of cisplatin administered, the greater the concentration of cisplatin that accumulates in the DRGs, increasing sensitivity to the agent. This can possibly have an effect on the molecular mechanisms involved, accounting for the difference in symptoms observed in the clinic as well as the severity of these symptoms (acute versus chronic). Researchers need to keep this in mind when developing rodent models because it will impact on the outcome of pharmacological experiments performed as well as translatability [185].

3.4.2 Cisplatin-induced DNA damage in sensory neurons

It is believed that neuropathic pain is a result of sensory neuronal damage depicted by reduction in IENF [68, 98, 393]. In this study, the in vitro models consisted of both primary DRG dissociated cell cultures and the human neuroblastoma cell line, SH-SY5Y. DRGs were utilized to evaluate the cytotoxicity of cisplatin due to their increased susceptibility to accumulating cisplatin. Following cisplatin treatment, the primary cell cultures illustrated a dose-dependent decrease in neurite length and neurite outgrowth with increasing concentrations of cisplatin, which coincides with the findings of other researchers [335, 338, 339, 394–396]. In the clinic, skin biopsies with measurement of IENF density are utilized to evaluate patients with peripheral

neuropathy [244, 379, 397]. These assessments have revealed significant reduction in IENF density in patients with neuropathic pain [164, 398–403]. Additionally, IENF loss following cisplatin treatment has been demonstrated in rodent models [404–406]. Comparative studies performed have proven the reliability of IENF density quantification as well as showing that it significantly correlates with changes in sensory NCV [405, 407].

Similar to the DRGs, a cell viability assay performed on SH-SY5Y cells supported the toxic nature of cisplatin, as there was a decrease in cell viability with increasing concentration of cisplatin. This result coincides with the findings of other studies which also demonstrated cisplatin to be cytotoxic [408–410]. These studies utilized a variety of human cancer cell lines including SH-SY5Y, A549, PC3 and A2780-cp cells. For my research, the SH-SY5Y cells were not differentiated because differentiation generates cells that express mature neuronal markers [411]. However, we are investigating childhood chemotherapy so we deemed undifferentiated cells to be more representative. For future research we can attempt differentiating the cells subsequent to cisplatin treatment, as a means of signifying development from childhood to adulthood.

In these in vitro neuronal models there is a prominent DNA damage response occurring represented by the induction of p53 following 24 hours cisplatin treatment, as well as increased phosphorylation of the DNA damage markers, p53 and histone H2A.X. Cisplatin binds with DNA, forming cisplatin-DNA adducts. The primary mechanism to detect and repair these adducts is the nucleotide excision repair (NER) pathway [152, 262–264], which is believed to be regulated by p53 [275, 276, 412]. Studies have revealed that the severity of CIPN depends on the efficiency of this DNA repair machinery to repair these cisplatin-DNA adducts [152, 265]. An increase in the repair of cisplatin-DNA adducts has also been associated with cisplatin resistance [270, 271].

The DDR pathway consists of different families of proteins that have varying roles; damage sensors, signal transducers and effectors [413]. Damage sensors identify damage signals and initiate cell signalling transduction. Signal transducers then transduce DNA damage chemical signals, activating downstream effectors. Effectors regulate various cellular processes including DNA repair and apoptosis. It is believed that cells undergo apoptotic cell death when the amount of DNA damage present exceeds the ability to achieve repair [414, 415]. One explanation for the absence of

CC3 staining in our cisplatin-treated DRGs could be that the neurons do not die but are only damaged following cisplatin treatment. However, there are some limitations to our experiment. There was no cell body (DAPI-staining) count performed for the DRG neurons in Figures 3.2A-D so there is no confirmation that the neurons are not dying. Additionally, there was no positive control staining for CC3 hence there is the possibility that there could have been an issue with the antibody. Studies have shown that p53 promoted DNA repair and protected against cisplatin-induced DNA damage and apoptosis [277–279], supporting the involvement of p53 in the modulation of various DNA damage response pathways [280]. Furthermore, p53 has been associated with cisplatin resistance [278, 416]. In experiments performed by Chee et al. [416], increased resistance to cisplatin was observed in human non-small cell lung carcinoma H1299 cells expressing high levels of both exogenous wild-type p53 and mutant p53. In a comparative study where cells expressing wild-type and mutant p53 were treated with an inducing agent to express p53 for 24 hours prior to cisplatin exposure, the induction of p53 resulted in better cell recovery when compared to cells that were not induced. Moreover, significantly higher density of cell growth was observed when p53 was induced in cells contained a mutant p53. This increased resistance to cisplatin was due to an inhibitory effect of p53 on caspase-9, an initiator caspase which has been shown to be required for apoptosis [417, 418]. Other investigations using various cancer cell lines have also associated p53 mutation with the development of cisplatin resistance and decreased susceptibility to apoptosis [419, 420]. Hence DDR and p53 may play a role in the onset of CIPN and should be explored further.

3.4.3 Role of inflammatory signalling in the delayed onset of neuropathic pain

The delayed onset of neuropathic pain observed following neonatal exposure to chemotherapeutic agents is believed to be a consequence of a change in the neuroimmune profile [98, 101]. An investigation into the gene expression signature of CIPN following cisplatin treatment revealed gene expression changes associated with a mixed inflammatory and neuropathic phenotype [421], hence supporting the involvement of inflammatory signalling in cisplatin-induced peripheral neuropathy. In a comparison study between infant (P10) and adult (P33) rodents [101], infant rodents which experienced nerve injury display no behavioural pain hypersensitivity until P38

for rats and P31 for mice. On the other hand, rapid decrease in mechanical threshold was observed in adult rodents within seven days following nerve injury. A closer look at the inflammatory response illustrated an initial anti-inflammatory immune response in the dorsal horn following infant nerve injury, which switches to a proinflammatory response upon reaching adolescence. In contrast, nerve injury in adult rodents initiated a proinflammatory response. It is believed that this delayed onset proinflammatory response is responsible for the delayed onset of neuropathic pain observed subsequent to infant nerve injury. Furthermore, it was discovered that following early life nerve injury, neuropathic pain is not absent but only suppressed, as blocking anti-inflammatory activity in the dorsal horn of infant rats caused significant decrease in withdrawal threshold following nerve injury.

A comprehensive network of contextualized protein-protein interactions (PPIs) specifically associated with pain [422] revealed NGF as one of the most enriched proteins in the network as well as one of the four proteins that more significantly regulate other proteins. Analysis of subnetworks specific to inflammatory and neuropathic pain showed that NGF was present in both pain datasets. Additionally, from anatomical categorization, NGF and BDNF were the only two found to be enriched in the brain, spinal cord and peripheral nervous system. As a result, the involvement of NGF and inflammatory signalling in CIPN will be investigated further in chapter 4.

3.5 Concluding Remarks

Cisplatin is cytotoxic in nature and causes sensory neuronal degeneration. Damage to the peripheral nerves early in life results in a delayed onset of chronic pain, exhibited as mechanical hypersensitivity. It is apparent that early life exposure to cisplatin disrupts the normal development of nociceptive pathways, heightening nociceptive processing and causing increased sensitivity to pain. The damage which ensues, induces DNA damage response pathways, leading to the activation of numerous downstream signalling pathways. Previous research has demonstrated an association between the TrkA receptor and chronic pain as well as implicated the type of inflammatory response as a cause for this delayed onset of chronic pain. Furthermore, NGF has been shown to be enhanced during inflammation, which induces nerve fibres to synthesize and release neurotransmitters and neuropeptides. This in turn can

activate receptors located on these nerve fibres. As a result, we decided to explore the mechanistic role of NGF-TrkA signalling in peripheral neuropathy.

Chapter 4: Involvement of NGF-TrkA signalling in the development of CIPN

4.1 Introduction

Early life exposure to cisplatin damages the peripheral sensory nerves and causes increased sensitivity to pain. This onset of chronic pain is delayed until adulthood and appears to involve an inflammatory component during development. McKelvey et al., [101] illustrated that there is an initial anti-inflammatory immune response in the dorsal horn following infant nerve injury, which switches to a proinflammatory response upon reaching adolescence, initiating neuropathic pain later in life. In contrast, nerve injury in adult rodents initiated a proinflammatory response from the outset, therefore is associated with the immediate onset of neuropathic pain behavioural phenotypes. Studies of patients and rodent models of inflammatory and chronic pain conditions [423–426, 64, 427] have demonstrated that inflammatory cytokine signalling can promote neurite growth and peripheral sensory neuronal sensitization. One such example is nerve growth factor (NGF), a neurotrophin essential for the growth, development and functioning of the nervous system [428] that acts via the receptor tyrosine TrkA signalling. Plantar skin retrieved from the hind paw at different time-points (P16 and P45) from a rodent model exposed to chemotherapy early in life and allowed to reach adulthood [340], demonstrated a change in nerve growth from degeneration at P16 to regeneration at P45. At P16, there was a decrease in intraepidermal nerve fibre (IENF) in the cisplatin-treated rats when compared to the vehicle controls. However, at P45, there was an increase in IENF in the cisplatin-treated rats when compared to the vehicle controls. Additionally, in DRGs, there was no change in TrkA+ve sensory neurons between vehicle control and cisplatin treated rats at P16. However, at P45, there was an increase in TrkA+ve sensory neurons in the cisplatin-treated group compared to the vehicle control group. Since this regeneration coincided with an increase in the number of DRG sensory neurons that express TrkA, it is believed to be modulated by TrkA dependence. However, it must be noted that during CIPN, recruited peripheral immune cells (such as macrophages and monocytes) as well as central glial cells [242, 429, 430], are potential sources of NGF [431, 432].

4.1.1 Nerve growth factor (NGF) and its association with peripheral neuropathy

NGF is one of four members of the neurotrophin family [433], essential for the growth, development and functioning of the peripheral nervous system [428]. During embryonic development, sensory DRG neurons, exclusively small diameter neurons, depend on NGF for survival [434]. In vivo, NGF knockout mice displayed extensive loss of DRG sensory and sympathetic neurons [435]. In vitro treatment with NGF stimulated neurite outgrowth in PC12 rat pheochromocytoma cells [436], superior cervical ganglion (SCG) [437] and DRG explants[438] in a dose-dependent and time-dependent manner. As a result, NGF has been trialled as a therapeutic in diabetic polyneuropathy [439]. Patients with stage 2 diabetic neuropathy were recruited, randomly divided into three groups and administered either a placebo or recombinant human NGF (rhNGF) at a dose of 0.1 µg/kg or 0.3 µg/kg. They were assessed 6 months later. Global symptom assessment, a measure of overall symptoms based on the subjects' perspective, revealed a greater global improvement in neuropathic symptoms in patients who received rhNGF treatment (73 % for the 0.1 µg/kg rhNGF group and 76 % for the 0.3 µg/kg rhNGF group) compared to the placebo group (42 %). Quantitative sensory testing, a measure of small diameter sensory fibre function, and neurological examination demonstrated more substantial improvements in both rhNGF treated groups compared to the placebo. However, rhNGF treatment did result in some adverse effects such as the development of myalgia (muscle aches and pain) and injection site hyperalgesia.

Two NGF-dependent neuropeptides are calcitonin gene-related peptide (CGRP) and substance P (SP) [440, 441]. Neuropeptides are messenger molecules that are produced and released by neurons to modulate synaptic activity. Examination of rodent models and patients of various disease conditions exhibited a direct correlation between NGF level and neuropeptide levels (CGRP and SP). Freund's adjuvant-induced paw inflammation in rats [442, 443], a rat model of chronic pancreatitis [444], patients with surgical degenerate intervertebral disc (IVD) [445] and patients with chronic daily headache (CDH) [446] all displayed increased levels of NGF, CGRP and SP. In vivo, intraplantar injection of NGF into rats stimulated neuropeptide production, evident by increased levels of CGRP and SP in the sciatic nerve [442, 447]. In streptozotocin-induced diabetic rat models [440, 448], chemotherapy-induced

neuropathy mice models [449, 450] as well as following sciatic nerve injury [451], the reduction in CGRP and SP levels detected in sciatic nerve and DRGs was prevented by the administration of rhNGF. In fact, in the diabetic models, NGF stimulated CGRP and SP levels to that greater than the control group. Hence CGRP and SP are widely used as a marker of peripheral sensory neuropathy.

Studies have also demonstrated NGF as being neuroprotective against the neurodegenerative effect of various chemotherapeutic agent, including cisplatin, vincristine and taxol [437, 438]. Co-treatment of SCG and DRG explant cultures with NGF and a chemotherapeutic agent promoted neuritogenesis. There was increased neurite outgrowth and neurite density compared to the culture treated with only the anti-cancer drug. Furthermore, the use of an anti-NGF antibody had the ability to block this regenerative effect of NGF. In contrast to developing DRG sensory neurons, NGF appears to only be required for the normal functioning of adult sensory neurons such as neurotransmitter production, not survival [452]. This was evident by reduction in substance P in the absence of NGF, without any effect on the survival or size of sensory neurons.

In addition to neurite growth, NGF has been implicated in the induction of pain. NGF levels, as well as those of CGRP and substance P, have been shown to increase in chronic pain states such as inflammation, rheumatoid arthritis, osteoarthritis and chronic pancreatitis [442–444, 453]. In both the clinic and animal models, the administration of a NGF neutralizing antibody has been trialled as a therapeutic to treat these chronic pain states [454–457], exhibiting reduction in nerve fibre growth, decreased levels of CGRP and SP and pain relief. In this chapter, we explored the involvement of NGF in the chronic pain which develops in CIPN and its link to the regeneration of sensory IENFs demonstrated by Hathway et al., [340].

4.1.2 Tropomyosin receptor kinase A (TrkA) and its activation

NGF binds to two receptors; TrkA, which is a high affinity receptor and p75NTR, which is a low affinity receptor [47–49]. TrkA, is expressed predominantly on small-diameter sensory neurons, some of which are nociceptors [5, 458]. 45 % of sensory neurons and 95 % of sympathetic neurons express TrkA [435]. During development, TrkA is expressed in all nociceptors and by about 80-85 % DRG sensory neurons [47,

40]. Postnatally, during the 3 weeks after birth in mice, TrkA expression is lost in approximately half of all nociceptors as there is a switch from expressing TrkA to expressing Ret [39, 40]. This gives rise to two populations; $TrkA^+$ peptidergic neurons that express the neuropeptides CGRP and substance P, and $TrkA^-$ non-peptidergic neurons that bind to isolectin B4 (IB4). Another difference in these two subsets is that TrkA-expressing neurons terminate in lamina I and the outer region of lamina II of the dorsal horn whereas IB4-binding neurons project to the interior of lamina II [39, 40, 459]. Nociceptors depend on TrkA signalling [460–462]. In mutant mice in which the *trkA* gene was inactivated (*trkA* -/-), thereby abolishing NGF/TrkA signalling, small DRG sensory neurons were eliminated [463]. The *trkA* -/- mice also exhibited a massive depletion in small myelinated and unmyelinated axons as well as a massive loss of small diameter peptidergic (CGRP+ve and SP+ve) neurons. Furthermore, primary afferent projections to laminae I and II of the dorsal horn were absent in *trkA* -/- mice. Similar results of extensive loss of small diameter DRG neurons in *trkA* -/- mice were demonstrated by Smeyne et al. [464]. Not only did these mutant mice experience severe sensory and sympathetic neuropathies; by P20, about half of them had died and none survived beyond P55. As a result, the focus of this research is on the $TrkA^+$ peptidergic neurons as they are modulated following early life exposure to cisplatin.

The binding of NGF to TrkA results in its activation via homodimerization and subsequent autophosphorylation and intracellular signalling [51]. It has also been shown that TrkA can be activated in the absence of NGF, through the G-protein-coupled receptor (GPCR) ligands adenosine and pituitary adenylate cyclase-activating polypeptide (PACAP) [54–56]. Using PC12 cells, both ligands were capable of activating TrkA receptor in the absence of NGF, although this was prolonged compared to NGF activation. Similar to NGF activation, the use a TrkA inhibitor, K252a, inhibited this increased activation. Furthermore, both adenosine and PACAP induced activation of AKT (protein kinase B) and resulted in increased cell survival subsequent to the withdrawal of NGF. Studies have also evidenced elongator complex protein 1 (Elp1) in the survival of TrkA neurons [465] and TrkA receptor phosphorylation [466]. In one study, Elp1 knockout caused TrkA neuron loss [465]. In another study [466], Elp1 was shown to bind to internalized TrkA receptors, in a NGF-dependent manner, and it maintained TrkA receptor phosphorylation by

negatively regulating the phosphatase activity of Shp1 (PTPN6). Furthermore, premature dephosphorylation of TrkA receptor was detected in Elp1-deficient neurons. Consequently, the NGF/TrkA signalling pathway was investigated both in the presence and absence of NGF to explore exogenous and endogenous activation of TrkA signalling.

4.1.3 Hypothesis

Cisplatin-induced DNA damage activates NGF-TrkA signalling, leading to neuritogenesis and the induction of neuropathic pain.

Specific Hypotheses

1) Cisplatin treatment results in the modulation of TrkA receptors.
2) Cisplatin induces nerve fibre growth and peripheral sensory neuronal sensitization by activating TrkA signalling.
3) Inhibition of TrkA signalling reduces this nerve fibre growth and ameliorates pain induced by peripheral sensory neuronal sensitization.

Experimental aims

1) To determine the effect of cisplatin treatment on TrkA receptors using SH-SY5Y cells.
2) To corroborate that in our cisplatin rodent model, the delayed onset of behavioural hypersensitivity observed following early life exposure to cisplatin is accompanied by nerve fibre growth.
3) To explore the involvement of TrkA signalling in these CIPN-associated phenotypes by using a model of NGF-induced TrkA activation.
4) To validate the involvement of TrkA signalling by investigating whether inhibiting this pathway in both models, thereby blocking TrkA activation, reverses these CIPN-associated phenotypes.

4.2 Method

4.2.1 Western blotting

4.2.1.1 NGF expression and inflammatory profile in splenocytes

Splenocytes were isolated from neonatal mice, cultured as described in Section 2.4.3.3 and allowed to grow. Approximately 1-week later, the cultures were treated with cisplatin (0 and 5 µg/ml) for 24 hours. Protein was extracted and quantified using the Bradford assay (see Sections 2.7.1 and 2.7.2 for full details). Western blotting was performed for determining protein expression of NGF (see Section 2.7.3 for protocol and antibody details). The housekeeping protein, β-actin, was used as the loading control. Between 30-50 µg of protein was loaded into each well. The protein expression level of NGF was normalized to that of β-actin. A graph was plotted using GraphPad Prism v9.0. A Mann-Whitney t-test was performed for the analysis of NGF expression level.

The extracted protein was also analyzed for 40 different cytokines and chemokines using the mouse cytokine array kit, ARY006 (R&D Systems; USA) (see Section 2.7.5 for full protocol). For each sample, 150 µg of protein was utilized. A graph of the protein expression levels was plotted using GraphPad Prism v9.0 and analysis performed using a two-way ANOVA.

4.2.1.2 TrkA and P-TrkA expression in SH-SY5Y cells

SH-SY5Y cells were cultured as described in Sections 2.4.1 and 2.4.2. Upon reaching 90-100 % confluency, cells were treated as followed:

Experiment 1: Varying concentrations of cisplatin (0, 1, 2, 5 µg/ml) for 24 hours

Experiment 2: 26.5 ng/ml NGF for different timepoints (0, 5 and 10 mins)

Experiment 3: Control vs NGF (26.5 ng/ml) vs TrkA inhibitor (100 nM) vs NGF + TrkA inhibitor

Protein was extracted and quantified using the Bradford assay (see Section 2.7.1 and 2.7.2 for full details). Western blotting was performed for determining protein expression of TrkA and P-TrkA (see Section 2.7.3 for protocol and antibody details). The housekeeping protein, β-actin, was used as the loading control. Between 30-70 µg of protein was loaded into each well. The protein expression levels of all target

proteins were normalized to that of β-actin. For P-TrkA, this normalized expression level was then expressed relative to that of total TrkA. All graphs were plotted using GraphPad Prism v9.0. A one-way ANOVA was performed for the analysis of TrkA and P-TrkA expression levels.

4.2.2 Behavioural testing for mechanical hypersensitivity

4.2.2.1 Cisplatin induction and TrkA activation inhibition

Neonatal Wistar Hans rats (weaned at P21, see chapter 2 for animal details) were randomly separated into 2 groups and injected twice on non-consecutive days with cisplatin (0.1mg/kg, i.p.) at Postnatal day (P) 14 and 16). An additional cohort of age-matched rats was injected with PBS (0.01 M, i.p.) and were used as vehicle controls. Mechanical withdrawal thresholds (using von Frey monofilament hairs test) were measured as described in Section 2.2.2. Testing was performed pre-dosing to obtain a baseline value, 24 hours post-dosing and then twice a week until the presentation and maintenance of pain at approximately P23-25. At this point, one group of cisplatin-treated rats were injected with a TrkA inhibitor, GW441756 (0.5mg/kg, i.p.). Behavioural testing for mechanical hypersensitivity was continued for 4 hours and 24 hours post-dosing. Experiments were performed in both male and female rats (see table 2.1 for number of animals per group).

4.2.2.2 NGF induction and NGF/TrkA signalling inhibition

For this study, two methods of dosing were utilized. Wistar Hans rats (8 weeks, see chapter 2 for animal details) were randomly separated into three groups and treated as followed:

Experiment 1: One cohort was injected with PBS (i.pl., n=6) and was used as vehicle controls. A second cohort was injected with NGF (1 µM, i.pl., n=6) followed by PBS (i.p.). A third cohort was injected with NGF (1 µM, i.pl., n=6) followed by a TrkA inhibitor, GW441756 (2mg/kg, i.p.).

Experiment 2: One cohort was injected with PBS (i.pl., n=6) and was used as vehicle controls. A second cohort was injected with NGF (26.5 µg/ml, i.pl., n=8). A third

cohort was injected with a mixture of NGF (26.5 µg/ml) and a TrkA inhibitor, GW441756 (100 nM) (i.pl., n=8).

Mechanical withdrawal thresholds (using von Frey monofilament hairs test) and thermal withdrawal thresholds (using Hargreaves test) were measured as described in Sections 2.2.2 and 2.2.3 respectively. Testing was performed pre-dosing to obtain two reciprocal baseline values, 4 hours post-dosing and then 24 hours post-dosing. Recordings were obtained for both the ipsilateral and contralateral hind paws.

4.2.3 Tissue extraction

For immunohistochemistry analysis, animals were terminally anaesthetized (i.p. sodium pentobarbital/dolethal), death confirmed by cervical dislocation, and plantar skin extracted. Tissues were either frozen and stored at -80 ℃ or submerged in 4 % paraformaldehyde (PFA) for 24 hours at 4 ℃. Following PFA submersion, tissues were cryoprotected in 30 % sucrose and stored at 4 ℃ overnight. Plantar skin was then embedded in OCT and either stored at -80 ℃ or processed for cryosectioning. 20 µm thick sections of plantar skin were sectioned onto labelled microscope slide (see Section 2.3.5 for details) and stored in slide boxes at -80 ℃ until required for immunohistochemistry staining.

4.2.4 Immunohistochemistry of plantar tissue

20 µm thick plantar skin sections on microscope slides (see Section 2.3.5 for tissue preparation) were immunostained using primary antibody targeted to CGRP, followed by the addition of an anti-Rabbit biotinylated antibody and then secondary antibody Alexa Fluor 555 streptavidin (see Section 2.5.2 for immunofluorescence and antibody details). Tissue sections were additionally incubated in a nuclear stain DAPI. Plantar skin was visualized using a Leica SP5 confocal microscope (Germany) at X20 magnification and images obtained were processed and analysed using the Fiji software (Image J2) version 2.15.0 (https://imagej.net/software/fiji/). IENF density and number of branch-points were calculated using randomly selected regions.

4.2.5 Data analysis

For Western blotting, graphs of protein expression level versus cisplatin concentration (μg/ml) and protein expression level versus treatment group were plotted. For inflammatory profile analysis, protein expression levels for each target protein were plotted. GraphPad Prism v9.0 was used to plot all graphs. Analysis of the expression levels of TrkA, P-TrkA and the various inflammatory marker were performed using a one-way ANOVA, whereas a t-test was implemented for NGF expression level; all comparisons were done to the control, or 0 μg/ml where applicable.

For the behavioural tests, GraphPad Prism v9.0 was used to plot withdrawal threshold (g) against time-point for mechanical hypersensitivity and withdrawal latency (s) against time-point for thermal hypersensitivity. Analysis was performed using a two-way ANOVA, compared to the NGF-treated group at each time-point.

For immunohistochemistry of plantar tissue, IENF density was determined by counting the number of nerve fibres per 1000 μm, for a minimum of three randomly selected areas, for each treatment group. A branch-point was denoted by a "V" shape. The number of branch-points per 1000 μm was counted. For each result, a graph was plotted using GraphPad Prism v9.0. Analysis was performed using a one-way ANOVA, compared to the NGF-treated group.

For microarray data analysis, the GSE125003 dataset was downloaded from the Gene Expression Omnibus (GEO) database [421]. GEO is a database repository of high throughput gene expression data and hybridization arrays, chips, microarrays. This dataset was based on the platform GPL19057 (Illumina NextSeq 500). The data presented was the gene expression signatures of chemotherapy-induced neuropathy induced by cisplatin. Whole DRGs (L3-L5) were extracted from either control groups (5 % glucose, n=3) or cisplatin-treated (40 μg, i.pl. n=3) C57BL/6J mice, 8-10 weeks old, 72 hours following treatment. Extracted DRGs underwent total RNA isolation using the Rneasy Mini kit (Qiagen) and RNA-Seq analysis performed. A differential expression analysis was performed using MatLab and Hochberg's Method. Differentially expressed genes (DEGs) were selected using a fold change (FC) of 1 (i.e. $\log2FC \geq 0$) and an adjusted $P < 0.05$. Pathway and process enrichment analyses, of selected upregulated genes, were carried out with Kyoto Encyclopedia of Genes and Genomes (KEGG) pathways [467] as well as Gene Ontology (GO) molecular

functions and cellular components [468]. Protein–protein interaction enrichment analysis was carried out using STRING (https://string-db.org/).

4.3 Results

4.3.1 Cisplatin treatment does not appear to exhibit an inflammatory aspect in our in vitro model

Splenocytes extracted from neonatal mice were treated 5 µg/ml cisplatin to investigate whether cisplatin treatment induces NGF production (Figure 4.1A). Following 24-hours cisplatin treatment, no significant difference in NGF expression levels was observed (vehicle control = 1±0.095 and cisplatin = 1.2±0.087). We then explored the effect of NGF on the inflammatory profile. Similarly, there was no significant change in the inflammatory profile following 24-hours cisplatin treatment [F (1, 28) = 0.1505, ns] (Figures 4.1B-D). Only a significant increase in soluble Intercellular adhesion molecule 1, sICAM-1 (CD54) expression level was observed in the cisplatin treated splenocytes (7454.898±201.616 *p<0.05), compared to the vehicle control (6386.692±335.89) (Figure 4.1D). sICAM-1 has been shown to promote both pro- and anti-inflammatory responses [469].

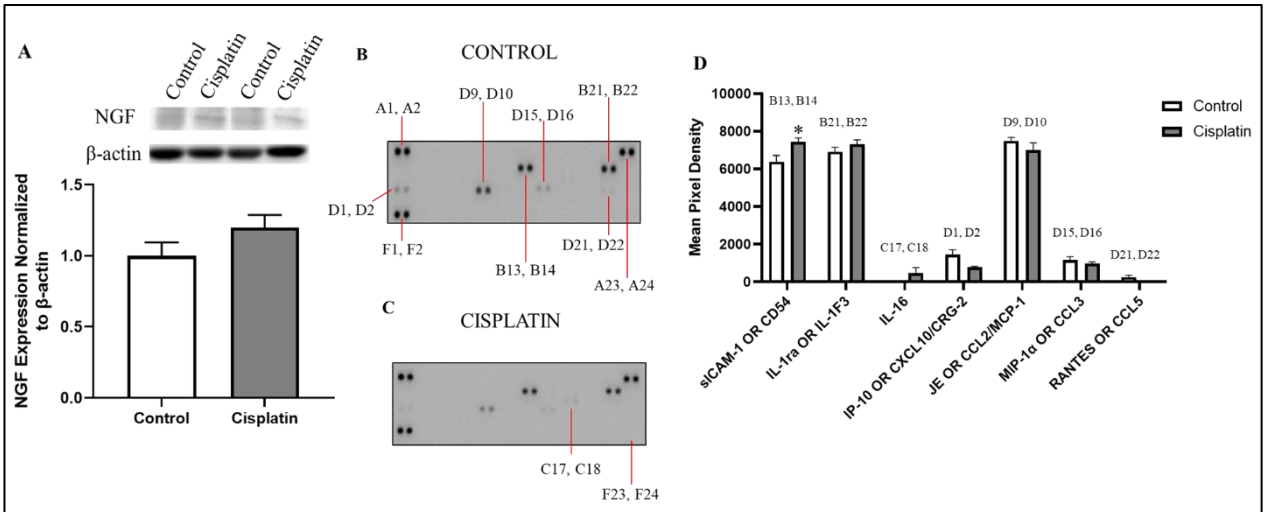

Figure 4.1 Cisplatin does not appear to exhibit an inflammatory aspect in our in vitro model. Splenocytes were isolated from neonatal mice, seeded in 6-well plates and allowed to grow. The cultures were then treated with cisplatin (0 or 5 µg/ml) for 24 hours, protein extracted and probed for NGF [A]. Cisplatin treatment did not result in a significant increase in NGF expression. β-actin was the loading control. The extracted proteins were also analysed using a mouse cytokine array kit for 40 different cytokines. The relative expression levels of the cytokines present in the control [B] and cisplatin-treated samples [C] did not show a significant change in the inflammatory profile following cisplatin treatment. Quantification of expression levels is illustrated in D. *p < 0.05, two-way ANOVA; n=3 per group. A1, A2, A23, A24, F1 and F2 are reference spots. F23 and F24 are negative controls (PBS).

4.3.2 Cisplatin activates TrkA receptors in vitro

SH-SY5Y cells treated with varying concentrations of cisplatin (0, 1, 2 and 5 µg/ml) illustrated no change in TrkA expression [F (3, 12) = 0.3889, ns] (Figure 4.2A). However, there was a dose-dependent increase in activated TrkA signalling after 24-hours cisplatin treatment [F (3, 12) = 3.229, $p < .05$] (Figure 4.2B), with significance observed at 5 µg/ml cisplatin (P-TrkA = 2.04±0.33 *$p<0.05$) when compared to the vehicle control (1±0.103). According to the data, it can be interpreted that there may be endogenous phosphorylation of the TrkA receptor.

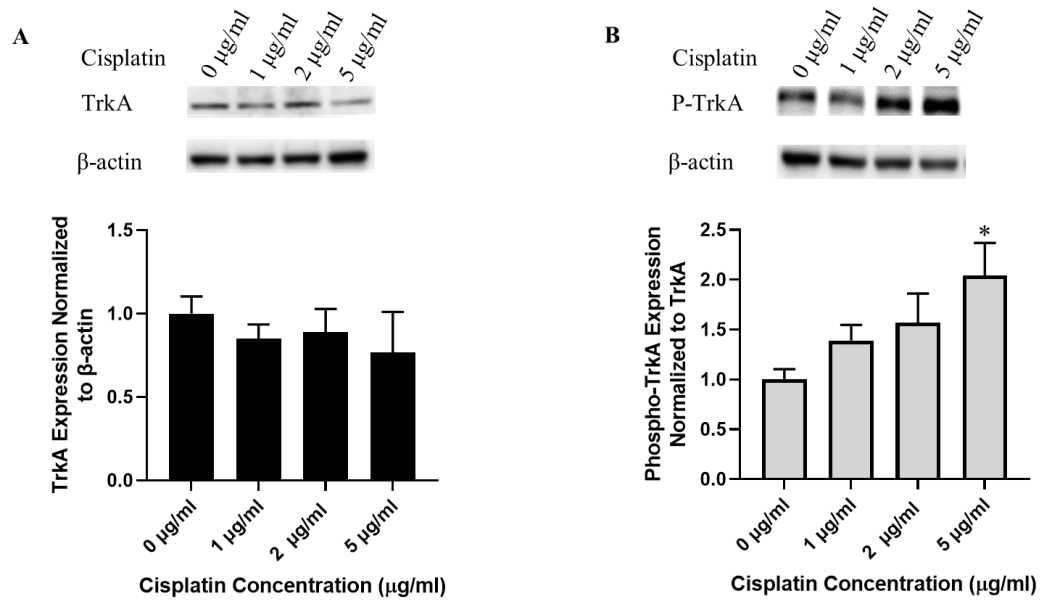

Figure 4.2 Cisplatin activates TrkA receptors. SH-SY5Y cells were seeded into gelatin-coated 90 mm petri dishes and allowed to reach 90-100 % confluency. Cells were then treated with varying concentrations of cisplatin (0, 1, 2, and 5 µg/ml) for 24 hours, protein extracted and probed for TrkA [A] and Phospho-TrkA (P-TrkA) [B]. TrkA expression appeared to remain unchanged following 24hrs cisplatin treatment. However, there was a dose-dependent increase in activated TrkA signalling after 24hrs cisplatin treatment. β-Actin was the loading control. For quantification, P-TrkA expression was normalized to total TrkA expression. *$p < 0.05$, one-way ANOVA (Kruskal-Wallis test) compared to control (0 µg/ml); n = 4. Error bars are mean+SEM.

4.3.3 NGF-induced activation of TrkA is prevented in the presence of a TrkA inhibitor in vitro

The impact of inhibiting NGF/TrkA signalling on NGF-induced activation was then investigated (Figure 4.3). SH-SY5Y cells were firstly treated with NGF (26.5 ng/ml) for 5 mins and 10 mins to determine if NGF induces TrkA activation (Figures 4.3A

and B). There was a trend of a time-dependent increase in both TrkA and P-TrkA following NGF treatment but the changes were not statistically significant. Next, it was investigated whether inhibiting NGF/TrkA signalling could prevent NGF-induced activation of TrkA (Figures 4.3C and D). The NGF-induced activation of TrkA observed (control = 0.875±0.152 and NGF = 6.122±3.197, *p<0.05) (Figure 4.3D), was prevented in the presence of a TrkA inhibitor, GW441756 (100 nM) (control = 0.875±0.152 and NGF+TrkA inhibitor = 0.935±0.353).

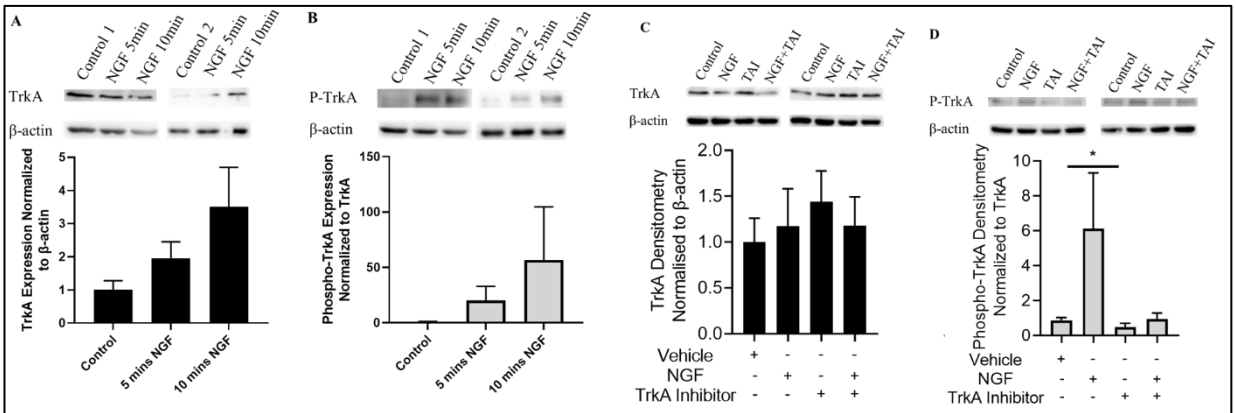

Figure 4.3 NGF-induced activation of TrkA is prevented in the presence of a TrkA inhibitor. SH-SY5Y cells were seeded into gelatin-coated 90 mm petri dishes and allowed to reach 90-100 % confluency. Cells were then treated with NGF (26.5 ng/ml) for varying timepoints (0, 5 and 10 mins), protein extracted and probed for TrkA [A] and Phospho-TrkA (P-TrkA) [B]. There is a trend of increasing TrkA and P-TrkA expression levels with longer NGF exposure, however this was not significant. SH-SY5Y cells, prepared as above, were treated with NGF (26.5 ng/ml), a TrkA inhibitor (100 nM) or a combination of both. Protein extracted and probed for TrkA [C] and P-TrkA [D] showed NGF-induced activation of TrkA, which was prevented in the presence of a TrkA inhibitor. β-actin was the loading control. For quantification, P-TrkA expression was normalized to total TrkA expression. *p < 0.05, one-way ANOVA (Kruskal-Wallis test); n = 6 for the NGF study and for the TrkA inhibitor study, n=7 for the control an NGF groups whereas n=4 for both TrkA inhibitor groups. Error bars are mean+SEM. TAI = TrkA inhibitor.

4.3.4 NGF induced hyperalgesia and aberrant nociceptor growth

There was a significant effect of treatment on the development of both mechanical [F (2, 29) = 4.521, p < .05] and thermal hypersensitivity [F (2, 27) = 3.441, p < .05]. NGF treatment (black) induced both mechanical [Figures 4.4A and E] and thermal [Figures 4.4B and F] hypersensitivity within 4 hours of dosing for both experiments. For mechanical hypersensitivity experiment 1, withdrawal threshold of the vehicle was 18.537±1.774 g while that of the NGF group was 11.267±1.141 g (*p<0.05) and for experiment 2, withdrawal threshold of the vehicle was 19.028±4.337 g while that of the NGF group 7.297±4.608 g (***p<0.001). For thermal hypersensitivity experiment 1, withdrawal latency of the vehicle was 9.684±1.403 g while that of the NGF group

was 7.037±1.697 g (*p<0.05) and for experiment 2, withdrawal latency of the vehicle was 10.408±3.079 g while that of the NGF group was 7.144±1.574 g (*p<0.05). Mechanical hypersensitivity was also observed in the untreated paws 4 hours post-dose for both experiments; experiment 1, (vehicle 21.893±3.103 g; NGF 10.162±1.112 g, *p<0.05) and experiment 2 (vehicle 19.995±7.675 g; NGF 13.9±6.956 g, **p<0.01) [Figures 4.4C and G respectively]. This was not observed with thermal sensitivity for either experiment; experiment 1 (vehicle 11.198±1.432 g vs. NGF 8.685±1.045 g) and experiment 2 (vehicle 10.449±3.222 g vs. NGF 8.118±2.046 g) [Figures 4.4D and H respectively]. The rodents recovered from NGF-induced mechanical sensitization within 24 hours, was evident in both the ipsilateral and contralateral hind paws. However, when it came to thermal sensitivity, for experiment 2, hypersensitivity disappeared within 24 hours (vehicle 11.605±2.278 g vs. NGF 8.573±1.767 g) [Figure 4.4F] whereas for experiment 1 it was still evident 24 hours following dosing (vehicle 12.454±2.955 g; NGF 8.551±1.603 g, *p<0.05) [Figure 4.4B]. Furthermore, NGF induced nerve fibre growth with regards to increased IENF density (vehicle 1.862±0.372 IENF/100 µm; NGF 7.3±0.606 IENF/100 µm, F (2, 33) = 16.91, ****p<0.0001) and increased branching (vehicle 0.186±0.186 branch-points/100 µm; NGF 3.724±0.695 branch-points/100 µm, F (2, 33) = 7.231, **p<0.01) [Figure 4.5].

4.3.5 Inhibiting NGF/TrkA signalling prevented NGF-induced mechanical and thermal hypersensitivity and reduced nerve fibre growth

Inhibiting NGF/TrkA signalling by administrating NGF in combination with a TrkA inhibitor, GW441756, ameliorated the NGF-induced mechanical hypersensitivity which occurred at 4 hours post-dose [Figures 4.4A and E]. For mechanical hypersensitivity experiment 1, withdrawal threshold of the NGF group was 11.267+1.141 g; while that of the NGF+TrkA inhibitor group was 25.68+0.14 g, (*p<0.05) and for experiment 2, withdrawal threshold of the NGF group was 7.297+4.608 g while that of the NGF+TrkA inhibitor group was 16.797+9.997 g, (***p<0.001). Alternatively, the TrkA inhibitor did not appear to prevent thermal hypersensitivity [Figures 4.4B and F], there was a trend of increasing withdrawal latency but no significance. For thermal hypersensitivity experiment 1, withdrawal

latency of the NGF group was 7.037+1.697 g while that of the NGF+TrkA inhibitor group was 10.972+3.01 g and for experiment 2, withdrawal threshold of the NGF

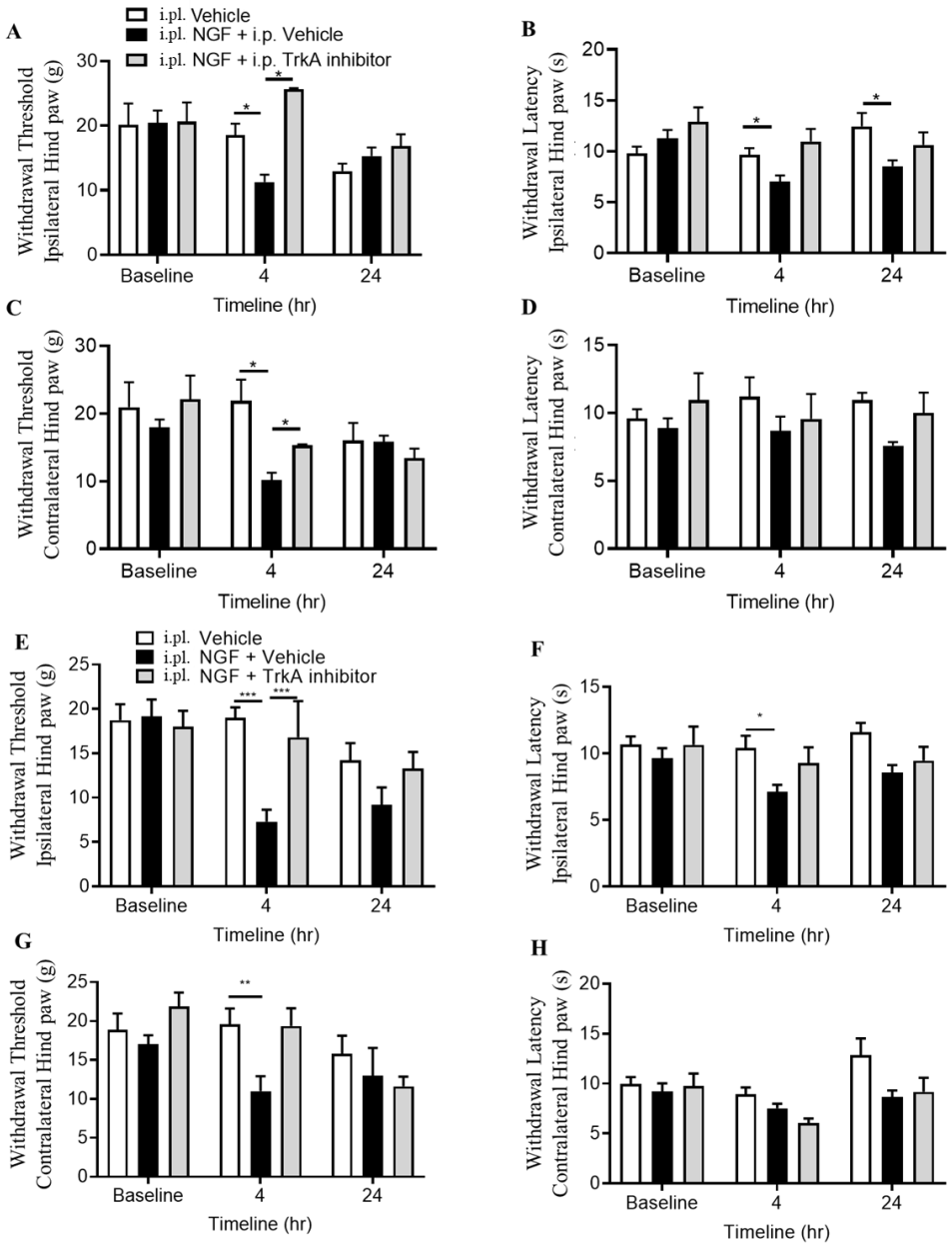

Figure 4.4 NGF-induced mechanical and thermal hypersensitivity are prevented by inhibiting NGF/TrkA signalling. Wistar Hans rats were injected with either PBS (white), NGF (26.5 µg/ml, black) or NGF along with a TrkA inhibitor, GW441756 (grey). In experiment 1, NGF and the inhibitor were administered separately, via intraplantar and intraperitoneal injection respectively [A-D] while in experiment 2, they were administered in combination as one intraplantar injection [E-H]. NGF induced both mechanical [A&E] and thermal [B&F] hypersensitivity within 4 hours of dosing. Contralateral sensitization was observed following NGF administration with regards to mechanical hypersensitization [C&G] but not thermal [D&H]. *$p < 0.05$, **$p < 0.01$ and ***$p < 0.001$, one-way ANOVA (Kruskal-Wallis test) compared to the NGF treated group. For experiment 1, n=6 for all groups; for experiment 2, n=6 for control and n=8 for both NGF and NGF+TrkA inhibitor groups. Error bars are mean+SEM.

group was 7.144+1.574 g while that of the NGF+TrkA inhibitor group was 9.299+3.487 g. The effect of the TrkA inhibitor in preventing mechanical sensitization was also observed in the contralateral, untreated paws for experiment 1 (NGF 10.162+1.112 g; NGF+TrkA inhibitor 15.32+0.14 g, *p<0.05) but not for experiment 2 (NGF 13.9+6.956 g; NGF+TrkA inhibitor 19.367+5.567 g) [Figures 4.4C and G respectively]. Additionally, administering NGF along with a TrkA inhibitor resulted in reduced nerve fibre growth (NGF 7.3+0.606 IENF/100 µm vs NGF+TrkA inhibitor 4.171+0.55 IENF/100 µm, F (2, 33) = 16.91, ***p<0.001) and branching (NGF 3.724+0.695 branch-points/100 µm vs NGF+TrkA inhibitor 1.788+0.419 branch-points/100 µm, F (2, 33) = 7.231, *p<0.05) [Figure 4.5].

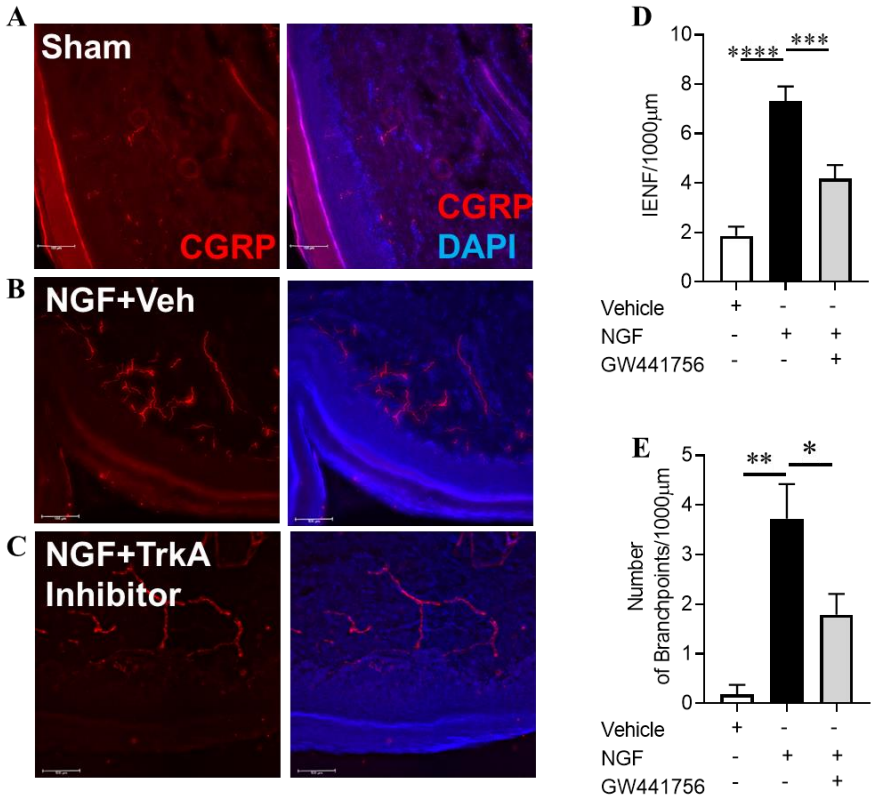

Figure 4.5 NGF-induced nerve fibre growth is prevented by inhibiting NGF/TrkA signalling. Plantar skin was extracted from Wistar Hans rats injected with either PBS (white), NGF (1 µM, black) or NGF along with a TrkA inhibitor, GW441756 (grey). Immunocytochemistry was performed using the nociceptor-specific marker, CGRP. Representative images [A-C], quantification of IENF density [D] and of number of branchpoints [E] showed that NGF resulted in increased nerve fibre growth. The administration of NGF along with a TrkA inhibitor reduced nerve fibre growth and branching. *p < 0.05, **p < 0.01. ***p < 0.001 and ****p < 0.0001, one-way ANOVA compared to NGF-treated group. For vehicle control, n=6 and for both NGF and NGF+TrkA inhibitor, n=15. Scale bar = 100 µm. Error bars are mean + SEM.

4.3.6 Cisplatin-induced mechanical hypersensitivity is ameliorated by inhibiting TrkA activation in vivo

We then investigated whether the cisplatin-induced mechanical hypersensitivity and nerve fibre growth observed in rodents following cisplatin treatment (0.1 mg/kg) in chapter 3 (Figure 3.1) could also be prevented by inhibiting TrkA activation (Figure 4.6). There was a significant effect of treatment on the development of mechanical hypersensitivity [F (1, 24) = 64.85, p < .0001]. As previously demonstrated, the administration of cisplatin at P14 and P16 resulted in a delayed onset of mechanical hypersensitivity, which was observed from P21 (P21: males, control 24.167±1.833 g; cisplatin 15 g **p<0.01; females, control 22.333±2.319 g; cisplatin 11.625±1.017 g **p<0.01) (P25: males, control 22.333±2.319 g; cisplatin 11.667±1.054 g **p<0.01; females, control 31.667±5.667 g; cisplatin 9.5±0.327 g **p<0.01).

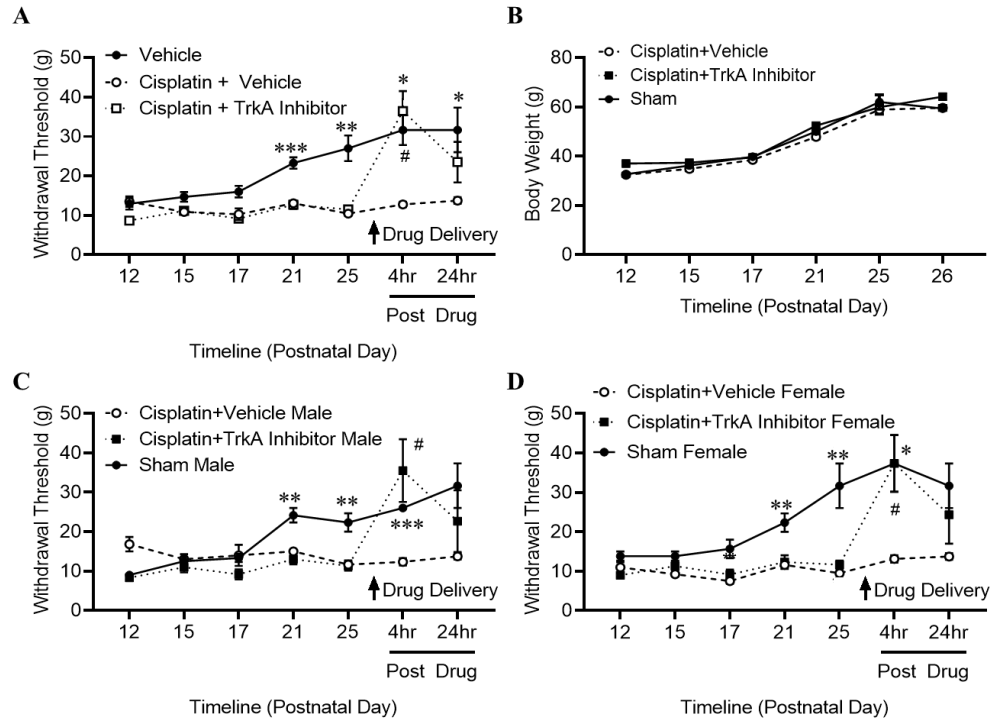

Figure 4.6 Inhibiting TrkA activation ameliorated cisplatin-induced mechanical hypersensitivity. Neonatal Wistar rats (~30g) were intraperitoneal injected with cisplatin (0.1mg/kg) at Postnatal day (P) 14 and 16 [A]. Increased mechanical hypersensitivity was observed from P21 until the end of experiment. Administration of either TrkA inhibitor, GW441756 (intraperitoneal 0.5mg/kg) at P25, ameliorated this cisplatin-induced mechanical hypersensitivity within 4 hrs. No weight loss [B] or gender-associated differences [C & D] were displayed. * compares cisplatin groups and sham group; # compares cisplatin and cisplatin+TrkA inhibitor groups. *p < 0.05, **p < 0.01, ***p < 0.001 and ****p < 0.0001, #p < 0.05, Two-way ANOVA; n = 6-8. Error bars are mean ± SEM.

Introducing a TrkA inhibitor, GW441756 (0.5mg/kg) [Figures 4.6C and D] at P25 ameliorated the mechanical hypersensitivity within 4 hours (males, cisplatin 12.333±0.919 g vs cisplatin+TrkA inhibitor 35.5±7.94 g #p<0.05; females, cisplatin 13.125±0.915 g vs cisplatin+TrkA inhibitor 37.333±7.168 g #p<0.05). The withdrawal threshold of those cisplatin-treated rodents returned to that of the vehicle control (sham). There were also no gender-associated differences.

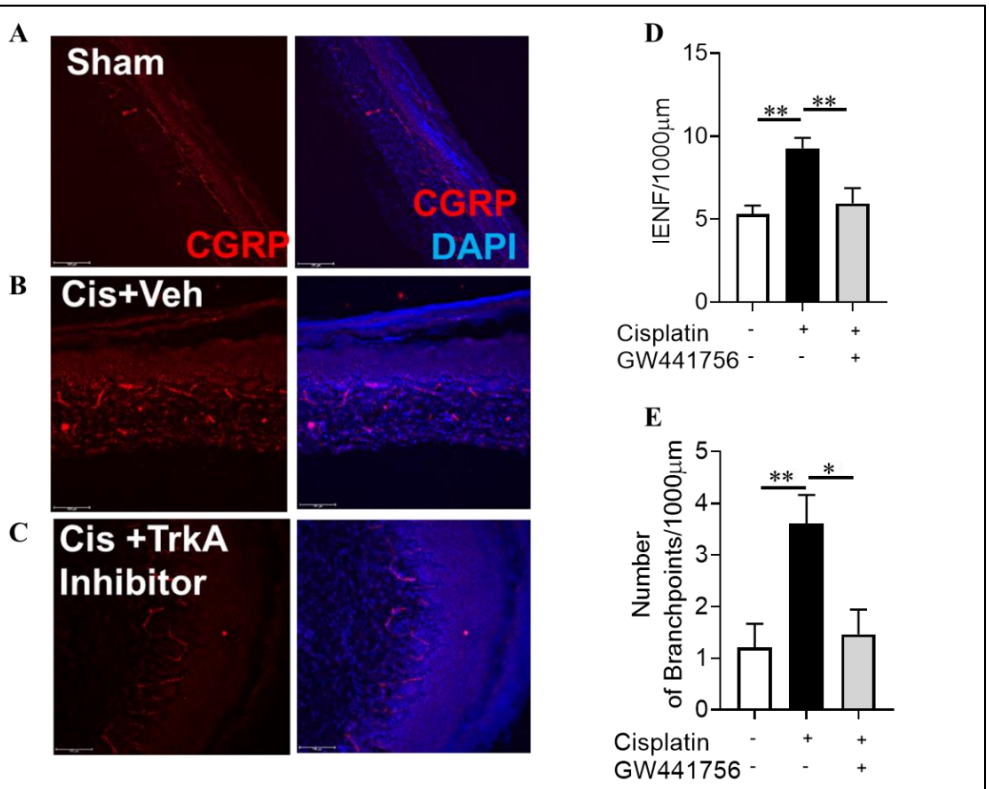

Figure 4.7 Cisplatin-induced nerve fibre growth is prevented by inhibiting TrkA signalling. Plantar skin was extracted from Wistar Hans rats injected with either PBS (white), cisplatin (0.1mg/kg, black) or cisplatin along with a TrkA inhibitor, GW441756 (grey). Immunocytochemistry was performed using the nociceptor-specific marker, CGRP. Representative images [A-C], quantification of IENF density [D] and of number of branchpoints [E] showed that cisplatin resulted in increased nerve fibre growth. The administration of cisplatin along with a TrkA inhibitor reduced nerve fibre growth and branching. *p < 0.05 and **p < 0.01, one-way ANOVA (Kruskal-Wallis test) compared to cisplatin-treated group. For vehicle control and cisplatin, n=13 and for cisplatin+TrkA inhibitor, n=18. Scale bar = 100 µm. Error bars are mean + SEM.

Additionally, the cisplatin-treated rodents illustrated increased nerve growth with regards to increased IENF density (vehicle 5.329+0.492 IENF/100 µm; cisplatin 9.282+0.625 IENF/100 µm, F (2, 41) = 7.012, **p<0.01) and increased branching (vehicle 1.203+0.464 branch-points/100 µm; cisplatin 3.61+0.554 branch-points/100

µm, F (2, 39) = 6.669, **p<0.01), which was prevented when a TrkA inhibitor was introduced (IENF density, cisplatin 9.282+0.625 IENF/100 µm vs cisplatin+TrkA inhibitor 5.959+0.912 IENF/100 µm, **p<0.01; and branching, cisplatin 3.61+0.554 branch-points/100 µm vs cisplatin+TrkA inhibitor 1.466+0.475 branch-points/100 µm, **p<0.01) [Figure 4.7]. Treatment did not result in any weight loss throughout the experiment [Figure 4.6B].

4.3.7 NGF/TrkA signalling can be linked to apoptosis and DNA repair

To further explore the damaging effect of cisplatin, data mining was performed on some RNA-Seq data retrieved from a Gene Expression Omnibus (GEO) database [GEO submission number: GSE125003] [421]. Samples consisted of whole DRGs (L3-L5) extracted from either control groups (5 % glucose, n=3) or cisplatin-treated (40 µg, i.pl. n=3) C57BL/6J mice, 9 weeks old, following 72 hours of treatment. From the RNA-Seq data, upregulated genes associated with NGF/TrkA signalling, apoptosis and DNA were identified using the criteria log2FC ≥ 0 and adjusted P < 0.05. STRING analysis of these selected upregulated genes illustrated that TrkA can be linked to ion channels activation (including NGF and TRPV1), apoptosis and DNA repair [Figure 4.8]. The colours of the lines identify how the genes are linked and are as follows [470, 471]; known interactions from curated data are light blue (—), known interactions experimentally determined are pink (—), predicted interactions due to gene neighbourhood (similar genomic context in different species suggest a similar function of the proteins) are green (—), predicted interactions due to gene fusions (proteins that are fused in some genomes are very likely to be functionally linked as in other genomes where the genes are not fused) are red (—), predicted interactions due to gene co-occurrence (proteins that have a similar function or an occurrence in the same metabolic pathway, must be expressed together and have similar phylogenetic profile) are blue (—), other interaction due to text mining (A large body of scientific texts are analyzed to search for statistically relevant co-occurrences of gene names) are light green (—) and other interaction due to co-expression (proteins that have a similar function or an occurrence in the same metabolic pathway, must be expressed together and have similar phylogenetic profile) are black (—).

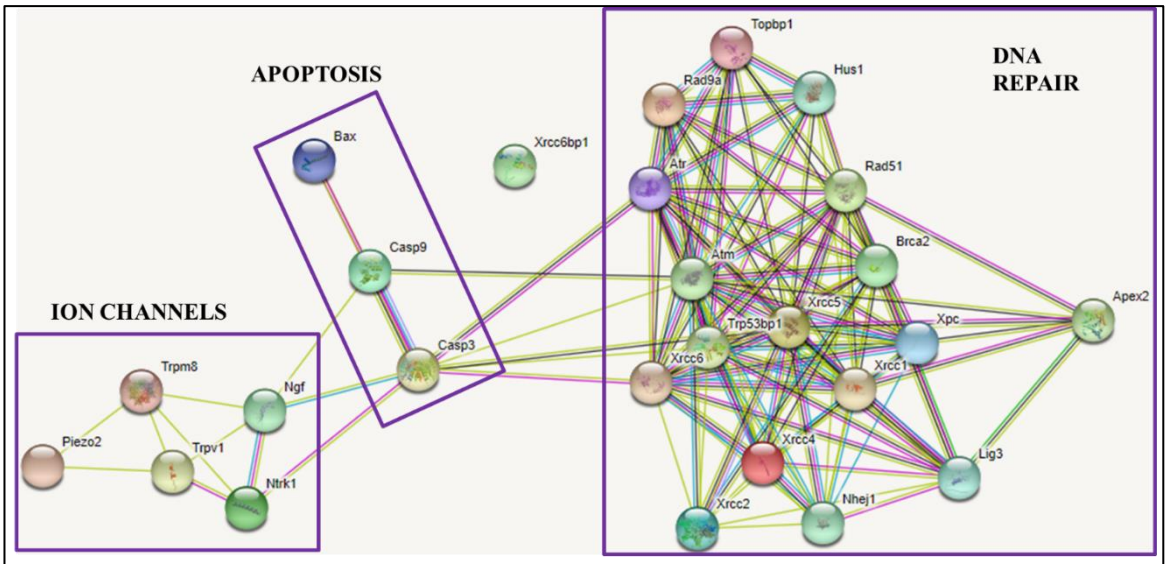

Figure 4.8 NGF/TrkA signalling can be linked to apoptosis and DNA repair. Data mining was performed on some RNA-Seq data retrieved from a Gene Expression Omnibus (GEO) database [GEO submission number: GSE125003]. STRING analysis of selected upregulated genes following 72 hours cisplatin treatment (40 µg, i.pl.) illustrated that TrkA can be linked to ion channels activation (NGF, TRPV1), apoptosis and DNA repair. The colours of the lines identify how the genes are linked and are as follows: Known interaction from curated data and experimentally determined, predicted interaction due to gene neighbourhood, gene fusions and gene co-occurrence and other interactions due to text mining and co-expression.

Pathway and process enrichment analyses are illustrated in Figure 4.9. KEGG pathways associated with the upregulated DEGs included non-homologous end joining, homologous recombination, apoptosis - multiple species, p53 signalling pathway and platinum drug resistance. GO analysis identified molecular functions associated with cysteine-type endopeptidase activity involved in apoptotic signalling pathway, 5′-deoxyribose-5-phosphate lyase activity, nerve growth factor binding, neurotrophin receptor binding and four-way junction DNA binding. Furthermore, associated cellular components included Ku70:Ku80 complex, RAD51B-RAD51C-RAD51D-XRCC2 complex, ERCC4-ERCC1 complex, non-homologous end joining complex, nucleotide-excision repair complex and DNA repair complex; all complexes involved in DNA repair. The false discovery rate (FDR) is the ratio of the number of false positive results to the number of total positive test results, giving an indication of any associated false positives.

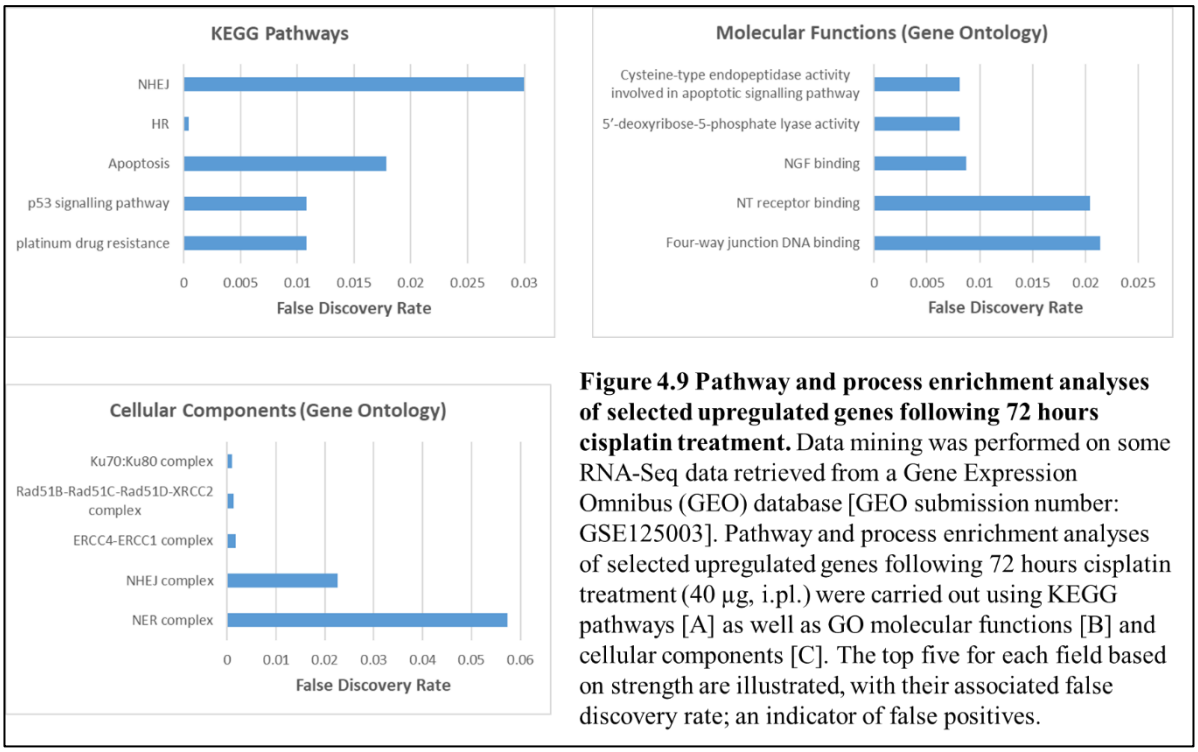

Figure 4.9 Pathway and process enrichment analyses of selected upregulated genes following 72 hours cisplatin treatment. Data mining was performed on some RNA-Seq data retrieved from a Gene Expression Omnibus (GEO) database [GEO submission number: GSE125003]. Pathway and process enrichment analyses of selected upregulated genes following 72 hours cisplatin treatment (40 µg, i.pl.) were carried out using KEGG pathways [A] as well as GO molecular functions [B] and cellular components [C]. The top five for each field based on strength are illustrated, with their associated false discovery rate; an indicator of false positives.

4.4 Discussion

Splenocytes treated with 5 µg/ml of cisplatin for 24 hours did not exhibit a significant change in NGF levels or the inflammatory profile (Figure 4.1). Only sICAM-1 (CD54) expression level was significantly increased following cisplatin treatment. sICAM-1, has been deemed an inflammatory biomarker [469], with elevated levels being identified in patients suffering with various inflammatory conditions such as coronary heart disease [472], pulmonary artery hypertension [473], atherosclerosis [474], asthma [475], intermediate uveitis [476], sepsis [477], rhinovirus infection [478] and cancer [479, 480]. However, sICAM-1 has been associated with promoting both proinflammatory [469, 481] and anti-inflammatory responses [469, 482]. A possible explanation for this lack of significance could be the low sample size utilized as each group only had an n number of 3.

4.4.1 Activation and subsequent inhibition of TrkA signalling in vitro

Our data supports a cisplatin-induced phosphorylation of receptor tyrosine kinase, TrkA. SH-SY5Y cells treated for 24 hours with increasing concentrations of cisplatin displayed no change in TrkA expression levels but a dose-dependent increase in activated TrkA signalling (Figure 4.2). This denotes endogenous activation of TrkA since this is an exclusive cell line system with no NGF present. Research by Fernandez-Calle et al. [487] discovered ethanol-induced activation of TrkA in SH-SY5Y neuroblastoma cells. Similarly, there was significant increase in phosphorylation of TrkA at Tyr 490 with no effect of treatment on total TrkA protein levels. This supports endogenous phosphorylation of the TrkA receptor, which was revealed in our in vitro model.

Activation of TrkA signalling pathway has proven vital to the sensitization of nociceptors [57], growth of sensory neurons [58] and onset of pain and chronic pain states [59, 60]. In this chapter we investigated the impact of blocking this TrkA signalling pathway using the TrkA inhibitor, GW441756. NGF is known to phosphorylate TrkA [488]. In our experiment, exposure to NGF (26.5 ng/ml) in vitro, for only 5 minutes and 10 minutes, did not result in a significant change in TrkA and phosphorylated TrkA expression levels, however, there was a trend of a time-dependent increase in both TrkA and P-TrkA following NGF treatment. (Figure 4.3A

and B). Following a longer incubation period of 24 hours, NGF caused a significant increase in phosphorylated TrkA (Figure 4.3D), however, there appeared to be no impact on TrkA levels after 24 hours (Figure 4.3C). Firstly, we will discuss NGF treatment and TrkA expression level. In our experiments, there was a trend of increasing TrkA expressing levels following 5-minutes and 10-minutes treatment with NGF however, 24-hour NGF treatment displayed no change in TrkA expression levels. In a study conducted by Chang et al. [489], PC12 cells treated with 50 ng/ml of NGF for varying time-points, ranging from 5 minutes to 7 days, displayed no significant change in total TrkA levels. In contrast, a study conducted by Zhou et al. [490], also using PC12 cells and the same concentration of NGF (50 ng/ml,) showed that after 5 minutes treatment with NGF, TrkA expression levels remained unchanged. In this same study, the effect of prolonged NGF exposure on TrkA was also investigated. Beyond 5 minutes (30 minutes and 60 minutes), there was a rapid downregulation of TrkA receptor, with only 33 % of that present before treatment detected subsequent to 60 minutes NGF treatment. However, NGF treatment for 2 days onwards displayed increased levels of TrkA receptor, but the TrkA level at 2-days exposure did not reach the level present as in the untreated cells. Thus TrkA receptor was down-regulated at 24-hours NGF exposure, compared to the untreated cells. On the contrary, another study [491], demonstrated that 24-hour treatment with 5 μg/ml β-NGF caused transient upregulation of TrkA receptor in HTB114 cells. As one can see, there is inconsistency in the literature when it comes to the effect of NGF on TrkA levels in vitro.

Previous studies, using different cell lines, have demonstrated rapid (within 5 minutes) tyrosine phosphorylation of TrkA by NGF [488, 490, 492, 493], which coincides with our study. However, this was achieved with 50-100 ng/ml NGF, higher concentrations than were utilized in our study. One study illustrated TrkA phosphorylation in PC12 cells using as little as 0.1 ng/ml NGF following 30 minutes incubation [488]. However, a comparison study [492] in which NGF-induced tyrosine phosphorylation was attained in both PC12 and SH-SY5Y cells following 5 minutes NGF treatment (100 ng/ml), showed that there was lower level of phosphorylated TrkA in the SH-SY5Y cells. It was insinuated that SH-SY5Y cells express about fourfold less trk mRNA than PC12 cells and this accounted for the lower level of phosphorylated TrkA. Hence, the lack of significance in our experiment can be due to the lower NGF concentration. In PC12 cells, maximum level of phosphorylation was reached after 5 minutes of NGF

treatment (50 ng/ml) [488], but decreased following prolonged incubation period (60 minutes, 2 days and 7 days). Nonetheless, a signal was still detected at all the time-points, validating our NGF-induced TrkA receptor activation following 24-hours NGF treatment. Using cultures of rat sympathetic neurons [494], tyrosine phosphorylation of TrkA was achieved using a wide range of NGF concentrations (10-200 ng/ml). This occurred in a dose-dependent manner. These cultures, however, were initially grown in medium supplemented with 200 ng/ml of NGF for 2 weeks. Medium was then replaced with NGF-free media for 2-4 hours prior to NGF treatment experiment. It is uncertain whether this initial exposure to NGF impacted on the experiment. As a recommendation, for the TrkA inhibitor study, treatment with 100 ng/ml NGF for 5 mins could be employed to achieve a stronger signal.

The TrkA inhibitor, GW441756 has been successfully used to inhibit TrkA signalling pathway [491, 495, 496]. In these studies, concentrations of GW441756 utilized ranged between 0.5-10 µM. In our experiment, a lower concentration of the TrkA inhibitor (100 nM) was sufficient to prevent TrkA activation. Similarly, to NGF, there was no significant effect on TrkA expression levels following 24-hours treatment (Figure 4.3C). This coincides with the literature [491] which shows GW441756 (0.5, 5.0, 10.0 µM) had minimal effect on TrkA expression; only treatment with 10 µM for 48 hours produced a minor, but significant downregulation of TrkA. Finally, the TrkA inhibitor prevented TrkA activation in the presence of NGF and absence, corroborating our concept of endogenous TrkA activation. Accordingly, the in vivo models were developed using 1 µM NGF and 100 nM TrkA inhibitor (GW441756) as the welfare of the animals were of utmost importance.

4.4.2 Activation and subsequent inhibition of TrkA signalling in vivo

In vitro, we demonstrated that both cisplatin and NGF have the ability to activate the TrkA receptor (Figures 4.2 and 4.3 respectively). In chapter 3, we also showed that cisplatin treatment resulted in mechanical hypersensitivity (Figure 3.1). Hence, we wanted to determine if activation of TrkA signalling in vivo, via treatment with NGF (Figure 4.4), would have a similar effect as cisplatin. In our study, NGF caused both mechanical and thermal hypersensitivity within 4 hours post injection, which, in most cases, lasted for less than 24 hours. NGF has been shown extensively to cause both mechanical [497–505] and thermal [497, 499–504, 506–508] hypersensitivity. The

onset of both mechanical and thermal hypersensitivity has been seen as early as 1 hour post injection [497, 501]. Administration of a single dose of NGF (0.3-5 µg, i.pl.) into adult male rats [497] induced mechanical hypersensitivity within 1 hour, which persisted for at least 1 week with all doses utilized (0.3, 1, 3 and 5 µg). At higher concentrations (3 µg and 5 µg), mechanical hypersensitivity was still detected 2 weeks post injection. With regards to thermal hypersensitivity, it also developed within 1 hour and persisted for at least 3 hours with all doses utilized. However, only at the highest concentration (5 µg) was hypersensitivity still detected at 24 hours post injection, which resolved by 48 hours. In another study [502] a single injection of NGF (1 µg/g, i.p.), at P35, resulted in a later onset of mechanical hypersensitivity at 6.5 hours post injection. Maximum hypersensitivity was reached between 24-48 hours, persisted for 3 days and was absent after 7 days. On the other hand, thermal hypersensitivity was induced much earlier at 15 mins post injection and reached max at 50 mins, but also persisted for 3 days and was absent after 7 days. Similarly, Rueff et al. [504] detected mechanical hypersensitivity at 7 hours post injection (i.p.) of both 1 mg/kg and 0.1 mg/kg NGF (1 mg/kg ≡ 1 µg/g). The decrease in withdrawal threshold was greater following 1 mg/kg NGF and persisted longer (4 days) compared to 0.1 mg/kg NGF, which only persisted for 50 hours. Likewise, to the previous study, thermal hypersensitivity developed earlier at 30 mins post injection but persisted for 100 hours (just over 4 days). In both studies, the onset of thermal hypersensitivity was sooner compared to mechanical hypersensitivity but both sensitization persisted for the same duration. In contrast, another study using the same dose but mice instead of rats and a different route of administration, a single injection (i.v.) of l µg/g NGF [508] did not observe any significant effect on thermal threshold. As one can see, species, dose and route of drug administration can all impact on results obtained, hence emphasizing the importance of standardization.

The phenomenon of contralateral sensitization, which has been demonstrated in various models [509–513], was observed in our study; hypersensitivity was also exhibited by the uninjected paw (Figures 4.4C and G). However, only contralateral mechanical hypersensitivity was detected, without contralateral thermal hyperalgesia. Similar findings were displayed by Chillingworth et al. [509] in mice that were induced with chronic inflammatory arthritis via intradermal injection of Freund's complete adjuvant around the left tibiotarsal joint, resulting in unilateral arthritis. A decrease in

mechanical withdrawal threshold was seen in both the ipsilateral and contralateral hind paws but only the ipsilateral hind paw showed a decrease in thermal withdrawal latency. Likewise, animal models of chronic muscle pain [510], induced by carrageenan injection into the left gastrocnemius muscle, resulting in unilateral inflammation, presented with bilateral decrease in mechanical withdrawal threshold. Contralateral sensitization is sometimes referred to as 'mirror pain' and is believed to be a form of secondary hypersensitivity, arising due to central sensitization in the spinal cord (explained in more detail in Section 1.3.1). In our study, however, contralateral hypersensitivity was inconsistent between experiments as it was not apparent in all rats.

Compared to humans, intradermal injection of 25 µg/ml NGF lead to both mechanical and thermal hypersensitivity within 1 hour [501]. However, it was still present at 24 hours post injection. In another study [514], patients receiving NGF at doses above 0.1 µg/kg (both i.v. and s.c.), described the onset of diffuse myalgias (muscle aches and pain). Following 1.0 µg/kg (i.v.) NGF, diffuse myalgias developed within 1-1.5 hours after dosing, worsened over the next 4-6 hours and resolved slowly over 2-8 days. Patients who received the same dose but via s.c. injection experienced mild diffuse myalgias which developed within 5-7 hours after dosing and resolved over 2-5 days. Similarly, injection of 1 or 3 µg of NGF into the skin resulted in both mechanical and thermal hypersensitivity within 3 hours of dosing and persisted to 21 days [500]. All these studies validate our rodent model as being representative to what occurs in human.

The administration of the TrkA inhibitor prevented mechanical hypersensitivity, regardless of whether it was given in combination with NGF (i.pl.) or immediately after (i.p.). Conversely, the TrkA inhibitor had no significant effect on preventing thermal hypersensitivity, however there appears to be a trend. The increase in sensitivity was accompanied by increased nerve fibre growth. This is believed to be linked to the onset of pain as the TrkA inhibitor also reduced nerve growth. Since the administration of NGF and cisplatin both resulted in mechanical and thermal hypersensitivity, we investigated whether blocking TrkA signalling, using a TrkA inhibitor, would have the same effect, which it did. Injection of a TrkA inhibitor ameliorated cisplatin-induced mechanical hypersensitivity within 4 hours of dosing. Furthermore, the associated nerve growth following cisplatin treatment was reduced

when NGF was given along with a TrkA inhibitor. These rodent models confirm the involvement of TrkA activation in cisplatin-induced pain. The next step will be to determine a source of this activation.

4.4.3 Cisplatin-induced ion channel activation and DDR signalling

Nociceptors express numerous TRP channels that allow us to identify different noxious stimuli such as heat, cold and mechanical. Various ion channels were upregulated following cisplatin treatment, including the mechanosensitive ion channels TRPV1 (capsaicin receptor), TRPM8 (cold receptor) and Piezo2 (proprioception and touch sensation channel). These TRP channels are modulated by TrkA which, from this dataset, seems to be possibly controlled by this DDR pathway. Of these, TRPV1 has been linked to mechanical and thermal hyperalgesia [515]. TRPV1 has been demonstrated to be key in the conduction of nociceptive signals [516, 517], with its phosphorylation resulting in sensitization. Both NGF and TrkA have the ability to activate TRPV1 [516]. TrkA activation promoted TRPV1 sensitization by NGF, in a time-dependent manner. There is also evidence that this TrkA-mediated sensitization of TRPV1 requires its downstream PI3K and MAPK signalling pathways [517]. Hence, the activation of TRPV1 to investigate cisplatin-induced TrkA activation is utilized in the next chapter.

The cisplatin-DNA adducts which form subsequent to cisplatin treatment damages the DNA, initiating DDR [318]. The efficiency to repair these adducts contributes to the severity of CIPN [152, 265] and is instrumental in cisplatin resistance [270, 271]. Studies have shown that p53 plays a role in both DNA repair [277] and cisplatin resistance [416]. In our in vitro neuronal model, 24 hours cisplatin treatment resulted in the induction of p53 (Chapter 3, Figure 3.3A). Additionally, there was increased levels of both phosphorylated p53 and phosphorylated histone H2A.X (Chapter 3, Figure 3.3B and D), signifying a prominent DNA damage response. Cisplatin has been shown to produce DNA double-stranded breaks (DSBs) [285, 286], which can be repaired by non-homologous DNA end joining (NHEJ) and homologous recombination (HR) [284]. The repair of cisplatin-DNA adducts also involves both the nuclear excision repair pathway (NER) and base excision repair (BER) pathway [152, 272, 518], both of which have been linked to p53 signalling pathway [275]. When the amount of DNA damage present exceeds the ability to achieve repair, cells undergo

apoptotic cell death [414, 415]. These events are supported by the STRING analysis performed on the RNA-Seq data retrieved from the GEO database (GSE125003) as those pathways were highlighted as key KEGG pathways. Furthermore, most of the associated molecular functions and cellular components highlighted from GO analysis are linked to DNA repair and the various DNA repair pathways [519–524], strengthening the involvement of DDR signalling.

4.5 Concluding remarks

In vitro, both NGF and cisplatin activated TrkA signalling. In vivo, both NGF and cisplatin induced mechanical and thermal hyperalgesia, which was accompanied by aberrant nerve fibre growth. Furthermore, inhibiting TrkA signalling using a TrkA inhibitor ameliorated this pain and reduced nerve fibre growth. These findings support our hypothesis that subsequent to cisplatin treatment, TrkA receptors on sensory neurons are activated. Activation of TrkA signalling then leads to peripheral sensory neuronal sensitization and induces neuritogenesis, resulting in increased sensitivity to pain. In our in vitro model, there was endogenous activation of the TrkA receptor following cisplatin treatment. If we are able to identify this mediator of TrkA activation, it can potentially be used as a therapeutic target. The next chapter explores a possible source for the activation of TrkA signalling.

Chapter 5: Topoisomerase modulation of nociceptor function following exposure to cisplatin

5.1 Introduction

5.1.1 DNA damage and sensory neuroregeneration

Thus far, we have identified that cisplatin treatment damages DNA, initiates DDR, activates the TrkA receptor, sensitizes nociceptors and causes pain. We also demonstrated that in vivo, subsequent to cisplatin treatment, there was increased nerve fibre growth (Figure 4.7). Studies have demonstrated topoisomerase inhibitors as inducers of the regeneration marker, activating transcription factor-3 (ATF-3) [525–528], onset by the generation of DNA DSBs. Since cisplatin has been shown to cause DNA DSBs [285, 286], it is then plausible that cisplatin treatment induces ATF-3, indicative of the nerve fibre growth observed.

Topoisomerases play an important role in various processes including DNA replication, transcription, genome stability and DNA repair [529–532]. They relieve DNA supercoils by transiently forming breaks in the DNA strand and then resealing them. In the absence of topoisomerase, DNA would supercoil and ultimately break, resulting in DNA damage. There are two types of DNA topoisomerases, TOP1 and TOP2. TOP1 generates single-strand breaks whereas TOP 2 causes double-strand breaks. These two types of topoisomerases can be further classified into four subfamilies; TOP1α, TOP1β, TOP2α and TOP2β.

Following the inhibition of topoisomerase, DNA breaks are induced and are accompanied by an upregulation of both γH2A.X and activating transcription factor-3 (ATF-3) [525–527]. Furthermore, Cheng et al. was able to link topoisomerase inhibition and peripheral nerve injury to ATF-3 expression and axonal regeneration [525]. It was discovered that subsequent to a sciatic nerve injury, the administration of a topoisomerase inhibitor (2 mg/kg; i.p.; given 30 mins after the injury and then for 5 consecutive days) resulted in axon regeneration as well as accelerated functional recovery. Additionally, inhibiting topoisomerase enhanced DNA breaks in injured DRG neurons. This enhancement occurred at the gene locus of ATF-3, further increasing ATF-3 expression. It is believed that this induction of ATF-3 promoted the axon regeneration that was observed. However, the elevation in ATF-3 expression

occurred only within 18-24 hours of nerve injury and had returned to levels similar to that of the vehicle controls at 36 hours after injury. Although this study investigated the TOP1 inhibitor camptothecin, both TOP1 and TOP2 inhibitors were identified as activators of ATF-3.

ATF-3, a basic leucine zipper transcription factor, is a member of the cAMP response element-binding protein (CREB)/ATF family of transcription factors. ATF-3 is induced in response to stress stimuli and cellular damage and has been demonstrated as being both pro-apoptotic [528, 533–535] and anti-apoptotic [536–540]. When it comes to neurons though, induction of ATF-3 expression has been closely linked to survival and regeneration [541]. In uninjured neurons, ATF-3 is either not expressed or expressed at very low levels [537, 542–546]. However, following peripheral axonal injury, but not central axonal injury, ATF-3 has been shown to be rapidly upregulated in all injured DRG neurons and downregulated after reinnervation of their target [545, 547]. Hence ATF-3 has been regarded as a marker of nerve injury [545] and regeneration [548].

5.1.1.1 ATF-3 as a marker of nerve injury and regeneration

Numerous studies have demonstrated an upregulation of ATF-3 following nerve injury [537, 542–546, 549, 550]. Some of these studies have also illustrated nerve regeneration as a result of ATF-3 induction or ATF-3 overexpression. Facial nerve transection in wild type mice resulted in increased ATF-3 expression in facial motoneurons (FMNs) [542], with maximal levels observed at 3 days post lesion. At 7 days post lesion, the number of ATF-3 positive FMNs was slightly reduced and after 21 days post lesion, ATF-3 expression was no longer detected in FMNs. A comparison was performed between these wild type mice and *atf3* mutant mice, which showed no ATF-3 expression at 3 days post lesion. Axonal regeneration, which was observed in the wild type mice, was reduced in the *atf3* mutant mice. At 23 and 31 days post lesion, facial muscles in wild type mice were re-innervated by regenerating axons at 65 and 82 % respectively. Conversely, in *atf3* mutant mice, the percentage of regenerated FMNs at 23 and 31 days post lesion were 45 and 60 % respectively. Furthermore, DRG neurons cultured for 24 hours displayed strong neurite growth, which was decreased by approximately 40 % in *atf3* mutant DRGs. In this same study, rodent and human Schwann cells also exhibited ATF-3 induction after peripheral nerve

injury. Schwann cells myelinate peripheral nerves and support cells of peripheral neurons [551]. Studies conducted by Seijffers et al. [543, 552], revealed that ATF-3 enhanced DRG neurite elongation in vitro and promoted peripheral nerve regeneration in vivo. ATF-3 delivered to cultured adult DRG neurons via a viral vector (herpes simplex virus (HSV) based amplicon vector), resulted in enhanced neurite outgrowth [543]. In addition, ATF-3 transgenic mice, which constitutively express ATF-3, showed increased peripheral nerve regeneration following sciatic nerve injury compared to controls [552]. However, both studies illustrated that in contrary to a peripheral nerve transection which induced ATF-3 expression in adult rodent DRG neurons and caused enhanced regeneration, injury to central axons of DRG neurons led to ATF-3 induction in only a few isolated neurons and no regeneration was observed following dorsal column injury. Hence ATF-3 is a suitable marker for peripheral nerve injury and regeneration.

Additionally, models of various disease states including ischemia [553], monoarthritis [554] and neurodegenerative diseases such as Huntington's disease [539] and amyotrophic lateral sclerosis (ALS) [555] have all resulted in the induction of ATF-3. Huntington's disease is caused by a polyglutamine expansion near the N-terminus of huntingtin. In a PC12 cell model of Huntington's disease [539], mutant huntingtin (Htt) resulted in cell death and significantly increased expression of ATF-3 at both the mRNA and protein level. It was observed that overexpression of ATF-3 protected against mutant Htt toxicity whereas knock down of ATF-3 enhanced mutant Htt toxicity. Similar effects were seen in an ALS mouse model [555]. These mice exhibited neuromuscular junction denervation and axonal degeneration, which resulted in motor neuron loss and loss of motor function. Overexpression of ATF-3 in the motor neurons of an ASL mouse model delayed neuromuscular junction denervation and muscle atrophy, improved muscle strength and function and delayed disease onset and mortality. However, lifespan was only slightly increased. Moreover, toxins such as cisplatin [346, 408], paclitaxel [556] and the DNA topoisomerase (TOP) inhibitors doxorubicin [557] and camptothecin resulted in ATF-3 induction both in vitro and in vivo.

5.1.2 TRPV1 dependent nociceptor sensitization

Transient receptor potential vanilloid 1 (TRPV1), a nociceptive ion channel [12, 558], is highly expressed in small diameter sensory neurons [517, 559], predominantly in peptidergic C-fibres [560, 561]. In addition to significant increase in AFT-3 following cisplatin treatment, studies have also demonstrated increased TRPV1 expression upon exposure to cisplatin [347, 562–564]. TRPV1 has been shown to be activated by inflammation and heat [565, 566] and its activation has been linked to the mediation of pain [567–569]. TRPV1 phosphorylation results in its sensitization, which, in DRG neurons, have been exhibited to be evoked by NGF [570–572]. Studies have revealed that NGF-induced sensitization of TRPV1 is mediated through the TrkA receptor [516, 517, 570, 571, 573]. Pre-treatment of adult rat DRG neurons with a TrkA receptor inhibitor abolished NGF-induced sensitization of TRPV1 [517]. Using African naked mole-rats, Omerbasic et al. [573] showed that NGF alone did not sensitize TRPV1 in isolated nociceptors. Furthermore, TRPV1 sensitization and subsequent NGF-induced hyperalgesia was decreased by reduced TrkA function. In a related study [497], a TRPV1 antagonist caused partial inhibition to the development of mechanical hypersensitivity as well as reduced the development of thermal hypersensitivity. However, the exact mechanism behind NGF-induced sensitization of TRPV1 is still unclear and a bit controversial [574] as the activation of TrkA leads to the activation of multiple major signalling pathways; phospholipase C (PLCγ), p42/p44 mitogen-activated protein kinase (MAPK, also referred to as Ras/MEK/ERK) and phosphoinositide-3-kinase (PI3K) [575]. There is evidence supporting PLCγ [576], Ras/MEK [577, 578] and PI3K [516, 570, 579] in TRPV1 sensitization.

Studies have also shown that TRPV1 plays a crucial role in cisplatin-induced thermal hyperalgesia in vivo [347, 580]. This receptor was upregulated following cisplatin treatment, leading to hypersensitivity to heat stimulation. However, in the absence of TRPV1 ($TRPV1^{-/-}$), cisplatin-induced thermal hyperalgesia was not exhibited, as was seen in the cisplatin-treated wild-type group. Additionally, the cisplatin-treated $TRPV1^{-/-}$ group was less sensitive to heat pain than the wild-type control group. Researchers have also demonstrated normal heat response or increased withdrawal latency in $TRPV1^{-/-}$ mice compared to wild-type mice [347, 565, 566, 580, 581], suggesting that although the ability to respond to noxious heat may not dependent on TRPV1, the absence of this receptor impairs nociception to thermal stimuli.

In chapter 4, our rodent models showed that inhibiting NGF/TrkA signalling ameliorated both NGF-induced mechanical and thermal hypersensitivity as well as cisplatin-induced mechanical hypersensitivity (Figures 4.4 and 4.6 respectively). TRPV1 is often used as a tool to look at nociceptor sensitization. Hence, in this chapter, TRPV1 activation in mice DRG neurons was utilized to explore TrkA activation following cisplatin treatment and determine a possible inhibitor to this activation.

5.1.3 Hypothesis

Research has suggested that DNA topoisomerases modulate nociceptor activity under stress and damage. Therefore, it is possible that a DNA topoisomerase could be mediating TrkA activation.

Experimental aims

1) To use mass spectrometry to identify if any DNA topoisomerases are upregulated following cisplatin treatment, thereby being a possible mediator of TrkA activation.
2) To select a potential candidate and investigate whether inhibiting that protein in SH-SY5Y cells prevents cisplatin-induced TrkA activation.
3) To validate that cisplatin results in TRPV1 sensitization in DRG neurons by using an in vitro model of nociceptor sensitization; a capsaicin model.
4) To utilize the capsaicin model to investigate whether inhibiting the potential candidate identified in experimental aim 2 reduces cisplatin-induced TRPV1 sensitization, thereby serving as a potential therapeutic target.

5.2 Method

5.2.1 Mass Spectrometry

SH-SY5Y cells were cultured as described in Sections 2.4.1 and 2.4.2. Upon reaching 90-100 % confluency, cells were treated with cisplatin (0 and 5 µg/ml). Protein was extracted and quantified using the Bradford assay (see Sections 2.7.1 and 2.7.2 for full details). Lysates (50 µg of protein) underwent proteomics analysis using mass spectrometry. See section 2.7.4 for full protocol details. In brief, lysates were purified, digested and then re-suspended for liquid chromatography separation using an Eksegent expert nano LC 452 upstream of a Sciex TripleTOF 6600 mass spectrometer. Data analysis was performed in both IDA and SWATH modes.

5.2.2 Cell viability

SH-SY5Y cells were cultured as described in Sections 2.4.1 and 2.4.2 and treated the following day as shown below:

Experiment 1: Varying concentrations of a TOP2 inhibitor, doxorubicin hydrochloride (Dox: 0, 0.5, 1, 2, 5, 10, 20 and 50 µM), either in the absence or presence of 5 µg/ml cisplatin, for 24 hours.

Experiment 2: Varying concentrations of a p53 inhibitor, pifithrin-α hydrobromide (Pif-α: 0, 0.5, 1, 2, 5, 10 and 20 µM), either in the absence or presence of 5 µg/ml cisplatin, for 24 hours.

A cell viability assay was performed using Cell Proliferation Reagent WST-1 (see Section 2.6 for full protocol). In brief, following 24 hours of treatment, Cell Proliferation Reagent WST-1 was added to each well and cells were incubated for 4 hours. The plate was then shaken and absorbance for each well measured, which directly correlates to the number of viable cells.

5.2.3 Western blotting

SH-SY5Y cells were cultured as described in Sections 2.4.1 and 2.4.2. Upon reaching 90-100 % confluency, cells were treated as followed:

Experiment 1: Control vs Cisplatin (5 µg/ml) for 24 hours

Experiment 2: Control vs Dox (0.5 µM) vs Cisplatin (5 µg/ml) vs Cisplatin + Dox

Experiment 3: Control vs Pif-α (1 µM) vs Cisplatin (5 µg/ml) vs Cisplatin + Dox

Protein was extracted and quantified using the Bradford assay (see Sections 2.7.1 and 2.7.2 for full details). Western blotting was performed for determining protein expression of TOP2 and ATF-3, for experiment 1, TrkA, P-TrkA and ATF-3, for experiment 2 and ATF-3 for experiment 3 (see Section 2.7.3 for protocol and antibody details). The housekeeping protein, β-actin, was used as the loading control. Between 50-60 µg of protein was loaded into each well. The protein expression levels of all target proteins were normalized to that of β-actin. For P-TrkA, this normalized expression level was then expressed relative to that of total TrkA. All graphs were plotted using GraphPad Prism v9.0. A Mann-Whitney t-test was performed for the analysis of TOP2 and ATF-3 expression levels in experiment 1 and a one-way ANOVA was performed for the analysis of TrkA and P-TrkA expression levels in experiment 2 and ATF-3 expression levels in experiment 3.

5.2.4 Calcium assay to asses TRPV1 activity

DRGs were isolated and cultured as described in Sections 2.4.3.1 and 2.4.3.2 and treated the next day as followed:

Experiment 1: Varying concentrations of Dox (0, 0.5, 1 and 2 µM) for 24 hours

Experiment 2: 5 µg/ml cisplatin with varying concentrations of Dox (0, 0.5, 1 and 2 µM) for 24 hours

After treatment, a calcium assay was performed using the fluo-4 direct assay (see Section 2.8 for full details). In brief, capsaicin (5 µM) was used to evoke TRPV1 activity and the resulting changes in Ca^{2+} ion influx and efflux were calculated as a measure of the changes in fluorescence using a Tecan Infinite 200 Pro microplate reader over a 300 second time frame.

5.2.5 Data analysis

For mass spectrometry, differentially expressed genes (DEGs) were selected using a fold change (FC) of 1 (i.e. $\log2FC \geq 0$) and an adjusted $P < 0.05$. A clustergram was generated in MATLAB.

For cell viability, graphs of Cell Viability (%) versus Drug Concentration (Log μM) was plotted using GraphPad Prism v9.0 and analysis performed using a two-way ANOVA, compared to the vehicle.

For Western blotting, graphs of protein expression level versus cisplatin concentration (μg/ml) and protein expression level versus treatment group were plotted. GraphPad Prism v9.0 was used to plot all graphs. Analysis of TOP2 and ATF-3 expression levels in experiment 1 were performed using a Mann-Whitney t-test, whereas a one-way ANOVA was implemented for ATF-3, TrkA and P-TrkA expression levels in experiment 2 and ATF-3 expression level in experiment 3; all comparisons were done to the control (0 μg/ml).

5.3 Results

5.3.1 Cisplatin upregulates key proteins

Quantitative mass spectrometry detected 1638 proteins. Following 24 hours cisplatin treatment, 908 proteins were upregulated and 730 proteins were downregulated. The clustergram illustrates the upregulation and downregulation of differentially expressed proteins (Figure 5.1A). The rows (genes) and columns (samples) are ordered according to hierarchical clustering; the groups are clustered together based on the similarity of their gene expression patterns. This helps in identifying samples that are more similar to each other based on their overall gene expression patterns. As you can see, the cisplatin treated group forms a cluster that is distinct from the control group. The cluster of genes that are upregulated in the cisplatin treated samples are downregulated in the control samples, and vice versa. Some key proteins that were upregulated following cisplatin treatment include p53 (p=1.07E-13, log2FC=2.7798), histone H2A.X (p=0, log2FC=2.7454) and TOP2 (p=1.79E-26, log2FC=3.7008 for TOP2A_HUMAN and p= 3.99E-18, log2FC= 3.1682 for TOP2A). These results were validated using Western blotting (see figure 3.3 for p53 and histone H2A.X). A list of the top 20 upregulated (red) and downregulated (green) proteins are provided in Table 5.1. The full list can be found using the link: Full List of DEGs Following 24 hours Cisplatin Treatment.xlsx. Following cisplatin treatment, there was a significant increase of TOP2 expression (12.780±2.755, **p<0.01), compared to the control (Figure 5.1B). Activating Transcription Factor 3 (ATF-3), a marker of regeneration [548, 552], was also significantly increased following cisplatin treatment (32.680±12.461, ****p<0.0001), compared to the control (Figure 5.1C). The upregulation of ATF-3 expression observed was independent of p53 (Figure 5.2B). Pifithrin-α hydrobromide (Pif-α) was used to inhibit p53. Under normal conditions, Pif-α did not have much of an effect on cell viability (Figure 5.2A). A decrease in cell viability was observed in the cisplatin treated cells, which was worsened when p53 was inhibited. In the absence of Pif-α, cisplatin caused a 60 % decrease in cell viability (control 100±6.066 % vs. cisplatin 59.479±5.286 %, **p<0.01); data not shown due to logarithm axis. This decrease in cell viability was worsened when p53 was inhibited (at 1 µM Pif-α: control 94.644±5.150 % vs. cisplatin 40.615±1.678 %, ****p<0.0001). Cisplatin treatment resulted in upregulation of ATF-3 to a similar degree both in the

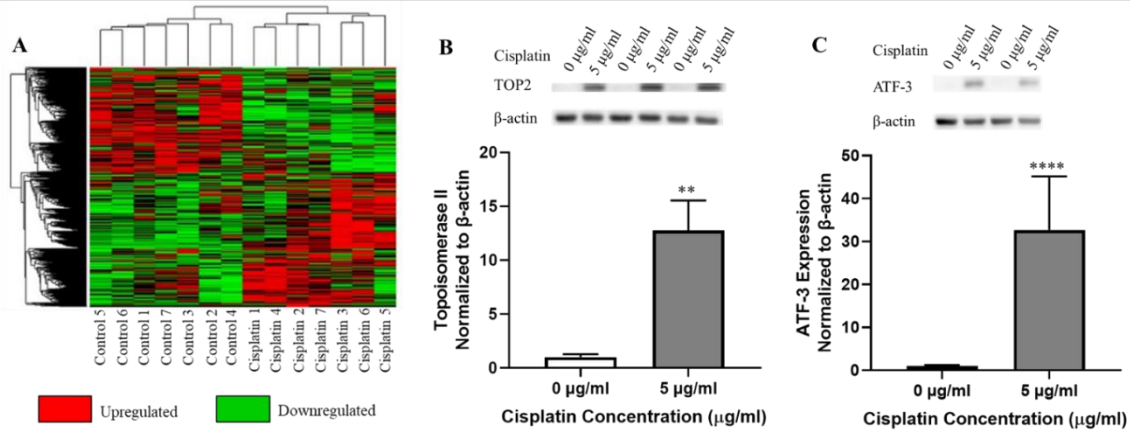

Figure 5.1 Cisplatin upregulates key proteins including topoisomerase II (TOP2) and ATF-3. SH-SY5Y cells were seeded into gelatin-coated 90 mm petri dishes and allowed to reach 90-100 % confluency. Cells were then treated with cisplatin (0 and 5 µg/ml) for 24 hours, protein extracted and sent for proteomics analysis using mass spectrometry [A]. The same samples were also probed for topoisomerase II (TOP2) [B] and ATF-3 [C]. Quantitative mass spectrometry identified key proteins that were upregulated following 24hrs cisplatin treatment, including p53, histone H2A.X and TOP2. This was validated by Western blotting as there was a significant increase in TOP2 expression following cisplatin treatment. There was also a significant increase in ATF-3. β-actin was the loading control. **$p < 0.01$ and ****$p < 0.0001$, Mann-Whitney t-test; n = 7 for mass spectrometry, n = 6 for TOP2 study and n = 12 for ATF-3 study. Error bars are mean+SEM.

Table 5.1 List of the top 20 upregulated and downregulated proteins

UPREGULATED			DOWNREGULATED		
Protein Name	p adjusted	log2FC	Protein Name	p adjusted	log2FC
GDF15_HUMAN	1.01E-214	6.6731	GPC6_HUMAN	1.66E-19	-4.9308
H2A1B_HUMAN	2.05E-20	6.0017	IRAK1_HUMAN	6.05E-09	-4.1188
H2AW_HUMAN	1.75E-54	4.7892	NIN_HUMAN	5.60E-28	-3.8136
MACROH2A1	1.51E-139	4.6343	CAN3_HUMAN	2.14E-27	-3.7787
CDN1A_HUMAN	5.09E-45	4.4481	MSRA_HUMAN	3.57E-06	-3.7223
HMOX1_HUMAN	8.09E-41	4.3132	ERR3_HUMAN	1.96E-19	-3.2959
NEBU_HUMAN	3.23E-34	4.0597	ERR3_HUMAN	1.96E-19	-3.2959
APOH_HUMAN	1.45E-09	3.8137	PARD3_HUMAN	4.39E-17	-3.1334
THBG_HUMAN	2.42E-10	3.7935	PLK1_HUMAN	2.60E-15	-2.9776
ZN594_HUMAN	4.49E-27	3.7341	ALAT2_HUMAN	8.56E-21	-2.9596
TOP2A_HUMAN	**1.79E-26**	**3.7008**	CFA91_HUMAN	9.90E-15	-2.9317
BRI3_HUMAN	9.58E-15	3.5382	ASAP2_HUMAN	0.000122013	-2.9068
SYNE1_HUMAN	2.82E-22	3.4612	LMBD2_HUMAN	1.89E-05	-2.8860
SMC5_HUMAN	5.56E-22	3.4362	KI20A_HUMAN	1.98E-11	-2.8329
S10A8_HUMAN	4.38E-21	3.3881	ANS1B_HUMAN	5.46E-13	-2.7566
AMBP_HUMAN	2.58E-27	3.2052	SMC1B_HUMAN	0.000140599	-2.6682
ABHGB_HUMAN	2.28E-157	3.1986	MYCB2_HUMAN	1.34E-05	-2.6429
TOP2A	**3.99E-18**	**3.1682**	NAV2_HUMAN	0.000154121	-2.5992
H4_HUMAN	0	3.0914	GT2D1_HUMAN	3.69E-06	-2.5388
PEDF_HUMAN	1.79E-32	3.0300	MCM10_HUMAN	4.64E-10	-2.5108

presence and absence of p53 (control 1.000±0.433 vs. cisplatin 9.478±3.145 vs. cisplatin+Pif-α 13.397±6.198, both *p<0.05 compared to the control) (Figure 5.2B).

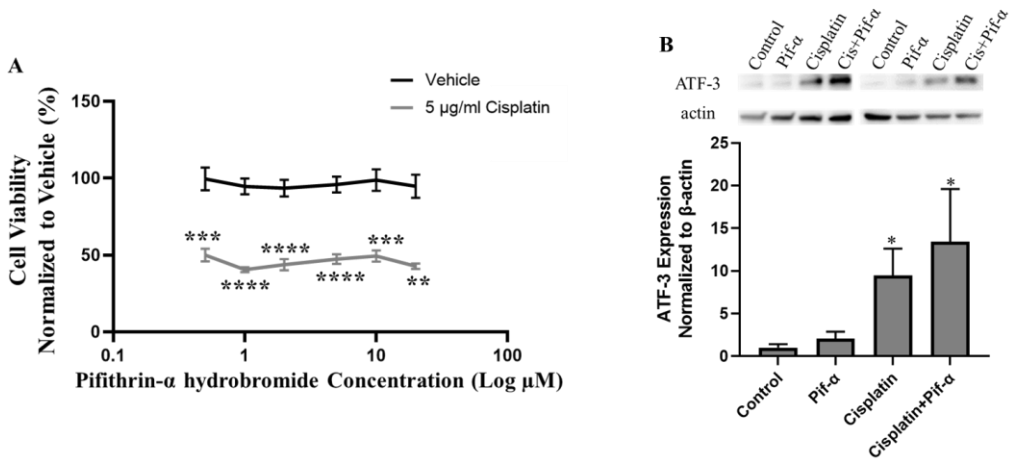

Figure 5.2 Cisplatin-induced upregulation of ATF-3 is independent of p53. SH-SY5Y cells were seeded into gelatin-coated 90 mm petri dishes and allowed to reach 90-100 % confluency. Cells were then treated with varying concentrations of the p53 inhibitor, pifithrin-α hydrobromide (Pif-α, 0-20 µM), in the absence of presence of cisplatin (Cis, 5 µg/ml), for 24 hours, and a cell viability assay performed using Cell Proliferation Reagent WST-1 [A]. A decrease in cell viability was observed in the cisplatin treated cells, which was exacerbated when p53 was inhibited. **p<0.01, ***p<0.001 and ****p < 0.0001, two-way ANOVA compared to the vehicle; n = 8. Error bars are mean+SEM. SH-SY5Y cells, prepared as above, were treated with Pif-α (1 µM), cisplatin (5 µg/ml) or a combination of both. Protein extracted and probed for ATF-3 [B] showed that cisplatin-induced upregulation of ATF-3 was independent of p53. β-actin was the loading control. For ATF-3 expression, n = 5. Error bars are mean+SEM.

5.3.2 Inhibiting topoisomerase II enhances cisplatin-induced ATF-3 upregulation but prevents cisplatin-induced activation of TrkA

Under normal conditions, doxorubicin hydrochloride (Dox) resulted in a dose-dependent decrease in cell viability (Figure 5.3A). At the 2 µM dose, less than 50 % of the cells were viable (43.680±4.066 %). In the cisplatin treated cells, a decrease in cell viability was observed which was exacerbated when TOP2 was inhibited. In the absence of Dox, cisplatin caused a 50 % decrease in cell viability (control 100±1.566 % vs. cisplatin 51.989±0.945 %, ****p<0.0001); data not shown due to logarithm axis. This decrease in cell viability was exacerbated when TOP2 was inhibited (at 0.5 µM Dox: control 66.157±5.192 % vs. cisplatin 12.613±0.773 % and at 2 µM Dox: control 43.680±4.066 % vs. cisplatin 5.143±0.461 %, both ***p<0.001). Cisplatin treatment

resulted in upregulation on ATF-3 (control 1.000±0.203 vs. cisplatin 4.472±1.218, F (3, 16) = 2.417, *p<0.05), which was enhanced when cisplatin was given simultaneously with Dox (control 1.000±0.203 vs. cisplatin+Dox 5.177±0.836, **p<0.01) (Figure 5.3B). In contrast, cisplatin-induced activation of TrkA (control 1.000±0.079 vs. cisplatin 2.010±0.412, *p<0.05) was prevented subsequent to TOP2 inhibition (control 1.000±0.079 vs. cisplatin+Dox 1.421±0.110, ns) F (3, 12) = 3.271 (Figure 5.3D). There appeared to be no effect on TrkA (control 1.000±0.041 vs. cisplatin 0.875±0.096, vs. cisplatin+Dox 0.888±0.039, ns) (Figure 5.3C).

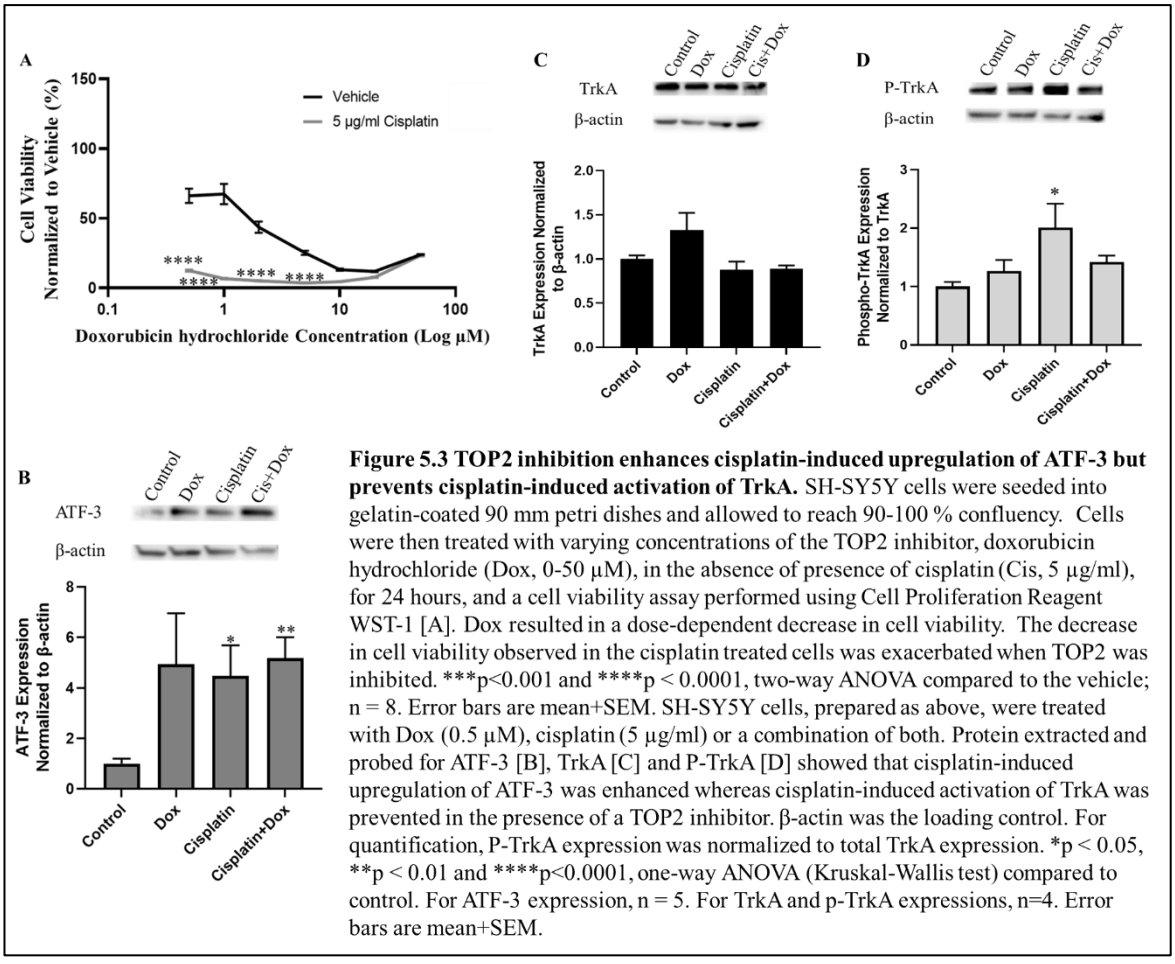

Figure 5.3 TOP2 inhibition enhances cisplatin-induced upregulation of ATF-3 but prevents cisplatin-induced activation of TrkA. SH-SY5Y cells were seeded into gelatin-coated 90 mm petri dishes and allowed to reach 90-100 % confluency. Cells were then treated with varying concentrations of the TOP2 inhibitor, doxorubicin hydrochloride (Dox, 0-50 µM), in the absence of presence of cisplatin (Cis, 5 µg/ml), for 24 hours, and a cell viability assay performed using Cell Proliferation Reagent WST-1 [A]. Dox resulted in a dose-dependent decrease in cell viability. The decrease in cell viability observed in the cisplatin treated cells was exacerbated when TOP2 was inhibited. ***p<0.001 and ****p < 0.0001, two-way ANOVA compared to the vehicle; n = 8. Error bars are mean+SEM. SH-SY5Y cells, prepared as above, were treated with Dox (0.5 µM), cisplatin (5 µg/ml) or a combination of both. Protein extracted and probed for ATF-3 [B], TrkA [C] and P-TrkA [D] showed that cisplatin-induced upregulation of ATF-3 was enhanced whereas cisplatin-induced activation of TrkA was prevented in the presence of a TOP2 inhibitor. β-actin was the loading control. For quantification, P-TrkA expression was normalized to total TrkA expression. *p < 0.05, **p < 0.01 and ****p<0.0001, one-way ANOVA (Kruskal-Wallis test) compared to control. For ATF-3 expression, n = 5. For TrkA and p-TrkA expressions, n=4. Error bars are mean+SEM.

5.3.3 Inhibiting topoisomerase II decreases capsaicin-induced TRPV1 activity

Capsaicin evoked an increase in calcium fluorescence over 300 seconds (Figure 5.4A). The AUC, interpreted as a measure of TRPV1 activity, illustrated capsaicin-induced TRPV1 activation (capsaicin = 12.948±3.675, ****p<0.0001) (Figure 5.4B). In the

absence of capsaicin, no noticeable effect on calcium fluorescence was observed. This capsaicin-induced TRPV1 activation (capsaicin = 13.703±3.910, **p<0.01 compared to control) was significantly diminished when TOP2 was inhibited (capsaicin+0.5 µM Dox = 2.144±2.189 and capsaicin+1 µM Dox = 2.500±1.940, both *p<0.05 compared to capsaicin only) F (4, 61) = 4.142, p < .01 (Figure 5.5B).

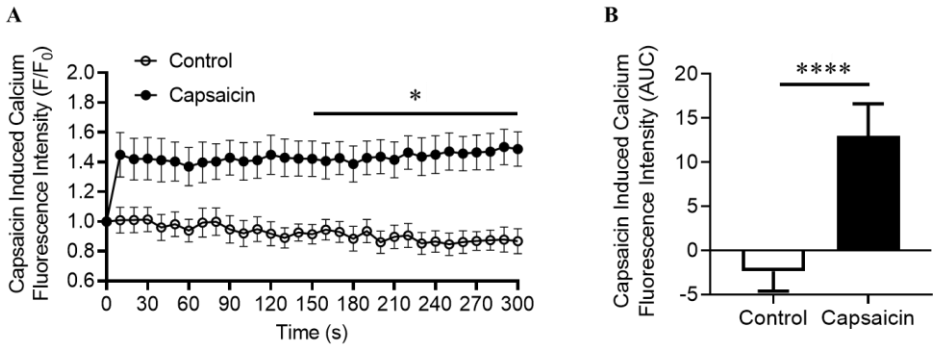

Figure 5.4 Capsaicin-induced TRPV1 activity in primary DRG neurons. Dorsal root ganglia (DRGs) from neonatal mice were isolated, enzymatically dissociated and seeded in the wells of a 96-well plate. Following 48 hours, a calcium flux assay was performed. An initial baseline fluorescence reading was taken (t=0). Capsaicin was then added to one group and fluorescence readings were taken every 10 seconds for 300 seconds. For each well, the fluorescence was expressed relative to it's own baseline, giving the fold change (F/F_0) in intracellular calcium fluorescence intensity [A]. AUC of this capsaicin-induced calcium fluorescence intensity fold change over the time course was interpreted as a measure of TRPV1 activity [B]. Capsaicin activated nociceptive primary sensory neurons. ****p < 0.0001, Mann-Whitney t-test. Error bars are mean+SEM.

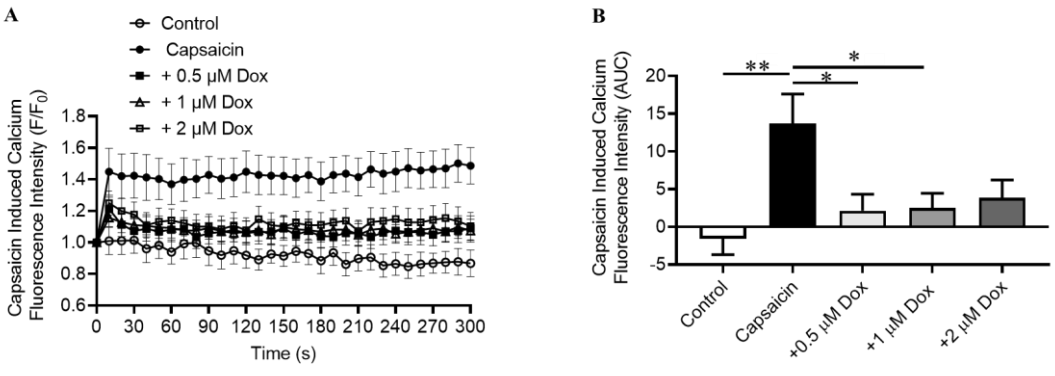

Figure 5.5 TOP2 inhibition diminished nociceptor activation. Dorsal root ganglia (DRGs) from neonatal mice were isolated, enzymatically dissociated and seeded in the wells of a 96-well plate. The following day, the cultures were treated for 24 hours with varying concentrations of doxorubicin hydrochloride (Dox: 0, 0.5, 1 and 2 µM). A calcium flux assay was then performed. In the presence of the TOP2 inhibitor, capsaicin-induced neuronal activation was diminished [A]. AUC showed a significant increase in TRPV1 activity following the addition of capsaicin (black), which was inhibited in the presence of a TOP2 inhibitor (0.5 and 1 µM) [B]. *p < 0.05 and **p < 0.01, one-way ANOVA (Kruskal-Wallis test) compared to the capsaicin group. Error bars are mean+SEM.

5.3.4 Cisplatin enhances capsaicin-induced TRPV1 activation, which is attenuated when topoisomerase II is inhibited

Capsaicin evoked an increase in calcium fluorescence over 300 seconds in both the vehicle and cisplatin groups (Figure 5.6A). Capsaicin-induced TRPV1 activation was greater following cisplatin treatment (control = 5.405±2.471 vs cisplatin = 15.840±3.176, **p<0.01) (Figure 5.6B). Capsaicin-induced TRPV1 activation was attenuated when TOP2 was inhibited (cisplatin+0.5 µM Dox = 8.246±2.746, cisplatin+1 µM Dox = 8.767±2.561 and cisplatin+2 µM Dox = 8.066±4.520); levels returned to almost that of the vehicle control (Figures 5.6C and D).

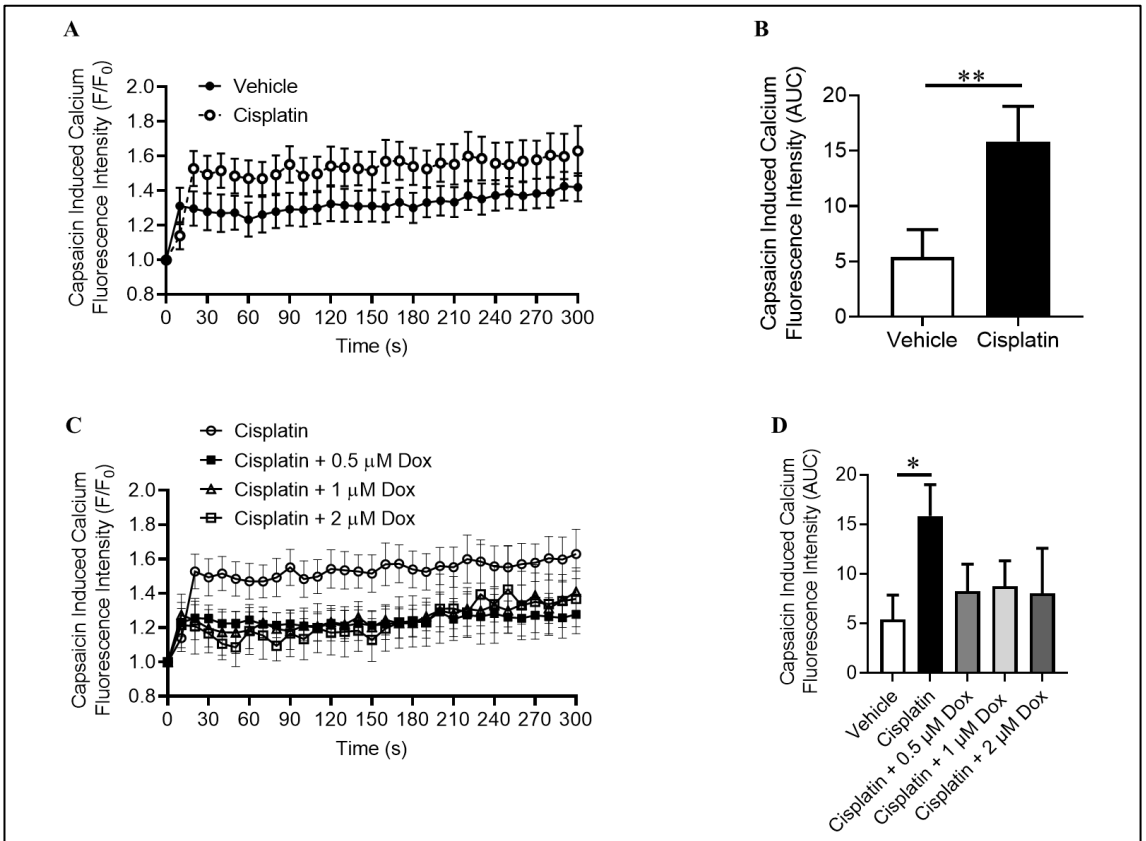

Figure 5.6 Effect of cisplatin and doxorubicin hydrochloride on nociceptor activation. Dorsal root ganglia (DRGs) from neonatal mice were isolated, enzymatically dissociated and seeded in the wells of a 96-well plate. The following day, the cultures were treated for 24 hours with 5µg/ml cisplatin and varying concentrations of doxorubicin hydrochloride (0, 0.5, 1 and 2 µM). A calcium flux assay was then performed. Cisplatin treatment resulted in greater TRPV1 activation compared to vehicle [A&B]. **p < 0.01, Mann-Whitney t-test. TOP2 inhibition in the presence of cisplatin attenuated neuronal activation to levels almost back to that of the vehicle control [C&D]. *p < 0.05, one-way ANOVA (Kruskal-Wallis test) compared to the vehicle). Error bars are mean+SEM.

5.4 Discussion

5.4.1 ATF-3 induction following cisplatin treatment

In our cisplatin rodent model, an increase in nerve fibre growth was observed subsequent to cisplatin treatment. Cisplatin causes DNA DSBs [285, 286]. Additionally DSBs have been shown to induce ATF-3 activation and promote regeneration following nerve injury [525]. Hence the induction of ATF-3 is indicative of nerve growth. Cisplatin treatment in SH-SY5Y cells significantly induced ATF-3, which have been demonstrated both in vitro and in vivo [346, 408]. ATF-3 was significantly induced in various human cancer-derived cell lines following 24-hours cisplatin treatment [408]. The cell lines utilized were MCF-7 (breast adenocarcinoma), A549 (lung carcinoma), SKOV-3 (ovarian carcinoma), PC3 (prostate carcinoma), and A2780-cp (ovarian carcinoma) and ATF-3 induction was evidenced at both the mRNA and protein levels. Treatment with 10 µg/ml cisplatin for 24 hours induced AFT-3 in all cell lines whereas 1 µg/ml, a non-cytotoxic dose, only induced ATF-3 in the SKOV-3 cell line. In our cell model, treatment with 5 µg/ml cisplatin increased ATF-3 expression by more than 30-folds. In chapter 3, this concentration of cisplatin decreased cell viability by about 40 % (Figure 3.2) as well as induced a DNA damage response (Figure 3.4). ATF-3, being a marker of nerve injury [545], it is not surprising that there was such a significant increase in ATF-3 expression. Cisplatin also resulted in a significant upregulation of p53 (Figure 3.4A) as part of the DNA damage response. Inhibiting p53 under normal conditions did not impact on cell viability because in normal cells, the protein level of p53 is low, due to Mdm2; the major regulator of p53 which is responsible for its degradation [296, 297]. Since ATF-3 expression levels following cisplatin treatment were not impacted when p53 was inhibited, cisplatin-induced upregulation of ATF-3 was independent of p53. This coincides with the findings of St. Germain et al. [408], which also illustrated that the induction of ATF-3 by cisplatin was independent of a p53 mechanism as cisplatin induced ATF-3 in two p53 functionally null cells lines (SKOV-3 and PC3). However, studies have shown that ATF-3 stabilizes and activates p53 by blocking its ubiquitination [582, 583].

5.4.2 TOP2 inhibition induces ATF-3

Another protein which was significantly increased following cisplatin treatment was Topoisomerase II (TOP2). TOP2, which has two isoforms, TOP2α and TOP2β, catalyses double stranded breaks by transiently cleaving a pair of complementary DNA strands; a process that is essential for preventing supercoiling of DNA [584]. Topoisomerases play an important role in various processes including DNA replication, transcription, genome stability and DNA repair [530–532, 585, 586]. In vertebrate cells, TOP2α and TOP2β have similar structure and function but different biological roles [529]. TOP2α is essential for proliferation [587] whereas TOP2β has a critical role in neural development [588]. Inhibiting TOP2 inhibits the resealing of cleaved DNA strands, resulting in increased DNA fragmentation and cell death [589]. In our study, the TOP2 inhibitor, doxorubicin hydrochloride, resulted in a drastic decrease in cell viability in SH-SY5Y cells. Combining with cisplatin exacerbated cytotoxicity. Other studies have also exhibited the toxicity of doxorubicin in a dose-dependent manner [557, 590, 591]. The sensitivity of SH-SY5Y cells to doxorubicin appeared to be similar to that of the gallbladder cancer cell line OCUG-1 [591], which had an IC_{50} of 1.5±0.04 µM. On the other hand, HK-2 cells, a proximal tubular cell line derived from normal kidney [557] ,and NOZ cells, a gallbladder cancer cell line [591], were both more resistant to doxorubicin cytotoxicity than the SH-SY5Y cells. A dose of 8 µM Dox (maximum dose utilized in the study) caused only a 60 % decrease in cell viability in HK-2 cells whereas NOZ cells had an IC_{50} of 16.1±0.02 µM.

Studies have shown that doxorubicin induces ATF-3 in a dose-dependent and time-dependent manner [557, 590]. Doxorubicin treatment also brought about an increase in the DNA damage markers p53 [557] and γH2AX [590], denoting activation of a DNA damage response, similar to what was observed in our in vitro model following cisplatin treatment (Figures 3.4A and D). Since ATF-3 is regarded as a marker of nerve injury [545], it is not surprising that doxorubicin induced ATF-3. In our study, doxorubicin resulted in elevated levels of ATF-3, however, it was not significant ($p = 0.0646$, one-way ANOVA). This may be due to sampling variability between the samples. Although, a t-test between the two groups (control vs Dox) indicated significance (**$p = 0.0079$).

In contrast to p53 inhibition, inhibiting TOP2 enhanced cisplatin-induced ATF-3 upregulation. As it has been evidenced that both cisplatin and doxorubicin are

cytotoxic and they both induce ATF-3, it is conceivable that they can have a synergistic effect, producing more damage in combination and hence increased upregulation of ATF-3. The fact that ATF-3 expression levels were upregulated following cisplatin treatment and enhanced when TOP2 was inhibited in combination with cisplatin, but unaffected when p53 was inhibited, supports the notion that the increase in ATF-3 was in response to DNA damage.

5.4.3 Effect of TOP2 inhibition on TrkA in vitro

In our study, Dox did not appear to impact upon TrkA and P-TrkA (as a ratio to TrkA) levels in SH-SY5Y cells. This coincides with the recent findings of Cappabianca et al. [592], which also demonstrated that Dox (0.5 and 1 µg/ml) did not induce TrkA phosphorylation. The only difference with this study and ours is that treatment was only performed for 6 hours as opposed to 24 hours. Contrary to our findings, a study performed by Liao et al. [593], illustrated a significant decrease in the levels of TrkA and P-TrkA/TrkA ratio in rat cardiomyocytes following doxorubicin treatment (total dose 17.5 mg/kg, i.p.). The disparity between the work of Liao et al., 2019 and our work may result from the different types of cells utilized for the study as well as method of treatment. With regards to cisplatin given in combination with Dox, cisplatin-induced activation of TrkA was prevented.

Neonatal primary DRG neurons were then used to further investigate the effect of TOP2 inhibition in combination with cisplatin treatment. TRPV1 is activated by capsaicin [569, 594], which results in an influx of Ca^{2+} into the cell, leading to depolarization of the neurons, generation of an action potential and finally sensation [595]. In our study, under normal conditions, capsaicin evoked TRPV1 activation. However, in the presence of Dox, this capsaicin-induced activation of TRPV1 was significantly decreased. In contrast, doxorubicin treatment in human breast cancer MCF-7 cells activated TRPV1 [596]. This discrepancy can possibly be accounted for by the difference in cell type. Cisplatin treatment caused greater TRPV1 activation compared to the control. It is believed that this is attributed to the activation of TrkA, which was demonstrated to be induced subsequent to cisplatin treatment (Figure 4.2). Studies have linked TRPV1 sensitization to TrkA activation [516, 517, 570, 571, 573]. Additionally, TRPV1 activation has been implicated in the development of mechanical and thermal hypersensitivity as a TRPV1 antagonist caused partial inhibition to the

development of mechanical hypersensitivity as well as reduced the development of thermal hypersensitivity [497]. As evidenced by our cisplatin rodent model, cisplatin treatment resulted in increased sensitivity to mechanical sensitization (Figure 3.1), which was ameliorated when TrkA activation was inhibited (Figure 4.6).

Similar to what occurred under normal conditions, Dox attenuated cisplatin-induced TRPV1 activation, to levels almost back to that of the vehicle control. In our cell model, we demonstrated that Dox prevented cisplatin-induced TrkA activation, which can possibly account for the diminished TRPV1 activation. If this is the case, it can be hypothesized that TOP2 may be a source of cisplatin-induced TrkA activation and thereby a contributing factor to nociceptor sensitization and cisplatin-induced survivorship pain.

5.5 Concluding remarks

In vitro, following cisplatin treatment in SH-SY5Y cells, there was increased activation of TrkA, alongside upregulation of TOP2 expression levels. When TOP2 was inhibited using Dox, in conjunction with cisplatin treatment, this cisplatin-induced activation was prevented. In DRGs, cisplatin treatment resulted in capsaicin-induced TRPV1 activation. Inhibiting TOP2 during cisplatin treatment attenuated TRPV1 activity to levels almost back to that of the vehicle control. It appears that TOP2 is mediating TrkA activation following cisplatin treatment and a probable facilitator of nociceptor sensitization and cisplatin-induced survivorship pain. As a result, TOP2 inhibition can be explored as a possible therapy for cisplatin-induced peripheral neuropathy.

Chapter 6: Concluding Discussion

The work in this thesis corroborates the involvement of TrkA signalling in the induction of aberrant nerve growth, nociceptor sensitization and the development of chronic pain subsequent to neonatal cisplatin treatment. Furthermore, the findings in this thesis have identified topoisomerase II as a potential target for inhibiting TrkA activation and doxorubicin as a potential therapeutic agent for alleviating nociceptor sensitization and thus cisplatin-induced peripheral neuropathy.

Both in vitro and in vivo modelling systems were utilized to investigate the effects of cisplatin treatment and the role of TrkA signalling in the development of cisplatin-induced peripheral neuropathy. In vitro, the cytotoxic effect of cisplatin was demonstrated. Following 24-hours cisplatin treatment, DRG sensory neurons underwent neurodegeneration in a dose-dependent manner; there was a decrease in neurite outgrowth with increasing concentration of cisplatin. Similarly, SH-SY5Y cells displayed a dose-dependent decrease in cell viability. This cisplatin-induced sensory neurodegeneration and pain was associated with the initiation of DDR signalling, evidenced by upregulation of p53, phosphorylated p53 and γH2A.X. In vivo, administration of cisplatin to neonatal rats resulted in a persistent but delayed onset of chronic pain. Rodents presented with increased sensitivity to mechanical stimuli (mechanical hypersensitivity). These models confirmed the hallmarks of CIPN, neurodegeneration and peripheral sensory neuronal sensitization.

This persistent but delayed onset of chronic pain that was observed subsequent to cisplatin treatment in neonatal rats was accompanied by aberrant nerve fibre growth. Inhibiting TrkA signalling via the introduction of a TrkA inhibitor ameliorated the cisplatin-induced mechanical hypersensitivity as well as prevented the accompanying aberrant nerve fibre growth. Moreover, these events coincided with those observed following NGF-induced activation of TrkA, further supporting the involvement of TrkA signalling in nociceptor sensitization, the induction of aberrant nerve fibre growth and the onset of chronic pain, all of which are linked to CIPN.

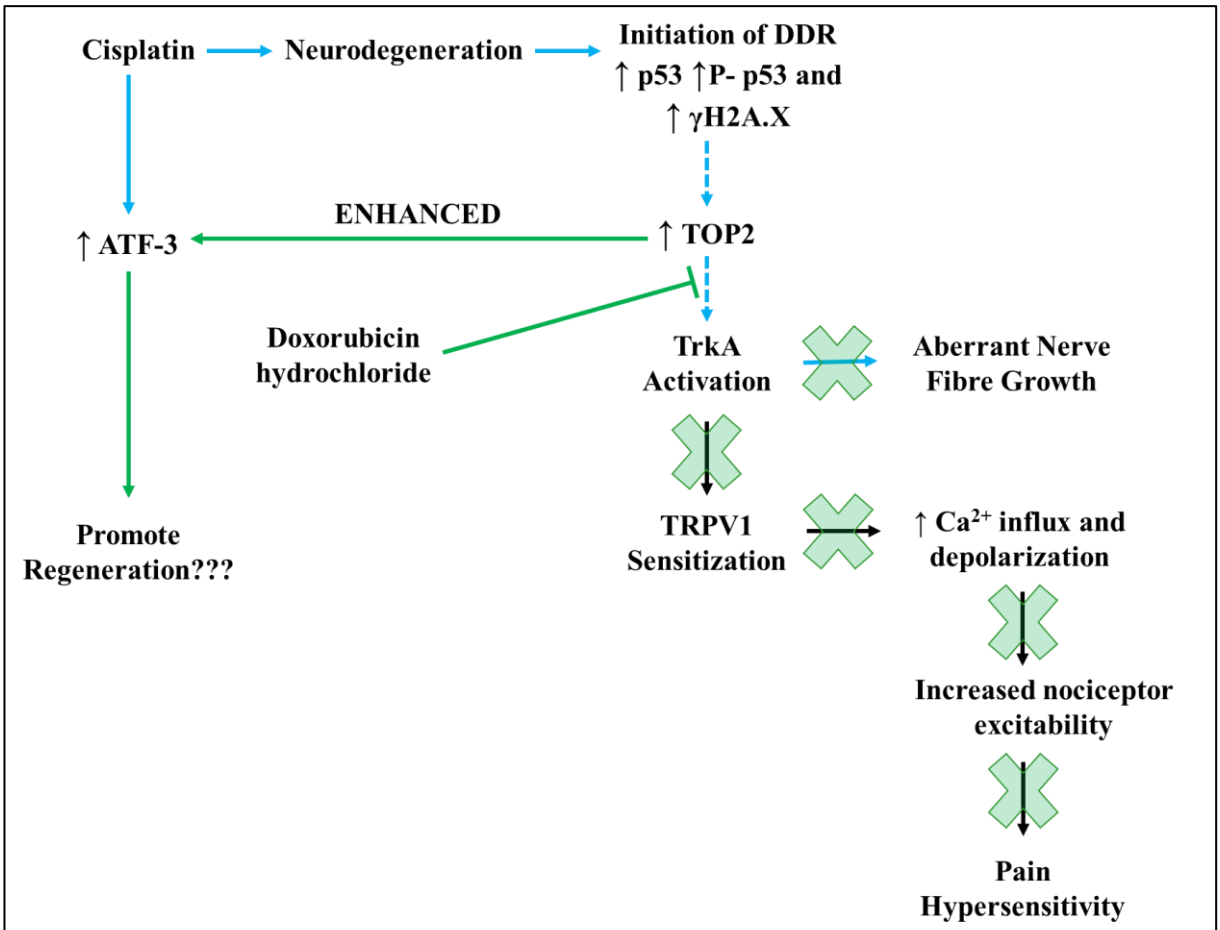

Figure 6.1 A schematic illustrating TOP2-associated TrkA activation as a proposed mechanism of CIPN in childhood cancer survivorship. Cisplatin treatment causes neurodegeneration of sensory neurons and induces a DDR, with upregulation of p53, P-p53 and γH2A.X. This in turns results in upregulation of TOP2 and subsequent activation of the TrkA receptors. TrkA activation results in aberrant nerve fibre growth and the onset of pain hypersensitivity through TRPV1 sensitization. Sensitization of TRPV1 leads to increased Ca^{2+} influx and membrane depolarization, resulting in increased nociceptor excitability and consequently increased nociception, which is exhibited as pain hypersensitivity. In vitro, inhibiting TOP2 using doxorubicin hydrochloride prevented TrkA activation and attenuated nociceptor activation. In vivo, inhibiting TrkA signalling ameliorated cisplatin-induced pain hypersensitivity and prevented cisplatin-induced aberrant nerve fibre growth. Additionally, TOP2 inhibition, in the presence of nerve injury, enhanced ATF-3 upregulation, which may play a regenerative role. Blue solid lines denote findings in this thesis; blue dashed lines denote a hypothesized mechanism based on the literature or inferred from the results of this thesis; black solid lines denote effects already established in the literature; green lines and Xs denote the inhibitory effects of doxorubicin hydrochloride.

In vitro, 24-hours cisplatin treatment of SH-SY5Y cells triggered endogenous activation of the TrkA receptor. Topoisomerase II was identified as a potential source of TrkA activation and doxorubicin a potential therapeutic agent for alleviating nociceptor sensitization and thus cisplatin-induced peripheral neuropathy. SH-SY5Y cells treated with cisplatin for 24 hours exhibited upregulated levels of both ATF-3 and TOP2. Inhibiting TOP2 using doxorubicin enhanced cisplatin-induced

upregulation of ATF-3 but prevented cisplatin-induced activation of TrkA. In addition, DRG sensory neurons displayed capsaicin-induced activation of TRPV1, which was increased following 24-hours cisplatin treatment, demonstrating sensitization of nociceptor activity subsequent to cisplatin treatment. Under normal conditions, TOP2 inhibition diminished nociceptor sensitization which was induced by capsaicin. Furthermore, giving cisplatin concomitantly with doxorubicin, thereby inhibiting TOP2 activity, suppressed the activity of these nociceptors down to normal levels. A schematic is presented in Figure 6.1.

6.1 Topoisomerase II (TOP2): A therapeutic target for nociceptor sensitization associated with cisplatin-induced peripheral neuropathy?

Literature has shown that DNA topoisomerases modulate nociceptor activity under stress and damage [525]. Topoisomerase inhibitors were demonstrated to be neuroprotective and induced neuroregeneration in an ATF-3 dependent manner. This work wanted to explore how DNA topoisomerases were modulating TrkA function as our cisplatin rodent model revealed an association between TrkA signalling and aberrant nerve fibre growth with the development of chronic pain. Using proteomics, topoisomerase II (TOP2) was identified as a key protein that was upregulated following cisplatin treatment. The study conducted by Cheng et al. [525] named doxorubicin as one of the topoisomerase inhibitors capable of inducing ATF-3 and promoting neuroregeneration. Furthermore, similar to this study, inhibiting TOP2 in the presence of damage enhanced ATF-3. The work in this thesis has demonstrated the involvement of TrkA signalling in the development of CIPN and shown the effectiveness of inhibiting TrkA activation in providing pain relief. In vitro, inhibiting TOP2 successfully prevented cisplatin-induced TrkA activation in SH-SY5Y cells as well as suppressed cisplatin-induced TRPV1 activation and subsequent nociceptor sensitization in DRG sensory neurons. It is possible that a novel target has been discovered that is capable of promoting regeneration whilst simultaneously providing pain relief.

However, there is a caveat. Doxorubicin is shown to be toxic. There is a possibility though that this toxicity may be only short-lived and once washed out, the stressed

incurred may be relieved. Doxorubicin also appears to inhibit the catalytic cycle of TOP2 via two different mechanisms depending on the concentration utilized, with low concentrations (<1 μM) producing a more toxic outcome than higher concentrations (>10 μM) [597]. Hence, a concentration of doxorubicin greater than 10 μM may be less toxic in nature. Otherwise, an alternative drug that inhibits TOP2 may need to be considered for in vivo analysis.

6.2 Doxorubicin as a therapeutic for cisplatin-induced peripheral neuropathy

DNA damage following cisplatin treatment has been shown to induce a state of senescence [598–600]. Recent studies have associated CIPN with the induction of senescence [601, 602]. One study revealed that cisplatin induced DDR activation and upregulation of p21, which lead to senescence as opposed to apoptosis [601]. DRG sensory neurons isolated from cisplatin-treated mice that developed CIPN showed upregulation of the cyclin-dependent kinase inhibitor 1a (*Cdkn1a*) gene, increased expression levels of p21, phospho-H2A.X and nuclear factor kappa B (NfκB)-p65 as well as significantly higher senescence-associated β- galactosidase (SA-β-Gal) staining, all of which are senescence hallmarks. Additionally, there was no difference in protein expression levels of cleaved caspase-3 (CC3). In another study, clearance of senescent-like cells from DRG sensory neurons of mice, using genetic and pharmacologic methods, reversed CIPN that was induced by cisplatin [602]. Cisplatin-induced upregulation of p21 and p16 expression levels also returned to levels similar to that of the control group control subsequent to the clearance of senescent cells. Doxorubicin has been demonstrated to be one of the most efficient cytotoxic drugs against senescent cells [603].

It has been revealed that post-mitotic cells can undergo senescence [604], which is associated with the acquisition of a senescence-associated secretory phenotype (SASP). Cells of post-mitotic cellular senescence secrete high levels of inflammatory cytokines, growth factors and proteases. These can contribute to the “inflammatory soup” (discussed in section 1.3), providing an additional source for nociceptor activation and subsequent sensitization. Henceforth, possible removal of senescent cells by doxorubicin could have led to a reduction in the levels of pro-inflammatory

SASP components, preventing activation of TrkA receptors. A further investigation into the mechanism behind the prevention of cisplatin-induced TrkA activation and the suppression of cisplatin-induced neuronal activation of DRG sensory neurons by doxorubicin is recommended. Exploring the effect of an alternative TOP2 inhibitor, as suggested in section 6.1, can provide an answer to this concept.

6.3. Future direction

The work in this thesis provides the first evidence that doxorubicin treatment prevents cisplatin-induced activation of TrkA and suppresses cisplatin-induced neuronal activation, which leads to nociceptor sensitization and development of CIPN. Two mechanisms of action of doxorubicin have been presented; TOP2 inhibition, implicating TOP2 as a source of TrkA activation, and senolysis, implicating cellular senescence as the contributing factor to the activation of TrkA receptors. There is also the possibility of a synergistic effect; both mechanisms working together to produce the observed outcomes. Much of this work, however, was performed in vitro and requires further validation in vivo. Once the mechanism of action of doxorubicin has been established, a suitable drug delivery system for in vivo investigation can be developed. This work provides the basis for the following experimental hypotheses to be tested.

1) Doxorubicin suppresses cisplatin-induced nociceptor activation by inhibiting TOP2 and/or via senolysis.
2) Doxorubicin treatment alleviates the symptoms of CIPN in rodent model.

Testing of experimental hypothesis one would involve trialling an alternative TOP2 inhibitor, presumably one that is less toxic. If TrkA activation is also suppressed, this strengthens the evidence of TOP2-mediated TrkA activation as a mechanism of long-term pain in childhood cancer survivorship. A less toxic drug would also be more favourable when it comes to in vivo analysis. Furthermore, inhibiting TOP2 enhanced cisplatin-induced ATF-3 upregulation. Cheng et al. demonstrated that topoisomerase inhibition, in the presence of peripheral nerve injury, had a regenerative effect in sensory neurons [525]. Taking this into account, it is possible that an analgesic with the ability to promote regeneration may have been discovered, thereby not only focusing on treating the symptom but the source. In contrast, if TOP2 is not the target,

this can be interpreted as doxorubicin possibly being a therapeutic agent. One challenge for the future would be developing an effective delivery system for the drug. TOP2 plays an important role in various processes including DNA replication and transcription so complete inhibition would detrimental. Instead, the drug would need to be delivered to a targeted region; perhaps the DRGs as they have been shown to have increased susceptibility to cisplatin.

One limitation of the study is that the in vivo analysis was performed in rats whereas the capsaicin model consisted of DRGs isolated from mice. Podratz et al. demonstrated that neurotoxicity to the DRG neurons varied between rodent strains following cisplatin treatment [338], with mice displaying greater sensitive to cisplatin than rats. At the time, mice were more readily available as they were already being utilized in the laboratory for the collection of other tissues. Additionally, more tools exist that are compatible with mice, such as neuron isolation, and we were planning for single cell sequencing. However, due to time constraints, we were unable to perform those experiments. Prior to in vivo experiments, the effect of the TOP2 inhibitor should be investigated on rat DRG neurons to validate TOP2-mediated TrkA activation subsequent to cisplatin treatment. Another limitation is the much lower dose of cisplatin used in the rodent model compared to what is administered in the clinic. CIPN is a dose-limiting side effect, which occurs in a dose-dependent manner. The severity of CIPN increases with higher cumulative doses so the higher the dose of drug administered, the greater the neurotoxicity. This needs to be taken into consideration when it comes to the in vivo studies as mechanisms of action may vary with varying drug concentrations.

6.4. Key observations

1) Cisplatin resulted in neurodegeneration in DRG sensory neurons and a dose-dependent decrease in cell viability in SH-SY5Y cells
2) Cisplatin induced a DNA damage response with upregulation of p53, P-p53 and γH2A.X in SH-SY5Y cells
3) Cisplatin induced TrkA activation in SH-SY5Y cells
4) In vivo, cisplatin treatment resulted in mechanical hypersensitivity which was accompanied by aberrant nerve fibre growth. Similar phenotypes were observed following NGF-induced TrkA activation, supporting the hypothesis of cisplatin-

induced TrkA activation as a possible instigator in the onset of cisplatin-induced peripheral neuropathy

5) Administration of the TrkA inhibitor GW441756, thereby inhibiting TrkA activation, ameliorated cisplatin-induced mechanical hypersensitivity and prevented cisplatin-induced nerve fibre growth. Similar outcomes were observed in our NGF model, providing further evidence for the involvement of TrkA activation in the onset of cisplatin-induced peripheral neuropathy
6) Cisplatin treatment upregulated TOP2 and ATF-3 in SH-SY5Y cells. This upregulation in ATF-3 was independent of p53
7) Inhibiting TOP2 using doxorubicin hydrochloride enhanced cisplatin-induced ATF-3 upregulation and prevented cisplatin-induced TrkA activation in SH-SY5Y cells
8) Cisplatin enhanced nociceptor activation in DRG sensory neurons, which was attenuated when TOP2 was inhibited.

References

1 Meltzer, S., Santiago, C., Sharma, N. and Ginty, D. D. (2021) The cellular and molecular basis of somatosensory neuron development. *Neuron* **109**, 3736–3757 https://doi.org/10.1016/j.neuron.2021.09.004

2 Krames, E. S. (2014) The Role of the Dorsal Root Ganglion in the Development of Neuropathic Pain. *Pain Med* **15**, 1669–1685 https://doi.org/10.1111/pme.12413

3 Dubin, A. E. and Patapoutian, A. (2010) Nociceptors: the sensors of the pain pathway. *J. Clin. Invest.* **120**, 3760–3772 https://doi.org/10.1172/JCI42843

4 Djouhri, L. and Lawson, S. N. (2004) Aβ-fiber nociceptive primary afferent neurons: a review of incidence and properties in relation to other afferent A-fiber neurons in mammals. *Brain Research Reviews* **46**, 131–145 https://doi.org/10.1016/j.brainresrev.2004.07.015

5 Rask, CynthiaA. (1999) Biological Actions of Nerve Growth Factor in the Peripheral Nervous System. *Eur Neurol* **41**, 14–19 https://doi.org/10.1159/000052075

6 Light, A. R. and Perl, E. R. (1993) Peripheral sensory systems. In Peripheral Neuropathy, pp 149–165, W.B Saunders, Philadelphia

7 Woolf, C. J. and Ma, Q. (2007) Nociceptors—Noxious Stimulus Detectors. *Neuron* **55**, 353–364 https://doi.org/10.1016/j.neuron.2007.07.016

8 Purves, D. (Ed.). (2012) Neuroscience 5th ed., Sinauer Associates, Sunderland, Mass

9 Basbaum, A. I., Bautista, D. M., Scherrer, G. and Julius, D. (2009) Cellular and Molecular Mechanisms of Pain. *Cell* **139**, 267–284 https://doi.org/10.1016/j.cell.2009.09.028

10 Schmidt, R., Schmelz, M., Forster, C., Ringkamp, M., Torebjork, E. and Handwerker, H. (1995) Novel classes of responsive and unresponsive C nociceptors in human skin. *J. Neurosci.* **15**, 333–341 https://doi.org/10.1523/JNEUROSCI.15-01-00333.1995

11 Van Hees, J. and Gybels, J. (1981) C nociceptor activity in human nerve during painful and non painful skin stimulation. *Journal of Neurology, Neurosurgery & Psychiatry* **44**, 600–607 https://doi.org/10.1136/jnnp.44.7.600

12 Venkatachalam, K. and Montell, C. (2007) TRP Channels. *Annu. Rev. Biochem.* **76**, 387–417 https://doi.org/10.1146/annurev.biochem.75.103004.142819

13 Levine, J. D. and Alessandri-Haber, N. (2007) TRP channels: Targets for the relief of pain. *Biochimica et Biophysica Acta (BBA) - Molecular Basis of Disease* **1772**, 989–1003 https://doi.org/10.1016/j.bbadis.2007.01.008

14 Dhaka, A., Viswanath, V. and Patapoutian, A. (2006) TRP ion channels and temperature sensation. *Annu. Rev. Neurosci.* **29**, 135–161 https://doi.org/10.1146/annurev.neuro.29.051605.112958

15 Le Pichon, C. E. and Chesler, A. T. (2014) The functional and anatomical dissection of somatosensory subpopulations using mouse genetics. *Front. Neuroanat.* **8**, article 21 https://doi.org/10.3389/fnana.2014.00021

16 Caterina, M. J. and Julius, D. (2001) The Vanilloid Receptor: A Molecular Gateway to the Pain Pathway. *Annu. Rev. Neurosci.* **24**, 487–517 https://doi.org/10.1146/annurev.neuro.24.1.487

17 Cavanaugh, D. J., Chesler, A. T., Braz, J. M., Shah, N. M., Julius, D. and Basbaum, A. I. (2011) Restriction of Transient Receptor Potential Vanilloid-1

to the Peptidergic Subset of Primary Afferent Neurons Follows Its Developmental Downregulation in Nonpeptidergic Neurons. *Journal of Neuroscience* **31**, 10119–10127 https://doi.org/10.1523/JNEUROSCI.1299-11.2011

18 Story, G. M., Peier, A. M., Reeve, A. J., Eid, S. R., Mosbacher, J., Hricik, T. R., et al. (2003) ANKTM1, a TRP-like Channel Expressed in Nociceptive Neurons, Is Activated by Cold Temperatures. *Cell* **112**, 819–829 https://doi.org/10.1016/S0092-8674(03)00158-2

19 Peier, A. M., Moqrich, A., Hergarden, A. C., Reeve, A. J., Andersson, D. A., Story, G. M., et al. (2002) A TRP Channel that Senses Cold Stimuli and Menthol. *Cell* **108**, 705–715 https://doi.org/10.1016/S0092-8674(02)00652-9

20 Sugiura, Y., Lee, C. L. and Perl, E. R. (1986) Central Projections of Identified, Unmyelinated (C) Afferent Fibers Innervating Mammalian Skin. *Science* **234**, 358–361 https://doi.org/10.1126/science.3764416

21 Rexed, B. (1952) The cytoarchitectonic organization of the spinal cord in the cat. *J. Comp. Neurol.* **96**, 415–495 https://doi.org/10.1002/cne.900960303

22 D'Mello, R. and Dickenson, A. H. (2008) Spinal cord mechanisms of pain. *British Journal of Anaesthesia* **101**, 8–16 https://doi.org/10.1093/bja/aen088

23 Todd, A. J. (2002) Anatomy of Primary Afferents and Projection Neurones in the Rat Spinal Dorsal Horn with Particular Emphasis on Substance P and the Neurokinin 1 Receptor. *Experimental Physiology* **87**, 245–249 https://doi.org/10.1113/eph8702351

24 Yam, M., Loh, Y., Tan, C., Khadijah Adam, S., Abdul Manan, N. and Basir, R. (2018) General Pathways of Pain Sensation and the Major Neurotransmitters Involved in Pain Regulation. *IJMS* **19**, article 2164 https://doi.org/10.3390/ijms19082164

25 Cioffi, C. L. (2018) Modulation of Glycine-Mediated Spinal Neurotransmission for the Treatment of Chronic Pain. *J. Med. Chem.* **61**, 2652–2679 https://doi.org/10.1021/acs.jmedchem.7b00956

26 Marmigère, F. and Ernfors, P. (2007) Specification and connectivity of neuronal subtypes in the sensory lineage. *Nat Rev Neurosci* **8**, 114–127 https://doi.org/10.1038/nrn2057

27 Ma, Q., Fode, C., Guillemot, F. and Anderson, D. J. (1999) NEUROGENIN1 and NEUROGENIN2 control two distinct waves of neurogenesis in developing dorsal root ganglia. *Genes & Development* **13**, 1717–1728 https://doi.org/10.1101/gad.13.13.1717

28 Lawson, S. N. and Biscoe, T. J. (1979) Development of mouse dorsal root ganglia: an autoradiographic and quantitative study. *J Neurocytol* **8**, 265–274 https://doi.org/10.1007/BF01236122

29 Fitzgerald, M. (2005) The development of nociceptive circuits. *Nat Rev Neurosci* **6**, 507–520 https://doi.org/10.1038/nrn1701

30 Frank, E. and Sanes, J. R. (1991) Lineage of neurons and glia in chick dorsal root ganglia: analysis in vivo with a recombinant retrovirus. *Development* **111**, 895–908 https://doi.org/10.1242/dev.111.4.895

31 Perez, S. E., Rebelo, S. and Anderson, D. J. (1999) Early specification of sensory neuron fate revealed by expression and function of neurogenins in the chick embryo. *Development* **126**, 1715–1728 https://doi.org/10.1242/dev.126.8.1715

32 George, L., Kasemeier-Kulesa, J., Nelson, B. R., Koyano-Nakagawa, N. and Lefcort, F. (2010) Patterned assembly and neurogenesis in the chick dorsal root ganglion. *J. Comp. Neurol.* **518**, 405–422 https://doi.org/10.1002/cne.22248
33 Blanchard, J. W., Eade, K. T., Szűcs, A., Lo Sardo, V., Tsunemoto, R. K., Williams, D., et al. (2015) Selective conversion of fibroblasts into peripheral sensory neurons. *Nat Neurosci* **18**, 25–35 https://doi.org/10.1038/nn.3887
34 Maro, G. S., Vermeren, M., Voiculescu, O., Melton, L., Cohen, J., Charnay, P., et al. (2004) Neural crest boundary cap cells constitute a source of neuronal and glial cells of the PNS. *Nat Neurosci* **7**, 930–938 https://doi.org/10.1038/nn1299
35 Kramer, I., Sigrist, M., de Nooij, J. C., Taniuchi, I., Jessell, T. M. and Arber, S. (2006) A Role for Runx Transcription Factor Signaling in Dorsal Root Ganglion Sensory Neuron Diversification. *Neuron* **49**, 379–393 https://doi.org/10.1016/j.neuron.2006.01.008
36 Chen, A. I., de Nooij, J. C. and Jessell, T. M. (2006) Graded Activity of Transcription Factor Runx3 Specifies the Laminar Termination Pattern of Sensory Axons in the Developing Spinal Cord. *Neuron* **49**, 395–408 https://doi.org/10.1016/j.neuron.2005.12.028
37 Chen, C.-L., Broom, D. C., Liu, Y., de Nooij, J. C., Li, Z., Cen, C., et al. (2006) Runx1 Determines Nociceptive Sensory Neuron Phenotype and Is Required for Thermal and Neuropathic Pain. *Neuron* **49**, 365–377 https://doi.org/10.1016/j.neuron.2005.10.036
38 Huang, E. J. and Reichardt, L. F. (2001) Neurotrophins: Roles in Neuronal Development and Function. *Annu. Rev. Neurosci.* **24**, 677–736 https://doi.org/10.1146/annurev.neuro.24.1.677
39 Molliver, D. C., Wright, D. E., Leitner, M. L., Parsadanian, A. S., Doster, K., Wen, D., et al. (1997) IB4-Binding DRG Neurons Switch from NGF to GDNF Dependence in Early Postnatal Life. *Neuron* **19**, 849–861 https://doi.org/10.1016/S0896-6273(00)80966-6
40 Molliver, D. C. and Snider, W. D. (1997) Nerve growth factor receptor trkA is down-regulated during postnatal development by a subset of dorsal root ganglion neurons. *J. Comp. Neurol.* **381**, 428–438 https://doi.org/10.1002/(SICI)1096-9861(19970519)381:4<428::AID-CNE3>3.0.CO;2-4
41 Weier, H.-U. G., Rhein, A. P., Shadravan, F., Collins, C. and Polikoff, D. (1995) Rapid physical mapping of the human trk protooncogene (NTRK1) to human chromosome 1q21–q22 by P1 clone selection, fluorescence in situ hybridization (FISH), and computer-assisted microscopy. *Genomics* **26**, 390–393 https://doi.org/10.1016/0888-7543(95)80226-C
42 Franco, M. L., Nadezhdin, K. D., Goncharuk, S. A., Mineev, K. S., Arseniev, A. S. and Vilar, M. (2020) Structural basis of the transmembrane domain dimerization and rotation in the activation mechanism of the TRKA receptor by nerve growth factor. *Journal of Biological Chemistry* **295**, 275–286 https://doi.org/10.1074/jbc.RA119.011312
43 Uren, R. T. and Turnley, A. M. (2014) Regulation of neurotrophin receptor (Trk) signaling: suppressor of cytokine signaling 2 (SOCS2) is a new player. *Front. Mol. Neurosci.* **7** https://doi.org/10.3389/fnmol.2014.00039
44 Stephens, R. M., Loeb, D. M., Copeland, T. D., Pawson, T., Greene, L. A. and Kaplan, D. R. (1994) Trk receptors use redundant signal transduction pathways involving SHC and PLC-γ1 to mediate NGF responses. *Neuron* **12**, 691–705 https://doi.org/10.1016/0896-6273(94)90223-2

45 Obermeier, A., Halfter, H., Wiesmüller, K. H., Jung, G., Schlessinger, J. and Ullrich, A. (1993) Tyrosine 785 is a major determinant of Trk--substrate interaction. *The EMBO Journal* **12**, 933–941 https://doi.org/10.1002/j.1460-2075.1993.tb05734.x
46 Cunningham, M. E., Stephens, R. M., Kaplan, D. R. and Greene, L. A. (1997) Autophosphorylation of Activation Loop Tyrosines Regulates Signaling by the TRK Nerve Growth Factor Receptor. *Journal of Biological Chemistry* **272**, 10957–10967 https://doi.org/10.1074/jbc.272.16.10957
47 Denk, F., Bennett, D. L. and McMahon, S. B. (2017) Nerve Growth Factor and Pain Mechanisms. *Annu. Rev. Neurosci.* **40**, 307–325 https://doi.org/10.1146/annurev-neuro-072116-031121
48 Raffioni, S., Bradshaw, R. A. and Buxser, S. E. (1993) The Receptors For Nerve Growth Factor And Other Neurotrophins. *Annu. Rev. Biochem.* **62**, 823–850 https://doi.org/10.1146/annurev.bi.62.070193.004135
49 Bothwell, M. (1995) Functional Interactions of Neurotrophins and Neurotrophin Receptors. *Annu. Rev. Neurosci.* **18**, 223–253 https://doi.org/10.1146/annurev.ne.18.030195.001255
50 Wiesmann, C., Ultsch, M. H., Bass, S. H. and de Vos, A. M. (1999) Crystal structure of nerve growth factor in complex with the ligand-binding domain of the TrkA receptor. *Nature* **401**, 184–188 https://doi.org/10.1038/43705
51 Jing, S., Tapley, P. and Barbacid, M. (1992) Nerve growth factor mediates signal transduction through trk homodimer receptors. *Neuron* **9**, 1067–1079 https://doi.org/10.1016/0896-6273(92)90066-M
52 Huang, E. J. and Reichardt, L. F. (2003) Trk Receptors: Roles in Neuronal Signal Transduction. *Annu. Rev. Biochem.* **72**, 609–642 https://doi.org/10.1146/annurev.biochem.72.121801.161629
53 Stoleru, B., Popescu, A. M., Tache, D. E., Neamtu, O. M., Emami, G., Tataranu, L. G., et al. (2013) Tropomyosin-receptor-kinases signaling in the nervous system. *Maedica (Bucur)* **8**, 43–48
54 Rajagopal, R. (2004) Transactivation of Trk Neurotrophin Receptors by G-Protein-Coupled Receptor Ligands Occurs on Intracellular Membranes. *Journal of Neuroscience* **24**, 6650–6658 https://doi.org/10.1523/JNEUROSCI.0010-04.2004
55 Lee, F. S. and Chao, M. V. (2001) Activation of Trk neurotrophin receptors in the absence of neurotrophins. *Proceedings of the National Academy of Sciences* **98**, 3555–3560 https://doi.org/10.1073/pnas.061020198
56 Lee, F. S., Rajagopal, R., Kim, A. H., Chang, P. C. and Chao, M. V. (2002) Activation of Trk Neurotrophin Receptor Signaling by Pituitary Adenylate Cyclase-activating Polypeptides. *Journal of Biological Chemistry* **277**, 9096–9102 https://doi.org/10.1074/jbc.M107421200
57 Obreja, O., Rukwied, R., Nagler, L., Schmidt, M., Schmelz, M. and Namer, B. (2018) Nerve growth factor locally sensitizes nociceptors in human skin. *Pain* **159**, 416–426 https://doi.org/10.1097/j.pain.0000000000001108
58 Gallo, G., Lefcort, F. B. and Letourneau, P. C. (1997) The trkA Receptor Mediates Growth Cone Turning toward a Localized Source of Nerve Growth Factor. *J. Neurosci.* **17**, 5445–5454 https://doi.org/10.1523/JNEUROSCI.17-14-05445.1997
59 Nwosu, L. N., Mapp, P. I., Chapman, V. and Walsh, D. A. (2016) Blocking the tropomyosin receptor kinase A (TrkA) receptor inhibits pain behaviour in two

rat models of osteoarthritis. *Ann Rheum Dis* **75**, 1246–1254 https://doi.org/10.1136/annrheumdis-2014-207203

60 Ashraf, S., Bouhana, K. S., Pheneger, J., Andrews, S. W. and Walsh, D. A. (2016) Selective inhibition of tropomyosin-receptor-kinase A (TrkA) reduces pain and joint damage in two rat models of inflammatory arthritis. *Arthritis Res Ther* **18**, article 97 https://doi.org/10.1186/s13075-016-0996-z

61 Swanson, A. G. (1963) Congenital Insensitivity to Pain with Anhydrosis: A Unique Syndrome in Two Male Siblings. *Arch Neurol* **8**, 299–306 https://doi.org/10.1001/archneur.1963.00460030083008

62 Indo, Y., Tsuruta, M., Hayashida, Y., Karim, M. A., Ohta, K., Kawano, T., et al. (1996) Mutations in the TRKA/NGF receptor gene in patients with congenital insensitivity to pain with anhidrosis. *Nat Genet* **13**, 485–488 https://doi.org/10.1038/ng0896-485

63 Neogi, T. (2013) The epidemiology and impact of pain in osteoarthritis. *Osteoarthritis and Cartilage* **21**, 1145–1153 https://doi.org/10.1016/j.joca.2013.03.018

64 Iannone, F. (2002) Increased expression of nerve growth factor (NGF) and high affinity NGF receptor (p140 TrkA) in human osteoarthritic chondrocytes. *Rheumatology* **41**, 1413–1418 https://doi.org/10.1093/rheumatology/41.12.1413

65 Fayaz, A., Croft, P., Langford, R. M., Donaldson, L. J. and Jones, G. T. (2016) Prevalence of chronic pain in the UK: a systematic review and meta-analysis of population studies. *BMJ Open* **6**, article e010364 https://doi.org/10.1136/bmjopen-2015-010364

66 Cervero, F. and Laird, J. M. A. (1996) Mechanisms of touch-evoked pain (allodynia): a new model. *Pain* **68**, 13–23 https://doi.org/10.1016/S0304-3959(96)03165-X

67 Urban, R., Scherrer, G., Goulding, E. H., Tecott, L. H. and Basbaum, A. I. (2011) Behavioral indices of ongoing pain are largely unchanged in male mice with tissue or nerve injury-induced mechanical hypersensitivity: *Pain* **152**, 990–1000 https://doi.org/10.1016/j.pain.2010.12.003

68 Decosterd, I. and Woolf, C. J. (2000) Spared nerve injury: an animal model of persistent peripheral neuropathic pain. *Pain* **87**, 149–158 https://doi.org/10.1016/S0304-3959(00)00276-1

69 Seltzer, Z., Dubner, R. and Shir, Y. (1990) A novel behavioral model of neuropathic pain disorders produced in rats by partial sciatic nerve injury. *Pain* **43**, 205–218 https://doi.org/10.1016/0304-3959(90)91074-S

70 Howard, R. F., Walker, S. M., Mota, M. P. and Fitzgerald, M. (2005) The ontogeny of neuropathic pain: Postnatal onset of mechanical allodynia in rat spared nerve injury (SNI) and chronic constriction injury (CCI) models: *Pain* **115**, 382–389 https://doi.org/10.1016/j.pain.2005.03.016

71 Bourquin, A.-F., Süveges, M., Pertin, M., Gilliard, N., Sardy, S., Davison, A. C., et al. (2006) Assessment and analysis of mechanical allodynia-like behavior induced by spared nerve injury (SNI) in the mouse. *Pain* **122**, 14e1-14e14 https://doi.org/10.1016/j.pain.2005.10.036

72 Hirai, T., Enomoto, M., Kaburagi, H., Sotome, S., Yoshida-Tanaka, K., Ukegawa, M., et al. (2014) Intrathecal AAV Serotype 9-mediated Delivery of shRNA Against TRPV1 Attenuates Thermal Hyperalgesia in a Mouse Model of Peripheral Nerve Injury. *Molecular Therapy* **22**, 409–419 https://doi.org/10.1038/mt.2013.247

73 Treede, R.-D., Meyer, R. A., Raja, S. N. and Campbell, J. N. (1992) Peripheral and central mechanisms of cutaneous hyperalgesia. *Progress in Neurobiology* **38**, 397–421 https://doi.org/10.1016/0301-0082(92)90027-C
74 Treede, R.-D. and Magerl, W. (2000) Multiple mechanisms of secondary hyperalgesia. In Progress in Brain Research, pp 331–341, Elsevier https://doi.org/10.1016/S0079-6123(00)29025-0
75 Meyer, R., Ringkamp, M., Campbell, J. and Raja, S. (2006) Peripheral mechanisms of cutaneous nociception. In Wall and Melzack's Textbook of Pain, pp 3–34, Elsevier, London
76 Frangogiannis, N. G. (2017) The Inflammatory Response in Tissue Repair. In Inflammation - From Molecular and Cellular Mechanisms to the Clinic, pp 1517–1538, Wiley-VCH Verlag GmbH & Co. KGaA, Weinheim, Germany https://doi.org/10.1002/9783527692156.ch60
77 Wei, S.-Q., Tao, Z.-Y., Xue, Y. and Cao, D.-Y. (2020) Peripheral Sensitization. In Peripheral Nerve Disorders and Treatment (Turker, H., Garcia Benavides, L., Ramos Gallardo, G., and Méndez Del Villar, M., eds.), IntechOpen https://doi.org/10.5772/intechopen.90319
78 Woller, S. A., Eddinger, K. A., Corr, M. and Yaksh, T. L. (2017) An overview of pathways encoding nociception. *Clin Exp Rheumatol* **35 Suppl 107**, 40–46
79 Woolf, C. J. (1983) Evidence for a central component of post-injury pain hypersensitivity. *Nature* **306**, 686–688 https://doi.org/10.1038/306686a0
80 Latremoliere, A. and Woolf, C. J. (2009) Central Sensitization: A Generator of Pain Hypersensitivity by Central Neural Plasticity. *The Journal of Pain* **10**, 895–926 https://doi.org/10.1016/j.jpain.2009.06.012
81 Duggan, A. W. and Johnston, G. A. R. (1970) Glutamate and Related Amino Acids in Cat Spinal Roots, Dorsal Root Ganglia and Peripheral Nerves. *J Neurochem* **17**, 1205–1208 https://doi.org/10.1111/j.1471-4159.1970.tb03369.x
82 Mayer, M. L., Westbrook, G. L. and Guthrie, P. B. (1984) Voltage-dependent block by Mg2+ of NMDA responses in spinal cord neurones. *Nature* **309**, 261–263 https://doi.org/10.1038/309261a0
83 Sivilotti, L. and Woolf, C. J. (1994) The contribution of GABAA and glycine receptors to central sensitization: disinhibition and touch-evoked allodynia in the spinal cord. *Journal of Neurophysiology* **72**, 169–179 https://doi.org/10.1152/jn.1994.72.1.169
84 Backman, S. B. and Henry, J. L. (1983) Effects of GABA and glycine on sympathetic preganglionic neurons in the upper thoracic intermediolateral nucleus of the cat. *Brain Research* **277**, 365–369 https://doi.org/10.1016/0006-8993(83)90947-2
85 Torsney, C. and MacDermott, A. B. (2006) Disinhibition Opens the Gate to Pathological Pain Signaling in Superficial Neurokinin 1 Receptor-Expressing Neurons in Rat Spinal Cord. *J. Neurosci.* **26**, 1833–1843 https://doi.org/10.1523/JNEUROSCI.4584-05.2006
86 Coull, J. A. M., Beggs, S., Boudreau, D., Boivin, D., Tsuda, M., Inoue, K., et al. (2005) BDNF from microglia causes the shift in neuronal anion gradient underlying neuropathic pain. *Nature* **438**, 1017–1021 https://doi.org/10.1038/nature04223
87 Long, T., He, W., Pan, Q., Zhang, S., Zhang, D., Qin, G., et al. (2020) Microglia P2X4R-BDNF signalling contributes to central sensitization in a recurrent nitroglycerin-induced chronic migraine model. *J Headache Pain* **21**, article 4 https://doi.org/10.1186/s10194-019-1070-4

88 Thompson, S. W. N., Bennett, D. L. H., Kerr, B. J., Bradbury, E. J. and McMahon, S. B. (1999) Brain-derived neurotrophic factor is an endogenous modulator of nociceptive responses in the spinal cord. *Proc. Natl. Acad. Sci. U.S.A.* **96**, 7714–7718 https://doi.org/10.1073/pnas.96.14.7714
89 Ulmann, L., Hatcher, J. P., Hughes, J. P., Chaumont, S., Green, P. J., Conquet, F., et al. (2008) Up-Regulation of P2X4 Receptors in Spinal Microglia after Peripheral Nerve Injury Mediates BDNF Release and Neuropathic Pain. *Journal of Neuroscience* **28**, 11263–11268 https://doi.org/10.1523/JNEUROSCI.2308-08.2008
90 Ji, R.-R., Berta, T. and Nedergaard, M. (2013) Glia and pain: Is chronic pain a gliopathy? *Pain* **154**, S10–S28 https://doi.org/10.1016/j.pain.2013.06.022
91 Westermann, A., Rönnau, A.-K., Krumova, E., Regeniter, S., Schwenkreis, P., Rolke, R., et al. (2011) Pain-associated Mild Sensory Deficits Without Hyperalgesia in Chronic Non-neuropathic Pain. *The Clinical Journal of Pain* **27**, 782–789 https://doi.org/10.1097/AJP.0b013e31821d8fce
92 Oaklander, A. L., Romans, K., Horasek, S., Stocks, A., Hauer, P. and Meyer, R. A. (1998) Unilateral postherpetic neuralgia is associated with bilateral sensory neuron damage. *Ann Neurol.* **44**, 789–795 https://doi.org/10.1002/ana.410440513
93 Dietz, C., Reinhold, A.-K., Escolano-Lozano, F., Mehling, K., Forer, L., Kress, M., et al. (2021) Complex regional pain syndrome: role of contralateral sensitisation. *British Journal of Anaesthesia* **127**, e1–e3 https://doi.org/10.1016/j.bja.2021.03.018
94 Mapp, P. I., Terenghi, G., Walsh, D. A., Chen, S. T., Cruwys, S. C., Garrett, N., et al. (1993) Monoarthritis in the rat knee induces bilateral and time-dependent changes in substance P and calcitonin gene-related peptide immunoreactivity in the spinal cord. *Neuroscience* **57**, 1091–1096 https://doi.org/10.1016/0306-4522(93)90051-G
95 Donaldson, L. F., Seckl, J. R. and McQueen, D. S. (1993) A discrete adjuvant-induced monoarthritis in the rat: effects of adjuvant dose. *Journal of Neuroscience Methods* **49**, 5–10 https://doi.org/10.1016/0165-0270(93)90103-X
96 Khodorova, A. and Strichartz, G. R. (2010) Contralateral paw sensitization following injection of endothelin-1: effects of local anesthetics differentiate peripheral and central processes. *Neuroscience* **165**, 553–560 https://doi.org/10.1016/j.neuroscience.2009.10.049
97 Levine, J., Dardick, S., Basbaum, A. and Scipio, E. (1985) Reflex neurogenic inflammation. I. Contribution of the peripheral nervous system to spatially remote inflammatory responses that follow injury. *J. Neurosci.* **5**, 1380–1386 https://doi.org/10.1523/JNEUROSCI.05-05-01380.1985
98 Fitzgerald, M. and McKelvey, R. (2016) Nerve injury and neuropathic pain - A question of age. *Exp. Neurol.* **275 Pt 2**, 296–302 https://doi.org/10.1016/j.expneurol.2015.07.013
99 Schwaller, F. and Fitzgerald, M. (2014) The consequences of pain in early life: injury-induced plasticity in developing pain pathways. *Eur J Neurosci* **39**, 344–352 https://doi.org/10.1111/ejn.12414
100 Vega-Avelaira, D., McKelvey, R., Hathway, G. and Fitzgerald, M. (2012) The Emergence of Adolescent Onset Pain Hypersensitivity following Neonatal Nerve Injury. *Mol Pain* **8**, article 30 https://doi.org/10.1186/1744-8069-8-30
101 McKelvey, R., Berta, T., Old, E., Ji, R.-R. and Fitzgerald, M. (2015) Neuropathic pain is constitutively suppressed in early life by anti-inflammatory

neuroimmune regulation. *J. Neurosci.* **35**, 457–466 https://doi.org/10.1523/JNEUROSCI.2315-14.2015
102 Costigan, M., Moss, A., Latremoliere, A., Johnston, C., Verma-Gandhu, M., Herbert, T. A., et al. (2009) T-Cell Infiltration and Signaling in the Adult Dorsal Spinal Cord Is a Major Contributor to Neuropathic Pain-Like Hypersensitivity. *Journal of Neuroscience* **29**, 14415–14422 https://doi.org/10.1523/JNEUROSCI.4569-09.2009
103 Fitzgerald, M., Millard, C. and McIntosh, N. (1989) Cutaneous hypersensitivity following peripheral tissue damage in newborn infants and its reversal with topical anaesthesia. *Pain* **39**, 31–36 https://doi.org/10.1016/0304-3959(89)90172-3
104 Andrews, K. and Fitzgerald, M. (1994) The cutaneous withdrawal reflex in human neonates: sensitization, receptive fields, and the effects of contralateral stimulation. *Pain* **56**, 95–101 https://doi.org/10.1016/0304-3959(94)90154-6
105 Moss, A., Beggs, S., Vega-Avelaira, D., Costigan, M., Hathway, G. J., Salter, M. W., et al. (2007) Spinal microglia and neuropathic pain in young rats. *Pain* **128**, 215–224 https://doi.org/10.1016/j.pain.2006.09.018
106 Vega-Avelaira, D., Moss, A. and Fitzgerald, M. (2007) Age-related changes in the spinal cord microglial and astrocytic response profile to nerve injury. *Brain, Behavior, and Immunity* **21**, 617–623 https://doi.org/10.1016/j.bbi.2006.10.007
107 Hathway, G. J., Vega-Avelaira, D., Moss, A., Ingram, R. and Fitzgerald, M. (2009) Brief, low frequency stimulation of rat peripheral C-fibres evokes prolonged microglial-induced central sensitization in adults but not in neonates. *Pain* **144**, 110–118 https://doi.org/10.1016/j.pain.2009.03.022
108 Scholz, J. and Woolf, C. J. (2002) Can we conquer pain? *Nat Neurosci* **5**, 1062–1067 https://doi.org/10.1038/nn942
109 Reynolds, M. L. and Fitzgerald, M. (1995) Long-term sensory hyperinnervation following neonatal skin wounds. *J. Comp. Neurol.* **358**, 487–498 https://doi.org/10.1002/cne.903580403
110 Shortland, P. and Fitzgerald, M. (1994) Neonatal Sciatic Nerve Section Results in a Rearrangement of the Central Terminals of Saphenous and Axotomized Sciatic Nerve Afferents in the Dorsal Horn of the Spinal Cord of the Adult Rat. *European Journal of Neuroscience* **6**, 75–86 https://doi.org/10.1111/j.1460-9568.1994.tb00249.x
111 Shortland, P. and Fitzgerald, M. (1991) Functional Connections Formed by Saphenous Nerve Terminal Sprouts in the Dorsal Horn Following Neonatal Sciatic Nerve Section. *Eur J Neurosci* **3**, 383–396 https://doi.org/10.1111/j.1460-9568.1991.tb00826.x
112 Fitzgerald, M., Woolf, C. J. and Shortland, P. (1990) Collateral sprouting of the central terminals of cutaneous primary afferent neurons in the rat spinal cord: Pattern, morphology, and influence of targets. *J. Comp. Neurol.* **300**, 370–385 https://doi.org/10.1002/cne.903000308
113 Fitzgerald, M. and Vrbová, G. (1985) Plasticity of acid phosphatase (FRAP) afferent terminal fields and of dorsal horn cell growth in the neonatal rat. *J. Comp. Neurol.* **240**, 414–422 https://doi.org/10.1002/cne.902400409
114 Himes, B. T. and Tessler, A. (1989) Death of some dorsal root ganglion neurons and plasticity of others following sciatic nerve section in adult and neonatal rats. *J. Comp. Neurol.* **284**, 215–230 https://doi.org/10.1002/cne.902840206

115 Woolf, C. J., Shortland, P. and Coggeshall, R. E. (1992) Peripheral nerve injury triggers central sprouting of myelinated afferents. *Nature* **355**, 75–78 https://doi.org/10.1038/355075a0
116 Lekan, H. A., Carlton, S. M. and Coggeshall, R. E. (1996) Sprouting of Aβ fibers into lamina II of the rat dorsal horn in peripheral neuropathy. *Neuroscience Letters* **208**, 147–150 https://doi.org/10.1016/0304-3940(96)12566-0
117 Woolf, C. J., Shortland, P., Reynolds, M., Ridings, J., Doubell, T. and Coggeshall, R. E. (1995) Reorganization of central terminals of myelinated primary afferents in the rat dorsal horn following peripheral axotomy. *J. Comp. Neurol.* **360**, 121–134 https://doi.org/10.1002/cne.903600109
118 Fitzgerald, M. and Beggs, S. (2001) Book Review: The Neurobiology of Pain: Developmental Aspects. *Neuroscientist* **7**, 246–257 https://doi.org/10.1177/107385840100700309
119 Beggs, S., Currie, G., Salter, M. W., Fitzgerald, M. and Walker, S. M. (2012) Priming of adult pain responses by neonatal pain experience: maintenance by central neuroimmune activity. *Brain* **135**, 404–417 https://doi.org/10.1093/brain/awr288
120 World Health Organization. (2020) The Top 10 Causes of Death https://www.who.int/news-room/fact-sheets/detail/the-top-10-causes-of-death
121 Cancer Research UK. (2018) Cancer Statistics for the UK https://www.cancerresearchuk.org/health-professional/cancer-statistics-for-the-uk
122 Macmillan Cancer Support. (2020) Calculating Cancer Prevalence https://www.macmillan.org.uk/about-us/what-we-do/evidence/using-cancer-data/calculating-cancer-prevalence.html#355989
123 Macmillan Cancer Support. (2011) Living after diagnosis median cancer survival times
124 Quaresma, M., Coleman, M. P. and Rachet, B. (2015) 40-year trends in an index of survival for all cancers combined and survival adjusted for age and sex for each cancer in England and Wales, 1971–2011: a population-based study. *The Lancet* **385**, 1206–1218 https://doi.org/10.1016/S0140-6736(14)61396-9
125 Mols, F., Beijers, T., Vreugdenhil, G. and van de Poll-Franse, L. (2014) Chemotherapy-induced peripheral neuropathy and its association with quality of life: a systematic review. *Support Care Cancer* **22**, 2261–2269 https://doi.org/10.1007/s00520-014-2255-7
126 Jones, D., Zhao, F., Brell, J., Lewis, M. A., Loprinzi, C. L., Weiss, M., et al. (2015) Neuropathic symptoms, quality of life, and clinician perception of patient care in medical oncology outpatients with colorectal, breast, lung, and prostate cancer. *J Cancer Surviv* **9**, 1–10 https://doi.org/10.1007/s11764-014-0379-x
127 Miaskowski, C., Mastick, J., Paul, S. M., Abrams, G., Cheung, S., Sabes, J. H., et al. (2018) Impact of chemotherapy-induced neurotoxicities on adult cancer survivors' symptom burden and quality of life. *J Cancer Surviv* **12**, 234–245 https://doi.org/10.1007/s11764-017-0662-8
128 Huang, I.-C., Brinkman, T. M., Kenzik, K., Gurney, J. G., Ness, K. K., Lanctot, J., et al. (2013) Association Between the Prevalence of Symptoms and Health-Related Quality of Life in Adult Survivors of Childhood Cancer: A Report From the St Jude Lifetime Cohort Study. *JCO* **31**, 4242–4251 https://doi.org/10.1200/JCO.2012.47.8867

129 Macmillan Cancer Support. (2018) Side Effects of Chemotherapy https://www.macmillan.org.uk/cancer-information-and-support/treatment/types-of-treatment/chemotherapy/side-effects-of-chemotherapy
130 American Cancer Society. (2020) Chemotherapy Side Effects https://www.cancer.org/treatment/treatments-and-side-effects/treatment-types/chemotherapy/chemotherapy-side-effects.html
131 Windebank, A. J. and Grisold, W. (2008) Chemotherapy-induced neuropathy. *J Peripher Nerv Syst* **13**, 27–46 https://doi.org/10.1111/j.1529-8027.2008.00156.x
132 Argyriou, A. A., Bruna, J., Marmiroli, P. and Cavaletti, G. (2012) Chemotherapy-induced peripheral neurotoxicity (CIPN): An update. *Critical Reviews in Oncology/Hematology* **82**, 51–77 https://doi.org/10.1016/j.critrevonc.2011.04.012
133 Park, S. B., Goldstein, D., Krishnan, A. V., Lin, C. S.-Y., Friedlander, M. L., Cassidy, J., et al. (2013) Chemotherapy-induced peripheral neurotoxicity: a critical analysis. *CA Cancer J Clin* **63**, 419–437 https://doi.org/10.3322/caac.21204
134 Carozzi, V. A., Canta, A. and Chiorazzi, A. (2015) Chemotherapy-induced peripheral neuropathy: What do we know about mechanisms? *Neuroscience Letters* **596**, 90–107 https://doi.org/10.1016/j.neulet.2014.10.014
135 Banach, M., Juranek, J. K. and Zygulska, A. L. (2017) Chemotherapy-induced neuropathies-a growing problem for patients and health care providers. *Brain Behav* **7**, article e00558 https://doi.org/10.1002/brb3.558
136 Thompson, S. W., Davis, L. E., Kornfeld, M., Hilgers, R. D. and Standefer, J. C. (1984) Cisplatin neuropathy. Clinical, electrophysiologic, morphologic, and toxicologic studies. *Cancer* **54**, 1269–1275 https://doi.org/10.1002/1097-0142(19841001)54:7<1269::aid-cncr2820540707>3.0.co;2-9
137 Roelofs, R. I., Hrushesky, W., Rogin, J. and Rosenberg, L. (1984) Peripheral sensory neuropathy and cisplatin chemotherapy. *Neurology* **34**, 934–934 https://doi.org/10.1212/WNL.34.7.934
138 Ta, L. E., Espeset, L., Podratz, J. and Windebank, A. J. (2006) Neurotoxicity of oxaliplatin and cisplatin for dorsal root ganglion neurons correlates with platinum–DNA binding. *NeuroToxicology* **27**, 992–1002 https://doi.org/10.1016/j.neuro.2006.04.010
139 McWhinney, S. R., Goldberg, R. M. and McLeod, H. L. (2009) Platinum neurotoxicity pharmacogenetics. *Mol Cancer Ther* **8**, 10–16 https://doi.org/10.1158/1535-7163.MCT-08-0840
140 Amptoulach, S. and Tsavaris, N. (2011) Neurotoxicity Caused by the Treatment with Platinum Analogues. *Chemotherapy Research and Practice* **2011**, 1–5 https://doi.org/10.1155/2011/843019
141 Bentzen, A. G., Balteskard, L., Wanderås, E. H., Frykholm, G., Wilsgaard, T., Dahl, O., et al. (2013) Impaired health-related quality of life after chemoradiotherapy for anal cancer: Late effects in a national cohort of 128 survivors. *Acta Oncologica* **52**, 736–744 https://doi.org/10.3109/0284186X.2013.770599
142 Jaggi, A. S. and Singh, N. (2012) Mechanisms in cancer-chemotherapeutic drugs-induced peripheral neuropathy. *Toxicology* **291**, 1–9 https://doi.org/10.1016/j.tox.2011.10.019

143 Starobova, H. and Vetter, I. (2017) Pathophysiology of chemotherapy-induced peripheral neuropathy. *Front. Mol. Neurosci.* **10**, 174 https://doi.org/10.3389/fnmol.2017.00174
144 Mora, E., Smith, E. M. L., Donohoe, C. and Hertz, D. L. (2016) Vincristine-induced peripheral neuropathy in pediatric cancer patients. *Am J Cancer Res* **6**, 2416–2430
145 Cersosimo, R. J. (2005) Oxaliplatin-Associated Neuropathy: A Review. *Ann Pharmacother* **39**, 128–135 https://doi.org/10.1345/aph.1E319
146 Tofthagen, C., McAllister, R. D. and Visovsky, C. (2013) Peripheral neuropathy caused by Paclitaxel and docetaxel: an evaluation and comparison of symptoms. *J Adv Pract Oncol* **4**, 204–215
147 Gomber, S., Dewan, P. and Chhonker, D. (2010) Vincristine induced neurotoxicity in cancer patients. *Indian J Pediatr* **77**, 97–100 https://doi.org/10.1007/s12098-009-0254-3
148 Staff, N. P., Grisold, A., Grisold, W. and Windebank, A. J. (2017) Chemotherapy-induced peripheral neuropathy: A current review. *Ann. Neurol.* **81**, 772–781 https://doi.org/10.1002/ana.24951
149 Fischer, S. J., McDonald, E. S., Gross, L. and Windebank, A. J. (2001) Alterations in Cell Cycle Regulation Underlie Cisplatin Induced Apoptosis of Dorsal Root Ganglion Neurons in Vivo. *Neurobiology of Disease* **8**, 1027–1035 https://doi.org/10.1006/nbdi.2001.0426
150 Podratz, J. L., Knight, A. M., Ta, L. E., Staff, N. P., Gass, J. M., Genelin, K., et al. (2011) Cisplatin induced mitochondrial DNA damage in dorsal root ganglion neurons. *Neurobiology of Disease* **41**, 661–668 https://doi.org/10.1016/j.nbd.2010.11.017
151 Allen, D. T. and Kiernan, J. A. (1994) Permeation of proteins from the blood into peripheral nerves and ganglia. *Neuroscience* **59**, 755–764 https://doi.org/10.1016/0306-4522(94)90192-9
152 Dzagnidze, A., Katsarava, Z., Makhalova, J., Liedert, B., Yoon, M.-S., Kaube, H., et al. (2007) Repair Capacity for Platinum-DNA Adducts Determines the Severity of Cisplatin-Induced Peripheral Neuropathy. *Journal of Neuroscience* **27**, 9451–9457 https://doi.org/10.1523/JNEUROSCI.0523-07.2007
153 Yang, Z., Faustino, P. J., Andrews, P. A., Monastra, R., Rasmussen, A. A., Ellison, C. D., et al. (2000) Decreased cisplatin/DNA adduct formation is associated with cisplatin resistance in human head and neck cancer cell lines. *Cancer Chemotherapy and Pharmacology* **46**, 255–262 https://doi.org/10.1007/s002800000167
154 Jamieson, E. R. and Lippard, S. J. (1999) Structure, Recognition, and Processing of Cisplatin−DNA Adducts. *Chem. Rev.* **99**, 2467–2498 https://doi.org/10.1021/cr980421n
155 Wang, D. and Lippard, S. J. (2005) Cellular processing of platinum anticancer drugs. *Nat Rev Drug Discov* **4**, 307–320 https://doi.org/10.1038/nrd1691
156 Rice, J. A., Crothers, D. M., Pinto, A. L. and Lippard, S. J. (1988) The major adduct of the antitumor drug cis-diamminedichloroplatinum(II) with DNA bends the duplex by approximately equal to 40 degrees toward the major groove. *Proceedings of the National Academy of Sciences* **85**, 4158–4161 https://doi.org/10.1073/pnas.85.12.4158
157 Scovell, W. M. and Collart, F. (1985) Unwinding of supercoiled DNA by cis- and trans-diamminedichloroplatinum(II): influence of the torsional strain on

DNA unwinding. *Nucl Acids Res* **13**, 2881–2895 https://doi.org/10.1093/nar/13.8.2881
158 McDonald, E. S. and Windebank, A. J. (2002) Cisplatin-Induced Apoptosis of DRG Neurons Involves Bax Redistribution and Cytochrome cRelease But Not fas Receptor Signaling. *Neurobiology of Disease* **9**, 220–233 https://doi.org/10.1006/nbdi.2001.0468
159 McDonald, E. S., Randon, K. R., Knight, A. and Windebank, A. J. (2005) Cisplatin preferentially binds to DNA in dorsal root ganglion neurons in vitro and in vivo: a potential mechanism for neurotoxicity. *Neurobiology of Disease* **18**, 305–313 https://doi.org/10.1016/j.nbd.2004.09.013
160 Screnci, D., McKeage, M. J., Galettis, P., Hambley, T. W., Palmer, B. D. and Baguley, B. C. (2000) Relationships between hydrophobicity, reactivity, accumulation and peripheral nerve toxicity of a series of platinum drugs. *Br J Cancer* **82**, 966–972 https://doi.org/10.1054/bjoc.1999.1026
161 Gregg, R. W., Molepo, J. M., Monpetit, V. J., Mikael, N. Z., Redmond, D., Gadia, M., et al. (1992) Cisplatin neurotoxicity: the relationship between dosage, time, and platinum concentration in neurologic tissues, and morphologic evidence of toxicity. *JCO* **10**, 795–803 https://doi.org/10.1200/JCO.1992.10.5.795
162 Quasthoff, S. and Hartung, H. P. (2002) Chemotherapy-induced peripheral neuropathy. *J Neurol* **249**, 9–17 https://doi.org/10.1007/PL00007853
163 Meijer, C., de Vries, E. G., Marmiroli, P., Tredici, G., Frattola, L. and Cavaletti, G. (1999) Cisplatin-induced DNA-platination in experimental dorsal root ganglia neuronopathy. *Neurotoxicology* **20**, 883–887
164 Krarup-Hansen, Rietz, Krarup, Heydorn, Rørth, and Schmalbruch. (1999) Histology and platinum content of sensory ganglia and sural nerves in patients treated with cisplatin and carboplatin: an autopsy study. *Neuropathology and Applied Neurobiology* **25**, 28–39 https://doi.org/10.1046/j.1365-2990.1999.00160.x
165 Jimenez-Andrade, J. M., Herrera, M. B., Ghilardi, J. R., Vardanyan, M., Melemedjian, O. K. and Mantyh, P. W. (2008) Vascularization of the Dorsal Root Ganglia and Peripheral Nerve of the Mouse: Implications for Chemical-Induced Peripheral Sensory Neuropathies. *Mol Pain* **4**, 1744-8069-4–10 https://doi.org/10.1186/1744-8069-4-10
166 Jacobs, J. M., Macfarlane, R. M. and Cavanagh, J. B. (1976) Vascular leakage in the dorsal root ganglia of the rat, studied with horseradish peroxidase. *Journal of the Neurological Sciences* **29**, 95–107 https://doi.org/10.1016/0022-510X(76)90083-6
167 Anzil, ArchintoP., Blinzinger, K. and Herrlinger, H. (1976) Fenestrated blood capillaries in rat cranio-spinal sensory ganglia. *Cell Tissue Res.* **167**, 563–567 https://doi.org/10.1007/BF00215185
168 Grundy, R. and Hulse, R. P. (2019) Chronic pain and childhood cancer survivorship. *Current Opinion in Physiology* **11**, 58–61 https://doi.org/10.1016/j.cophys.2019.06.002
169 Mohamed, M. H. N. and Mohamed, H. A. B. (2019) Chemotherapy-induced peripheral neuropathy and its association with quality of life among cancer patients. *JNEP* **9**, 29 https://doi.org/10.5430/jnep.v9n10p29
170 Ness, K. K., Jones, K. E., Smith, W. A., Spunt, S. L., Wilson, C. L., Armstrong, G. T., et al. (2013) Chemotherapy-Related Neuropathic Symptoms and Functional Impairment in Adult Survivors of Extracranial Solid Tumors of

Childhood: Results From the St. Jude Lifetime Cohort Study. *Archives of Physical Medicine and Rehabilitation* **94**, 1451–1457 https://doi.org/10.1016/j.apmr.2013.03.009
171 Argyriou, A., Kyritsis, A., Makatsoris, T. and Kalofonos, H. (2014) Chemotherapy-induced peripheral neuropathy in adults: a comprehensive update of the literature. *CMAR* **6**, 135–147 https://doi.org/10.2147/CMAR.S44261
172 Malik, B. and Stillman, M. (2008) Chemotherapy-induced peripheral neuropathy. *Curr Neurol Neurosci Rep* **8**, 56–65 https://doi.org/10.1007/s11910-008-0010-5
173 Dasari, S. and Bernard Tchounwou, P. (2014) Cisplatin in cancer therapy: Molecular mechanisms of action. *European Journal of Pharmacology* **740**, 364–378 https://doi.org/10.1016/j.ejphar.2014.07.025
174 Melli, G., Taiana, M., Camozzi, F., Triolo, D., Podini, P., Quattrini, A., et al. (2008) Alpha-lipoic acid prevents mitochondrial damage and neurotoxicity in experimental chemotherapy neuropathy. *Experimental Neurology* **214**, 276–284 https://doi.org/10.1016/j.expneurol.2008.08.013
175 Bulua, A. C., Simon, A., Maddipati, R., Pelletier, M., Park, H., Kim, K.-Y., et al. (2011) Mitochondrial reactive oxygen species promote production of proinflammatory cytokines and are elevated in TNFR1-associated periodic syndrome (TRAPS). *Journal of Experimental Medicine* **208**, 519–533 https://doi.org/10.1084/jem.20102049
176 Kanat, O., Ertas, H. and Caner, B. (2017) Platinum-induced neurotoxicity: A review of possible mechanisms. *WJCO* **8**, 329–335 https://doi.org/10.5306/wjco.v8.i4.329
177 Canta, A., Pozzi, E. and Carozzi, V. (2015) Mitochondrial Dysfunction in Chemotherapy-Induced Peripheral Neuropathy (CIPN). *Toxics* **3**, 198–223 https://doi.org/10.3390/toxics3020198
178 Lazic, A., Popović, J., Paunesku, T., Woloschak, G. and Stevanović, M. (2020) Insights into platinum-induced peripheral neuropathy–current perspective. *Neural Regen Res* **15**, 1623–1630 https://doi.org/10.4103/1673-5374.276321
179 Kelley, M. R., Jiang, Y., Guo, C., Reed, A., Meng, H. and Vasko, M. R. (2014) Role of the DNA Base Excision Repair Protein, APE1 in Cisplatin, Oxaliplatin, or Carboplatin Induced Sensory Neuropathy. *PLoS ONE* (Kirchmair, R., ed.) **9**, e106485 https://doi.org/10.1371/journal.pone.0106485
180 Areti, A., Yerra, V. G., Naidu, V. and Kumar, A. (2014) Oxidative stress and nerve damage: Role in chemotherapy induced peripheral neuropathy. *Redox Biology* **2**, 289–295 https://doi.org/10.1016/j.redox.2014.01.006
181 Cashman, C. R. and Höke, A. (2015) Mechanisms of distal axonal degeneration in peripheral neuropathies. *Neuroscience Letters* **596**, 33–50 https://doi.org/10.1016/j.neulet.2015.01.048
182 Leo, M., Schmitt, L.-I., Erkel, M., Melnikova, M., Thomale, J. and Hagenacker, T. (2017) Cisplatin-induced neuropathic pain is mediated by upregulation of N-type voltage-gated calcium channels in dorsal root ganglion neurons. *Experimental Neurology* **288**, 62–74 https://doi.org/10.1016/j.expneurol.2016.11.003
183 Rybak, L. P., Whitworth, C. A., Mukherjea, D. and Ramkumar, V. (2007) Mechanisms of cisplatin-induced ototoxicity and prevention. *Hearing Research* **226**, 157–167 https://doi.org/10.1016/j.heares.2006.09.015

184 Miller, R. P., Tadagavadi, R. K., Ramesh, G. and Reeves, W. B. (2010) Mechanisms of Cisplatin Nephrotoxicity. *Toxins* **2**, 2490–2518 https://doi.org/10.3390/toxins2112490
185 Perše, M. (2021) Cisplatin Mouse Models: Treatment, Toxicity and Translatability. *Biomedicines* **9**, 1406 https://doi.org/10.3390/biomedicines9101406
186 Argyriou, A. A., Polychronopoulos, P., Iconomou, G., Chroni, E. and Kalofonos, H. P. (2008) A review on oxaliplatin-induced peripheral nerve damage. *Cancer Treatment Reviews* **34**, 368–377 https://doi.org/10.1016/j.ctrv.2008.01.003
187 Deuis, J. R., Zimmermann, K., Romanovsky, A. A., Possani, L. D., Cabot, P. J., Lewis, R. J., et al. (2013) An animal model of oxaliplatin-induced cold allodynia reveals a crucial role for Nav1.6 in peripheral pain pathways. *Pain* **154**, 1749–1757 https://doi.org/10.1016/j.pain.2013.05.032
188 Park, S. B., Lin, C. S.-Y., Krishnan, A. V., Goldstein, D., Friedlander, M. L. and Kiernan, M. C. (2009) Oxaliplatin-induced neurotoxicity: changes in axonal excitability precede development of neuropathy. *Brain* **132**, 2712–2723 https://doi.org/10.1093/brain/awp219
189 Webster, R. G., Brain, K. L., Wilson, R. H., Grem, J. L. and Vincent, A. (2005) Oxaliplatin induces hyperexcitability at motor and autonomic neuromuscular junctions through effects on voltage-gated sodium channels: Oxaliplatin-induced hyperexcitability at NMJ. *British Journal of Pharmacology* **146**, 1027–1039 https://doi.org/10.1038/sj.bjp.0706407
190 Sahenk, Z., Brady, S. T. and Mendell, J. R. (1987) Studies on the pathogenesis of vincristine-induced neuropathy. *Muscle Nerve* **10**, 80–84 https://doi.org/10.1002/mus.880100115
191 Gan, P. P., McCarroll, J. A., Po'uha, S. T., Kamath, K., Jordan, M. A. and Kavallaris, M. (2010) Microtubule Dynamics, Mitotic Arrest, and Apoptosis: Drug-Induced Differential Effects of βIII-Tubulin. *Mol Cancer Ther* **9**, 1339–1348 https://doi.org/10.1158/1535-7163.MCT-09-0679
192 Jordan, M. A. and Wilson, L. (2004) Microtubules as a target for anticancer drugs. *Nat Rev Cancer* **4**, 253–265 https://doi.org/10.1038/nrc1317
193 Chantal, T., Nancy, F., Claudette, B., Gaston, D. and Aime´, C. (1986) Action of vinca alraloides on calcium movements through mitochondrial membrane. *Pharmacological Research Communications* **18**, 519–528 https://doi.org/10.1016/0031-6989(86)90147-5
194 Siau, C. and Bennett, G. J. (2006) Dysregulation of Cellular Calcium Homeostasis in Chemotherapy-Evoked Painful Peripheral Neuropathy: *Anesthesia & Analgesia* **102**, 1485–1490 https://doi.org/10.1213/01.ane.0000204318.35194.ed
195 Chen, X.-J., Wang, L. and Song, X.-Y. (2020) Mitoquinone alleviates vincristine-induced neuropathic pain through inhibiting oxidative stress and apoptosis via the improvement of mitochondrial dysfunction. *Biomedicine & Pharmacotherapy* **125**, 110003 https://doi.org/10.1016/j.biopha.2020.110003
196 Kidd, J. F., Pilkington, M. F., Schell, M. J., Fogarty, K. E., Skepper, J. N., Taylor, C. W., et al. (2002) Paclitaxel Affects Cytosolic Calcium Signals by Opening the Mitochondrial Permeability Transition Pore. *Journal of Biological Chemistry* **277**, 6504–6510 https://doi.org/10.1074/jbc.M106802200
197 Vashistha, B., Sharma, A. and Jain, V. (2017) Ameliorative potential of ferulic acid in vincristine-induced painful neuropathy in rats: An evidence of

behavioral and biochemical examination. *Nutritional Neuroscience* **20**, 60–70 https://doi.org/10.1179/1476830514Y.0000000165
198 Duggett, N. A., Griffiths, L. A., McKenna, O. E., de Santis, V., Yongsanguanchai, N., Mokori, E. B., et al. (2016) Oxidative stress in the development, maintenance and resolution of paclitaxel-induced painful neuropathy. *Neuroscience* **333**, 13–26 https://doi.org/10.1016/j.neuroscience.2016.06.050
199 Lv, Z., Shen, J., Gao, X., Ruan, Y., Ling, J., Sun, R., et al. (2021) Herbal formula Huangqi Guizhi Wuwu decoction attenuates paclitaxel-related neurotoxicity via inhibition of inflammation and oxidative stress. *Chin Med* **16**, 76 https://doi.org/10.1186/s13020-021-00488-1
200 Haritha, P., Satyanarayana, S. P., Bharathi, K. and Prasad VSRG, K. (2021) Curcumin Ameliorates Paclitaxel-Induced Pain Hypersensitivity via Alleviation of Inflammation and Oxidative Stress in Rats. *Int J Pharma Bio Sci* **11**, 58–67 https://doi.org/10.22376/ijpbs/lpr.2021.11.4.P58-67
201 Siau, C., Xiao, W. and Bennett, G. J. (2006) Paclitaxel- and vincristine-evoked painful peripheral neuropathies: loss of epidermal innervation and activation of Langerhans cells. *Exp. Neurol.* **201**, 507–514 https://doi.org/10.1016/j.expneurol.2006.05.007
202 Poruchynsky, M. S., Sackett, D. L., Robey, R. W., Ward, Y., Annunziata, C. and Fojo, T. (2008) Proteasome inhibitors increase tubulin polymerization and stabilization in tissue culture cells: a possible mechanism contributing to peripheral neuropathy and cellular toxicity following proteasome inhibition. *Cell Cycle* **7**, 940–949 https://doi.org/10.4161/cc.7.7.5625
203 Meregalli, C., Chiorazzi, A., Carozzi, V. A., Canta, A., Sala, B., Colombo, M., et al. (2014) Evaluation of tubulin polymerization and chronic inhibition of proteasome as citotoxicity mechanisms in bortezomib-induced peripheral neuropathy. *Cell Cycle* **13**, 612–621 https://doi.org/10.4161/cc.27476
204 Staff, N. P., Podratz, J. L., Grassner, L., Bader, M., Paz, J., Knight, A. M., et al. (2013) Bortezomib alters microtubule polymerization and axonal transport in rat dorsal root ganglion neurons. *NeuroToxicology* **39**, 124–131 https://doi.org/10.1016/j.neuro.2013.09.001
205 Broyl, A., Corthals, S. L., Jongen, J. L., van der Holt, B., Kuiper, R., de Knegt, Y., et al. (2010) Mechanisms of peripheral neuropathy associated with bortezomib and vincristine in patients with newly diagnosed multiple myeloma: a prospective analysis of data from the HOVON-65/GMMG-HD4 trial. *The Lancet Oncology* **11**, 1057–1065 https://doi.org/10.1016/S1470-2045(10)70206-0
206 Palanca, A., Casafont, I., Berciano, M. T. and Lafarga, M. (2014) Proteasome inhibition induces DNA damage and reorganizes nuclear architecture and protein synthesis machinery in sensory ganglion neurons. *Cell. Mol. Life Sci.* **71**, 1961–1975 https://doi.org/10.1007/s00018-013-1474-2
207 Wang, H., Liu, Z., Yang, W., Liao, A., Zhang, R., Wu, B., et al. (2011) Study on mechanism of bortezomib inducing peripheral neuropathy and the reversing effect of reduced glutathione. *Zhonghua Xue Ye Xue Za Zhi* **32**, 107–111
208 Duggett, N. A. and Flatters, S. J. L. (2017) Characterization of a rat model of bortezomib-induced painful neuropathy: Rat model of bortezomib-induced painful neuropathy. *British Journal of Pharmacology* **174**, 4812–4825 https://doi.org/10.1111/bph.14063

209 Cavaletti, G., Gilardini, A., Canta, A., Rigamonti, L., Rodriguez-Menendez, V., Ceresa, C., et al. (2007) Bortezomib-induced peripheral neurotoxicity: A neurophysiological and pathological study in the rat. *Experimental Neurology* **204**, 317–325 https://doi.org/10.1016/j.expneurol.2006.11.010
210 Landowski, T. H., Megli, C. J., Nullmeyer, K. D., Lynch, R. M. and Dorr, R. T. (2005) Mitochondrial-Mediated Disregulation of Ca2+ Is a Critical Determinant of Velcade (PS-341/Bortezomib) Cytotoxicity in Myeloma Cell Lines. *Cancer Res* **65**, 3828–3836 https://doi.org/10.1158/0008-5472.CAN-04-3684
211 Misra, U., Kalita, J. and Nair, P. (2008) Diagnostic approach to peripheral neuropathy. *Ann Indian Acad Neurol* **11**, 89–97 https://doi.org/10.4103/0972-2327.41875
212 Menkes, D. L., Swenson, M. R. and Sander, H. W. (2000) Current perception threshold: an adjunctive test for detection of acquired demyelinating polyneuropathies. *Electromyogr Clin Neurophysiol* **40**, 205–210
213 Lv, S., Fang, C., Hu, J., Huang, Y., Yang, B., Zou, R., et al. (2015) Assessment of Peripheral Neuropathy Using Measurement of the Current Perception Threshold with the Neurometer® in patients with type 1 diabetes mellitus. *Diabetes Research and Clinical Practice* **109**, 130–134 https://doi.org/10.1016/j.diabres.2015.04.018
214 Young, M. J., Boulton, A. J. M., Macleod, A. F., Williams, D. R. R. and Sonksen, P. H. (1993) A multicentre study of the prevalence of diabetic peripheral neuropathy in the United Kingdom hospital clinic population. *Diabetologia* **36**, 150–154 https://doi.org/10.1007/BF00400697
215 Myftiu, B., Hundozi, Z., Sermaxhaj, F., Blyta, A., Shala, N., Jashari, F., et al. (2022) Chemotherapy-Induced Peripheral Neuropathy (CIPN) in Patients Receiving 4-6 Cycles of Platinum-Based and Taxane-Based Chemotherapy: A Prospective, Single-Center Study from Kosovo. *Med Sci Monit* **28** https://doi.org/10.12659/MSM.937856
216 Chung, T., Prasad, K. and Lloyd, T. E. (2014) Peripheral Neuropathy - Clinical and Electrophysiological Considerations. *Neuroimaging Clinics of North America* **24**, 49–65 https://doi.org/10.1016/j.nic.2013.03.023
217 Griffith, K. A., Couture, D. J., Zhu, S., Pandya, N., Johantgen, M. E., Cavaletti, G., et al. (2014) Evaluation of chemotherapy-induced peripheral neuropathy using current perception threshold and clinical evaluations. *Support Care Cancer* **22**, 1161–1169 https://doi.org/10.1007/s00520-013-2068-0
218 Doi, D., Ota, Y., Konishi, H., Yoneyama, K. and Araki, T. (2003) Evaluation of the Neurotoxicity of Paclitaxel and Carboplatin by Current Perception Threshold in Ovarian Cancer Patients. *J Nippon Med Sch* **70**, 129–134 https://doi.org/10.1272/jnms.70.129
219 Hansen, S. W. (1990) Autonomic neuropathy after treatment with cisplatin, vinblastine, and bleomycin for germ cell cancer. *BMJ* **300**, 511–512 https://doi.org/10.1136/bmj.300.6723.511
220 Mayo Clinic. (2020) Autonomic Neuropathy https://www.mayoclinic.org/diseases-conditions/autonomic-neuropathy/diagnosis-treatment/drc-20369836
221 Postma, T. J., Aaronson, N. K., Heimans, J. J., Muller, M. J., Hildebrand, J. G., Delattre, J. Y., et al. (2005) The development of an EORTC quality of life questionnaire to assess chemotherapy-induced peripheral neuropathy: The QLQ-CIPN20. *European Journal of Cancer* **41**, 1135–1139 https://doi.org/10.1016/j.ejca.2005.02.012

222 Pachman, D. R., Qin, R., Seisler, D. K., Smith, E. M. L., Beutler, A. S., Ta, L. E., et al. (2015) Clinical Course of Oxaliplatin-Induced Neuropathy: Results From the Randomized Phase III Trial N08CB (Alliance). *JCO* **33**, 3416–3422 https://doi.org/10.1200/JCO.2014.58.8533
223 Binda, D., Vanhoutte, E. K., Cavaletti, G., Cornblath, D. R., Postma, T. J., Frigeni, B., et al. (2013) Rasch-built Overall Disability Scale for patients with chemotherapy-induced peripheral neuropathy (CIPN-R-ODS). *European Journal of Cancer* **49**, 2910–2918 https://doi.org/10.1016/j.ejca.2013.04.004
224 Seretny, M., Currie, G. L., Sena, E. S., Ramnarine, S., Grant, R., MacLeod, M. R., et al. (2014) Incidence, prevalence, and predictors of chemotherapy-induced peripheral neuropathy: A systematic review and meta-analysis. *Pain* **155**, 2461–2470 https://doi.org/10.1016/j.pain.2014.09.020
225 Grisold, W., Cavaletti, G. and Windebank, A. J. (2012) Peripheral neuropathies from chemotherapeutics and targeted agents: diagnosis, treatment, and prevention. *Neuro-Oncology* **14**, iv45–iv54 https://doi.org/10.1093/neuonc/nos203
226 Lehtinen, S. S., Huuskonen, U. E., Harila-Saari, A. H., Tolonen, U., Vainionpää, L. K. and Lanning, B. M. (2002) Motor nervous system impairment persists in long-term survivors of childhood acute lymphoblastic leukemia: Motor Pathway Lesions in Patients with ALL. *Cancer* **94**, 2466–2473 https://doi.org/10.1002/cncr.10503
227 Postma, T. J., Benard, B. A., Huijgens, P. C., Ossenkoppele, G. J. and Heimans, J. J. (1993) Long term effects of vincristine on the peripheral nervous system. *J Neuro-Oncol* **15**, 23–27 https://doi.org/10.1007/BF01050259
228 Gidding, C. (1999) Vincristine revisited. *Critical Reviews in Oncology/Hematology* **29**, 267–287 https://doi.org/10.1016/S1040-8428(98)00023-7
229 Chaudhry, V., Cornblath, D. R., Polydefkis, M., Ferguson, A. and Borrello, I. (2008) Characteristics of bortezomib- and thalidomide-induced peripheral neuropathy. *Journal of the Peripheral Nervous System* **13**, 275–282 https://doi.org/10.1111/j.1529-8027.2008.00193.x
230 Tanabe, Y., Hashimoto, K., Shimizu, C., Hirakawa, A., Harano, K., Yunokawa, M., et al. (2013) Paclitaxel-induced peripheral neuropathy in patients receiving adjuvant chemotherapy for breast cancer. *Int J Clin Oncol* **18**, 132–138 https://doi.org/10.1007/s10147-011-0352-x
231 Bhatnagar, B., Gilmore, S., Goloubeva, O., Pelser, C., Medeiros, M., Chumsri, S., et al. (2014) Chemotherapy dose reduction due to chemotherapy induced peripheral neuropathy in breast cancer patients receiving chemotherapy in the neoadjuvant or adjuvant settings: a single-center experience. *Springerplus* **3**, 366 https://doi.org/10.1186/2193-1801-3-366
232 Colvin, L. A. (2019) Chemotherapy-induced peripheral neuropathy: where are we now? *Pain* **160 Suppl 1**, S1–S10 https://doi.org/10.1097/j.pain.0000000000001540
233 Hershman, D. L., Lacchetti, C., Dworkin, R. H., Lavoie Smith, E. M., Bleeker, J., Cavaletti, G., et al. (2014) Prevention and Management of Chemotherapy-Induced Peripheral Neuropathy in Survivors of Adult Cancers: American Society of Clinical Oncology Clinical Practice Guideline. *JCO* **32**, 1941–1967 https://doi.org/10.1200/JCO.2013.54.0914
234 Loprinzi, C. L., Lacchetti, C., Bleeker, J., Cavaletti, G., Chauhan, C., Hertz, D. L., et al. (2020) Prevention and Management of Chemotherapy-Induced

Peripheral Neuropathy in Survivors of Adult Cancers: ASCO Guideline Update. *JCO* **38**, 3325–3348 https://doi.org/10.1200/JCO.20.01399
235 Smith, E. M. L., Kuisell, C., Cho, Y., Kanzawa-Lee, G. A., Gilchrist, L. S., Park, S. B., et al. (2021) Characteristics and patterns of pediatric chemotherapy-induced peripheral neuropathy: A systematic review. *Cancer Treatment and Research Communications* **28**, 100420 https://doi.org/10.1016/j.ctarc.2021.100420
236 Kandula, T., Park, S. B., Cohn, R. J., Krishnan, A. V. and Farrar, M. A. (2016) Pediatric chemotherapy induced peripheral neuropathy: A systematic review of current knowledge. *Cancer Treatment Reviews* **50**, 118–128 https://doi.org/10.1016/j.ctrv.2016.09.005
237 Lu, Q., Krull, K. R., Leisenring, W., Owen, J. E., Kawashima, T., Tsao, J. C. I., et al. (2011) Pain in long-term adult survivors of childhood cancers and their siblings: A report from the Childhood Cancer Survivor Study. *Pain* **152**, 2616–2624 https://doi.org/10.1016/j.pain.2011.08.006
238 Gilchrist, L. S., Marais, L. and Tanner, L. (2014) Comparison of two chemotherapy-induced peripheral neuropathy measurement approaches in children. *Support Care Cancer* **22**, 359–366 https://doi.org/10.1007/s00520-013-1981-6
239 Clanton, N. R., Klosky, J. L., Li, C., Jain, N., Srivastava, D. K., Mulrooney, D., et al. (2011) Fatigue, vitality, sleep, and neurocognitive functioning in adult survivors of childhood cancer: A report from the childhood cancer survivor study. *Cancer* **117**, 2559–2568 https://doi.org/10.1002/cncr.25797
240 Alberts, N. M., Gagnon, M. M. and Stinson, J. N. (2018) Chronic pain in survivors of childhood cancer: a developmental model of pain across the cancer trajectory. *Pain* **159**, 1916–1927 https://doi.org/10.1097/j.pain.0000000000001261
241 Cavaletti, G., Alberti, P., Argyriou, A. A., Lustberg, M., Staff, N. P., Tamburin, S., et al. (2019) Chemotherapy-induced peripheral neurotoxicity: A multifaceted, still unsolved issue. *J Peripher Nerv Syst* **24**, S6–S12 https://doi.org/10.1111/jns.12337
242 Salat, K. (2020) Chemotherapy-induced peripheral neuropathy: part 1—current state of knowledge and perspectives for pharmacotherapy. *Pharmacol. Rep* **72**, 486–507 https://doi.org/10.1007/s43440-020-00109-y
243 Majithia, N., Temkin, S. M., Ruddy, K. J., Beutler, A. S., Hershman, D. L. and Loprinzi, C. L. (2016) National Cancer Institute-supported chemotherapy-induced peripheral neuropathy trials: outcomes and lessons. *Support Care Cancer* **24**, 1439–1447 https://doi.org/10.1007/s00520-015-3063-4
244 Flatters, S. J. L., Dougherty, P. M. and Colvin, L. A. (2017) Clinical and preclinical perspectives on Chemotherapy-Induced Peripheral Neuropathy (CIPN): a narrative review. *British Journal of Anaesthesia* **119**, 737–749 https://doi.org/10.1093/bja/aex229
245 Hou, S., Huh, B., Kim, H. K., Kim, K.-H. and Abdi, S. (2018) Treatment of Chemotherapy-Induced Peripheral Neuropathy: Systematic Review and Recommendations. *Pain Physician* **21**, 571–592
246 Maihöfner, C., Diel, I., Tesch, H., Quandel, T. and Baron, R. (2021) Chemotherapy-induced peripheral neuropathy (CIPN): current therapies and topical treatment option with high-concentration capsaicin. *Support Care Cancer* **29**, 4223–4238 https://doi.org/10.1007/s00520-021-06042-x

247 Cartoni, C., Brunetti, G. A., Federico, V., Efficace, F., Grammatico, S., Tendas, A., et al. (2012) Controlled-release oxycodone for the treatment of bortezomib-induced neuropathic pain in patients with multiple myeloma. *Support Care Cancer* **20**, 2621–2626 https://doi.org/10.1007/s00520-012-1511-y
248 Nagashima, M., Ooshiro, M., Moriyama, A., Sugishita, Y., Kadoya, K., Sato, A., et al. (2014) Efficacy and tolerability of controlled-release oxycodone for oxaliplatin-induced peripheral neuropathy and the extension of FOLFOX therapy in advanced colorectal cancer patients. *Support Care Cancer* **22**, 1579–1584 https://doi.org/10.1007/s00520-014-2132-4
249 Højsted, J., Nielsen, P. R., Guldstrand, S. K., Frich, L. and Sjøgren, P. (2010) Classification and identification of opioid addiction in chronic pain patients. *European Journal of Pain* **14**, 1014–1020 https://doi.org/10.1016/j.ejpain.2010.04.006
250 Bykov, K., Bateman, B. T., Franklin, J. M., Vine, S. M. and Patorno, E. (2020) Association of Gabapentinoids With the Risk of Opioid-Related Adverse Events in Surgical Patients in the United States. *JAMA Netw Open* **3**, article e2031647 https://doi.org/10.1001/jamanetworkopen.2020.31647
251 Meng, J., Zhang, Q., Yang, C., Xiao, L., Xue, Z. and Zhu, J. (2019) Duloxetine, a Balanced Serotonin-Norepinephrine Reuptake Inhibitor, Improves Painful Chemotherapy-Induced Peripheral Neuropathy by Inhibiting Activation of p38 MAPK and NF-κB. *Front. Pharmacol.* **10**, 365 https://doi.org/10.3389/fphar.2019.00365
252 Smith, E. M. L., Pang, H., Cirrincione, C., Fleishman, S., Paskett, E. D., Ahles, T., et al. (2013) Effect of Duloxetine on Pain, Function, and Quality of Life Among Patients With Chemotherapy-Induced Painful Peripheral Neuropathy: A Randomized Clinical Trial. *JAMA* **309**, 1359–1367 https://doi.org/10.1001/jama.2013.2813
253 Ibrahim, W. (2018) Effectiveness of duloxetine in treatment of painful chemotherapy-induced peripheral neuropathy: a systematic review. *JCSO* **16**, e243–e249 https://doi.org/10.12788/jcso.0436
254 Jin, Y., Wang, Y., Zhang, J., Xiao, X. and Zhang, Q. (2020) Efficacy and Safety of Acupuncture against Chemotherapy-Induced Peripheral Neuropathy: A Systematic Review and Meta-Analysis. *Evid Based Complement Alternat Med* **2020**, article 8875433 https://doi.org/10.1155/2020/8875433
255 Lin, W.-L., Wang, R.-H., Chou, F.-H., Feng, I.-J., Fang, C.-J. and Wang, H.-H. (2021) The effects of exercise on chemotherapy-induced peripheral neuropathy symptoms in cancer patients: a systematic review and meta-analysis. *Support Care Cancer* **29**, 5303–5311 https://doi.org/10.1007/s00520-021-06082-3
256 Kleckner, I. R., Kamen, C., Gewandter, J. S., Mohile, N. A., Heckler, C. E., Culakova, E., et al. (2018) Effects of exercise during chemotherapy on chemotherapy-induced peripheral neuropathy: a multicenter, randomized controlled trial. *Support Care Cancer* **26**, 1019–1028 https://doi.org/10.1007/s00520-017-4013-0
257 Zimmer, P., Trebing, S., Timmers-Trebing, U., Schenk, A., Paust, R., Bloch, W., et al. (2018) Eight-week, multimodal exercise counteracts a progress of chemotherapy-induced peripheral neuropathy and improves balance and strength in metastasized colorectal cancer patients: a randomized controlled trial. *Support Care Cancer* **26**, 615–624 https://doi.org/10.1007/s00520-017-3875-5

258 Filipczak-Bryniarska, I., Krzyzewski, R. M., Kucharz, J., Michalowska-Kaczmarczyk, A., Kleja, J., Woron, J., et al. (2017) High-dose 8% capsaicin patch in treatment of chemotherapy-induced peripheral neuropathy: single-center experience. *Med Oncol* **34**, 162 https://doi.org/10.1007/s12032-017-1015-1
259 Kennedy, W. R., Vanhove, G. F., Lu, S., Tobias, J., Bley, K. R., Walk, D., et al. (2010) A Randomized, Controlled, Open-Label Study of the Long-Term Effects of NGX-4010, a High-Concentration Capsaicin Patch, on Epidermal Nerve Fiber Density and Sensory Function in Healthy Volunteers. *The Journal of Pain* **11**, 579–587 https://doi.org/10.1016/j.jpain.2009.09.019
260 Anand, P., Elsafa, E., Privitera, R., Naidoo, K., Yiangou, Y., Donatien, P., et al. (2019) Rational treatment of chemotherapy-induced peripheral neuropathy with capsaicin 8% patch: from pain relief towards disease modification. *JPR* **Volume 12**, 2039–2052 https://doi.org/10.2147/JPR.S213912
261 Bienfait, F., Julienne, A., Jubier-Hamon, S., Seegers, V., Delorme, T., Jaoul, V., et al. (2023) Evaluation of 8% Capsaicin Patches in Chemotherapy-Induced Peripheral Neuropathy: A Retrospective Study in a Comprehensive Cancer Center. *Cancers* **15**, article 349 https://doi.org/10.3390/cancers15020349
262 Reed, E. (1998) Platinum-DNA adduct, nucleotide excision repair and platinum based anti-cancer chemotherapy. *Cancer Treatment Reviews* **24**, 331–344 https://doi.org/10.1016/S0305-7372(98)90056-1
263 Furuta, T., Ueda, T., Aune, G., Sarasin, A., Kraemer, K. H. and Pommier, Y. (2002) Transcription-coupled nucleotide excision repair as a determinant of cisplatin sensitivity of human cells. *Cancer Res* **62**, 4899–4902
264 Wang, D., Hara, R., Singh, G., Sancar, A. and Lippard, S. J. (2003) Nucleotide Excision Repair from Site-Specifically Platinum-Modified Nucleosomes. *Biochemistry* **42**, 6747–6753 https://doi.org/10.1021/bi034264k
265 Zhang, M., Du, W., Acklin, S., Jin, S. and Xia, F. (2020) SIRT2 protects peripheral neurons from cisplatin-induced injury by enhancing nucleotide excision repair. *Journal of Clinical Investigation* 10.1172/JCI123159 https://doi.org/10.1172/JCI123159
266 Shu, X., Xiong, X., Song, J., He, C. and Yi, C. (2016) Base-Resolution Analysis of Cisplatin-DNA Adducts at the Genome Scale. *Angew. Chem. Int. Ed.* **55**, 14246–14249 https://doi.org/10.1002/anie.201607380
267 Giurgiovich, A. (1997) Elevated mitochondrial cisplatin-DNA adduct levels in rat tissues after transplacental cisplatin exposure. *Carcinogenesis* **18**, 93–96 https://doi.org/10.1093/carcin/18.1.93
268 Croteau, D. L., Stierum, Rob. H. and Bohr, V. A. (1999) Mitochondrial DNA repair pathways. *Mutation Research/DNA Repair* **434**, 137–148 https://doi.org/10.1016/S0921-8777(99)00025-7
269 Clayton, D. A., Doda, J. N. and Friedberg, E. C. (1974) The Absence of a Pyrimidine Dimer Repair Mechanism in Mammalian Mitochondria. *Proc. Natl. Acad. Sci. U.S.A.* **71**, 2777–2781 https://doi.org/10.1073/pnas.71.7.2777
270 Basu, A. and Krishnamurthy, S. (2010) Cellular Responses to Cisplatin-Induced DNA Damage. *Journal of Nucleic Acids* **2010**, 1–16 https://doi.org/10.4061/2010/201367
271 Perez, R. P. (1998) Cellular and molecular determinants of cisplatin resistance. *European Journal of Cancer* **34**, 1535–1542 https://doi.org/10.1016/S0959-8049(98)00227-5

272 Jiang, Y., Guo, C., Vasko, M. R. and Kelley, M. R. (2008) Implications of Apurinic/Apyrimidinic Endonuclease in Reactive Oxygen Signaling Response after Cisplatin Treatment of Dorsal Root Ganglion Neurons. *Cancer Research* **68**, 6425–6434 https://doi.org/10.1158/0008-5472.CAN-08-1173
273 Auten, R. L. and Davis, J. M. (2009) Oxygen Toxicity and Reactive Oxygen Species: The Devil Is in the Details. *Pediatr Res* **66**, 121–127 https://doi.org/10.1203/PDR.0b013e3181a9eafb
274 Cooke, M. S., Evans, M. D., Dizdaroglu, M. and Lunec, J. (2003) Oxidative DNA damage: mechanisms, mutation, and disease. *FASEB j.* **17**, 1195–1214 https://doi.org/10.1096/fj.02-0752rev
275 Smith, M. L. and Seo, Y. R. (2002) p53 regulation of DNA excision repair pathways. *Mutagenesis* **17**, 149–156 https://doi.org/10.1093/mutage/17.2.149
276 Seo, Y. R. and Jung, H. J. (2004) The potential roles of p53 tumor suppressor in nucleotide excision repair (NER) and base excision repair (BER). *Exp Mol Med* **36**, 505–509 https://doi.org/10.1038/emm.2004.64
277 McKay, B. C., Becerril, C. and Ljungman, M. (2001) P53 plays a protective role against UV- and cisplatin-induced apoptosis in transcription-coupled repair proficient fibroblasts. *Oncogene* **20**, 6805–6808 https://doi.org/10.1038/sj.onc.1204901
278 Lin, X., Ramamurthi, K., Mishima, M., Kondo, A., Christen, R. D. and Howell, S. B. (2001) P53 modulates the effect of loss of DNA mismatch repair on the sensitivity of human colon cancer cells to the cytotoxic and mutagenic effects of cisplatin. *Cancer Res* **61**, 1508–1516
279 Vikhanskaya, F., Colella, G., Valenti, M., Parodi, S., D'Incalci, M. and Broggini, M. (1999) Cooperation between p53 and hMLH1 in a human colocarcinoma cell line in response to DNA damage. *Clin Cancer Res* **5**, 937–941
280 Helton, E. S. and Chen, X. (2007) p53 modulation of the DNA damage response. *J. Cell. Biochem.* **100**, 883–896 https://doi.org/10.1002/jcb.21091
281 Kiss, R. C., Xia, F. and Acklin, S. (2021) Targeting DNA Damage Response and Repair to Enhance Therapeutic Index in Cisplatin-Based Cancer Treatment. *IJMS* **22**, article 8199 https://doi.org/10.3390/ijms22158199
282 Aloyz, R., Xu, Z.-Y., Bello, V., Bergeron, J., Han, F.-Y., Yan, Y., et al. (2002) Regulation of cisplatin resistance and homologous recombinational repair by the TFIIH subunit XPD. *Cancer Res* **62**, 5457–5462
283 Diggle, C. P. (2005) Inhibition of double-strand break non-homologous end-joining by cisplatin adducts in human cell extracts. *Nucleic Acids Research* **33**, 2531–2539 https://doi.org/10.1093/nar/gki528
284 Lieber, M. R. (2010) The Mechanism of Double-Strand DNA Break Repair by the Nonhomologous DNA End-Joining Pathway. *Annu. Rev. Biochem.* **79**, 181–211 https://doi.org/10.1146/annurev.biochem.052308.093131
285 Frankenberg-Schwager, M., Kirchermeier, D., Greif, G., Baer, K., Becker, M. and Frankenberg, D. (2005) Cisplatin-mediated DNA double-strand breaks in replicating but not in quiescent cells of the yeast Saccharomyces cerevisiae. *Toxicology* **212**, 175–184 https://doi.org/10.1016/j.tox.2005.04.015
286 Nowosielska, A. and Marinus, M. G. (2005) Cisplatin induces DNA double-strand break formation in Escherichia coli dam mutants. *DNA Repair* **4**, 773–781 https://doi.org/10.1016/j.dnarep.2005.03.006
287 Ray, A., Blevins, C., Wani, G. and Wani, A. A. (2016) ATR- and ATM-Mediated DNA Damage Response Is Dependent on Excision Repair Assembly

during G1 but Not in S Phase of Cell Cycle. *PLoS ONE* (Huen, M. S.-Y., ed.) **11**, e0159344 https://doi.org/10.1371/journal.pone.0159344
288 Marechal, A. and Zou, L. (2013) DNA Damage Sensing by the ATM and ATR Kinases. *Cold Spring Harbor Perspectives in Biology* **5**, a012716–a012716 https://doi.org/10.1101/cshperspect.a012716
289 Yang, J., Yu, Y., Hamrick, H. E. and Duerksen-Hughes, P. J. (2003) ATM, ATR and DNA-PK: initiators of the cellular genotoxic stress responses. *Carcinogenesis* **24**, 1571–1580 https://doi.org/10.1093/carcin/bgg137
290 Matsuoka, S., Ballif, B. A., Smogorzewska, A., McDonald, E. R., Hurov, K. E., Luo, J., et al. (2007) ATM and ATR Substrate Analysis Reveals Extensive Protein Networks Responsive to DNA Damage. *Science* **316**, 1160–1166 https://doi.org/10.1126/science.1140321
291 Bekker-Jensen, S., Lukas, C., Kitagawa, R., Melander, F., Kastan, M. B., Bartek, J., et al. (2006) Spatial organization of the mammalian genome surveillance machinery in response to DNA strand breaks. *Journal of Cell Biology* **173**, 195–206 https://doi.org/10.1083/jcb.200510130
292 Banin, S., Moyal, L., Shieh, S.-Y., Taya, Y., Anderson, C. W., Chessa, L., et al. (1998) Enhanced Phosphorylation of p53 by ATM in Response to DNA Damage. *Science* **281**, 1674–1677 https://doi.org/10.1126/science.281.5383.1674
293 Tibbetts, R. S., Brumbaugh, K. M., Williams, J. M., Sarkaria, J. N., Cliby, W. A., Shieh, S.-Y., et al. (1999) A role for ATR in the DNA damage-induced phosphorylation of p53. *Genes & Development* **13**, 152–157 https://doi.org/10.1101/gad.13.2.152
294 Burma, S., Chen, B. P., Murphy, M., Kurimasa, A. and Chen, D. J. (2001) ATM Phosphorylates Histone H2AX in Response to DNA Double-strand Breaks. *Journal of Biological Chemistry* **276**, 42462–42467 https://doi.org/10.1074/jbc.C100466200
295 Hanasoge, S. and Ljungman, M. (2007) H2AX phosphorylation after UV irradiation is triggered by DNA repair intermediates and is mediated by the ATR kinase. *Carcinogenesis* **28**, 2298–2304 https://doi.org/10.1093/carcin/bgm157
296 Haupt, Y., Maya, R., Kazaz, A. and Oren, M. (1997) Mdm2 promotes the rapid degradation of p53. *Nature* **387**, 296–299 https://doi.org/10.1038/387296a0
297 Kulikov, R., Letienne, J., Kaur, M., Grossman, S. R., Arts, J. and Blattner, C. (2010) Mdm2 facilitates the association of p53 with the proteasome. *Proc. Natl. Acad. Sci. U.S.A.* **107**, 10038–10043 https://doi.org/10.1073/pnas.0911716107
298 Gao, Y., Sun, N., Wang, L., Wu, Y., Ma, L., Hong, J., et al. (2018) Bioinformatics Analysis Identifies p53 as a Candidate Prognostic Biomarker for Neuropathic Pain. *Front. Genet.* **9** https://doi.org/10.3389/fgene.2018.00320
299 Lai, L., Wang, Y., Peng, S., Guo, W., Li, F. and Xu, S. (2022) P53 and taurine upregulated gene 1 promotes the repair of the DeoxyriboNucleic Acid damage induced by bupivacaine in murine primary sensory neurons. *Bioengineered* **13**, 7439–7456 https://doi.org/10.1080/21655979.2022.2048985
300 Shieh, S.-Y., Ikeda, M., Taya, Y. and Prives, C. (1997) DNA Damage-Induced Phosphorylation of p53 Alleviates Inhibition by MDM2. *Cell* **91**, 325–334 https://doi.org/10.1016/S0092-8674(00)80416-X
301 Firsanov, D. V., Solovjeva, L. V. and Svetlova, M. P. (2011) H2AX phosphorylation at the sites of DNA double-strand breaks in cultivated

mammalian cells and tissues. *Clin Epigenet* **2**, 283–297 https://doi.org/10.1007/s13148-011-0044-4
302 Rogakou, E. P., Pilch, D. R., Orr, A. H., Ivanova, V. S. and Bonner, W. M. (1998) DNA Double-stranded Breaks Induce Histone H2AX Phosphorylation on Serine 139. *Journal of Biological Chemistry* **273**, 5858–5868 https://doi.org/10.1074/jbc.273.10.5858
303 Olive, P. L. and Banáth, J. P. (2009) Kinetics of H2AX phosphorylation after exposure to cisplatin. *Cytometry* **76B**, 79–90 https://doi.org/10.1002/cyto.b.20450
304 Clingen, P. H., Wu, J. Y.-H., Miller, J., Mistry, N., Chin, F., Wynne, P., et al. (2008) Histone H2AX phosphorylation as a molecular pharmacological marker for DNA interstrand crosslink cancer chemotherapy. *Biochemical Pharmacology* **76**, 19–27 https://doi.org/10.1016/j.bcp.2008.03.025
305 Modesti, M. and Kanaar, R. (2001) DNA repair: Spot(light)s on chromatin. *Current Biology* **11**, R229–R232 https://doi.org/10.1016/S0960-9822(01)00112-9
306 Paull, T. T., Rogakou, E. P., Yamazaki, V., Kirchgessner, C. U., Gellert, M. and Bonner, W. M. (2000) A critical role for histone H2AX in recruitment of repair factors to nuclear foci after DNA damage. *Current Biology* **10**, 886–895 https://doi.org/10.1016/S0960-9822(00)00610-2
307 Bassing, C. H. and Alt, F. W. (2004) H2AX May Function as an Anchor to Hold Broken Chromosomal DNA Ends in Close Proximity. *Cell Cycle* **3**, 147–148 https://doi.org/10.4161/cc.3.2.684
308 Yuan, J., Adamski, R. and Chen, J. (2010) Focus on histone variant H2AX: To be or not to be. *FEBS Letters* **584**, 3717–3724 https://doi.org/10.1016/j.febslet.2010.05.021
309 Mah, L.-J., El-Osta, A. and Karagiannis, T. C. (2010) γH2AX: a sensitive molecular marker of DNA damage and repair. *Leukemia* **24**, 679–686 https://doi.org/10.1038/leu.2010.6
310 Stucki, M., Clapperton, J. A., Mohammad, D., Yaffe, M. B., Smerdon, S. J. and Jackson, S. P. (2005) MDC1 Directly Binds Phosphorylated Histone H2AX to Regulate Cellular Responses to DNA Double-Strand Breaks. *Cell* **123**, 1213–1226 https://doi.org/10.1016/j.cell.2005.09.038
311 Riballo, E., Kühne, M., Rief, N., Doherty, A., Smith, G. C. M., Recio, M.-J., et al. (2004) A Pathway of Double-Strand Break Rejoining Dependent upon ATM, Artemis, and Proteins Locating to γ-H2AX Foci. *Molecular Cell* **16**, 715–724 https://doi.org/10.1016/j.molcel.2004.10.029
312 Lukas, C., Melander, F., Stucki, M., Falck, J., Bekker-Jensen, S., Goldberg, M., et al. (2004) Mdc1 couples DNA double-strand break recognition by Nbs1 with its H2AX-dependent chromatin retention. *EMBO J* **23**, 2674–2683 https://doi.org/10.1038/sj.emboj.7600269
313 Ward, I. M., Minn, K., Jorda, K. G. and Chen, J. (2003) Accumulation of Checkpoint Protein 53BP1 at DNA Breaks Involves Its Binding to Phosphorylated Histone H2AX. *Journal of Biological Chemistry* **278**, 19579–19582 https://doi.org/10.1074/jbc.C300117200
314 Celeste, A., Fernandez-Capetillo, O., Kruhlak, M. J., Pilch, D. R., Staudt, D. W., Lee, A., et al. (2003) Histone H2AX phosphorylation is dispensable for the initial recognition of DNA breaks. *Nat Cell Biol* **5**, 675–679 https://doi.org/10.1038/ncb1004

315 Kinner, A., Wu, W., Staudt, C. and Iliakis, G. (2008) γ-H2AX in recognition and signaling of DNA double-strand breaks in the context of chromatin. *Nucleic Acids Research* **36**, 5678–5694 https://doi.org/10.1093/nar/gkn550
316 Chen, H. T., Bhandoola, A., Difilippantonio, M. J., Zhu, J., Brown, M. J., Tai, X., et al. (2000) Response to RAG-Mediated V(D)J Cleavage by NBS1 and γ-H2AX. *Science* **290**, 1962–1964 https://doi.org/10.1126/science.290.5498.1962
317 Giglia-Mari, G., Zotter, A. and Vermeulen, W. (2011) DNA Damage Response. *Cold Spring Harbor Perspectives in Biology* **3**, article a000745 https://doi.org/10.1101/cshperspect.a000745
318 Rocha, C. R. R., Silva, M. M., Quinet, A., Cabral-Neto, J. B. and Menck, C. F. M. (2018) DNA repair pathways and cisplatin resistance: an intimate relationship. *Clinics* **73**, article e478s https://doi.org/10.6061/clinics/2018/e478s
319 Hegde, M. L., Hazra, T. K. and Mitra, S. (2008) Early steps in the DNA base excision/single-strand interruption repair pathway in mammalian cells. *Cell Res* **18**, 27–47 https://doi.org/10.1038/cr.2008.8
320 Matsumoto, Y. (2001) Molecular mechanism of PCNA-dependent base excision repair. In Progress in Nucleic Acid Research and Molecular Biology, pp 129–138, Elsevier https://doi.org/10.1016/S0079-6603(01)68095-4
321 Jackson, S. P. (2002) Sensing and repairing DNA double-strand breaks. *Carcinogenesis* **23**, 687–696 https://doi.org/10.1093/carcin/23.5.687
322 Hoke, A. and Ray, M. (2014) Rodent Models of Chemotherapy-Induced Peripheral Neuropathy. *ILAR Journal* **54**, 273–281 https://doi.org/10.1093/ilar/ilt053
323 Hopkins, H. L., Duggett, N. A. and Flatters, S. J. L. (2016) Chemotherapy-induced painful neuropathy: pain-like behaviours in rodent models and their response to commonly used analgesics. *Current Opinion in Supportive & Palliative Care* **10**, 119–128 https://doi.org/10.1097/SPC.0000000000000204
324 Ozols, R. F. and Young, R. C. (1985) High-dose cisplatin therapy in ovarian cancer. *Semin Oncol* **12**, 21–30
325 Joseph, E. K. and Levine, J. D. (2009) Comparison of Oxaliplatin- and Cisplatin-Induced Painful Peripheral Neuropathy in the Rat. *The Journal of Pain* **10**, 534–541 https://doi.org/10.1016/j.jpain.2008.12.003
326 Guindon, J., Lai, Y., Takacs, S. M., Bradshaw, H. B. and Hohmann, A. G. (2013) Alterations in endocannabinoid tone following chemotherapy-induced peripheral neuropathy: Effects of endocannabinoid deactivation inhibitors targeting fatty-acid amide hydrolase and monoacylglycerol lipase in comparison to reference analgesics following cisplatin treatment. *Pharmacological Research* **67**, 94–109 https://doi.org/10.1016/j.phrs.2012.10.013
327 Woller, S. A., Corr, M. and Yaksh, T. L. (2015) Differences in cisplatin-induced mechanical allodynia in male and female mice. *Eur J Pain* **19**, 1476–1485 https://doi.org/10.1002/ejp.679
328 Ta, L. E., Low, P. A. and Windebank, A. J. (2009) Mice with Cisplatin and Oxaliplatin-Induced Painful Neuropathy Develop Distinct Early Responses to Thermal Stimuli. *Mol Pain* **5**, 5–9 https://doi.org/10.1186/1744-8069-5-9
329 Authier, N. (2003) An animal model of nociceptive peripheral neuropathy following repeated cisplatin injections. *Experimental Neurology* **182**, 12–20 https://doi.org/10.1016/S0014-4886(03)00003-7

330 Authier, N., Fialip, J., Eschalier, A. and Coudoré, F. (2000) Assessment of allodynia and hyperalgesia after cisplatin administration to rats. *Neuroscience Letters* **291**, 73–76 https://doi.org/10.1016/S0304-3940(00)01373-2
331 Boehmerle, W., Huehnchen, P., Peruzzaro, S., Balkaya, M. and Endres, M. (2015) Electrophysiological, behavioral and histological characterization of paclitaxel, cisplatin, vincristine and bortezomib-induced neuropathy in C57Bl/6 mice. *Sci Rep* **4**, 6370 https://doi.org/10.1038/srep06370
332 Brewer, J. R., Morrison, G., Dolan, M. E. and Fleming, G. F. (2016) Chemotherapy-induced peripheral neuropathy: Current status and progress. *Gynecologic Oncology* **140**, 176–183 https://doi.org/10.1016/j.ygyno.2015.11.011
333 Mao-Ying, Q.-L., Kavelaars, A., Krukowski, K., Huo, X.-J., Zhou, W., Price, T. J., et al. (2014) The Anti-Diabetic Drug Metformin Protects against Chemotherapy-Induced Peripheral Neuropathy in a Mouse Model. *PLoS ONE* (McKemy, D. D., ed.) **9**, e100701 https://doi.org/10.1371/journal.pone.0100701
334 Hu, L.-Y., Zhou, Y., Cui, W.-Q., Hu, X.-M., Du, L.-X., Mi, W.-L., et al. (2018) Triggering receptor expressed on myeloid cells 2 (TREM2) dependent microglial activation promotes cisplatin-induced peripheral neuropathy in mice. *Brain, Behavior, and Immunity* **68**, 132–145 https://doi.org/10.1016/j.bbi.2017.10.011
335 Vencappa, S., Donaldson, L. F. and Hulse, R. P. (2015) Cisplatin induced sensory neuropathy is prevented by vascular endothelial growth factor-A. *Am J Transl Res* **7**, 1032–1044
336 English, K., Shepherd, A., Uzor, N.-E., Trinh, R., Kavelaars, A. and Heijnen, C. J. (2020) Astrocytes rescue neuronal health after cisplatin treatment through mitochondrial transfer. *acta neuropathol commun* **8**, article 36 https://doi.org/10.1186/s40478-020-00897-7
337 Schinke, C., Fernandez Vallone, V., Ivanov, A., Peng, Y., Körtvelyessy, P., Nolte, L., et al. (2021) Modeling chemotherapy induced neurotoxicity with human induced pluripotent stem cell (iPSC) -derived sensory neurons. *Neurobiology of Disease* **155**, 105391 https://doi.org/10.1016/j.nbd.2021.105391
338 Podratz, J. L., Kulkarni, A., Pleticha, J., Kanwar, R., Beutler, A. S., Staff, N. P., et al. (2016) Neurotoxicity to DRG neurons varies between rodent strains treated with cisplatin and bortezomib. *Journal of the Neurological Sciences* **362**, 131–135 https://doi.org/10.1016/j.jns.2015.12.038
339 Wheeler, H. E., Wing, C., Delaney, S. M., Komatsu, M. and Dolan, M. E. (2015) Modeling Chemotherapeutic Neurotoxicity with Human Induced Pluripotent Stem Cell-Derived Neuronal Cells. *PLoS ONE* (Zheng, J. C., ed.) **10**, e0118020 https://doi.org/10.1371/journal.pone.0118020
340 Hathway, G. J., Murphy, E., Lloyd, J., Greenspon, C. and Hulse, R. P. (2018) Cancer Chemotherapy in Early Life Significantly Alters the Maturation of Pain Processing. *Neuroscience* **387**, 214–229 https://doi.org/10.1016/j.neuroscience.2017.11.032
341 Verdú, E., Vilches, J. J., Rodríguez, F. J., Ceballos, D., Valero, A. and Navarro, X. (1999) Physiological and immunohistochemical characterization of cisplatin-induced neuropathy in mice. *Muscle Nerve* **22**, 329–340 https://doi.org/10.1002/(SICI)1097-4598(199903)22:3<329::AID-MUS5>3.0.CO;2-8

342 Cataldo, G., Erb, S. J., Lunzer, M. M., Luong, N., Akgün, E., Portoghese, P. S., et al. (2019) The bivalent ligand MCC22 potently attenuates hyperalgesia in a mouse model of cisplatin-evoked neuropathic pain without tolerance or reward. *Neuropharmacology* **158** https://doi.org/10.1016/j.neuropharm.2019.04.004
343 Lin, H., Heo, B. H. and Yoon, M. H. (2015) A New Rat Model of Cisplatin-induced Neuropathic Pain. *Korean J Pain* **28**, 236–243 https://doi.org/10.3344/kjp.2015.28.4.236
344 Marcus, D. J., Zee, M., Hughes, A., Yuill, M. B., Hohmann, A. G., Mackie, K., et al. (2015) Tolerance to the Antinociceptive Effects of Chronic Morphine Requires C-Jun N-Terminal Kinase. *Mol Pain* **11**, s12990-015–0031 https://doi.org/10.1186/s12990-015-0031-4
345 Uhelski, M. L., Khasabova, I. A. and Simone, D. A. (2015) Inhibition of anandamide hydrolysis attenuates nociceptor sensitization in a murine model of chemotherapy-induced peripheral neuropathy. *Journal of Neurophysiology* **113**, 1501–1510 https://doi.org/10.1152/jn.00692.2014
346 Park, H. J., Stokes, J. A., Pirie, E., Skahen, J., Shtaerman, Y. and Yaksh, T. L. (2013) Persistent Hyperalgesia in the Cisplatin-Treated Mouse as Defined by Threshold Measures, the Conditioned Place Preference Paradigm, and Changes in Dorsal Root Ganglia Activated Transcription Factor 3: The Effects of Gabapentin, Ketorolac, and Etanercept. *Anesthesia & Analgesia* **116**, 224–231 https://doi.org/10.1213/ANE.0b013e31826e1007
347 Ta, L. E., Bieber, A. J., Carlton, S. M., Loprinzi, C. L., Low, P. A. and Windebank, A. J. (2010) Transient Receptor Potential Vanilloid 1 is Essential for Cisplatin-Induced Heat Hyperalgesia in Mice. *Mol Pain* **6**, 1744-8069-6–15 https://doi.org/10.1186/1744-8069-6-15
348 Cata, J. P., Weng, H.-R. and Dougherty, P. M. (2008) Behavioral and electrophysiological studies in rats with cisplatin-induced chemoneuropathy. *Brain Research* **1230**, 91–98 https://doi.org/10.1016/j.brainres.2008.07.022
349 Vera, G., Chiarlone, A., Cabezos, P. A., Pascual, D., Martín, M. I. and Abalo, R. (2007) WIN 55,212-2 prevents mechanical allodynia but not alterations in feeding behaviour induced by chronic cisplatin in the rat. *Life Sciences* **81**, 468–479 https://doi.org/10.1016/j.lfs.2007.06.012
350 Carozzi, V. A., Canta, A., Oggioni, N., Sala, B., Chiorazzi, A., Meregalli, C., et al. (2010) Neurophysiological and neuropathological characterization of new murine models of chemotherapy-induced chronic peripheral neuropathies. *Experimental Neurology* **226**, 301–309 https://doi.org/10.1016/j.expneurol.2010.09.004
351 Schappacher, K. A., Styczynski, L. and Baccei, M. L. (2017) Early life vincristine exposure evokes mechanical pain hypersensitivity in the developing rat: *PAIN* **158**, 1647–1655 https://doi.org/10.1097/j.pain.0000000000000953
352 Schappacher, K. A., Xie, W., Zhang, J.-M. and Baccei, M. L. (2019) Neonatal vincristine administration modulates intrinsic neuronal excitability in the rat dorsal root ganglion and spinal dorsal horn during adolescence: *PAIN* **160**, 645–657 https://doi.org/10.1097/j.pain.0000000000001444
353 Chaplan, S. R., Bach, F. W., Pogrel, J. W., Chung, J. M. and Yaksh, T. L. (1994) Quantitative assessment of tactile allodynia in the rat paw. *Journal of Neuroscience Methods* **53**, 55–63 https://doi.org/10.1016/0165-0270(94)90144-9

354 Hargreaves, K., Dubner, R., Brown, F., Flores, C. and Joris, J. (1988) A new and sensitive method for measuring thermal nociception in cutaneous hyperalgesia. *Pain* **32**, 77–88 https://doi.org/10.1016/0304-3959(88)90026-7
355 Coelho, A., Wolf-Johnston, A. S., Shinde, S., Cruz, C. D., Cruz, F., Avelino, A., et al. (2015) Urinary bladder inflammation induces changes in urothelial nerve growth factor and TRPV1 channels: Changes on urothelial cells during inflammation. *Br J Pharmacol* **172**, 1691–1699 https://doi.org/10.1111/bph.12958
356 Wood, E. R., Kuyper, L., Petrov, K. G., Hunter, R. N., Harris, P. A. and Lackey, K. (2004) Discovery and in vitro evaluation of potent TrkA kinase inhibitors: oxindole and aza-oxindoles. *Bioorganic & Medicinal Chemistry Letters* **14**, 953–957 https://doi.org/10.1016/j.bmcl.2003.12.002
357 LoMonaco, M., Milone, M., Batocchi, A. P., Padua, L., Restuccia, D. and Tonali, P. (1992) Cisplatin neuropathy: clinical course and neurophysiological findings. *J Neurol* **239**, 199–204 https://doi.org/10.1007/BF00839140
358 Mollman, J. E., Glover, D. J., Hogan, W. M. and Furman, R. E. (1988) Cisplatin neuropathy. Risk factors, prognosis, and protection by WR-2721. *Cancer* **61**, 2192–2195 https://doi.org/10.1002/1097-0142(19880601)61:11<2192::AID-CNCR2820611110>3.0.CO;2-A
359 Khan, R. B., Hudson, M. M., Ledet, D. S., Morris, E. B., Pui, C.-H., Howard, S. C., et al. (2014) Neurologic morbidity and quality of life in survivors of childhood acute lymphoblastic leukemia: a prospective cross-sectional study. *J Cancer Surviv* **8**, 688–696 https://doi.org/10.1007/s11764-014-0375-1
360 Phillips, S. M., Padgett, L. S., Leisenring, W. M., Stratton, K. K., Bishop, K., Krull, K. R., et al. (2015) Survivors of Childhood Cancer in the United States: Prevalence and Burden of Morbidity. *Cancer Epidemiology Biomarkers & Prevention* **24**, 653–663 https://doi.org/10.1158/1055-9965.EPI-14-1418
361 Glare, P., Aubrey, K., Gulati, A., Lee, Y. C., Moryl, N. and Overton, S. (2022) Pharmacologic Management of Persistent Pain in Cancer Survivors. *Drugs* **82**, 275–291 https://doi.org/10.1007/s40265-022-01675-6
362 Jiang, C., Wang, H., Wang, Q., Luo, Y., Sidlow, R. and Han, X. (2019) Prevalence of Chronic Pain and High-Impact Chronic Pain in Cancer Survivors in the United States. *JAMA Oncol* **5**, 1224–1226 https://doi.org/10.1001/jamaoncol.2019.1439
363 Couceiro, T. C. de M., Lima, L. C., Coutinho Júnior, M. P., Mello, P. F. da L. S. de O., Ferreira, T. M. M. L. and Firmino, A. L. P. (2018) Prevalence of neuropathic pain in patients with cancer. *Brazilian Journal Of Pain* **1** https://doi.org/10.5935/2595-0118.20180045
364 van den Beuken-van Everdingen, M. (2012) Chronic Pain in Cancer Survivors: A Growing Issue. *Journal of Pain & Palliative Care Pharmacotherapy* **26**, 385–387 https://doi.org/10.3109/15360288.2012.734908
365 Kurita, G. P. and Sjøgren, P. (2015) Pain management in cancer survivorship. *Acta Oncologica* **54**, 629–634 https://doi.org/10.3109/0284186X.2014.996662
366 Bennett, M. I., Rayment, C., Hjermstad, M., Aass, N., Caraceni, A. and Kaasa, S. (2012) Prevalence and aetiology of neuropathic pain in cancer patients: a systematic review. *Pain* **153**, 359–365 https://doi.org/10.1016/j.pain.2011.10.028
367 Boland, B. A., Sherry, V. and Polomano, R. C. (2010) Chemotherapy-Induced Peripheral Neuropathy in Cancer Survivors. *Oncol. Nurse Edn* **24**, 33–38, 42–43

368 Boogerd, W., ten Bokkel Huinink, W. W., Dalesio, O., Hoppenbrouwers, W. J. J. F. and van der Sande, J. J. (1990) Cisplatin induced neuropathy: Central, peripheral and autonomic nerve involvement. *J Neuro-Oncol* **9**, 255–263 https://doi.org/10.1007/BF02341156
369 Daugaard, G. K., Petrera, J. and Trojaborg, W. (1987) Electrophysiological study of the peripheral and central neurotoxic effect of cisplatin. *Acta Neurologica Scandinavica* **76**, 86–93 https://doi.org/10.1111/j.1600-0404.1987.tb03551.x
370 Hansen, S. W., Helweg-Larsen, S. and Trojaborg, W. (1989) Long-term neurotoxicity in patients treated with cisplatin, vinblastine, and bleomycin for metastatic germ cell cancer. *JCO* **7**, 1457–1461 https://doi.org/10.1200/JCO.1989.7.10.1457
371 Krarup-Hansen, A., Helweg-Larsen, S., Schmalbruch, H., Rorth, M. and Krarup, C. (2007) Neuronal involvement in cisplatin neuropathy: prospective clinical and neurophysiological studies. *Brain* **130**, 1076–1088 https://doi.org/10.1093/brain/awl356
372 Fukuda, Y., Li, Y. and Segal, R. A. (2017) A Mechanistic Understanding of Axon Degeneration in Chemotherapy-Induced Peripheral Neuropathy. *Front. Neurosci.* **11** https://doi.org/10.3389/fnins.2017.00481
373 Rach, A. M., Crabtree, V. M., Brinkman, T. M., Zeltzer, L., Marchak, J. G., Srivastava, D., et al. (2017) Predictors of fatigue and poor sleep in adult survivors of childhood Hodgkin's lymphoma: a report from the Childhood Cancer Survivor Study. *J Cancer Surviv* **11**, 256–263 https://doi.org/10.1007/s11764-016-0583-y
374 Ness, K. K., Hudson, M. M., Jones, K. E., Leisenring, W., Yasui, Y., Chen, Y., et al. (2017) Effect of Temporal Changes in Therapeutic Exposure on Self-reported Health Status in Childhood Cancer Survivors. *Ann Intern Med* **166**, 89–98 https://doi.org/10.7326/M16-0742
375 Curcio, K. (2016) Instruments for Assessing Chemotherapy-Induced Peripheral Neuropathy: A Review of the Literature. *CJON* **20**, 144–151 https://doi.org/10.1188/16.CJON.20-01AP
376 Haryani, H., Fetzer, S., Wu, C.-L. and Hsu, Y.-Y. (2017) Chemotherapy-Induced Peripheral Neuropathy Assessment Tools: A Systematic Review. *ONF* **44**, E111–E123 https://doi.org/10.1188/17.ONF.E111-E123
377 Molassiotis, A., Cheng, H. L., Lopez, V., Au, J. S. K., Chan, A., Bandla, A., et al. (2019) Are we mis-estimating chemotherapy-induced peripheral neuropathy? Analysis of assessment methodologies from a prospective, multinational, longitudinal cohort study of patients receiving neurotoxic chemotherapy. *BMC Cancer* **19**, 132 https://doi.org/10.1186/s12885-019-5302-4
378 Shimozuma, K., Ohashi, Y., Takeuchi, A., Aranishi, T., Morita, S., Kuroi, K., et al. (2009) Feasibility and validity of the Patient Neurotoxicity Questionnaire during taxane chemotherapy in a phase III randomized trial in patients with breast cancer: N-SAS BC 02. *Support Care Cancer* **17**, 1483–1491 https://doi.org/10.1007/s00520-009-0613-7
379 Hausheer, F. H., Schilsky, R. L., Bain, S., Berghorn, E. J. and Lieberman, F. (2006) Diagnosis, Management, and Evaluation of Chemotherapy-Induced Peripheral Neuropathy. *Seminars in Oncology* **33**, 15–49 https://doi.org/10.1053/j.seminoncol.2005.12.010

380 Kawashiri, T., Miyagi, A., Shimizu, S., Shigematsu, N., Kobayashi, D. and Shimazoe, T. (2018) Dimethyl fumarate ameliorates chemotherapy agent-induced neurotoxicity in vitro. *Journal of Pharmacological Sciences* **137**, 202–211 https://doi.org/10.1016/j.jphs.2018.06.008
381 Walco, G. A., Dworkin, R. H., Krane, E. J., LeBel, A. A. and Treede, R.-D. (2010) Neuropathic Pain in Children: Special Considerations. *Mayo Clinic Proceedings* **85**, S33–S41 https://doi.org/10.4065/mcp.2009.0647
382 Atherton, D. D., Taherzadeh, O., Elliot, D. and Anand, P. (2008) Age-Dependent Development Of Chronic Neuropathic Pain, Allodynia and Sensory Recovery after Upper Limb Nerve Injury in Children. *J Hand Surg Eur Vol* **33**, 186–191 https://doi.org/10.1177/1753193408087029
383 Robison, L. L., Mertens, A. C., Boice, J. D., Breslow, N. E., Donaldson, S. S., Green, D. M., et al. (2002) Study design and cohort characteristics of the childhood cancer survivor study: A multi-institutional collaborative project. *Med. Pediatr. Oncol.* **38**, 229–239 https://doi.org/10.1002/mpo.1316
384 Picut, C. A., Ziejewski, M. K. and Stanislaus, D. (2018) Comparative Aspects of Pre- and Postnatal Development of the Male Reproductive System: Development of the Male Reproductive System. *Birth Defects Research* **110**, 190–227 https://doi.org/10.1002/bdr2.1133
385 Bell, M. R. (2018) Comparing Postnatal Development of Gonadal Hormones and Associated Social Behaviors in Rats, Mice, and Humans. *Endocrinology* **159**, 2596–2613 https://doi.org/10.1210/en.2018-00220
386 Marty, M. S., Chapin, R. E., Parks, L. G. and Thorsrud, B. A. (2003) Development and maturation of the male reproductive system. *Birth Defect Res B* **68**, 125–136 https://doi.org/10.1002/bdrb.10015
387 Strumberg, D., Brügge, S., Korn, M. W., Koeppen, S., Ranft, J., Scheiber, G., et al. (2002) Evaluation of long-term toxicity in patients after cisplatin-based chemotherapy for non-seminomatous testicular cancer. *Annals of Oncology* **13**, 229–236 https://doi.org/10.1093/annonc/mdf058
388 Glendenning, J. L., Barbachano, Y., Norman, A. R., Dearnaley, D. P., Horwich, A. and Huddart, R. A. (2010) Long-term neurologic and peripheral vascular toxicity after chemotherapy treatment of testicular cancer. *Cancer* **116**, 2322–2331 https://doi.org/10.1002/cncr.24981
389 Guindon, J., Deng, L., Fan, B., Wager-Miller, J. and Hohmann, A. G. (2014) Optimization of a Cisplatin Model of Chemotherapy-Induced Peripheral Neuropathy in Mice: Use of Vitamin C and Sodium Bicarbonate Pretreatments to Reduce Nephrotoxicity and Improve Animal Health Status. *Mol Pain* **10**, 1744-8069-10–56 https://doi.org/10.1186/1744-8069-10-56
390 Nair, A. and Jacob, S. (2016) A simple practice guide for dose conversion between animals and human. *J Basic Clin Pharma* **7**, 27–31 https://doi.org/10.4103/0976-0105.177703
391 Talbot, S. R., Biernot, S., Bleich, A., van Dijk, R. M., Ernst, L., Häger, C., et al. (2020) Defining body-weight reduction as a humane endpoint: a critical appraisal. *Lab Anim* **54**, 99–110 https://doi.org/10.1177/0023677219883319
392 Astolfi, L., Ghiselli, S., Guaran, V., Chicca, M., Simoni, E., Olivetto, E., et al. (2013) Correlation of adverse effects of cisplatin administration in patients affected by solid tumours: A retrospective evaluation. *Oncology Reports* **29**, 1285–1292 https://doi.org/10.3892/or.2013.2279

393 Gilron, I., Baron, R. and Jensen, T. (2015) Neuropathic Pain: Principles of Diagnosis and Treatment. *Mayo Clinic Proceedings* **90**, 532–545 https://doi.org/10.1016/j.mayocp.2015.01.018
394 Wainger, B. J., Buttermore, E. D., Oliveira, J. T., Mellin, C., Lee, S., Saber, W. A., et al. (2015) Modeling pain in vitro using nociceptor neurons reprogrammed from fibroblasts. *Nat Neurosci* **18**, 17–24 https://doi.org/10.1038/nn.3886
395 Hol, E. M., Mandys, V., Sodaar, P., Gispen, W. H. and Bär, P. R. (1994) Protection by an ACTH4-9 analogue against the toxic effects of cisplatin and taxol on sensory neurons and glial cells in vitro: Neuroprotection by Melanocortins. *J. Neurosci. Res.* **39**, 178–185 https://doi.org/10.1002/jnr.490390208
396 Wing, C., Komatsu, M., Delaney, S. M., Krause, M., Wheeler, H. E. and Dolan, M. E. (2017) Application of stem cell derived neuronal cells to evaluate neurotoxic chemotherapy. *Stem Cell Research* **22**, 79–88 https://doi.org/10.1016/j.scr.2017.06.006
397 Krøigård, T., Schrøder, H. D., Qvortrup, C., Eckhoff, L., Pfeiffer, P., Gaist, D., et al. (2014) Characterization and diagnostic evaluation of chronic polyneuropathies induced by oxaliplatin and docetaxel comparing skin biopsy to quantitative sensory testing and nerve conduction studies. *Eur J Neurol* **21**, 623–629 https://doi.org/10.1111/ene.12353
398 Herrmann, D. N., Griffin, J. W., Hauer, P., Cornblath, D. R. and McArthur, J. C. (1999) Epidermal nerve fiber density and sural nerve morphometry in peripheral neuropathies. *Neurology* **53**, 1634–1634 https://doi.org/10.1212/WNL.53.8.1634
399 Holland, N. R., Crawford, T. O., Hauer, P., Cornblath, D. R., Griffin, J. W. and McArthur, J. C. (1998) Small-fiber sensory neuropathies: Clinical course and neuropathology of idiopathic cases. *Ann Neurol.* **44**, 47–59 https://doi.org/10.1002/ana.410440111
400 Holland, N. R., Stocks, A., Hauer, P., Cornblath, D. R., Griffin, J. W. and McArthur, J. C. (1997) Intraepidermal nerve fiber density in patients with painful sensory neuropathy. *Neurology* **48**, 708–711 https://doi.org/10.1212/WNL.48.3.708
401 McCarthy, B. G., Hsieh, S.-T., Stocks, A., Hauer, P., Macko, C., Cornblath, D. R., et al. (1995) Cutaneous innervation in sensory neuropathies: Evaluation by skin biopsy. *Neurology* **45**, 1848–1855 https://doi.org/10.1212/WNL.45.10.1848
402 Lauria, G., Morbin, M., Lombardi, R., Capobianco, R., Camozzi, F., Pareyson, D., et al. (2006) Expression of capsaicin receptor immunoreactivity in human peripheral nervous system and in painful neuropathies. *J Peripher Nerv Syst* **11**, 262–271 https://doi.org/10.1111/j.1529-8027.2006.0097.x
403 Periquet, M. I., Novak, V., Collins, M. P., Nagaraja, H. N., Erdem, S., Nash, S. M., et al. (1999) Painful sensory neuropathy: Prospective evaluation using skin biopsy. *Neurology* **53**, 1641–1641 https://doi.org/10.1212/WNL.53.8.1641
404 Eldridge, S., Guo, L. and Hamre, J. (2020) A Comparative Review of Chemotherapy-Induced Peripheral Neuropathy in In Vivo and In Vitro Models. *Toxicol Pathol* **48**, 190–201 https://doi.org/10.1177/0192623319861937
405 Lauria, G., Lombardi, R., Borgna, M., Penza, P., Bianchi, R., Savino, C., et al. (2005) Intraepidermal nerve fiber density in rat foot pad: neuropathologic-neurophysiologic correlation. *J Peripher Nerv Syst* **10**, 202–208 https://doi.org/10.1111/j.1085-9489.2005.0010210.x

406 Cavaletti, G., Tredici, G., Marmiroli, P., Petruccioli, M. G., Barajon, I. and Fabbrica, D. (1992) Morphometric study of the sensory neuron and peripheral nerve changes induced by chronic cisplatin (DDP) administration in rats. *Acta Neuropathol* **84** https://doi.org/10.1007/BF00227662
407 Smith, A. G., Howard, J. R., Kroll, R., Ramachandran, P., Hauer, P., Singleton, J. R., et al. (2005) The reliability of skin biopsy with measurement of intraepidermal nerve fiber density. *Journal of the Neurological Sciences* **228**, 65–69 https://doi.org/10.1016/j.jns.2004.09.032
408 St. Germain, C., Niknejad, N., Ma, L., Garbuio, K., Hai, T. and Dimitroulakos, J. (2010) Cisplatin Induces Cytotoxicity through the Mitogen-Activated Protein Kinase Pathways ana Activating Transcription Factor 3. *Neoplasia* **12**, 527–538 https://doi.org/10.1593/neo.92048
409 Donzelli, E., Carfì, M., Miloso, M., Strada, A., Galbiati, S., Bayssas, M., et al. (2004) Neurotoxicity of Platinum Compounds: Comparison of the Effects of Cisplatin and Oxaliplatin on the Human Neuroblastoma Cell Line SH-SY5Y. *J Neurooncol* **67**, 65–73 https://doi.org/10.1023/B:NEON.0000021787.70029.ce
410 Cece, R., Barajon, I. and Tredici, G. (1995) Cisplatin induces apoptosis in SH-SY5Y human neuroblastoma cell line. *Anticancer Res* **15**, 777–782
411 Dravid, A., Raos, B., Svirskis, D. and O'Carroll, S. J. (2021) Differentiated SH-SY5Y Cells for High-Throughput Screening in a 96-Well Plate Format: Protocol Optimisation and Application for Neurite Outgrowth Assays, preprint, In Review https://doi.org/10.21203/rs.3.rs-792905/v1
412 Adimoolam, S. and Ford, J. M. (2003) p53 and regulation of DNA damage recognition during nucleotide excision repair. *DNA Repair* **2**, 947–954 https://doi.org/10.1016/S1568-7864(03)00087-9
413 Lam, F. C. (2022) The DNA damage response - from cell biology to human disease. *J Transl Genet Genom* **6**, 204–222 https://doi.org/10.20517/jtgg.2021.61
414 Eastman, A. (1990) Activation of programmed cell death by anticancer agents: cisplatin as a model system. *Cancer Cells* **2**, 275–280
415 Offer, H., Erez, N., Zurer, I., Tang, X., Milyavsky, M., Goldfinger, N., et al. (2002) The onset of p53-dependent DNA repair or apoptosis is determined by the level of accumulated damaged DNA. *Carcinogenesis* **23**, 1025–1032 https://doi.org/10.1093/carcin/23.6.1025
416 Chee, J. L. Y., Saidin, S., Lane, D. P., Leong, S. M., Noll, J. E., Neilsen, P. M., et al. (2013) Wild-type and mutant p53 mediate cisplatin resistance through interaction and inhibition of active caspase-9. *Cell Cycle* **12**, 278–288 https://doi.org/10.4161/cc.23054
417 D'Sa-Eipper, C., Leonard, J. R., Putcha, G., Zheng, T. S., Flavell, R. A., Rakic, P., et al. (2001) DNA damage-induced neural precursor cell apoptosis requires p53 and caspase 9 but neither Bax nor caspase 3. *Development* **128**, 137–146 https://doi.org/10.1242/dev.128.1.137
418 Brentnall, M., Rodriguez-Menocal, L., De Guevara, R. L., Cepero, E. and Boise, L. H. (2013) Caspase-9, caspase-3 and caspase-7 have distinct roles during intrinsic apoptosis. *BMC Cell Biol* **14**, article 32 https://doi.org/10.1186/1471-2121-14-32
419 Perego, P., Giarola, M., Righetti, S. C., Supino, R., Caserini, C., Delia, D., et al. (1996) Association between cisplatin resistance and mutation of p53 gene and reduced bax expression in ovarian carcinoma cell systems. *Cancer Res* **56**, 556–562

420 Han, J. Y., Chung, Y. J., Kim, J. S., Rhyu, M. G., Kim, H. K., Lee, K. S., et al. (1999) The relationship between cisplatin - induced apoptosis and p53 , bcl - 2 and bax expression in human lung cancer cells. *Korean J Intern Med* **14**, 42–52 https://doi.org/10.3904/kjim.1999.14.1.42
421 Starobova, H., Mueller, A., Deuis, J. R., Carter, D. A. and Vetter, I. (2019) Inflammatory and Neuropathic Gene Expression Signatures of Chemotherapy-Induced Neuropathy Induced by Vincristine, Cisplatin, and Oxaliplatin in C57BL/6J Mice. *The Journal of Pain* **21**, 182–194 https://doi.org/10.1016/j.jpain.2019.06.008
422 Jamieson, D. G., Moss, A., Kennedy, M., Jones, S., Nenadic, G., Robertson, D. L., et al. (2014) The pain interactome: Connecting pain-specific protein interactions: *Pain* **155**, 2243–2252 https://doi.org/10.1016/j.pain.2014.06.020
423 Minnone, G., De Benedetti, F. and Bracci-Laudiero, L. (2017) NGF and Its Receptors in the Regulation of Inflammatory Response. *IJMS* **18**, article 1028 https://doi.org/10.3390/ijms18051028
424 Safieh-Garabedian, B., Poole, S., Allchorne, A., Winter, J. and Woolf, C. J. (1995) Contribution of interleukin-1β to the inflammation-induced increase in nerve growth factor levels and inflammatory hyperalgesia. *British Journal of Pharmacology* **115**, 1265–1275 https://doi.org/10.1111/j.1476-5381.1995.tb15035.x
425 Oddiah, D., Anand, P., McMahon, S. B. and Rattray, M. (1998) Rapid increase of NGF, BDNF and NT-3 mRNAs in inflamed bladder. *NeuroReport* **9**, 1455–1458 https://doi.org/10.1097/00001756-199805110-00038
426 Barthel, C., Yeremenko, N., Jacobs, R., Schmidt, R. E., Bernateck, M., Zeidler, H., et al. (2009) Nerve growth factor and receptor expression in rheumatoid arthritis and spondyloarthritis. *Arthritis Res Ther* **11**, R82 https://doi.org/10.1186/ar2716
427 Aloe, L., Rocco, M., Bianchi, P. and Manni, L. (2012) Nerve growth factor: from the early discoveries to the potential clinical use. *J Transl Med* **10**, 239 https://doi.org/10.1186/1479-5876-10-239
428 Thoenen, H., Bandtlow, C. and Heumann, R. (1987) The physiological function of nerve growth factor in the central nervous system: Comparison with the periphery. In Reviews of Physiology, Biochemistry and Pharmacology, Volume 94, pp 145–178, Springer Berlin Heidelberg, Berlin, Heidelberg https://doi.org/10.1007/BFb0031026
429 Lees, J. G., Makker, P. G. S., Tonkin, R. S., Abdulla, M., Park, S. B., Goldstein, D., et al. (2017) Immune-mediated processes implicated in chemotherapy-induced peripheral neuropathy. *European Journal of Cancer* **73**, 22–29 https://doi.org/10.1016/j.ejca.2016.12.006
430 Watkins, L. R. and Maier, S. F. (2002) Beyond Neurons: Evidence That Immune and Glial Cells Contribute to Pathological Pain States. *Physiological Reviews* **82**, 981–1011 https://doi.org/10.1152/physrev.00011.2002
431 Aloe, L., Bracci-Laudiero, L., Bonini, S., Manni, L. and Aloe, L. (1997) The expanding role of nerve growth factor: from neurotrophic activity to immunologic diseases. *Allergy* **52**, 883–994 https://doi.org/10.1111/j.1398-9995.1997.tb01247.x
432 Bonini, S., Rasi, G., Bracci-Laudiero, M. L., Procoli, A. and Aloe, L. (2003) Nerve Growth Factor: Neurotrophin or Cytokine? *Int Arch Allergy Immunol* **131**, 80–84 https://doi.org/10.1159/000070922

433 Ebendal, T. (1992) Function and evolution in the NGF family and its receptors. *J. Neurosci. Res.* **32**, 461–470 https://doi.org/10.1002/jnr.490320402
434 Ruit, K. G., Elliott, J. L., Osborne, P. A., Yan, Q. and Snider, W. D. (1992) Selective dependence of mammalian dorsal root ganglion neurons on nerve growth factor during embryonic development. *Neuron* **8**, 573–587 https://doi.org/10.1016/0896-6273(92)90284-K
435 McMahon, S. B. and Priestley, J. V. (1995) Peripheral neuropathies and neurotrophic factors: animal models and clinical perspectives. *Current Opinion in Neurobiology* **5**, 616–624 https://doi.org/10.1016/0959-4388(95)80067-0
436 Geldof, A. A. (1995) Nerve-growth-factor-dependent neurite outgrowth assay; a research model for chemotherapy-induced neuropathy. *J Cancer Res Clin Oncol* **121**, 657–660 https://doi.org/10.1007/BF01218523
437 Hayakawa, K., Sobue, G., Itoh, T. and Mitsuma, T. (1994) Nerve growth factor prevents neurotoxic effects of cisplatin, vincristine and taxol, on adult rat sympathetic ganglion explants in vitro. *Life Sciences* **55**, 519–525 https://doi.org/10.1016/0024-3205(94)00744-6
438 Konings, P. N. M., Karolien Makkink, W., van Delft, A. M. L. and Ruigt, G. F. (1994) Reversal by NGF of cytostatic drug-induced reduction of neurite outgrowth in rat dorsal root ganglia in vitro. *Brain Research* **640**, 195–204 https://doi.org/10.1016/0006-8993(94)91873-2
439 Apfel, S. C., Kessler, J. A., Adornato, B. T., Litchy, W. J., Sanders, C., Rask, C. A., et al. (1998) Recombinant human nerve growth factor in the treatment of diabetic polyneuropathy. *Neurology* **51**, 695–702 https://doi.org/10.1212/WNL.51.3.695
440 Diemel, L. T., Brewster, W. J., Fernyhough, P. and Tomlinson, D. R. (1994) Expression of neuropeptides in experimental diabetes; effects of treatment with nerve growth factor or brain-derived neurotrophic factor. *Molecular Brain Research* **21**, 171–175 https://doi.org/10.1016/0169-328X(94)90391-3
441 Sango, K., Verdes, J. M., Hikawa, N., Horie, H., Tanaka, S., Inoue, S., et al. (1994) Nerve growth factor (NGF) restores depletions of calcitonin gene-related peptide and substance P in sensory neurons from diabetic mice in vitro. *Journal of the Neurological Sciences* **126**, 1–5 https://doi.org/10.1016/0022-510X(94)90087-6
442 Donnerer, J., Schuligoi, R. and Stein, C. (1992) Increased content and transport of substance P and calcitonin gene-related peptide in sensory nerves innervating inflamed tissue: Evidence for a regulatory function of nerve growth factor in vivo. *Neuroscience* **49**, 693–698 https://doi.org/10.1016/0306-4522(92)90237-V
443 Woolf, C. J., Safieh-Garabedian, B., Ma, Q.-P., Crilly, P. and Winter, J. (1994) Nerve growth factor contributes to the generation of inflammatory sensory hypersensitivity. *Neuroscience* **62**, 327–331 https://doi.org/10.1016/0306-4522(94)90366-2
444 Winston, J. H., He, Z.-J., Shenoy, M., Xiao, S.-Y. and Pasricha, P. J. (2005) Molecular and behavioral changes in nociception in a novel rat model of chronic pancreatitis for the study of pain. *Pain* **117**, 214–222 https://doi.org/10.1016/j.pain.2005.06.013
445 Richardson, S. M., Doyle, P., Minogue, B. M., Gnanalingham, K. and Hoyland, J. A. (2009) Increased expression of matrix metalloproteinase-10, nerve growth factor and substance P in the painful degenerate intervertebral disc. *Arthritis Res Ther* **11**, R126 https://doi.org/10.1186/ar2793

446 Sarchielli, P., Alberti, A., Floridi, A. and Gallai, V. (2001) Levels of nerve growth factor in cerebrospinal fluid of chronic daily headache patients. *Neurology* **57**, 132–134 https://doi.org/10.1212/WNL.57.1.132
447 Amann, R., Schuligoi, R., Herzeg, G. and Donnerer, J. (1996) Intraplantar injection of nerve growth factor into the rat hind paw: local edema and effects on thermal nociceptive threshold: *Pain* **64**, 323–329 https://doi.org/10.1016/0304-3959(95)00120-4
448 Apfel, S. C., Arezzo, J. C., Brownlee, M., Federoff, H. and Kessler, J. A. (1994) Nerve growth factor administration protects against experimental diabetic sensory neuropathy. *Brain Research* **634**, 7–12 https://doi.org/10.1016/0006-8993(94)90252-6
449 Apfel, S. C., Lipton, R. B., Arezzo, J. C. and Kessler, J. A. (1991) Nerve growth factor prevents toxic neuropathy in mice. *Ann Neurol.* **29**, 87–90 https://doi.org/10.1002/ana.410290115
450 Apfel, S. C., Arezzo, J. C., Lipson, L. and Kessler, J. A. (1992) Nerve growth factor prevents experimental cisplatin neuropathy. *Ann Neurol* **31**, 76–80 https://doi.org/10.1002/ana.410310114
451 Verge, V., Richardson, P., Wiesenfeld-Hallin, Z. and Hokfelt, T. (1995) Differential influence of nerve growth factor on neuropeptide expression in vivo: a novel role in peptide suppression in adult sensory neurons. *J. Neurosci.* **15**, 2081–2096 https://doi.org/10.1523/JNEUROSCI.15-03-02081.1995
452 Schwartz, J. P., Pearson, J. and Johnson, E. M. (1982) Effect of exposure to anti-NGF on sensory neurons of adult rats and guinea pigs. *Brain Research* **244**, 378–381 https://doi.org/10.1016/0006-8993(82)90102-0
453 Barker, P. A., Mantyh, P., Arendt-Nielsen, L., Viktrup, L. and Tive, L. (2020) Nerve Growth Factor Signaling and Its Contribution to Pain. *JPR* **Volume 13**, 1223–1241 https://doi.org/10.2147/JPR.S247472
454 Ghilardi, J. R., Freeman, K. T., Jimenez-Andrade, J. M., Coughlin, K. A., Kaczmarska, M. J., Castaneda-Corral, G., et al. (2012) Neuroplasticity of sensory and sympathetic nerve fibers in a mouse model of a painful arthritic joint. *Arthritis & Rheumatism* **64**, 2223–2232 https://doi.org/10.1002/art.34385
455 Schmelz, M., Mantyh, P., Malfait, A.-M., Farrar, J., Yaksh, T., Tive, L., et al. (2019) Nerve growth factor antibody for the treatment of osteoarthritis pain and chronic low-back pain: mechanism of action in the context of efficacy and safety. *Pain* **160**, 2210–2220 https://doi.org/10.1097/j.pain.0000000000001625
456 Katz, N., Borenstein, D. G., Birbara, C., Bramson, C., Nemeth, M. A., Smith, M. D., et al. (2011) Efficacy and safety of tanezumab in the treatment of chronic low back pain. *Pain* **152**, 2248–2258 https://doi.org/10.1016/j.pain.2011.05.003
457 Schnitzer, T. J. and Marks, J. A. (2015) A systematic review of the efficacy and general safety of antibodies to NGF in the treatment of OA of the hip or knee. *Osteoarthritis and Cartilage* **23**, S8–S17 https://doi.org/10.1016/j.joca.2014.10.003
458 Fang, X., Djouhri, L., McMullan, S., Berry, C., Okuse, K., Waxman, S. G., et al. (2005) trkA Is Expressed in Nociceptive Neurons and Influences Electrophysiological Properties via Nav1.8 Expression in Rapidly Conducting Nociceptors. *Journal of Neuroscience* **25**, 4868–4878 https://doi.org/10.1523/JNEUROSCI.0249-05.2005
459 Molliver, D. C., Radeke, M. J., Feinstein, S. C. and Snider, W. D. (1995) Presence or absence of TrKA protein distinguishes subsets of small sensory

neurons with unique cytochemical characteristics and dorsal horn projections. *J. Comp. Neurol.* **361**, 404–416 https://doi.org/10.1002/cne.903610305
460 Ernsberger, U. (2009) Role of neurotrophin signalling in the differentiation of neurons from dorsal root ganglia and sympathetic ganglia. *Cell Tissue Res* **336**, 349–384 https://doi.org/10.1007/s00441-009-0784-z
461 Snider, W. D. (1994) Functions of the neurotrophins during nervous system development: What the knockouts are teaching us. *Cell* **77**, 627–638 https://doi.org/10.1016/0092-8674(94)90048-5
462 Snider, W. D. and Silos-Santiago, I. (1996) Dorsal root ganglion neurons require functional neurotrophin receptors for survival during development. *Phil. Trans. R. Soc. Lond. B* **351**, 395–403 https://doi.org/10.1098/rstb.1996.0034
463 Silos-Santiago, I., Molliver, D., Ozaki, S., Smeyne, R., Fagan, A., Barbacid, M., et al. (1995) Non-TrkA-expressing small DRG neurons are lost in TrkA deficient mice. *J. Neurosci.* **15**, 5929–5942 https://doi.org/10.1523/JNEUROSCI.15-09-05929.1995
464 Smeyne, R. J., Klein, R., Schnapp, A., Long, L. K., Bryant, S., Lewin, A., et al. (1994) Severe sensory and sympathetic neuropathies in mice carrying a disrupted Trk/NGF receptor gene. *Nature* **368**, 246–249 https://doi.org/10.1038/368246a0
465 Leonard, C. E., Quiros, J., Lefcort, F. and Taneyhill, L. A. (2022) Loss of Elp1 disrupts trigeminal ganglion neurodevelopment in a model of familial dysautonomia. *eLife* **11**, article e71455 https://doi.org/10.7554/eLife.71455
466 Li, L., Gruner, K. and Tourtellotte, W. G. (2020) Retrograde nerve growth factor signaling abnormalities in familial dysautonomia. *Journal of Clinical Investigation* **130**, 2478–2487 https://doi.org/10.1172/JCI130401
467 Kanehisa, M. (2000) KEGG: Kyoto Encyclopedia of Genes and Genomes. *Nucleic Acids Research* **28**, 27–30 https://doi.org/10.1093/nar/28.1.27
468 Ashburner, M., Ball, C. A., Blake, J. A., Botstein, D., Butler, H., Cherry, J. M., et al. (2000) Gene Ontology: tool for the unification of biology. *Nat Genet* **25**, 25–29 https://doi.org/10.1038/75556
469 Bui, T. M., Wiesolek, H. L. and Sumagin, R. (2020) ICAM-1: A master regulator of cellular responses in inflammation, injury resolution, and tumorigenesis. *J Leukoc Biol* **108**, 787–799 https://doi.org/10.1002/JLB.2MR0220-549R
470 Szklarczyk, D., Gable, A. L., Nastou, K. C., Lyon, D., Kirsch, R., Pyysalo, S., et al. (2021) The STRING database in 2021: customizable protein–protein networks, and functional characterization of user-uploaded gene/measurement sets. *Nucleic Acids Research* **49**, D605–D612 https://doi.org/10.1093/nar/gkaa1074
471 Szklarczyk, D., Gable, A. L., Lyon, D., Junge, A., Wyder, S., Huerta-Cepas, J., et al. (2019) STRING v11: protein–protein association networks with increased coverage, supporting functional discovery in genome-wide experimental datasets. *Nucleic Acids Research* **47**, D607–D613 https://doi.org/10.1093/nar/gky1131
472 Luc, G., Arveiler, D., Evans, A., Amouyel, P., Ferrieres, J., Bard, J.-M., et al. (2003) Circulating soluble adhesion molecules ICAM-1 and VCAM-1 and incident coronary heart disease: The PRIME Study. *Atherosclerosis* **170**, 169–176 https://doi.org/10.1016/S0021-9150(03)00280-6

473 Oguz, M. M., Oguz, A. D., Sanli, C. and Cevik, A. (2014) Serum Levels of Soluble ICAM-1 in Children with Pulmonary Artery Hypertension. *Texas Heart Institute Journal* **41**, 159–164 https://doi.org/10.14503/THIJ-12-3012
474 Gross, M. D., Bielinski, S. J., Suarez-Lopez, J. R., Reiner, A. P., Bailey, K., Thyagarajan, B., et al. (2012) Circulating Soluble Intercellular Adhesion Molecule 1 and Subclinical Atherosclerosis: the Coronary Artery Risk Development in Young Adults Study. *Clinical Chemistry* **58**, 411–420 https://doi.org/10.1373/clinchem.2011.168559
475 Shiota, Y., Sato, T. and Ono, T. (1993) [Serum levels of soluble ICAM-1 in asthmatic patients]. *Arerugi* **42**, 1782–1787
476 Klok, A.-M., Luyendijk, L., Zaal, M. J. W., Rothova, A. and Kijlstra, A. (1999) Soluble ICAM-1 serum levels in patients with intermediate uveitis. *British Journal of Ophthalmology* **83**, 847–851 https://doi.org/10.1136/bjo.83.7.847
477 Zonneveld, R., Martinelli, R., Shapiro, N. I., Kuijpers, T. W., Plötz, F. B. and Carman, C. V. (2014) Soluble adhesion molecules as markers for sepsis and the potential pathophysiological discrepancy in neonates, children and adults. *Crit Care* **18**, article 204 https://doi.org/10.1186/cc13733
478 Winther, B., Arruda, E., Witek, T. J., Marlin, S. D., Tsianco, M. M., Innes, D. J., et al. (2002) Expression of ICAM-1 in Nasal Epithelium and Levels of Soluble ICAM-1 in Nasal Lavage Fluid During Human Experimental Rhinovirus Infection. *Arch Otolaryngol Head Neck Surg* **128**, 131 https://doi.org/10.1001/archotol.128.2.131
479 Terol, M. J., Tormo, M., Martinez-Climent, J. A., Marugan, I., Benet, I., Ferrandez, A., et al. (2003) Soluble intercellular adhesion molecule-1 (s-ICAM-1/s-CD54) in diffuse large B-cell lymphoma: association with clinical characteristics and outcome. *Annals of Oncology* **14**, 467–474 https://doi.org/10.1093/annonc/mdg057
480 Giannoulis, K., Angouridaki, C., Fountzilas, G., Papapolychroniadis, C., Giannoulis, E. and Gamvros, O. (2004) Serum concentrations of soluble ICAM-1 and VCAM-1 in patients with colorectal cancer. Clinical implications. *Tech Coloproctol* **8**, s65–s67 https://doi.org/10.1007/s10151-004-0115-z
481 Lawson, C. and Wolf, S. (2009) ICAM-1 signaling in endothelial cells. *Pharmacological Reports* **61**, 22–32 https://doi.org/10.1016/S1734-1140(09)70004-0
482 Wiesolek, H. L., Bui, T. M., Lee, J. J., Dalal, P., Finkielsztein, A., Batra, A., et al. (2020) Intercellular Adhesion Molecule 1 Functions as an Efferocytosis Receptor in Inflammatory Macrophages. *The American Journal of Pathology* **190**, 874–885 https://doi.org/10.1016/j.ajpath.2019.12.006
483 Liu, M., Guo, S., Hibbert, J. M., Jain, V., Singh, N., Wilson, N. O., et al. (2011) CXCL10/IP-10 in infectious diseases pathogenesis and potential therapeutic implications. *Cytokine & Growth Factor Reviews* S1359610111000293 https://doi.org/10.1016/j.cytogfr.2011.06.001
484 Cid, M. C., Hoffman, M. P., Hernández-Rodríguez, J., Segarra, M., Elkin, M., Sánchez, M., et al. (2006) Association between increased CCL2 (MCP-1) expression in lesions and persistence of disease activity in giant-cell arteritis*. *Rheumatology* **45**, 1356–1363 https://doi.org/10.1093/rheumatology/kel128
485 Škuljec, J., Sun, H., Pul, R., Bénardais, K., Ragancokova, D., Moharregh-Khiabani, D., et al. (2011) CCL5 induces a pro-inflammatory profile in microglia in vitro. *Cellular Immunology* **270**, 164–171 https://doi.org/10.1016/j.cellimm.2011.05.001

486 Quaranta, D. V., Weaver, R. R., Baumann, K. K., Fujimoto, T., Williams, L. M., Kim, H. C., et al. (2022) Transport of the pro-inflammatory chemokines CCL2 (MCP-1) and CCL5 (RANTES) across the intact mouse blood-brain barrier is inhibited by heparin and eprodisate and increased with systemic inflammation. *J Pharmacol Exp Ther* JPET-AR-2022-001380 https://doi.org/10.1124/jpet.122.001380
487 Fernández-Calle, R., Vicente-Rodríguez, M., Pastor, M., Gramage, E., Di Geronimo, B., Zapico, J. M., et al. (2018) Pharmacological inhibition of Receptor Protein Tyrosine Phosphatase β/ζ (PTPRZ1) modulates behavioral responses to ethanol. *Neuropharmacology* **137**, 86–95 https://doi.org/10.1016/j.neuropharm.2018.04.027
488 Kaplan, D. R., Martin-Zanca, D. and Parada, L. F. (1991) Tyrosine phosphorylation and tyrosine kinase activity of the trk proto-oncogene product induced by NGF. *Nature* **350**, 158–160 https://doi.org/10.1038/350158a0
489 Chang, J. H., Mellon, E., Schanen, N. C. and Twiss, J. L. (2003) Persistent TrkA Activity Is Necessary to Maintain Transcription in Neuronally Differentiated PC12 Cells. *Journal of Biological Chemistry* **278**, 42877–42885 https://doi.org/10.1074/jbc.M308155200
490 Zhou, J., Valletta, J. S., Grimes, M. L. and Mobley, W. C. (2002) Multiple Levels for Regulation of TrkA in PC12 Cells by Nerve Growth Factor. *Journal of Neurochemistry* **65**, 1146–1156 https://doi.org/10.1046/j.1471-4159.1995.65031146.x
491 M. Stabile, A., Montagnoli, C., Pistilli, A., Grazia Rambotti, M., Pula, G. and Rende, M. (2013) Antiproliferative and Proapoptotic Effects of the TrK-inhibitor GW441756 in Human Myosarcomas and Prostatic Carcinoma. *CST* **8**, 74–83 https://doi.org/10.2174/1574362411308010010
492 Kaplan, D. R., Hempstead, B. L., Martin-Zanca, D., Chao, M. V. and Parada, L. F. (1991) The trk Proto-Oncogene Product: a Signal Transducing Receptor for Nerve Growth Factor. *Science* **252**, 554–558 https://doi.org/10.1126/science.1850549
493 Klein, R., Jing, S., Nanduri, V., O'Rourke, E. and Barbacid, M. (1991) The trk proto-oncogene encodes a receptor for nerve growth factor. *Cell* **65**, 189–197 https://doi.org/10.1016/0092-8674(91)90419-Y
494 Senger, D. L. and Campenot, R. B. (1997) Rapid Retrograde Tyrosine Phosphorylation of trkA and Other Proteins in Rat Sympathetic Neurons in Compartmented Cultures. *Journal of Cell Biology* **138**, 411–421 https://doi.org/10.1083/jcb.138.2.411
495 Di Donato, M., Galasso, G., Giovannelli, P., Sinisi, A. A., Migliaccio, A. and Castoria, G. (2021) Targeting the Nerve Growth Factor Signaling Impairs the Proliferative and Migratory Phenotype of Triple-Negative Breast Cancer Cells. *Front. Cell Dev. Biol.* **9**, 676568 https://doi.org/10.3389/fcell.2021.676568
496 Jung, E. J. and Kim, D. R. (2008) Apoptotic cell death in TrkA-overexpressing cells: kinetic regulation of ERK phosphorylation and caspase-7 activation. *Mol. Cells* **26**, 12–17
497 Mills, C. D., Nguyen, T., Tanga, F. Y., Zhong, C., Gauvin, D. M., Mikusa, J., et al. (2013) Characterization of nerve growth factor-induced mechanical and thermal hypersensitivity in rats: Characterization of NGF-induced pain in rats. *EJP* **17**, 469–479 https://doi.org/10.1002/j.1532-2149.2012.00202.x
498 Svensson, P., Cairns, B. E., Wang, K. and Arendt-Nielsen, L. (2003) Injection of nerve growth factor into human masseter muscle evokes long-lasting

mechanical allodynia and hyperalgesia: *Pain* **104**, 241–247 https://doi.org/10.1016/S0304-3959(03)00012-5

499 Rukwied, R., Mayer, A., Kluschina, O., Obreja, O., Schley, M. and Schmelz, M. (2010) NGF induces non-inflammatory localized and lasting mechanical and thermal hypersensitivity in human skin. *Pain* **148**, 407–413 https://doi.org/10.1016/j.pain.2009.11.022

500 Dyck, P. J., Peroutka, S., Rask, C., Burton, E., Baker, M. K., Lehman, K. A., et al. (1997) Intradermal recombinant human nerve growth factor induces pressure allodynia and lowered heat-pain threshold in humans. *Neurology* **48**, 501–505 https://doi.org/10.1212/WNL.48.2.501

501 Andresen, T., Nilsson, M., Nielsen, A. K., Lassen, D., Arendt-Nielsen, L. and Drewes, A. M. (2016) Intradermal Injection with Nerve Growth Factor: A Reproducible Model to Induce Experimental Allodynia and Hyperalgesia. *Pain Pract* **16**, 12–23 https://doi.org/10.1111/papr.12267

502 Lewin, G., Ritter, A. and Mendell, L. (1993) Nerve growth factor-induced hyperalgesia in the neonatal and adult rat. *J. Neurosci.* **13**, 2136–2148 https://doi.org/10.1523/JNEUROSCI.13-05-02136.1993

503 Lewin, G. R., Rueff, A. and Mendell, L. M. (1994) Peripheral and Central Mechanisms of NGF-induced Hyperalgesia. *European Journal of Neuroscience* **6**, 1903–1912 https://doi.org/10.1111/j.1460-9568.1994.tb00581.x

504 Rueff, A., Dawson, A. J. L. R. and Mendell, L. M. (1996) Characteristics of nerve growth factor induced hyperalgesia in adult rats: dependence on enhanced bradykinin-1 receptor activity but not neurokinin-1 receptor activation: *Pain* **66**, 359–372 https://doi.org/10.1016/0304-3959(96)03060-6

505 Hirth, M., Rukwied, R., Gromann, A., Turnquist, B., Weinkauf, B., Francke, K., et al. (2013) Nerve growth factor induces sensitization of nociceptors without evidence for increased intraepidermal nerve fiber density. *Pain* **154**, 2500–2511 https://doi.org/10.1016/j.pain.2013.07.036

506 Andreev, N. Yu., Dimitrieva, N., Koltzenburg, M. and McMahon, S. B. (1995) Peripheral administration of nerve growth factor in the adult rat produces a thermal hyperalgesia that requires the presence of sympathetic post-ganglionic neurones. *Pain* **63**, 109–115 https://doi.org/10.1016/0304-3959(95)00024-M

507 Ruiz, G., Ceballos, D. and Baños, J.-E. (2004) Behavioral and histological effects of endoneurial administration of nerve growth factor: possible implications in neuropathic pain. *Brain Research* **1011**, 1–6 https://doi.org/10.1016/j.brainres.2004.02.001

508 Della Seta, D., de Acetis, L., Aloe, L. and Alleva, E. (1994) NGF effects on hot plate behaviors in mice. *Pharmacology Biochemistry and Behavior* **49**, 701–705 https://doi.org/10.1016/0091-3057(94)90090-6

509 Chillingworth, N. L., Morham, S. G. and Donaldson, L. F. (2006) Sex differences in inflammation and inflammatory pain in cyclooxygenase-deficient mice. *American Journal of Physiology-Regulatory, Integrative and Comparative Physiology* **291**, R327–R334 https://doi.org/10.1152/ajpregu.00901.2005

510 Ainsworth, L., Budelier, K., Clinesmith, M., Fiedler, A., Landstrom, R., Leeper, B. J., et al. (2006) Transcutaneous electrical nerve stimulation (TENS) reduces chronic hyperalgesia induced by muscle inflammation. *Pain* **120**, 182–187 https://doi.org/10.1016/j.pain.2005.10.030

511 Sluka, K. A., Kalra, A. and Moore, S. A. (2001) Unilateral intramuscular injections of acidic saline produce a bilateral, long-lasting hyperalgesia. *Muscle*

Nerve **24**, 37–46 https://doi.org/10.1002/1097-4598(200101)24:1<37::AID-MUS4>3.0.CO;2-8

512 Chen, J., Luo, C., Li, H.-L. and Chen, H.-S. (1999) Primary hyperalgesia to mechanical and heat stimuli following subcutaneous bee venom injection into the plantar surface of hindpaw in the conscious rat: a comparative study with the formalin test: *Pain* **83**, 67–76 https://doi.org/10.1016/S0304-3959(99)00075-5

513 Aloisi, A. M., Porro, C. A., Cavazzuti, M., Baraldi, P. and Carli, G. (1993) 'Mirror pain' in the formalin test: behavioral and 2-deoxyglucose studies. *Pain* **55**, 267–273 https://doi.org/10.1016/0304-3959(93)90156-J

514 Petty, B. G., Cornblath, D. R., Adornato, B. T., Chaudhry, V., Flexner, C., Wachsman, M., et al. (1994) The effect of systemically administered recombinant human nerve growth factor in healthy human subjects. *Ann Neurol.* **36**, 244–246 https://doi.org/10.1002/ana.410360221

515 Chung, M.-K., Jung, S. J. and Oh, S. B. (2011) Role of TRP Channels in Pain Sensation. In Transient Receptor Potential Channels (Islam, Md. S., ed.), pp 615–636, Springer Netherlands, Dordrecht https://doi.org/10.1007/978-94-007-0265-3_33

516 Zhang, X., Huang, J. and McNaughton, P. A. (2005) NGF rapidly increases membrane expression of TRPV1 heat-gated ion channels. *EMBO J* **24**, 4211–4223 https://doi.org/10.1038/sj.emboj.7600893

517 Zhu, W. and Oxford, G. S. (2007) Phosphoinositide-3-kinase and mitogen activated protein kinase signaling pathways mediate acute NGF sensitization of TRPV1. *Molecular and Cellular Neuroscience* **34**, 689–700 https://doi.org/10.1016/j.mcn.2007.01.005

518 Englander, E. W. (2013) DNA damage response in peripheral nervous system: Coping with cancer therapy-induced DNA lesions. *DNA Repair* **12**, 685–690 https://doi.org/10.1016/j.dnarep.2013.04.020

519 García-Díaz, M., Bebenek, K., Kunkel, T. A. and Blanco, L. (2001) Identification of an Intrinsic 5′-Deoxyribose-5-phosphate Lyase Activity in Human DNA Polymerase λ. *Journal of Biological Chemistry* **276**, 34659–34663 https://doi.org/10.1074/jbc.M106336200

520 Koike, M. (2002) Dimerization, Translocation and Localization of Ku70 and Ku80 Proteins. *JRR* **43**, 223–236 https://doi.org/10.1269/jrr.43.223

521 Hopfner, K.-P., Putnam, C. D. and Tainer, J. A. (2002) DNA double-strand break repair from head to tail. *Current Opinion in Structural Biology* **12**, 115–122 https://doi.org/10.1016/S0959-440X(02)00297-X

522 Harris, J. L., Rabellino, A. and Khanna, K. K. (2018) RAD51 paralogs promote genomic integrity and chemoresistance in cancer by facilitating homologous recombination. *Ann. Transl. Med* **6**, S122–S122 https://doi.org/10.21037/atm.2018.12.30

523 Yonetani, Y., Hochegger, H., Sonoda, E., Shinya, S., Yoshikawa, H., Takeda, S., et al. (2005) Differential and collaborative actions of Rad51 paralog proteins in cellular response to DNA damage. *Nucleic Acids Research* **33**, 4544–4552 https://doi.org/10.1093/nar/gki766

524 McNeil, E. M. and Melton, D. W. (2012) DNA repair endonuclease ERCC1-XPF as a novel therapeutic target to overcome chemoresistance in cancer therapy. *Nucleic Acids Research* **40**, 9990–10004 https://doi.org/10.1093/nar/gks818

525 Cheng, Y.-C., Snavely, A., Barrett, L. B., Zhang, X., Herman, C., Frost, D. J., et al. (2021) Topoisomerase I inhibition and peripheral nerve injury induce DNA breaks and ATF3-associated axon regeneration in sensory neurons. *Cell Reports* **36**, 109666 https://doi.org/10.1016/j.celrep.2021.109666
526 Deng, S., Yan, T., Nikolova, T., Fuhrmann, D., Nemecek, A., Gödtel-Armbrust, U., et al. (2015) The catalytic topoisomerase II inhibitor dexrazoxane induces DNA breaks, ATF3 and the DNA damage response in cancer cells. *Br J Pharmacol* **172**, 2246–2257 https://doi.org/10.1111/bph.13046
527 Liu, Y., Gao, F., Jiang, H., Niu, L., Bi, Y., Young, C. Y. F., et al. (2013) Induction of DNA damage and ATF3 by retigeric acid B, a novel topoisomerase II inhibitor, promotes apoptosis in prostate cancer cells. *Cancer Letters* **337**, 66–76 https://doi.org/10.1016/j.canlet.2013.05.022
528 Mashima, T., Udagawa, S. and Tsuruo, T. (2001) Involvement of transcriptional repressor ATF3 in acceleration of caspase protease activation during DNA damaging agent-induced apoptosis. *J. Cell. Physiol.* **188**, 352–358 https://doi.org/10.1002/jcp.1130
529 Wang, J. C. (2002) Cellular roles of DNA topoisomerases: a molecular perspective. *Nat Rev Mol Cell Biol* **3**, 430–440 https://doi.org/10.1038/nrm831
530 Nitiss, J. L. (1998) DNA Topoisomerases in DNA Repair and DNA Damage Tolerance. In DNA Damage and Repair (Nickoloff, J. A., and Hoekstra, M. F., eds.), pp 517–537, Humana Press, Totowa, NJ https://doi.org/10.1007/978-1-59259-455-9_23
531 Downes, C. S. and Johnson, R. T. (1988) DNA topoisomerases and DNA repair. *Bioessays* **8**, 179–184 https://doi.org/10.1002/bies.950080602
532 Pommier, Y., Nussenzweig, A., Takeda, S. and Austin, C. (2022) Human topoisomerases and their roles in genome stability and organization. *Nat Rev Mol Cell Biol* **23**, 407–427 https://doi.org/10.1038/s41580-022-00452-3
533 Fan, F., Jin, S., Amundson, S. A., Tong, T., Fan, W., Zhao, H., et al. (2002) ATF3 induction following DNA damage is regulated by distinct signaling pathways and over-expression of ATF3 protein suppresses cells growth. *Oncogene* **21**, 7488–7496 https://doi.org/10.1038/sj.onc.1205896
534 Hartman, M. G., Lu, D., Kim, M.-L., Kociba, G. J., Shukri, T., Buteau, J., et al. (2004) Role for Activating Transcription Factor 3 in Stress-Induced β-Cell Apoptosis. *Mol Cell Biol* **24**, 5721–5732 https://doi.org/10.1128/MCB.24.13.5721-5732.2004
535 Lu, D., Wolfgang, C. D. and Hai, T. (2006) Activating Transcription Factor 3, a Stress-inducible Gene, Suppresses Ras-stimulated Tumorigenesis. *Journal of Biological Chemistry* **281**, 10473–10481 https://doi.org/10.1074/jbc.M509278200
536 Francis, J. S., Dragunow, M. and During, M. J. (2004) Over expression of ATF-3 protects rat hippocampal neurons from in vivo injection of kainic acid. *Molecular Brain Research* **124**, 199–203 https://doi.org/10.1016/j.molbrainres.2003.10.027
537 Nakagomi, S., Suzuki, Y., Namikawa, K., Kiryu-Seo, S. and Kiyama, H. (2003) Expression of the Activating Transcription Factor 3 Prevents c-Jun N-Terminal Kinase-Induced Neuronal Death by Promoting Heat Shock Protein 27 Expression and Akt Activation. *J. Neurosci.* **23**, 5187–5196 https://doi.org/10.1523/JNEUROSCI.23-12-05187.2003
538 Nobori, K., Ito, H., Tamamori-Adachi, M., Adachi, S., Ono, Y., Kawauchi, J., et al. (2002) ATF3 Inhibits Doxorubicin-induced Apoptosis in Cardiac

Myocytes: A Novel Cardioprotective Role of ATF3. *Journal of Molecular and Cellular Cardiology* **34**, 1387–1397 https://doi.org/10.1006/jmcc.2002.2091

539 Liang, Y., Jiang, H., Ratovitski, T., Jie, C., Nakamura, M., Hirschhorn, R. R., et al. (2009) ATF3 plays a protective role against toxicity by N-terminal fragment of mutant huntingtin in stable PC12 cell line. *Brain Research* **1286**, 221–229 https://doi.org/10.1016/j.brainres.2009.06.049

540 Allan, A. L., Albanese, C., Pestell, R. G. and LaMarre, J. (2001) Activating Transcription Factor 3 Induces DNA Synthesis and Expression of Cyclin D1 in Hepatocytes. *Journal of Biological Chemistry* **276**, 27272–27280 https://doi.org/10.1074/jbc.M103196200

541 Hunt, D., Raivich, G. and Anderson, P. N. (2012) Activating Transcription Factor 3 and the Nervous System. *Front. Mol. Neurosci.* **5** https://doi.org/10.3389/fnmol.2012.00007

542 Gey, M., Wanner, R., Schilling, C., Pedro, M. T., Sinske, D. and Knöll, B. (2016) Atf3 mutant mice show reduced axon regeneration and impaired regeneration-associated gene induction after peripheral nerve injury. *Open Biol.* **6**, article 160091 https://doi.org/10.1098/rsob.160091

543 Seijffers, R., Allchorne, A. J. and Woolf, C. J. (2006) The transcription factor ATF-3 promotes neurite outgrowth. *Molecular and Cellular Neuroscience* **32**, 143–154 https://doi.org/10.1016/j.mcn.2006.03.005

544 Averill, S., Michael, G. J., Shortland, P. J., Leavesley, R. C., King, V. R., Bradbury, E. J., et al. (2004) NGF and GDNF ameliorate the increase in ATF3 expression which occurs in dorsal root ganglion cells in response to peripheral nerve injury. *Eur J Neurosci* **19**, 1437–1445 https://doi.org/10.1111/j.1460-9568.2004.03241.x

545 Tsujino, H., Kondo, E., Fukuoka, T., Dai, Y., Tokunaga, A., Miki, K., et al. (2000) Activating Transcription Factor 3 (ATF3) Induction by Axotomy in Sensory and Motoneurons: A Novel Neuronal Marker of Nerve Injury. *Molecular and Cellular Neuroscience* **15**, 170–182 https://doi.org/10.1006/mcne.1999.0814

546 Hyatt Sachs, H., Schreiber, R. C., Shoemaker, S. E., Sabe, A., Reed, E. and Zigmond, R. E. (2007) Activating transcription factor 3 induction in sympathetic neurons after axotomy: Response to decreased neurotrophin availability. *Neuroscience* **150**, 887–897 https://doi.org/10.1016/j.neuroscience.2007.10.008

547 Bloechlinger, S., Karchewski, L. A. and Woolf, C. J. (2004) Dynamic changes in glypican-1 expression in dorsal root ganglion neurons after peripheral and central axonal injury. *Eur J Neurosci* **19**, 1119–1132 https://doi.org/10.1111/j.1460-9568.2004.03262.x

548 Lindå, H., Sköld, M. K. and Ochsmann, T. (2011) Activating Transcription Factor 3, a Useful Marker for Regenerative Response after Nerve Root Injury. *Front. Neur.* **2**, article 30 https://doi.org/10.3389/fneur.2011.00030

549 Payne, S. C., Belleville, P. J. and Keast, J. R. (2015) Regeneration of sensory but not motor axons following visceral nerve injury. *Experimental Neurology* **266**, 127–142 https://doi.org/10.1016/j.expneurol.2015.02.026

550 Boeshore, K. L., Schreiber, R. C., Vaccariello, S. A., Sachs, H. H., Salazar, R., Lee, J., et al. (2004) Novel changes in gene expression following axotomy of a sympathetic ganglion: A microarray analysis. *J. Neurobiol.* **59**, 216–235 https://doi.org/10.1002/neu.10308

551 Fallon, M. and Tadi, P. (2022) Histology, Schwann Cells. In StatPearls, StatPearls Publishing, Treasure Island (FL)
552 Seijffers, R., Mills, C. D. and Woolf, C. J. (2007) ATF3 Increases the Intrinsic Growth State of DRG Neurons to Enhance Peripheral Nerve Regeneration. *Journal of Neuroscience* **27**, 7911–7920 https://doi.org/10.1523/JNEUROSCI.5313-06.2007
553 Chen, B. P., Wolfgang, C. D. and Hai, T. (1996) Analysis of ATF3, a transcription factor induced by physiological stresses and modulated by gadd153/Chop10. *Mol Cell Biol* **16**, 1157–1168 https://doi.org/10.1128/MCB.16.3.1157
554 Nascimento, D., Pozza, D. H., Castro-Lopes, J. M. and Neto, F. L. (2011) Neuronal Injury Marker ATF-3 Is Induced in Primary Afferent Neurons of Monoarthritic Rats. *Neurosignals* **19**, 210–221 https://doi.org/10.1159/000330195
555 Seijffers, R., Zhang, J., Matthews, J. C., Chen, A., Tamrazian, E., Babaniyi, O., et al. (2014) ATF3 expression improves motor function in the ALS mouse model by promoting motor neuron survival and retaining muscle innervation. *Proc. Natl. Acad. Sci. U.S.A.* **111**, 1622–1627 https://doi.org/10.1073/pnas.1314826111
556 Jimenez-Andrade, J. M., Peters, C. M., Mejia, N. A., Ghilardi, J. R., Kuskowski, M. A. and Mantyh, P. W. (2006) Sensory neurons and their supporting cells located in the trigeminal, thoracic and lumbar ganglia differentially express markers of injury following intravenous administration of paclitaxel in the rat. *Neuroscience Letters* **405**, 62–67 https://doi.org/10.1016/j.neulet.2006.06.043
557 Park, E.-J., Kwon, H.-K., Choi, Y.-M., Shin, H.-J. and Choi, S. (2012) Doxorubicin Induces Cytotoxicity through Upregulation of pERK–Dependent ATF3. *PLoS ONE* (Mukhopadhyay, P., ed.) **7**, article e44990 https://doi.org/10.1371/journal.pone.0044990
558 Jardín, I., López, J. J., Diez, R., Sánchez-Collado, J., Cantonero, C., Albarrán, L., et al. (2017) TRPs in Pain Sensation. *Front. Physiol.* **8**, article 392 https://doi.org/10.3389/fphys.2017.00392
559 Mantyh, P. W., Koltzenburg, M., Mendell, L. M., Tive, L. and Shelton, D. L. (2011) Antagonism of Nerve Growth Factor-TrkA Signaling and the Relief of Pain: *Anesthesiology* **115**, 189–204 https://doi.org/10.1097/ALN.0b013e31821b1ac5
560 Guo, A., Vulchanova, L., Wang, J., Li, X. and Elde, R. (1999) Immunocytochemical localization of the vanilloid receptor 1 (VR1): relationship to neuropeptides, the P2X3 purinoceptor and IB4 binding sites. *European Journal of Neuroscience* **11**, 946–958 https://doi.org/10.1046/j.1460-9568.1999.00503.x
561 Tominaga, M., Caterina, M. J., Malmberg, A. B., Rosen, T. A., Gilbert, H., Skinner, K., et al. (1998) The Cloned Capsaicin Receptor Integrates Multiple Pain-Producing Stimuli. *Neuron* **21**, 531–543 https://doi.org/10.1016/S0896-6273(00)80564-4
562 OuYang, Y., Zhang, X., Liu, X., Liu, X., Cao, Y., Qiu, J., et al. (2020) TRPV 1 Regulates the Proliferation and Cisplatin Sensitivity of Esophageal Cancer. *International Journal of Radiation Oncology*Biology*Physics* **108**, article e501 https://doi.org/10.1016/j.ijrobp.2020.07.1583

563 Ghosh, S., Sheth, S., Sheehan, K., Mukherjea, D., Dhukhwa, A., Borse, V., et al. (2018) The Endocannabinoid/Cannabinoid Receptor 2 System Protects Against Cisplatin-Induced Hearing Loss. *Front. Cell. Neurosci.* **12**, article 271 https://doi.org/10.3389/fncel.2018.00271
564 Waissbluth, S. and Daniel, S. J. (2013) Cisplatin-induced ototoxicity: Transporters playing a role in cisplatin toxicity. *Hearing Research* **299**, 37–45 https://doi.org/10.1016/j.heares.2013.02.002
565 Caterina, M. J., Leffler, A., Malmberg, A. B., Martin, W. J., Trafton, J., Petersen-Zeitz, K. R., et al. (2000) Impaired Nociception and Pain Sensation in Mice Lacking the Capsaicin Receptor. *Science* **288**, 306–313 https://doi.org/10.1126/science.288.5464.306
566 Davis, J. B., Gray, J., Gunthorpe, M. J., Hatcher, J. P., Davey, P. T., Overend, P., et al. (2000) Vanilloid receptor-1 is essential for inflammatory thermal hyperalgesia. *Nature* **405**, 183–187 https://doi.org/10.1038/35012076
567 Iftinca, M., Defaye, M. and Altier, C. (2021) TRPV1-Targeted Drugs in Development for Human Pain Conditions. *Drugs* **81**, 7–27 https://doi.org/10.1007/s40265-020-01429-2
568 Kargbo, R. B. (2019) TRPV1 Modulators for the Treatment of Pain and Inflammation. *ACS Med. Chem. Lett.* **10**, 143–144 https://doi.org/10.1021/acsmedchemlett.8b00618
569 Szolcsányi, J. and Sándor, Z. (2012) Multisteric TRPV1 nocisensor: a target for analgesics. *Trends in Pharmacological Sciences* **33**, 646–655 https://doi.org/10.1016/j.tips.2012.09.002
570 Bonnington, J. K. and McNaughton, P. A. (2003) Signalling pathways involved in the sensitisation of mouse nociceptive neurones by nerve growth factor. *The Journal of Physiology* **551**, 433–446 https://doi.org/10.1113/jphysiol.2003.039990
571 Galoyan, S. M., Petruska, J. C. and Mendell, L. M. (2003) Mechanisms of sensitization of the response of single dorsal root ganglion cells from adult rat to noxious heat. *Eur J Neurosci* **18**, 535–541 https://doi.org/10.1046/j.1460-9568.2003.02775.x
572 Shu, X. and Mendell, L. M. (1999) Nerve growth factor acutely sensitizes the response of adult rat sensory neurons to capsaicin. *Neuroscience Letters* **274**, 159–162 https://doi.org/10.1016/S0304-3940(99)00701-6
573 Omerbašić, D., Smith, E. St. J., Moroni, M., Homfeld, J., Eigenbrod, O., Bennett, N. C., et al. (2016) Hypofunctional TrkA Accounts for the Absence of Pain Sensitization in the African Naked Mole-Rat. *Cell Reports* **17**, 748–758 https://doi.org/10.1016/j.celrep.2016.09.035
574 Zhang, X. and McNaughton, P. A. (2006) Why Pain Gets Worse: The Mechanism of Heat Hyperalgesia. *Journal of General Physiology* **128**, 491–493 https://doi.org/10.1085/jgp.200609676
575 Marlin, M. C. and Li, G. (2015) Biogenesis and Function of the NGF/TrkA Signaling Endosome. In International Review of Cell and Molecular Biology, pp 239–257, Elsevier https://doi.org/10.1016/bs.ircmb.2014.10.002
576 Chuang, H., Prescott, E. D., Kong, H., Shields, S., Jordt, S.-E., Basbaum, A. I., et al. (2001) Bradykinin and nerve growth factor release the capsaicin receptor from PtdIns(4,5)P2-mediated inhibition. *Nature* **411**, 957–962 https://doi.org/10.1038/35082088
577 Bron, R., Klesse, L. J., Shah, K., Parada, L. F. and Winter, J. (2003) Activation of Ras is necessary and sufficient for upregulation of vanilloid receptor type 1

in sensory neurons by neurotrophic factors. *Molecular and Cellular Neuroscience* **22**, 118–132 https://doi.org/10.1016/S1044-7431(02)00022-2
578 Ji, R.-R., Samad, T. A., Jin, S.-X., Schmoll, R. and Woolf, C. J. (2002) p38 MAPK Activation by NGF in Primary Sensory Neurons after Inflammation Increases TRPV1 Levels and Maintains Heat Hyperalgesia. *Neuron* **36**, 57–68 https://doi.org/10.1016/S0896-6273(02)00908-X
579 Zhuang, Z.-Y., Xu, H., Clapham, D. E. and Ji, R.-R. (2004) Phosphatidylinositol 3-Kinase Activates ERK in Primary Sensory Neurons and Mediates Inflammatory Heat Hyperalgesia through TRPV1 Sensitization. *Journal of Neuroscience* **24**, 8300–8309 https://doi.org/10.1523/JNEUROSCI.2893-04.2004
580 Meng, J., Qiu, S., Zhang, L., You, M., Xing, H. and Zhu, J. (2022) Berberine Alleviate Cisplatin-Induced Peripheral Neuropathy by Modulating Inflammation Signal via TRPV1. *Front. Pharmacol.* **12** https://doi.org/10.3389/fphar.2021.774795
581 Woodbury, C. J. (2004) Nociceptors Lacking TRPV1 and TRPV2 Have Normal Heat Responses. *Journal of Neuroscience* **24**, 6410–6415 https://doi.org/10.1523/JNEUROSCI.1421-04.2004
582 Li, X., Guo, M., Cai, L., Du, T., Liu, Y., Ding, H.-F., et al. (2020) Competitive ubiquitination activates the tumor suppressor p53. *Cell Death Differ* **27**, 1807–1818 https://doi.org/10.1038/s41418-019-0463-x
583 Yan, C., Lu, D., Hai, T. and Boyd, D. D. (2005) Activating transcription factor 3, a stress sensor, activates p53 by blocking its ubiquitination. *EMBO J* **24**, 2425–2435 https://doi.org/10.1038/sj.emboj.7600712
584 Wang, J. C. (1996) DNA Topoisomerases. *Annu. Rev. Biochem.* **65**, 635–692 https://doi.org/10.1146/annurev.bi.65.070196.003223
585 Martinez-Garcia, M., White, C. I., Franklin, F. Chris. H. and Sanchez-Moran, E. (2021) The Role of Topoisomerase II in DNA Repair and Recombination in Arabidopsis thaliana. *IJMS* **22**, 13115 https://doi.org/10.3390/ijms222313115
586 Morotomi-Yano, K., Saito, S., Adachi, N. and Yano, K. (2018) Dynamic behavior of DNA topoisomerase IIβ in response to DNA double-strand breaks. *Sci Rep* **8**, 10344 https://doi.org/10.1038/s41598-018-28690-6
587 Akimitsu, N., Adachi, N., Hirai, H., Hossain, M. S., Hamamoto, H., Kobayashi, M., et al. (2003) Enforced cytokinesis without complete nuclear division in embryonic cells depleting the activity of DNA topoisomerase IIα: Role of DNA topoisomerase IIa in mouse development. *Genes to Cells* **8**, 393–402 https://doi.org/10.1046/j.1365-2443.2003.00643.x
588 Yang, X., Li, W., Prescott, E. D., Burden, S. J. and Wang, J. C. (2000) DNA Topoisomerase IIβ and Neural Development. *Science* **287**, 131–134 https://doi.org/10.1126/science.287.5450.131
589 Jurisicova, A., Lee, H.-J., D'Estaing, S. G., Tilly, J. and Perez, G. I. (2006) Molecular requirements for doxorubicin-mediated death in murine oocytes. *Cell Death Differ* **13**, 1466–1474 https://doi.org/10.1038/sj.cdd.4401819
590 Hasim, M. S., Nessim, C., Villeneuve, P. J., Vanderhyden, B. C. and Dimitroulakos, J. (2018) Activating Transcription Factor 3 as a Novel Regulator of Chemotherapy Response in Breast Cancer. *Translational Oncology* **11**, 988–998 https://doi.org/10.1016/j.tranon.2018.06.001
591 Washiro, M., Ohtsuka, M., Kimura, F., Shimizu, H., Yoshidome, H., Sugimoto, T., et al. (2008) Upregulation of topoisomerase IIα expression in advanced

gallbladder carcinoma: a potential chemotherapeutic target. *J Cancer Res Clin Oncol* **134**, 793–801 https://doi.org/10.1007/s00432-007-0348-0

592 Cappabianca, L., Sebastiano, M., Ruggieri, M., Sbaffone, M., Zelli, V., Farina, A. R., et al. (2022) Doxorubicin-Induced TrkAIII Activation: A Selection Mechanism for Resistant Dormant Neuroblastoma Cells. *IJMS* **23**, 10895 https://doi.org/10.3390/ijms231810895

593 Liao, D., Zhang, C., Liu, N., Cao, L., Wang, C., Feng, Q., et al. (2019) Involvement of neurotrophic signaling in doxorubicin-induced cardiotoxicity. *Exp Ther Med* **19**, 1129–1135 https://doi.org/10.3892/etm.2019.8276

594 Yang, F. and Zheng, J. (2017) Understand spiciness: mechanism of TRPV1 channel activation by capsaicin. *Protein Cell* **8**, 169–177 https://doi.org/10.1007/s13238-016-0353-7

595 Caterina, M. J., Schumacher, M. A., Tominaga, M., Rosen, T. A., Levine, J. D. and Julius, D. (1997) The capsaicin receptor: a heat-activated ion channel in the pain pathway. *Nature* **389**, 816–824 https://doi.org/10.1038/39807

596 Koşar, P. A., Nazıroğlu, M., Övey, İ. S. and Çiğ, B. (2016) Synergic Effects of Doxorubicin and Melatonin on Apoptosis and Mitochondrial Oxidative Stress in MCF-7 Breast Cancer Cells: Involvement of TRPV1 Channels. *J Membrane Biol* **249**, 129–140 https://doi.org/10.1007/s00232-015-9855-0

597 Pommier, Y., Leo, E., Zhang, H. and Marchand, C. (2010) DNA Topoisomerases and Their Poisoning by Anticancer and Antibacterial Drugs. *Chemistry & Biology* **17**, 421–433 https://doi.org/10.1016/j.chembiol.2010.04.012

598 Du, D., Tang, X., Li, Y., Gao, Y., Chen, R., Chen, Q., et al. (2022) Senotherapy Protects against Cisplatin-Induced Ovarian Injury by Removing Senescent Cells and Alleviating DNA Damage. *Oxidative Medicine and Cellular Longevity* (Georgieva, M., ed.) **2022**, article 9144644 https://doi.org/10.1155/2022/9144644

599 Ahmadinejad, F., Bos, T., Hu, B., Britt, E., Koblinski, J., Souers, A. J., et al. (2022) Senolytic-Mediated Elimination of Head and Neck Tumor Cells Induced Into Senescence by Cisplatin. *Mol Pharmacol* **101**, 168–180 https://doi.org/10.1124/molpharm.121.000354

600 Fang, K., Chiu, C.-C., Li, C.-H., Chang, Y. and Hwang, H. (2007) Cisplatin-Induced Senescence and Growth Inhibition in Human Non-Small Cell Lung Cancer Cells With Ectopic Transfer of p16INK4a. *or* **16**, 479–488 https://doi.org/10.3727/096504007783338331

601 Calls, A., Torres-Espin, A., Navarro, X., Yuste, V. J., Udina, E. and Bruna, J. (2021) Cisplatin-induced peripheral neuropathy is associated with neuronal senescence-like response. *Neuro-Oncology* **23**, 88–99 https://doi.org/10.1093/neuonc/noaa151

602 Acklin, S., Zhang, M., Du, W., Zhao, X., Plotkin, M., Chang, J., et al. (2020) Depletion of senescent-like neuronal cells alleviates cisplatin-induced peripheral neuropathy in mice. *Sci Rep* **10**, article 14170 https://doi.org/10.1038/s41598-020-71042-6

603 Muñoz-Espín, D., Rovira, M., Galiana, I., Giménez, C., Lozano-Torres, B., Paez-Ribes, M., et al. (2018) A versatile drug delivery system targeting senescent cells. *EMBO Mol Med* **10**, article e9355 https://doi.org/10.15252/emmm.201809355

604 Sapieha, P. and Mallette, F. A. (2018) Cellular Senescence in Postmitotic Cells: Beyond Growth Arrest. *Trends in Cell Biology* **28**, 595–607 https://doi.org/10.1016/j.tcb.2018.03.003